Universitetet i Stavanger

FACULTY OF SCIENCE AND TECHNOLOGY

MASTER'S THESIS

Study programme/specialisation: Mechanical and structural engineering and materials science/ Civil engineering structures	Spring / ~~Autumn~~ semester, 2019 Open/~~Confidential~~
Author: Fredrik Bjørheim	…… … (signature of author)
Programme coordinator: Dimitrios Pavlou Supervisor(s): Kristen Rege	
Title of master's thesis: Practical comparison of crack meshing in ANSYS mechanical APDL 19.2	
Credits: 30	
Keywords: - FEM - XFEM - Crack analysis - Mesh - Stress intensity factors	Number of pages: 90 + Appendix: 68 Stavanger, 15.06.2019 date/year

Abstract

Structures under cyclic loading are typically subjected to formation of cracks, and thereafter crack propagation. To be able to analyse the crack propagation numerically with the goal of estimating a structure or a structural part's life span, many methods have been proposed, where two examples are:

1. Finite element method, with collapsed Q8 elements to describe the singularity present near the crack tip. In this case, remeshing is required as the crack grows.
2. Extended finite element method, where the elements are enriched with extra nodes to be able to describe the discontinuity, and singularity present. By using this method, the crack can propagate through the elements, hence no requirement for remeshing.

Both methods depend on the numerical evaluation of stress intensity factors (SIFS). This means that the accuracy of a crack propagation analysis, will depend on the accuracy achieved for the SIFS. This thesis will focus on the accuracy obtained for SIF evaluation on a stationary crack, from a practical perspective, where the obtained results will be compared to analytical solutions.

In this project two geometries have been tested, using both methods, and checking which parameters are of importance regarding the method used. The first geometry is a slanted through thickness crack, and the second is a curved through thickness crack. Both of these cracks have analytical formulas if the crack is present in an infinite plate.

The findings are that explicitly modelling the crack using the finite element method gives higher accuracy and requires fewer elements, than the extended finite element method.

When the cracks were explicitly modelled, it was possible to obtain results within 0,1% deviation with very few elements. Whereas the extended finite element method required a rather high mesh density to obtain a deviation within 1%.

This thesis contains a theoretical and an experimental section. The theoretical section describes general linear elastic fracture mechanics and the numerical methods used.

Acknowledgements

My personal experience with finite element analysis and linear fracture mechanics was limited to two courses of finite element method, and a course of structural integrity.

Throughout this master thesis, I have gained valuable knowledge with finite element analysis, and its capabilities to analyse cracks.

I want to express my gratitude to my supervisors Kristen Rege and Dimitrios Pavlou, for their support throughout the project. They helped me with good literature in regard to stress intensity factor analysis using FEM and XFEM, and suggestions for how the testing could be performed.

Innhold

Chapter 1 Introduction

Crack growth and fracture is a problem that can be seen both in nature, and in man-made structures. Where the common cause of the propagation is the presence of tensile or shear stress within the material.

An example of crack growth which can be seen in nature, could be the freeze-thaw erosion in mountains, where the crack in a rock is partly driven by the volumetric expansion of the water. This freeze-thaw erosion develops a cyclic tensile stress near the crack tip and will typically continue until the crack growth has reached a critical state. When the critical state has been reached, the crack will fracture.

Traditionally, the problem of crack growth and fracture has not been an issue, as the materials used for large structures typically were brick and mortar. As these materials are not reliable for carrying tensile loads, the structural components commonly used were columns and arches. The use of columns and arches guarantee that the stresses within the material will not experience tensile stresses.

When steel started being used as a structural material, the limitation to only carry compressive loads was no longer an issue, as steel is a material which is highly capable of carrying tensile loads. It was early noted that structures which used steel to carry tensile loads, would sometimes fail unexpectedly, at stresses well below the expected tensile strength of the material. An example of such a failure, was the rupture of a molasses tank in Boston in 1919 where 12 people died, 40 were injured with the addition of massive property damage, as 7500 m^3 was spilled. The cause of the failure was a mystery at the time [1].

The field of fracture mechanics was drastically accelerated after what happened to the Liberty ships during World War II. During the war, U.S. supplied Great Britain with planes and ships through the Lend-Lease Act. The problem with the supply, was that the ships used were sunk faster than the U.S could produce them. This led to the development of welding the ships instead of using rivets, which greatly accelerated the process of construction. Initially this seemed to be a great success, until one of the ships suddenly broke in two, during a voyage between Siberia and Alaska in 1943. Several of the other ships also experienced fractures of variable degree.

An investigation of the liberty ships was performed, and it was found that the failures were due to a combination of:

1. The welds contained crack-like flaws.
2. Most of the fractures initiated on the deck at square hatch corners, due to local stress concentration.
3. The steel from which the Liberty ships were made had poor toughness.

The steel which was used for the Liberty ships had been good enough for the riveted ships previously built, as the cracks would not be able to propagate across riveted panels. The issue which arose when the ships were welded, was that the hull in practice became one solid plate, with no significant barriers for the crack propagation.

The accelerated research within the field of fracture mechanics, led to the stress intensity factor which is a parameter which can describe the stresses and displacements near the crack tip. It was George R Irwin who first showed that the stresses and displacements near the crack tip can be described using a single constant which has a relation to the energy release rate. Irwin used the Westergaard approach, which is a technique for analysing stresses and displacements ahead of a sharp crack [1].

The stress intensity factor can be used in relation to the fracture assessment diagram, to check if the structure itself is safe for a given crack. Another practical use for the stress intensity factor, is related to fatigue crack growth. When a crack is subjected to cyclic loading, it can still successively propagate. As the crack grows larger, the stress intensity factor increases, until it reaches a critical level, where the structure might fracture.

A recent accident related to fracture mechanics is the Aleksander Kielland accident in 1981, where it was found during the investigation that the cause of the structural collapse, was a fatigue fracture in one of the bracings. The fatigue crack had started in a welded support for a hydrophone, which is an instrument used for positioning control. The report further states that the crack was most likely already present from construction in Dunkerque, due to paint residue on the crack surface. It also states that the shape of the welding bead of the fillet welds which were used, were poor. On Alexander Kielland, there were all together 212 people on board when the accident occurred, and this structural failure due to fatigue fracture cost 123 of them their lives [2].

Another recent accident is the accident, where the main rotor suddenly disconnected on a helicopter of the type Airbus Helicopters EC 225 LP Super Puma, which occurred on the 29th of April 2016. The investigating report, carried out by Accident Investigation Board Norway or AIBN, found that this structural failure was a result of fatigue fracture in one of the eight second stage planet gears in the main rotor gearbox. This accident resulted in the death of 13 people in total, as a result of fatigue fracture [3].

As explained throughout the introduction, fracture mechanics is an important field of study when it comes to engineering, thus much work has been done to determine the stress intensity factor for various geometries.

Many closed form solutions have been developed, but it’s not always possible to determine the closed form solution for an arbitrary geometry. This leads to the second option, which is numerical estimation, where accuracy of the method used is of high importance.

The objective of this thesis is to assess the accuracy achieved with two different methods of numerically estimating the stress intensity factor:

1. FEM – Where the crack is explicitly modelled, and singularity elements are used at the crack tip.
2. XFEM – Where the crack can grow through the elements themselves by enriching the nodes with extra degrees of freedom.

Two cracks which have an analytical solution were tested, and the results obtained numerically were compared to the analytical solutions throughout. The cracks chosen, were the slanted through thickness crack, and a curved through thickness crack. The choice of cracks, were based on presence of mixed mode loading, and the curved crack has a somewhat advanced geometry to model in FEM.

The thesis starts with a theory section, where the relevant information for the analysis is given, together with the information found in a literature study. The next part outlines the methodology used through the testing, for then to present the results obtained.

XFEM is currently limited to the use of bilinear rectangle (Q4) elements due to limitations of the software used, whereas quadratic rectangle (Q8) elements were used when FEM was applied.

The choice to perform the analysis in this manner, is from a practical perspective, rather than a "fair" perspective. If the analysis were to be performed for an arbitrary geometry using ANSYS mechanical APDL 19.2, this would be the two available options.

Chapter 2 Theory

This chapter will briefly explain the theory of linear elastic fracture mechanics, and crack propagation. Thereafter it will proceed with numerical methods which will be used, and take a look at what has been found previously, using the methods FEM and XFEM.

2.1 Stress intensity factor

The stresses near a crack tip in linear elastic fracture mechanics can be described by the following equation given in [1]:

$$\sigma_{ij} = \left(\frac{k}{\sqrt{r}}\right) f_{ij}(\theta) + \sum_{m=0}^{\infty} A_m r^{\frac{m}{2}} g_{ij}^{(m)}(\theta) \tag{1}$$

Where

σ_{ij} = Stress tensor

r = Distance from crack tip

θ = Angle in relation to crack plane

k = Constant

f_{ij} = Dimensionless function of θ in the leading term.

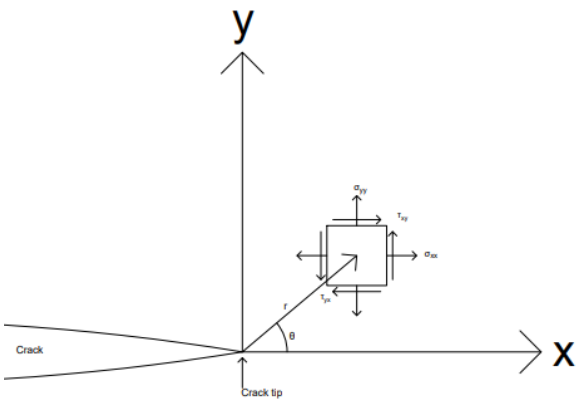

Figure 1. Definition of the polar coordinates used in equation 1.

The higher order terms (A_m and g_{ij}) will be neglected in this case, as the focus here will be the region close to the crack tip. As r approaches 0, the leading term will go towards infinity, as the other terms of the equation will approach 0. Hence, the equation near the crack tip reduces to:

$$\sigma_{ij} = \left(\frac{k}{\sqrt{r}}\right) f_{ij}(\theta) \tag{2}$$

Where the stress near the crack tip is proportional to $1/\sqrt{r}$. This leads to the introduction of the stress intensity factor, where $K = k\sqrt{2\pi}$. There are three modes of fracture, which are opening, in-plane shear, and out-of-plane shear, noted K_I, K_{II} and K_{III} respectively. In each mode of loading, the $1/\sqrt{r}$ singularity at the crack tip will be present, but the stress intensity factor and the function $f_{ij}(\theta)$ will vary for the different modes. The functions for the stress fields ahead of the crack tip can be found in [1]. The three modes of fracture can be seen in Figure 2.

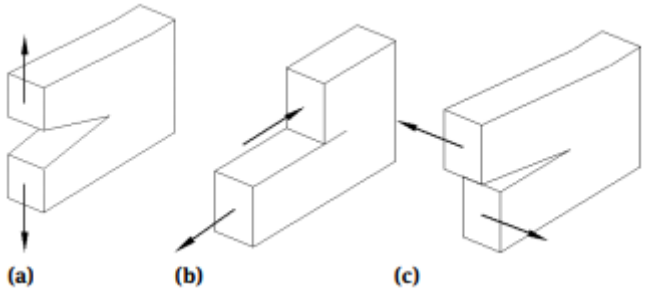

Figure 2.Three modes of fracture, (a) mode I - opening, (b) mode II - in plane shear, (c) mode III - out-of-plane shear. Found in [4] and is unmodified. CC BY-NC-ND 3.0.

2.1.1 Closed form solutions for stress intensity factors

When it comes to determining the stress intensity factors (SIFS) analytically, there are some closed form solutions. Where the required parameters to calculate the SIFS are the geometry of the crack and the remote loading. Two examples of closed form solutions are shown beneath; the slanted through thickness crack in an infinite plate, and a curved crack in an infinite plate. The reason why these will be shown, is that they will be later used in the testing Chapter 4.

SIFS for the slanted through thickness crack in an infinite plate are given by:

$$K_I = \sigma \cos^2(\beta)\sqrt{\pi a} \tag{3}$$

$$K_{II} = \sigma \sin(\beta)\cos(\beta)\sqrt{\pi a} \tag{4}$$

Where:

σ = The remote stress

β = The angle of the slanted crack.

a = Half the crack length

This formula can be found in [1] and this solution is exact according to [5]. The crack geometry can be seen in Figure 3.

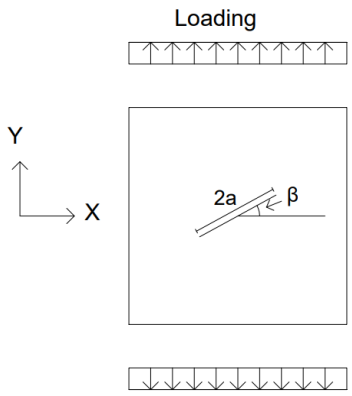

Figure 3. Slanted through thickness crack in an "infinite" plate

Another example of a closed form solution for SIFS, is the curved crack in an infinite plate. The solution can be found in [5]. SIFS are given by:

$$K_I = \frac{\sigma}{2}\sqrt{\pi R \sin\beta}\left[\frac{\left(1-\sin\left(\frac{\beta}{2}\right)\cos^2\left(\frac{\beta}{2}\right)\right)\cos\left(\frac{\beta}{2}\right)}{1+\sin^2\left(\frac{\beta}{2}\right)}+\cos\left(-\frac{3\beta}{2}\right)\right] \quad (5)$$

$$K_{II} = \frac{\sigma}{2}\sqrt{\pi R \sin\beta}\left[\frac{\left(1-sin^2\left(\frac{\beta}{2}\right)\cos^2\left(\frac{\beta}{2}\right)\right)\sin\left(\frac{\beta}{2}\right)}{1+\sin^2\left(\frac{\beta}{2}\right)}+\sin\left(-\frac{3\beta}{2}\right)\right] \quad (6)$$

Where:

σ = The remote stress

R = The radius of the circular arc

β = Half the subtended angle of the arc

This solution for the stress intensity factors is exact, according to [5]. The geometry can be seen in Figure 4.

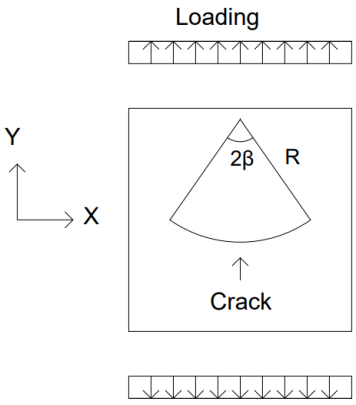

Figure 4. Curved crack in an "infinite" plate

It's not always possible to derive a closed form analytical solution for the stress intensity factor. Which leads to the use of numerical methods to estimate the SIFS, this will further be discussed in chapter 2.

2.2 Crack propagation

The stress intensity factor can be used to describe displacements and stresses near the crack tip for linear elastic fracture mechanics. But another practical use of the stress intensity factor is analysis of fatigue crack growth.

In a paper by Paris et al. [6] it was hypothesized that the propagation of a flaw in a linear elastic material could be defined by the stress intensity factor, and a relation factor between max and min, as follows.

$$\frac{\Delta a}{\Delta N} = f(K_{MAX}, \beta) \tag{7}$$

Where K_{MAX} is the maximum stress intensity factor, and $\beta = \frac{K_{MAX}}{K_{MIN}}$.

There are several proposed solutions for what a formula like this can be, where the limitations for the formulas vary. The most commonly used, is known as Paris law [1]:

$$\frac{da}{dN} = C\Delta K^m \tag{8}$$

Where C and m are material constants, that must be determined experimentally, and the parameter ΔK is the stress intensity range defined as $\Delta K = K_{max} - K_{\min}$. This formula is viable in region II, the linear section of a typical fatigue crack growth behaviour graph for metals, which can be seen in Figure 5.

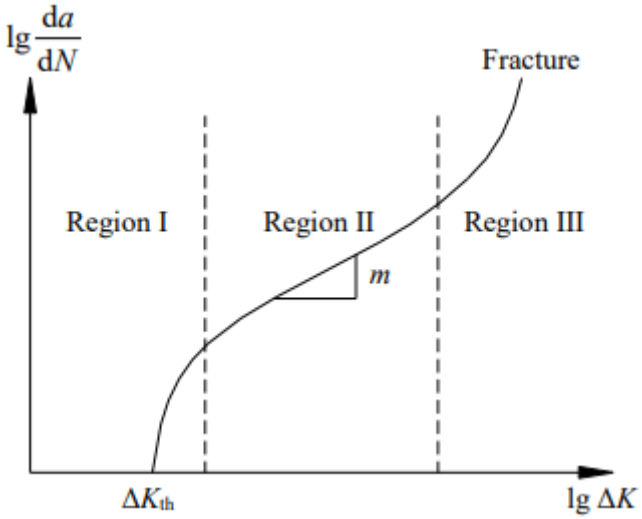

Figure 5. Typical fatigue crack growth curve. The figure was found in [7] unmodified. CC BY 3.0.

2.3 Mixed mode crack propagation

The formulas for crack propagation previously shown, are given as a function of one stress intensity mode and does not specify which direction the crack propagation will have. Several methods have been proposed to account for mixed mode crack propagation, as in finding the direction of crack

propagation, and finding a ΔK_{eqv}, ref equation 10. The methods proposed are for example, maximum circumferential stress criterion, maximum strain criterion, min strain energy density and max energy release rate [8-10].

In the publication "Quasi-automatic simulation of crack propagation for 2D LEFM problems" [8] it was found that the trajectories were very similar between the methods max circumferential stress, max energy release rate and min strain energy density, in comparison with an observed test. Which means that there are many good proposed solutions for the direction of crack growth.

2.3.1 ANSYS mechanical APDL 19.2

In the information provided in the documentation for ANSYS mechanical APDL 19.2 [11]. It can be found that when using XFEM, the crack growth simulation is restricted to region 2 of the typical fatigue crack growth behaviour graph, which can be described by equation 8.

The software does consider mixed mode loading where the maximum circumferential stress criterion is used. The function determining a ΔK_{eqv} for the crack propagation law, and the function determining the direction of the crack propagation can be seen below.

The formula for the direction of the crack propagation in ANSYS is as follows:

$$\theta = \cos^{-1}\left(\frac{3K_{II}^2 + K_I\sqrt{K_I^2 + 8K_{II}^2}}{K_I^2 + 9K_{II}^2}\right) \tag{9}$$

Where:

$K_I =$ Max mode 1 stress intensity factor during cyclic loading

$K_{II} =$ Max mode 2 stress intensity factor during cyclic loading

The formula for an equivalent range for the stress intensity factor can be found as:

$$\Delta K_{eqv} = \frac{1}{2}\cos\frac{\theta}{2}\left[\{\Delta K_I(1+\cos\theta)\} - 3\Delta K_{II}\sin\theta\right] \tag{10}$$

Where:

$\Delta K_I =$ The range of stress intensity factor in mode 1 loading

$\Delta K_{II} =$ The range of stress intensity factor in mode 2 loading

When it comes to what kind of remeshing alternatives ANSYS mechanical APDL 19.2 has, reference is made to a method called SMART. The SMART method is currently limited to 3-D mode I crack growth only [11]. Based on the implementation of crack growth in 2-D for the extended finite element, and what was found in [8], it should be possible to implement a 2-D remeshing method for ANSYS, by means of a script.

2.4 Numerical estimation of SIFS

When it comes to determining the stress intensity factor based on a numerical analysis, there are several methods proposed, both using FEM and other numerical methods. Some examples of the methods using FEM are stress extrapolation, displacement extrapolation, node displacement method

and the interaction integral method. Generally, the method which has the highest accuracy, and is able to determine K_I and K_{II} separately, is the interaction integral method [12].

2.4.1 Interaction integral method

The method which will be shown and described in this section, is the interaction integral method, as it's the one which will be used later on. This method is in principle the domain integral method, where an auxiliary field is applied to be able to separate K_I and K_{II}, as the domain integral on its own lacks this ability.

The domain integral method, which the interaction integral depends on, is the transformation of the line integral of J to a domain integral. This can be achieved by applying the divergence theorem, as shown by Shih et al. [13], where a line integral is transformed into an area integral for 2-D, and a surface integral is transformed into a volume integral for 3-D. The advantage of the transformation, is that area and volume integrals offer better accuracy, and are easier to implement numerically [7, 11].

The domain integral method is performed by first taking the J integral of the crack, for then to convert the J integral to the stress intensity factor. In the case for mixed mode stress intensity factor, it is necessary to also apply the interaction integral, to extract KI and KII separately.

The proof for the interaction integral is shown below, in case of a line integral.

The J-integral is defined as follows

$$J = \int_{\Gamma} W\, dy - T_i \frac{\partial u_i}{\partial x} ds \tag{11}$$

$$\Gamma = Arbitraty\ curve\ around\ the\ crack\ tip$$

$$W = Strain\ energy\ density$$

$$T_i = \sigma_{ij} n_j$$

$$\sigma_{ij} = Stress\ tensor$$

$$n_j = Outward\ normal\ unit\ vector$$

$$u_i = Displacement\ vector$$

$$\varepsilon_{ij} = Strain\ tensor$$

The relation between J and the stress intensity factor, in the case of linear elastic material is as follows (when K_{III} is not present)

$$J = \frac{K_I^2}{E'} + \frac{K_{II}^2}{E'} \tag{12}$$

$$E' = \begin{cases} E & for\ plane\ stress \\ \dfrac{E}{1-\nu^2} & for\ plane\ strain \end{cases} \tag{13}$$

In this situation, there is one equation and two unknowns. Hence the interaction integral must be applied to separate the two unknowns, K_I and K_{II}

The interaction integral is performed by applying an auxiliary field, which represents a pure stress intensity loading, leading to one of KI, KII and KIII being equal to 1 [14-16]. The auxiliary field, which makes one of the stress intensity factors be equal to 1, is also the SIF which will be calculated.

The principles used in the interaction integral is shown beneath.

First, the auxiliary field is applied to the actual field, where the actual field is given superindex 1, and the auxiliary field is given superindex 2.

$$\begin{cases} \sigma_{ij}^{(1,2)} = \sigma_{ij}^{(1)} + \sigma_{ij}^{(2)} \\ \varepsilon_{ij}^{(1,2)} = \varepsilon_{ij}^{(1)} + \varepsilon_{ij}^{(2)} \\ u_i^{(1,2)} = u_i^{(1)} + u_i^{(2)} \end{cases} \tag{14}$$

The J integral for the combined field is defined.

$$J^{(1,2)} = \int_{\Gamma} \frac{1}{2}\left(\sigma_{ij}^{(1)} + \sigma_{ij}^{(2)}\right)\left(\varepsilon_{ij}^{(1)} + \varepsilon_{ij}^{(2)}\right) dy - n_j\left(\sigma_{ij}^{(1)} + \sigma_{ij}^{(2)}\right)\frac{\partial(u_i^{(1)} + u_i^{(2)})}{\partial x} ds \tag{15}$$

Collecting terms, and organizing the equation lead to:

$$\begin{aligned} J^{(1,2)} = \int_{\Gamma} &\left(W^{(1)} + W^{(2)} + W^{*}\right) dy \\ &- \left[T_i^{(1)}\left(\frac{\partial u_i}{\partial x}\right)^{(1)} + T_i^{(2)}\left(\frac{\partial u_i}{\partial x}\right)^{(2)} + T_i^{(1)}\left(\frac{\partial u_i}{\partial x}\right)^{(2)} + T_i^{(2)}\left(\frac{\partial u_i}{\partial x}\right)^{(1)}\right] ds \end{aligned} \tag{16}$$

Which can also be written as:

$$J^{(1,2)} = J^{(1)} + J^{(2)} + I \tag{17}$$

Where:

$$J^{(1)} = \int_{\Gamma} W^{(1)}\, dy - \left[T_i^{(1)}\left(\frac{\partial u_i}{\partial x}\right)^{(1)}\right] ds \tag{18}$$

$$J^{(2)} = \int_{\Gamma} W^{(2)}\, dy - \left[T_i^{(2)}\left(\frac{\partial u_i}{\partial x}\right)^{(2)}\right] ds \tag{19}$$

$$I = \int_{\Gamma} W^{*}\, dy - \left[T_i^{(1)}\left(\frac{\partial u_i}{\partial x}\right)^{(2)} + T_i^{(2)}\left(\frac{\partial u_i}{\partial x}\right)^{(1)}\right] ds \tag{20}$$

In a linear elastic situation, the energy release rate can be written as

$$J^{(1,2)} = G^{(1,2)} = \frac{(K_I^{(1)} + K_I^{(2)})^2}{E'} + \frac{(K_{II}^{(1)} + K_{II}^{(2)})^2}{E'} \tag{21}$$

By expanding this equation, the result will be:

$$J^{(1,2)} = G^{(1,2)} = \frac{K_I^{(1)^2} + K_I^{(2)^2} + 2K_I^{(1)}K_I^{(2)} + K_{II}^{(1)^2} + K_{II}^{(2)^2} + 2K_{II}^{(1)}K_{II}^{(2)}}{E'} \quad (22)$$

By comparing the equation above, with the J integral equation, it can be seen that:

$$J^{(1)} = \frac{K_I^{(1)^2} + K_{II}^{(1)^2}}{E'} \quad (23)$$

$$J^{(2)} = \frac{K_I^{(2)^2} + K_{II}^{(2)^2}}{E'} \quad (24)$$

$$I = \frac{2K_I^{(1)}K_I^{(2)} + 2K_{II}^{(1)}K_{II}^{(2)}}{E'} \quad (25)$$

After having obtained this formulation, it is possible to apply an auxiliary field where either K_I or K_{II} is equal to 1, and the other would be set to 0. By doing that, it is possible to extract the other stress intensity factor by setting:

For the case where the auxiliary field leads to $K_I^{(2)}$= 1

$$I = \frac{2K_I^{(1)}K_I^{(2)}}{E'} \rightarrow K_I^{(1)} = \frac{1}{2}IE' \quad (26)$$

For the case where the auxiliary field leads to $K_{II}^{(2)}$= 1

$$I = \frac{2K_{II}^{(1)}K_{II}^{(2)}}{E'} \rightarrow K_{II}^{(1)} = \frac{1}{2}IE' \quad (27)$$

In the case of a two-dimensional analysis, it is possible to consider one of the equations, for then to obtain the other by the equation shown earlier:

$$J = \frac{K_I^2}{E'} + \frac{K_{II}^2}{E'} \quad (28)$$

Further reading about determining the auxiliary field, and the method in general can be found in [14, 15, 17].

When obtaining the SIF by a numerical evaluation, the main objective should be accuracy of the method used. In the case of numerical analysis using finite element method, the best accuracy is obtained by using the domain integral method. The argument for why the domain integral method will achieve the highest accuracy, is because it's an integral along a contour near the crack tip, which means it will be less subjected to local errors. The extrapolation methods depend heavily on correct stresses or displacements to be described by the finite element method [12].

As a curved crack will be tested later on in Section 4.3, it should be mentioned that the interaction integral is defined for a straight crack, but if contours are chosen close to the crack tip, it is still a viable option [18].

2.5 FEM and XFEM

There are two well established methods of meshing when it comes to using the finite element method for fracture mechanics. The first method is the traditional finite element method, where it is advantageous to use singularity elements near the crack tip, which will be further described in Section 2.6.2. The other method used is the extended finite element method, also called XFEM. In the extended finite element method, the nodes near the crack are enriched with extra degrees of freedom to account for the displacement jump which describes the crack.

Q4 and Q8 elements will briefly be explained in the following sections, because XFEM enrichment is currently limited to the use of Q4 elements, whereas Q8 elements will be used when FEM is applied.

2.5.1 Bilinear rectangle (Q4)

The bilinear rectangle element, also called Q4, has four nodes. Each node has two degrees of freedom. This element has a disadvantage when it comes to describing advanced stress states. For example, the element is unable to describe pure bending. In the case of pure bending applied to a Q4 element, the element will display shear strain in addition to the bending strain. The parasitic shear will absorb strain energy, also called shear locking behaviour, and hence the deformations will be underestimated. Beneath, in equations 29-33, displacement and strain functions are shown in terms of generalized degrees of freedom a_i found in [19].

The functions describing u and v for the Q4 element can be described as:

$$u = a_1 + a_2 x + a_3 y + a_4 xy \tag{29}$$

$$v = a_5 + a_6 x + a_7 y + a_8 xy \tag{30}$$

And the functions describing the strain field are:

$$\varepsilon_x = a_2 + a_4 y \tag{31}$$

$$\varepsilon_y = a_7 + a_8 x \tag{32}$$

$$\gamma_{xy} = (a_3 + a_6) + a_4 x + a_8 y \tag{33}$$

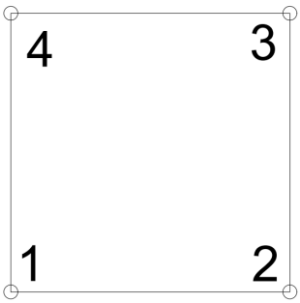

Figure 6. The bilinear rectangle Q4, with 4 nodes.

2.5.2 Quadratic rectangle (Q8)

The quadratic rectangle, also called Q8, has eight nodes. Each node has two degrees of freedom. This element is more frequently used in finite element analysis than the Q4 element, as it has the capability to describe a more advanced strain state than the Q4. For example, this element can display pure bending when it is undistorted. Beneath, in equations 34-38, the displacement and strain functions are shown in terms of generalized degrees of freedom a_i found in [19].

The functions describing u and v for the Q8 element can be described as:

$$u = a_1 + a_2x + a_3y + a_4x^2 + a_5xy + a_6y^2 + a_7x^2y + a_8xy^2 \quad (34)$$

$$v = a_9 + a_{10}x + a_{11}y + a_{12}x^2 + a_{13}xy + a_{14}y^2 + a_{15}x^2y + a_{16}xy^2 \quad (35)$$

And the functions describing the strain field are:

$$\varepsilon_x = a_2 + 2a_4x + a_5y + 2a_7xy + a_8y^2 \quad (36)$$

$$\varepsilon_y = a_{11} + a_{13}x + 2a_{14}y + a_{15}x^2 + 2a_{16}xy \quad (37)$$

$$\gamma_{xy} = (a_3 + a_{10}) + (a_5 + 2a_{12})x + (2a_6 + a_{13})y + a_7x^2 + 2(a_8 + a_{15})xy + a_{16}y^2 \quad (38)$$

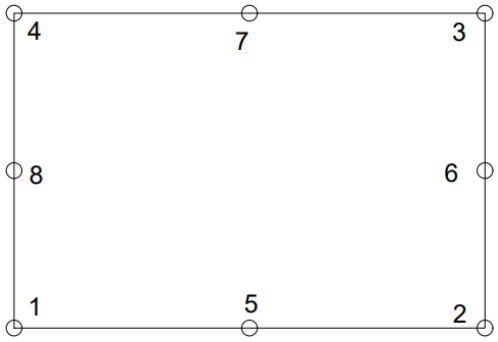

Figure 7. The quadratic rectangle (Q8) with 8 nodes.

2.5.3 Comparison of Q8 and Q4

The Q8 element has more nodes than the Q4 element, but in an example given in [19] it was shown the number of nodes required to get reasonable accuracy for a cantilever beam was significantly reduced by the use of Q8 elements. When the beam was meshed by the use of Q4 with 40 d.o.f, the displacement at the end of the beam was given as 67% of the analytical result. Whereas when the beam was meshed with the use of Q8 elements, with 20 d.o.f the displacement would be 93% of the analytical result. This shows that in an analysis, it would be advantageous to use the Q8 element over the Q4 element.

It is also noted by the functions describing the strain fields, that the Q8 element is a better element than the Q4 element. Because the Q8 element is able to describe quadratic strains, compared to the Q4 element, which is limited to linear strains.

2.6 FEM

A crack is simply a discontinuity in the material, where tensile stress cannot be transferred. The simplest method to model this is by making a small discontinuity or a 'gap' in the geometry where the crack should be, and mesh around it. If the gap is set to be very small, it will not have a significant effect on the results of the analysis.

2.6.1 Modelling of the general mesh

Beneath is an example of how to model a crack in the case of an edge crack in a plate. The nodes on the right side are connected, whereas the nodes on the left side will not be connected due to the gap introduced to the model. The main parameter governing how small this discontinuity can be, is based on the limit when the software will merge the nodes or consider them as one. It is not required to reduce it to the limits of the software to obtain good results for the analysis.

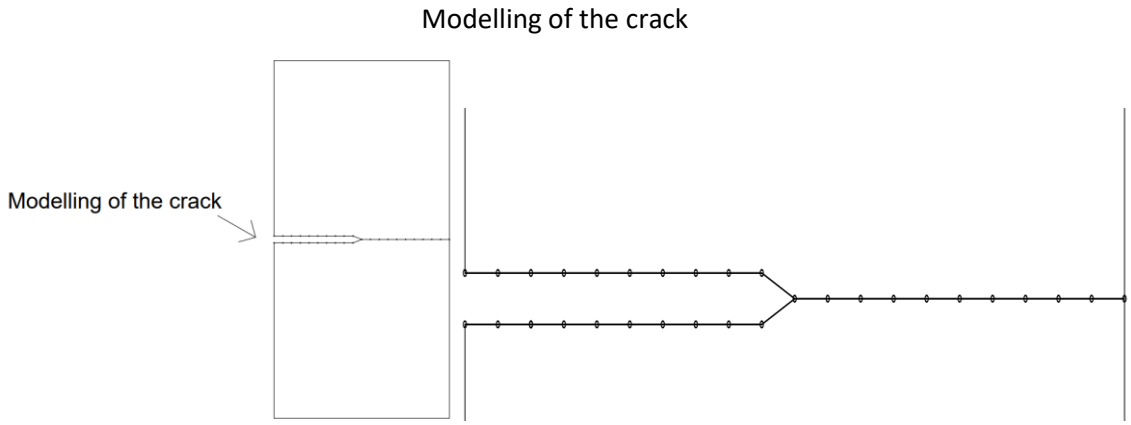

Figure 8. Example of explicitly meshing the crack using FEM.

2.6.2 Quarter point elements

Modelling a crack in ANSYS can be performed simply by using traditional elements such as Q8 or Q4, and still get a reasonable accurate result, if the domain integral method is used. Whereas if the displacement or stress extrapolations are used, the result strongly depends on the use of singularity elements at the crack tip, as shown in [12]. It is advantageous to use singularity elements because they have the capability to describe the strain singularity state which is present at the crack tip. It can also be advantageous to use this kind of elements when the domain integral method is used, as it will reduce the required mesh density near the crack tip to obtain an accurate result.

There are many examples on how a singularity element can be developed, where the most practical of the proposed methods is the quarter point element. The quarter point element is a regular isoparametric Q8 element, which is collapsed, and the side nodes are moved to a quarter point rather than being in the middle. The reason why this is the most practical is that this element is already available in most FE software, which means that it can be generated simply by specifying node locations for an element that already is in use [19]. Beneath in Figure 9 is an illustration of the described singularity element.

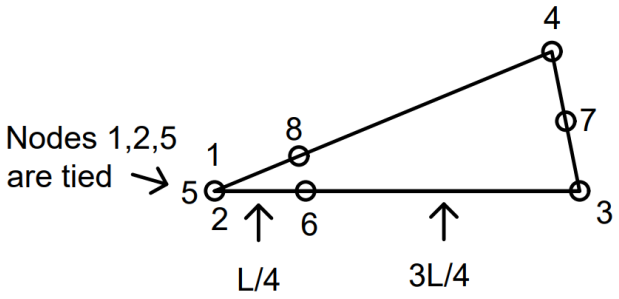

Figure 9. Collapsed isoparametric Q8 element as singularity element.

The advantage of using this element in the case of a crack tip, is that it will have a singularity at the tip and describe strains throughout with the relation $1/\sqrt{r}$. In normal finite element analysis with the absence of cracks, this is not desirable, but in the case of crack analysis it will improve the results obtained. Especially in the case where stress or displacement extrapolation is used.

The proof that the singularity will be present within the element itself was first shown by Barsoum [20] and Henshell and Shaw [21], and has been further checked in for example [22].

Some important characteristics for the element in regard to the finite element method, are explained in [19], and will be shortly mentioned here. The characteristics are that the element retains the ability to represent rigid body motion, the ability to represent constant strain state and can pass the patch test. Further reading about the element can be found in [1, 19, 20, 22]

2.6.3 Parameters of the crack tip mesh:

The singularity element has mainly two parameters which are significant to the result obtained, which are the length of the element, and the angle between the upper and lower line of the element. The angle will also be directly linked to the number of elements surrounding the crack tip.

Another parameter is the number of rows surrounding the crack tip. The additional rows of elements surrounding the crack tip will have two functions.

1. Help describe the region of high strain gradients.
2. Guarantee good paths for the interaction integral to be performed over.

The requirement for extra rows is mainly related to coarse mesh, as sufficient number of elements to describe the region of high strain gradients will typically be present in a fine mesh.

Using a fine mesh also increases the possibility of good paths to be developed through the automatic mesh generation in FE software.

2.7 XFEM

As mentioned earlier, there is a method called the extended finite element method. This method is performed by enriching the nodes near the crack region with extra degrees of freedom. Adding degrees of freedom, allows the crack to be located within an element, instead being explicitly modelled. The method also has the possibility to add a singularity field near the crack tip, the size of the singularity field must be determined by the user. A disadvantage of the method, at least in ANSYS mechanical APDL 19.2 is that XFEM enrichment is currently limited to use Q4 elements, which can be seen from the ANSYS help section [11]. The use of Q4 elements instead of Q8 elements, means that

the mesh will have more problems describing the strains within the model, which leads to the mesh requiring higher mesh density to achieve convergence. Most of the theory in the proceeding section about XFEM theory can be found in [23].

2.7.1 XFEM Theory

The general displacement function in finite element can be rewritten, as follows:

$$u^h(x) = \sum_{\forall I} N_I(x)u_I \Rightarrow u^h(x) = \sum N_I(x)\Psi(x)u_I \tag{39}$$

In the case above, the $\Psi(x)$ term can simply be equal to 1 hence, the equation is still certainly valid. The interesting part in this case, is when $\Psi(x)$ is modified to for example a discontinuity function. By adding the discontinuity function, and splitting the function into two terms, it leads to the formulation below.

$$u^h(x) = \sum_{\forall I} N_I(x)u_I + \sum_{\forall I} \varphi_I(x)\Psi(x)q_I \tag{40}$$

The first term of the function is the standard finite element displacements, and the second part is the partition of unity enrichment.

Two important notes about the function above are that:

1. The displacement field has been decomposed into the combination of u and q, which means that the displacement vectors have lost their kinematic meaning on their own.
2. In the function given above, the terms $N_I(x)$ and $\varphi(x)$ are the shape functions. They are noted differently, as it's not required that they are equal, but they are typically equal as in, $N_I(x)$= $\varphi(x)$ which will be seen in the case of application in ANSYS.

An example for a 1-D case can be a bar, which is cut at a location x_c. This example for a 1-D crack, will lack many of the interesting points when it comes to 2-D or 3-D fractures, but it is a good example, to show how the nodes are enriched.

To be able to model a strong discontinuity, the function $\Psi(x)$ should contain a strong discontinuity. This can be achieved by applying the Heaviside function, with the formulation shown beneath:

$$H(\alpha) = \begin{cases} 1, \alpha \geq 0 \\ 0, \alpha < 0 \end{cases} \tag{41}$$

To describe the crack, it is also required to have a signed distance function, also called a level set, which for this case, can be:

$$\phi(x) = x - x_C \tag{42}$$

Where x_c is the location of the fracture in the bar being considered.

Combining the equations with the equation shown under theory, leads to:

$$u^h(x) = \sum N_i(x)u_i + \Sigma N_j(x)H\big(\phi(x)\big)q_j \tag{43}$$

The function given above works well for a single element, but it will lead to an incompatibility at the shared nodes, with the neighbouring elements. To compensate for this, a method called shifting will be applied. The purpose of this is to remove the effects of q_i on the nodes. This can be done by redefining the $\Psi(x)$ function, as follows:

$$\Psi_j(x) = H\big(\phi(x)\big) - H\left(\phi\big(x_j\big)\right) \tag{44}$$

Where the displacement function would be:

$$u^h(x) = \sum N_i(x)u_i + \Sigma N_j(x)\Psi_j(x)q_j \tag{45}$$

Further explanation of XFEM for a 1-D situation will not be carried out here. Further reading and an example can be found in [23], where it's clearly shown that the conventional nodes will lose their kinematic meaning on their own, unless shifting is applied.

2.7.2 2-D XFEM theory

The two-dimensional case of XFEM works on the same principle as the one-dimensional case explained previously, but there is one important difference. In the two-dimensional case of a crack, there will be high stress gradients near the crack tip, in relation to the singularity which will occur. To deal with the gradients in the extended finite element method, enrichments can be added with the purpose of obtaining a better description of the singularity. This chapter will contain a simple explanation of the functions used, further reading in relation to this subject can be found in [23] where this theory was found.

The function for the 2-D case, for m enrichment terms is as follows.

$$u^h(x) = \sum_{\forall I} N_I(x)u_I + \sum_{j=1}^{m} \sum_{i \in I_j} \varphi_I(x)\big[\Psi^j(x) - \Psi^j(x_i)\big]q_i^j \tag{46}$$

Where I_j are the nodal subsets of the enriched nodes, Ψ^j are the corresponding enrichment functions. Note how the bracketed term here uses the principle of shifting, so that the conventional nodes retain their kinematic meaning, which was explained in the previous section.

The crack which is modelled by the use of XFEM might go through several elements, where the tip enrichment function should be applied in the near vicinity of the crack tip, and the general enrichment should be applied to the elements which the crack pass through. This can be achieved by writing the equation as follows:

$$\begin{aligned} u^h(x) = \sum_{\forall I} N_I(x)u_I + \sum_{J \in S_H} N_J(x)\left[H\big(\phi(x)\big) - H\left(\phi\big(x_J\big)\right)\right]q_J^O \\ + \sum_{j} \sum_{k \in S_c} N_k(x)\left[\Psi^{(j)}(x) - \Psi^{(j)}(x_k)\right]q_k^{(j)} \end{aligned} \tag{47}$$

This equation is for the example where $N_I = \varphi_I$ which generally tends to be the case. As seen from the function, the traditional FE equation $\sum_{\forall I} N_I(x)u_I$ is always applied. S_H contains the nodes to the elements where the crack simply passes through, and $S_C$contains the nodes of the elements where the crack tip enrichment is applied.

It can be noted that elements which are enriched will simply produce the general solution for the finite element method, if they do not have a crack. This means that it's not damaging to enrich more elements than required, but it will be at a cost of computing time.

2.7.3 Level set method

Now that the general method of XFEM is explained, the next step is how to describe the position and the shape of the crack mathematically. It is not required, but it is convenient to apply the level set method [7, 23-25]. The level set method uses two signed distance functions, where the first one is equal to 0 along the crack surface, and the sign of the function is positive and negative on opposite sides of the crack. This function alone will be able to describe the position and geometry of the crack, but it will not be able to describe where it ends. This leads to another level set function, which is orthogonal to the first level set function. The second level set function is equal to 0 at the location where the crack ends, or the crack tip.

This leads to the formula given in [25] which describes the crack:

$$\Gamma_c = \{x: \phi(x) = 0 \; and \; \gamma(x) \leq 0\} \tag{48}$$

Where $\phi(x)$ is the first level set function, which is equal to 0 along the crack surface, with opposite sign on each side of the crack surface. $\gamma(x)$ is the orthogonal level set function, which is 0 at the crack tip.

2.7.4 XFEM in ANSYS mechanical APDL 19.2

In ANSYS mechanical APDL 19.2 [11] it can be seen in the help section, that the software offers two methods. Singularity-Based Method, and Phantom-Node Method. The focus in this section will be on the Singularity-Based Method, as it's the method which is used in this thesis.

In the documentation for the Singularity-Based Method it states that the displacement function is as follows:

$$u(x) = N_I(x)u_I + H(x)N_I(x)a_I + N_I(x)\sum_j F_j(x)b_I^j \tag{49}$$

Where:

$u(x)$ = Displacement vector

$N_I(x) =$ Traditional nodal shape functions

$u_I =$ Nodal displacement vectors

$H(x) =$ Heaviside step function, which takes on values of -1 or +1 depending on which side of the crack the sampling point is located

$a_I =$ Enriched nodal d.o.f accounting for the jump in displacement

$F_j(x) =$ Crack-tip functions

$b_I^j =$ Nodal degrees of freedom accounting for the crack-tip singularity

It can also be found that the crack-tip function for a stationary crack analysis is as follows:

$$F_j(x) = \left[\sqrt{r}\sin\left(\frac{\theta}{2}\right), \sqrt{r}\cos\left(\frac{\theta}{2}\right), \sqrt{r}\sin\theta\sin\left(\frac{\theta}{2}\right), \sqrt{r}\sin\theta\cos\frac{\theta}{2}\right] \quad (50)$$

Where r and θ represents the polar coordinates, of a polar coordinate system where the origin is centred at the crack tip. In ANSYS it is possible to decide the size of this region, but if the region is set to 0, the crack tip element would still be enriched by this enrichment.

As the level set method will in practice be a local coordinate system for the crack tip, it can be found that ANSYS uses this to find r and θ, by the following formulas which can also be found in [24]:

$$r = \sqrt{\phi^2 + \psi^2} \quad (51)$$

$$\theta = \tan^{-1}\left(\frac{\Psi}{\phi}\right) \quad (52)$$

2.8 Literature study

This section contains the recommendations found for FEM and XFEM in the performed literature study. An attempt was made to find literature which specifically compares the accuracy obtained with XFEM and FEM for a given crack geometry. The result was negative, no literature was found.

2.8.1 FEM

2.8.1.1 Recommendations for the singularity element

In Cook et al. [19] the recommendations are to limit L < a/8 and the angle of the element should be between 30 and 40 degrees, where the reference for the recommendations are ANSYS. It was found that it was a previous recommendation from ANSYS, for version 17.0.

In the help section for ANSYS mechanical APDL 19.2 [11] the recommendations for how to model the crack tip is in agreement with [19] when it comes to the length of the element, which is set to the radius having a size a/8 or smaller. When it comes to the opening angle of each element, the recommendations are to have an opening of 15 to 30 degrees, to obtain reasonable results.

In a paper by Alegre et al. [10] it was concluded that 16 elements around the crack tip are enough to get a good agreement between simulation and experimental results. The paper also recommends the crack tip elements to be a/10, with the use of $a_0/10$ as the crack propagate, where a_0 is half the initial crack size before propagation. The use of 16 elements surrounding the crack tip which would mean an opening of 22,5 degrees if the crack tip opening is neglected.

In a paper by Menandro et al. [26]. It can be seen that 16 singularity elements surrounding the crack tip was used.

In a paper by Fang et al. [27], it was found that the opening angle should be between 15-20 degrees, and the singularity elements should have a radius about 0,05mm. From looking at the figures of the mesh used, it can be seen that 2 rows of elements were used.

2.8.1.2 Recommendations for the rows

There are not many clear recommendations when it comes to rows surrounding the crack tip elements. The reason might be that the elements are traditional Q8 elements, thus simply leading to a controlled refinement of the region.

2.8.2 XFEM

Conclusive recommendations for XFEM was not possible to find. One interesting finding through the literature study, is that XFEM for higher order elements should be possible. A method of how to implement the discontinuous partitions of unity, and crack tip enrichment in higher order elements was described in Stazi et al. [28]. The paper also contains numerical examples, where it's shown that the use of higher order elements with the implementation of XFEM will lead to higher accuracy with fewer nodes used.

The accuracy of the stress intensity factors shown to highly depend on selection of domain in Zhong Liang et al. [29]. The paper does not state how large the singularity region was, through the analysis performed.

Chapter 3 Methodology

The test program in this thesis includes two different crack geometries, where two methods of analysis were applied. The cracks considered are the slanted through thickness crack and a curved through thickness crack. FEM and XFEM are applied to both geometries, to compare the methods.

When the geometry is modelled in FEM, the elements used are the isoparametric Q8 elements, with the collapsed isoparametric Q8 elements around the crack tips, as explained in Section 2.6.2. ANSYS mechanical APDL 19.2 is limited to use of isoparametric Q4 elements when it comes to applying the XFEM enrichment functions, hence Q4 was used for XFEM. To compare FEM with XFEM when FEM is modelled with Q8 elements and the XFEM is modelled with Q4 elements is not necessarily fair, as the Q8 element is much better at describing advanced strain states. Nevertheless, from a practical perspective this is the comparison which can be done with the use of ANSYS mechanical APDL 19.2.

The two geometries which were tested, were initially found in [28], which are the slanted through thickness crack, and a curved crack, but the size of the plate and loading was changed. The choice of the geometries was because they both are subjected to mixed mode loading, and that a curved crack is more difficult to properly model.

The method used in both cases is briefly be explained below.

First, the analytical formulas for each crack in the case of an infinite plate was found, as these were the formulas which the numerical result would be compared to. The plate has a finite size when modelling, hence it was required to check how large the plate had to be, so that the effect of finite size would be limited. This was done by using a very refined mesh, for then to increase the size of the plate, until the solution converged. After the required size was found, the mesh was coarsened, and various changes in the meshing near the crack tip were studied.

Next step was to use the XFEM and repeat the process in reverse. This means starting from a coarse mesh for then to refine it. This was because the geometry decided upon for FEM was assumed to still be valid with XFEM.

The values used for youngs modulus and poisson's ratio are 210GPa and 0,3 respectively. The plate is modelled in millimetres, and the loading applied is a tensile stress in MPa. Plane strain was assumed throughout the testing. The desired accuracy for both methods, is to be within 0,1% deviation.

The geometries were modelled in 2-D, as it reduces the number of nodes to describe the geometry, which leads to less computational time required.

The method used for XFEM is the singularity-based method. It accounts for crack-tip singularity effects, discontinuity in displacements at the crack surfaces, and termination of cracks within an element [11].

The methodology in relation to how the mesh was generated, and parameters/definitions are shown in Sections 3.1, 3.2 and 3.3.

3.1 Universal Definitions

This section contains the definitions and descriptions which are used, for both FEM and XFEM.

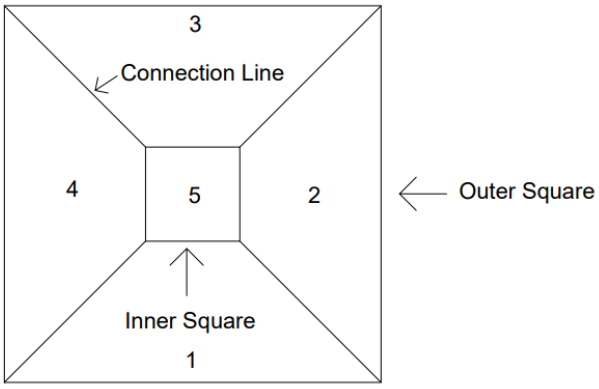

Figure 10. Illustration of how the plate was meshed as a whole.

Figure 10 illustrates how the overall mesh was generated in both FEM and XFEM. Region 1,2,3,4 were meshed using structured mesh, where the divisions for the connection lines and outer square lines would govern the mesh density in the regions. The inner and outer square line divisions were combined under one category, namely “NDIV square lines” as this was found practical for the mesh generation.

It’s mainly region 5 which differ for FEM and XFEM, because it is the region which contains the crack. Further explanation of region 5 is found in Section 3.2 for FEM and 3.3 for XFEM.

The parameters which can be adjusted for the overall geometry are as shown in Table 1:

Table 1. Parameters for the overall plate in relation to Figure 10.

Parameter	Unit/explanation
Outer square size	Millimetres x millimetres of the square
Inner square size	Millimetres x millimetres of the square
NDIV Square lines	Number of divisions used along square lines
NDIV Connection lines	Number of divisions used along the connection lines

Generally, contours 3-8 were considered throughout, with some exceptions in Section 4.1, where some other contours were considered in addition. Contours considered, means that the average value is calculated from these contours.

The domain integral, and thus the interaction integral, is performed over a domain. This means that contour 1 is the integral performed over the first element row surrounding the crack tip, for then contour 2 to be the next rows of elements. Further description of this will be shown in Section 3.2, for the application of FEM.

3.2 FEM Definitions

This section contains definitions and descriptions only used for FEM.

When FEM is applied, the geometry has to be explicitly modelled, as mentioned in 2.6. Figure 11 illustrates how a crack can be placed within region 5 in Figure 10. The two regions at the crack tips,

illustrate user specified elements. Further, region 5 is meshed by free meshing, where the input parameters are the square lines, the crack surface lines, and the outer edge lines for the user defined elements surrounding the crack tips as shown in Figure 12.

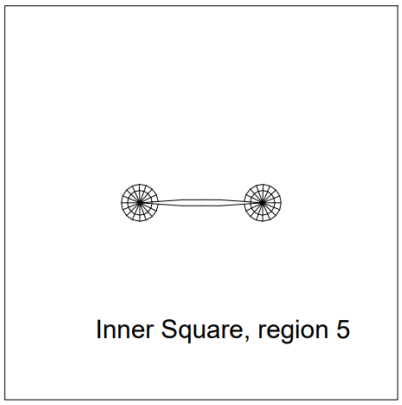

Figure 11. Inner square, region 5 for FEM

The use of singularity elements was adopted for FEM, because it was found to reduce the required refinement near the crack tip, also when the interaction integral is applied. An illustration of how the mesh is user defined near the crack tip, is shown in Figure 12. RRAT is here 0,5, as it can be seen that the CTSize is twice as large as CTSize*RRAT.

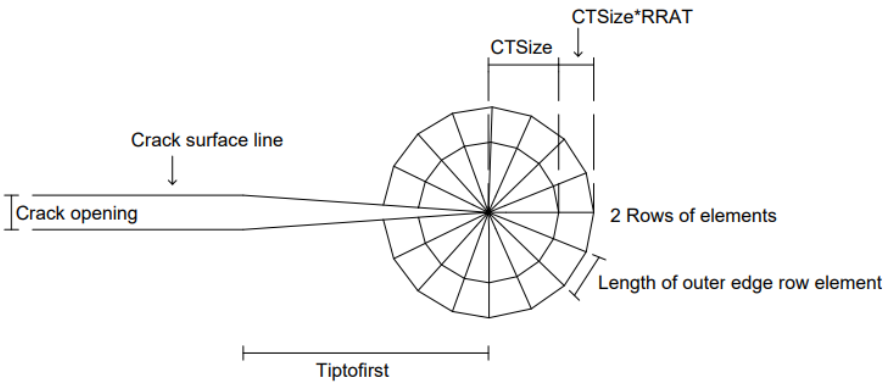

Figure 12. Illustration of refinement near crack tips.

The number of singularity elements surrounding the crack tip, was set to 16, as it was found in [10] that 16 elements around the crack tip are enough to get a good agreement between simulation and experimental results. The choice of 16 singularity elements is also in agreement with recommendations by ANSYS [11]. The singularity element, which is used, is the collapsed isoparametric Q8 element with quarter point nodes, as described in Section 2.6.2.

The parameters which were adjusted, were Crack surface line, CTSize, RRAT, rows of elements and tiptofirst. The parameters are described in Table 2 and illustrated in Figure 11

Table 2. Parameters relevant to crack tip and lines.

Parameter	Explanation
CTSize	The radial length of the crack tip elements, always as a function of a.
RRAT	Scaling factor, to determine radial length of rows of elements.
Rows of elements	Total number of rows of elements surrounding the crack tip.
NDIV crack surface lines	Defines the crack surface lines by divisions.
LESIZE crack surface lines	Defines the crack surface lines by element lengths. ANSYS will round up to the nearest integer, thus making the elements smaller than requested.
Crack opening	Maximum crack opening along the crack surface lines
tiptofirst	Distance from crack tip, till crack geometry flattens out
Length of outer edge row element	The length, as shown in Figure 12

Figure 13 shows how the refined region near the crack tip, when 4 rows of elements are used, and RRAT is set to 0,5. The rows of elements are numbered 1, 2, 3 and 4, and these are also the rows of elements that the interaction integral will be performed along. Thus, contour number 1 is the interaction integral performed along the 1st row of elements, contour number 2 would be the interaction integral performed along the 2nd row of elements.

Two methods of meshing rows are performed, these are explained in Section 3.2.1.

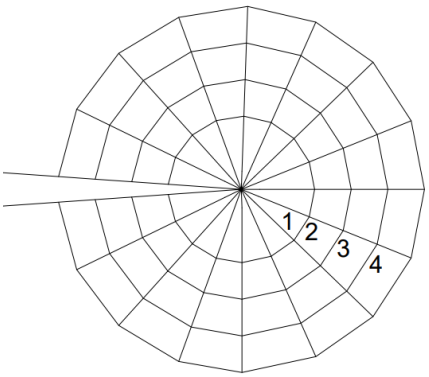

Figure 13. Illustration of contours.

The interaction integral does not depend on rows of elements defined by the user, it can integrate over rows of elements which are generated by automatic mesh generation.

The contours considered are 3-8, unless otherwise specified.

3.2.1 Rows of elements

Two methods of meshing the rows of elements were applied in this thesis.

The first method is defined here as “Traditional”. The first row of elements, which is the singularity element row, is defined by CTSize. The proceeding rows of elements, are defined by the CTSize multiplied by RRAT, as shown in Figure 12.

The second method is defined here as “New”, where the first row of element is still determined by the CTSize and is the row of singularity elements surrounding the crack tip. The difference in this method, is that the radial length for each proceeding row, is determined based on the previous row of elements. This is performed by checking the length, for one of the previous outer row elements, and using this as the radial length for the next row of elements.

The advantage with the second method, is that it will be an automatic coarsening of the mesh, as the distance to the crack tip increases.

An example of the “traditional” and “new” method of meshing rows is shown in Figure 14. The parameters used for CTSize and rows of elements are equal.

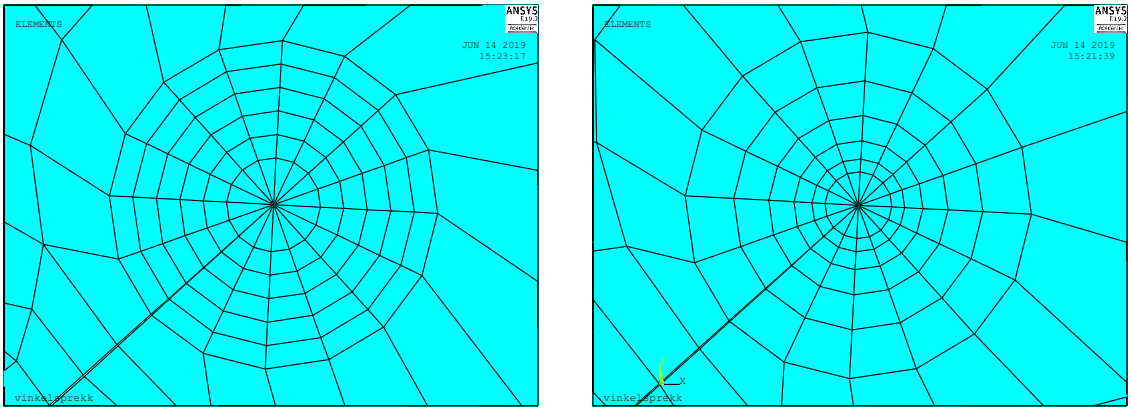

Figure 14. Illustration of “traditional” to the left, and “new” to the right, images used courtesy of ANSYS, inc. [11]

3.3 XFEM Definitions

This section contains definitions and descriptions only relevant for XFEM

Figure 15 Illustrates what the mesh would look like using XFEM, the main difference when XFEM is applied, is that the crack will grow through the mesh itself as previously described in Section 2.7.

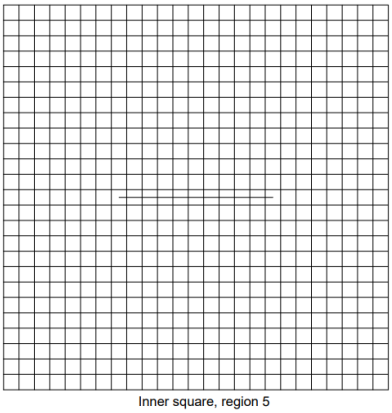

Figure 15. Inner square region 5

Figure 15 illustrates how the inner square region 5 is meshed by a structured mesh, where the parameter used is the previously defined NDIV Square lines, as it will define the mesh density.

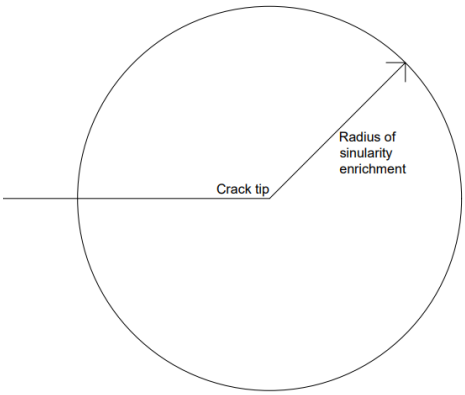

Figure 16. SING enrichment field, XFEM.

An additional parameter which is applied for XFEM, is the parameter which defines the radius of singularity enrichment.

Parameter	Explanation
SING	Defines singularity radius. The singularity enrichment function will still be applied to the crack tip element, If SING 0 is used

Chapter 4 Results

4.1 Slanted through thickness crack FEM

The first geometry considered is the slanted through thickness crack, as shown in Figure 17.

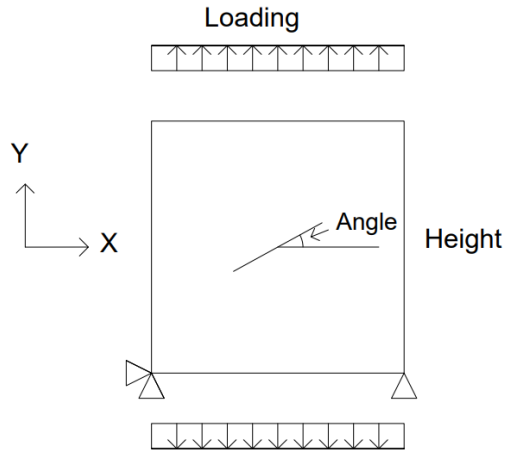

Figure 17. The geometry, with loading and restraints.

The plate is square, with the height equal to the width of the plate. The total length of the crack is 2a and the angle is defined as the angle the crack makes with the x axis, as shown in the figure. The loading applied is a tensile stress on both the upper and the lower edge of the plate. The loading is equal and opposite. The restraints are in x and y on the left side, and only in y on the right side, as shown in Figure 17. The restraints will not have a significant effect on the solution, as the plate is loaded equally from the top and bottom.

In ANSYS, the crack was plotted as coordinates, where one crack tip was located at (1, 0,9) and the other was located at (-1, -0,9) on the form (x, y). The formula to calculate the analytical solution requires the values σ, a and β.

σ is known, whereas a and β can be calculated as follows:

$$a = \sqrt{0{,}9^2 + 1^2} \approx 1{,}3454 \ldots \text{ mm}$$

$$\beta = \cos^{-1}\left(\frac{1}{a}\right) \approx 0{,}7328 \ldots \text{ rad}$$

$$\sigma = 100\ MPa$$

Now equation 3 and 4 for the stress intensity factors can be used:

$$K_I = 100 \cos^2(0{,}7328 \ldots)\sqrt{\pi * 1{,}3454 \ldots} \approx 113{,}58\ MPa\sqrt{\text{mm}}$$

$$K_{II} = 100 \sin(0{,}7328 \ldots) \cos(0{,}7328)\sqrt{\pi * 1{,}3454 \ldots} \approx 102{,}23\ MPa\sqrt{mm}$$

The calculations above were performed in MATLAB R2016b, which uses 16 significant digits throughout the calculations. The number of significant digits used throughout the testing was determined to be 5, this should be sufficient to determine an accuracy within 0,1%.

4.1.1 Plate sizing

The first objective is to determine how large the plate should be, to make size effects insignificant. The number of elements used for plate sizing, were 9040, to ensure that the mesh is more than enough refined.

Important parameters, which are kept constant for the test, are as follows:

Table 3. Initial parameters for slanted through thickness, using FEM.

Elements	9040
Rows of elements	2
CTSize	a/8
RRAT	0,5
LESIZE crack surface lines	0,0981mm
a	1,3454mm
tiptofirst	a/4
Crack opening	a/200
NDIV Square lines	40
NDIV Connection lines	40
Inner square size	10x10

Beneath is a figure where the deviations of the SIFS are plotted against the plate size.

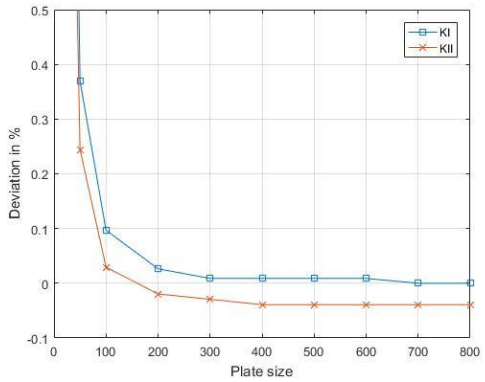

Figure 18. Plot of deviation as a function of plate size, ref Table A 2 in appendix.

From the graph, it can be seen that the effect of finite size was drastically reduced as the plate was set to 400x400, which will be used throughout the testing of this crack geometry.

4.1.2 Inner Square Size

The plate has now been determined to have an outer square size of 400x400, the next step is to determine a reasonable size of the inner square. This was first attempted by using the previously defined parameters, but the number of elements used is reduced as the inner square size gets smaller.

All the parameters are equal to the ones for the plate sizing section, except that the inner square size is now the variable, and outer square size is now kept constant; 400x400.

Beneath is a plot between Deviation of the SIFS against inner square size.

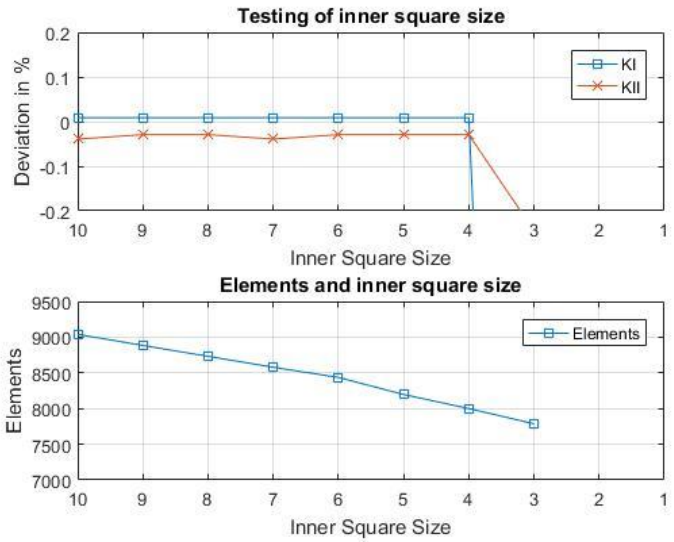

Figure 19. Plot of how the deviation change for various inner square sizes, in a fine mesh, ref Table A 3 in appendix.

From this first test, it seems like the inner square size can be very small in comparison to the crack size, and still give an accurate result. The results are nearly constant until the sudden change when the dimensions of the inner square size is set to 3x3. The difference between elements used when the inner square is 10x10 and 4x4 are 9040 and 8000 respectively, hence the number of elements has been reduced, but it's still a very fine mesh.

The reason why the 4x4 inner square size got an accurate result, was due to the high refinement of the outer region, as in regions, ref Figure 10. The outer regions of the plate are large and will not have high gradients of stresses or strains far away from the crack tip. This means it is a waste of elements and computing power to have a refined mesh throughout the plate. Hence a test matrix was proposed, with the purpose of checking the effect of a coarse mesh in the outer region, and a more refined mesh in region 5, which contains the crack. The test matrix uses 3 dimensions which are:

1. Inner square size, which are set to 4x4, 6x6, 8x8 and 10x10.
2. NDIV square lines, which are checked for 40, 30, 20, 10 and 1, with the addition of also testing the NDIV-interval from 10 to 1 for the 10x10 inner square size.
3. NDIV connection lines between the squares, which are tested for 1, 2, 3 and 4.

The complete test matrix can be found in appendix Table A 5 to Table A 8, whereas this section will focus on the result obtained with the connection lines having NDIV of 1. This means that the number of elements, in each of the 4 sections surrounding the inner square, will be equal to NDIV square lines. Increasing the NDIV along the connection lines is not considered to increase the accuracy, as long as the high gradients of strain in relation to the crack tips, are captured within the refined region.

The results obtained as various inner square sizes were coarsened by reduction of NDIV square lines, can be seen in Figure 20.

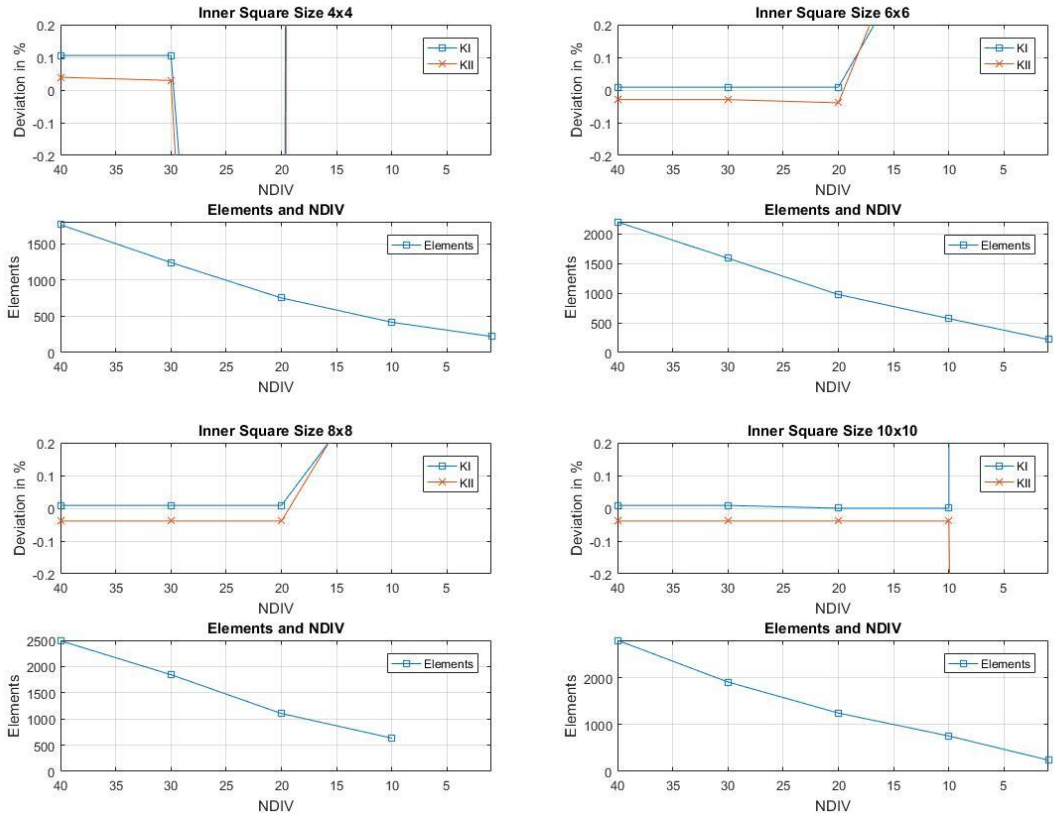

Figure 20. Plots of how the deviation varies for different inner square sizes, as they are coarsened, ref Table A 5 in appendix.

As expected, when the outer region of the plate is coarsened, the 4x4 will not achieve accuracy within the defined limit, even if the inner region is very refined. The remaining 3 options starts with an acceptable accuracy. The 6x6 and 8x8 options starts to deviate somewhere in the region between NDIV 10 and 20. The 10x10 option is still stable with NDIV 10. This leads to one more test done, to check how the 10x10 inner square performs as NDIV is reduced further, which can be seen in Figure 21.

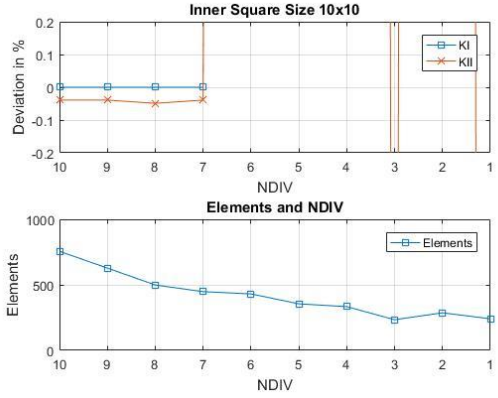

Figure 21. Plot of how the deviation changes as the inner square of size 10x10 is further coarsened, ref Table A 5 in appendix.

The plot above shows that the solution is still stable when NDIV square lines is set to 7 with a total of 448 elements used in the model as can be seen in Table A 5 in appendix.

This leads to the conclusion that the option of a 10x10 inner square size should be sufficient to capture the high stress/strain gradients, and hence give a good result.

It was also noted here that the contours considered will have a significant effect on how coarse the mesh can be. The integral requires paths of elements which it can integrated over, near the crack tip. As the mesh is coarsened, it is difficult to assure good paths for integration in the vicinity of the crack tip.

Testing was done on the accuracy of contours. The results in Table 4 shows the variation depending on different contours considered, the parameters used are as previously defined in Table 3, with the addition that the outer square size is 400x400 and inner square size is set to 10x10 with NDIV connection lines is set to having 1 division.

Table 4. Different contours considered, for plate size 400x400, inner square 10x10, and connection lines set to 1 NDIV, ref Table A 5, Table A 9 and Table A 10 in appendix.

Inner square size		10x10			
Contours	2-5				
Elements	NDIV Square lines	KI	KII	KI% ERROR	KII% ERROR
2800	40	113,58	102,1	0,00 %	-0,13 %
1909	30	113,58	102,1	0,00 %	-0,13 %
1246	20	113,58	102,11	0,00 %	-0,12 %
756	10	113,58	102,1	0,00 %	-0,13 %
241	1	107,04	103,87	-5,76 %	1,60 %
Contours	3-6				
Elements	NDIV square lines	KI	KII	KI% ERROR	KII% ERROR
2800	40	113,59	102,17	0,01 %	-0,06 %
1909	30	113,58	102,17	0,00 %	-0,06 %
1246	20	113,58	102,17	0,00 %	-0,06 %
756	10	113,58	102,16	0,00 %	-0,07 %
241	1	274,62	103,6	141,79 %	1,34 %
Contours	3-8				
Elements	NDIV Square lines	KI	KII	KI% ERROR	KII% ERROR
2800	40	113,59	102,19	0,01 %	-0,04 %
1909	30	113,59	102,19	0,01 %	-0,04 %
1246	20	113,58	102,19	0,00 %	-0,04 %
756	10	113,58	102,19	0,00 %	-0,04 %
241	1	626,94	76,49	451,98 %	-25,18 %

The results show that by using the contours 2-5, KII will be underestimated beyond the point of acceptable deviation. When the contours 3-6 are used, the result is within an acceptable limit, but deviates further than for the results achieved by 3-8. It should be noted that KI remains rather stable, whereas KII is the one which deviates, depending on contours considered. By looking at the results, it seems that the lower contours might underestimate KII. The parameters defined thus far, which will be used unless specified otherwise, is shown in Table 5.

Table 5. Defined parameters 1.

Defined parameters	
NDIV square lines	7
NDIV connection lines	1
Outer square size	400x400
Inner square size	10x10

4.1.3 Tiptofirst test

As mentioned previously in Chapter 3 methodology, tiptofirst was used as the parameter explaining when the crack tip will flatten out as shown in Figure 12. The result which was expected and shown, is that the distance does not matter significantly. When the distance is increased the crack will become sharper. As earlier mentioned, the issue that can arise with a sharp crack is in relation to the node merge command, which is used to merge the automatically generated mesh, with the user specified mesh. This command will typically have a threshold for the distance between nodes.

Other than the issue described above, the result shouldn't be too affected by the variable tiptofirst.

The first test was performed by using the previously defined parameters found in Table 5 where the lacking parameters can be found in Table 3. The only variable for this test, was the change in the parameter tiptofirst, and the results can be seen in Figure 22. The crack opening was not modified, thus making the crack sharper as tiptofirst is increased.

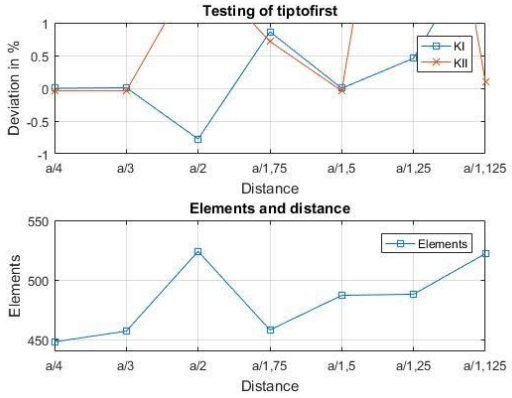

Figure 22. Plot of the results obtained for various tip to first, ref Table A 12 in appendix.

At first it seems as if the size used has a rather large effect on the result, but as this seemed unreasonable, further testing was done. The main reason why the results change so drastically in relation to this parameter could be due to how the mesh is generated in the vicinity of the crack tip. As previously mentioned, the interaction integral requires eight good paths which it can integrate over when contours 3-8 are considered.

Next part of testing was checking how adding more rows of elements can affect the result, as this will generate more good paths for the integral to be performed over. Some of the results are shown in Figure 23, for tiptofirst set as a/2, a/1,75 and a/1,125, as they had some of the highest initial deviation, which can be seen from Figure 22 above, and in Table A 12 in appendix.

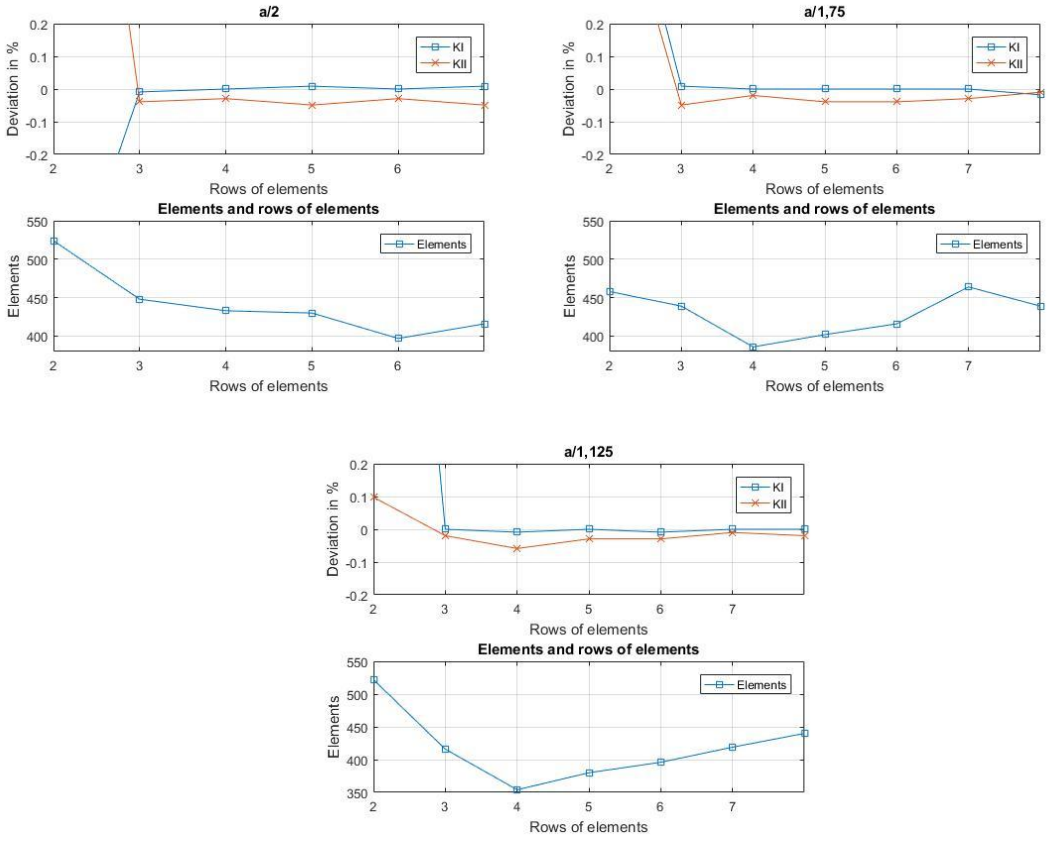

Figure 23. Plots of how various tiptofirst performs as rows of elements are added, ref Table A 13, Table A 14 and Table A 17 in appendix.

In each case, the result initially had a higher deviation than 0,1%, but the results always converged within the region of 0,1% deviation as more rows of elements were added, in the vicinity of the crack tip. Each row of elements, excluding the row consisting of singularity elements, had equal radial length, which was set to 50% of the CTSize. It was also checked that the nodes near the crack tip did not merge as the crack tip got sharper.

It can be noted that the graph of a/2 in Figure 23 stops at 7 rows of elements. This is as it was not enough room along the line before the crack flattens out to plot 8 rows of elements along it. The script used to calculate the node locations could be modified to fix this issue, but as the results showed that the parameter did not matter, it was not done.

The results shown and discussed led to the conclusion that this parameter is not of importance to the result. The only important parameters regarding the crack geometry, is that the discontinuity gap should be small, and nodes should not merge. In the further testing, the parameter tiptofirst was defined as a/1,25 simply because it's convenient to have space for many rows of elements in the current script.

Table 6. Defined parameters 2.

Defined parameters	
NDIV square lines	7
NDIV connection lines	1
Outer square size	400x400
Inner square size	10x10
Tiptofirst	a/1,25

4.1.4 Sizing of crack surface lines.

As this crack contains two crack tips and two crack surface lines, where the high stress/strain gradients are mainly located near the crack tips, it should be possible to reduce the number of elements along the crack surface lines.

This was done by changing the LESIZE crack surface lines, where the results can be seen in Figure 24.

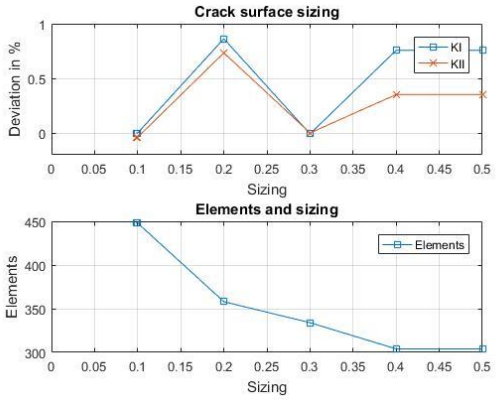

Figure 24. Plot of deviations obtained for various crack surface sizing, ref Table A 18 in appendix.

The testing was done for the initial size of 0,0981, which is equal to outer row element length, for then to be tested for 0,1, 0,2, 0,3, 0,4 and 0,5. The test was only performed with 2 rows of elements being generated near the crack tip, with CTSize a/8. Whereas the remaining paths were developed by the ANSYS mesh generation. The results show that it's not possible to significantly reduce the LESIZING of the mesh when 8 paths are required, but only 2 rows of elements were used near the crack tip.

The next section will have some relevance to this one, as the sizing of the lines between the crack tip will be determined by the length of outer edge row element in relation to the crack tip. The reason why this was chosen, was due to the assumption that higher refinement near the crack tips would lead to a lower requirement of refinement for the crack surface lines.

Table 7. Defined parameters 3.

Defined parameters	
NDIV square lines	7
NDIV connection lines	1
Outer square size	400x400
Inner square size	10x10
Tiptofirst	a/1,25
LESIZE crack surface lines	Length of outer edge row element

4.1.5 Rows and square divisions

As it was seen in Section 4.1.3, more rows of elements surrounding the crack tip leads to a more accurate result, probably due to the 8 “good paths” which are required. It was decided to do a test for rows 2-8 where the NDIV of the square lines started at 10, for then to be reduced towards 1, one step at a time, until the result diverged. Some examples from the results are shown in this section, but the full test matrix can be found in appendix, Table A 19 for traditional rows and Table A 20 for new rows.

Two methods of generating the rows were used, hence it will be separated into two sub sections, and a third sub section for a short discussion. The methods used were “traditional” and “new”, previously described in Section 3.2.1.

The singularity element size was set to a/8 throughout the testing of rows and square divisions, and RRAT was set to 0,5 when the traditional method was used.

4.1.5.1 Traditional rows

Some of the results obtained can be seen in Figure 25, where 4 plots are shown, for 2, 4, 6 and 7 rows of elements. The parameters compered are the NDIV square lines, where the number of elements used also are plotted to compare element usage and accuracy with different number of rows of elements.

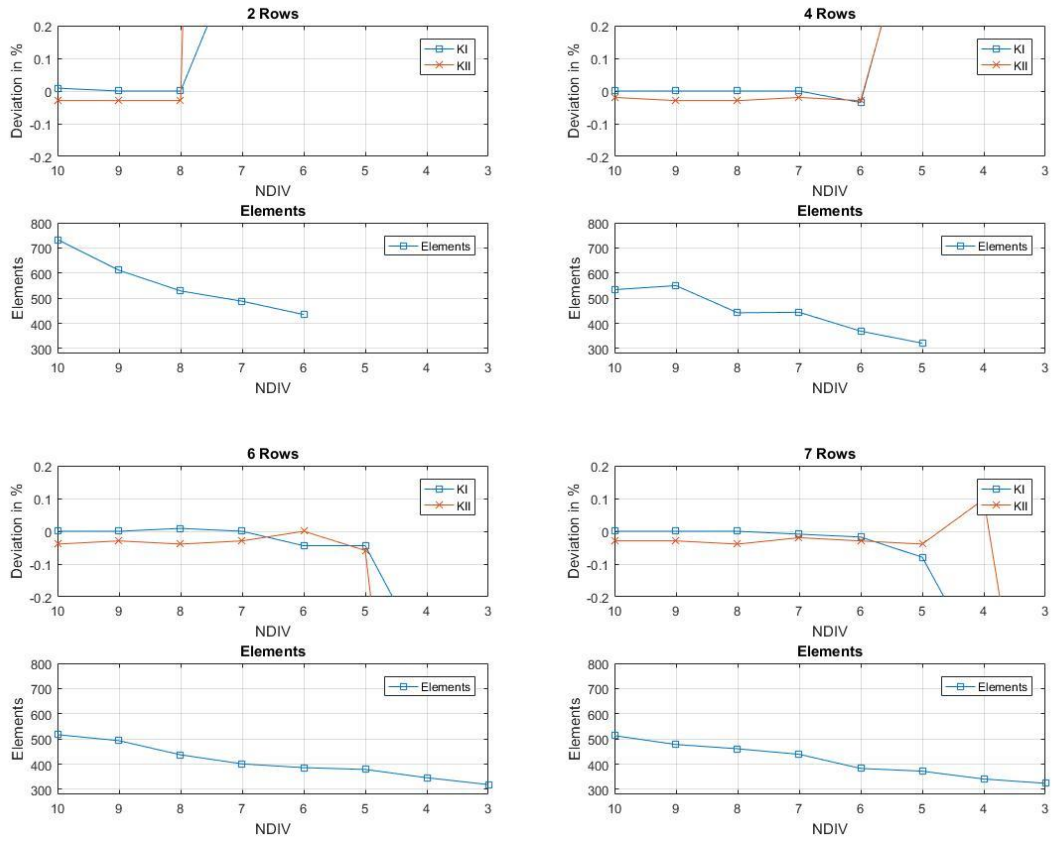

Figure 25. Plots of how square lines can be reduced further as more rows are used. Traditional, ref Table A 19 in appendix.

It can be seen from the plots that adding more rows, while reducing the number of divisions in relation to the square lines, leads to a reduction of elements used, while the deviation is kept within an acceptable level. This is very clear by comparing the graphs for 2 and 7 rows of elements. The last result within an acceptable limit as 2 rows of elements were used, was when NDIV was set to 8 with a total of 529 elements used. The last result within an acceptable limit when 7 rows of elements were used, was when NDIV was set to 5 with a total of 372 elements. The mesh near the crack tip, for the two examples mentioned, can be seen in Figure 26.

Arguments for the kept accuracy:

1. Higher refinement near the crack tip.
2. Good paths for the interaction integral are developed.

The reason for the reduction of elements for the same number of NDIV, is because the divisions of crack surface lines is determined based on the outer length, of the outer row element.

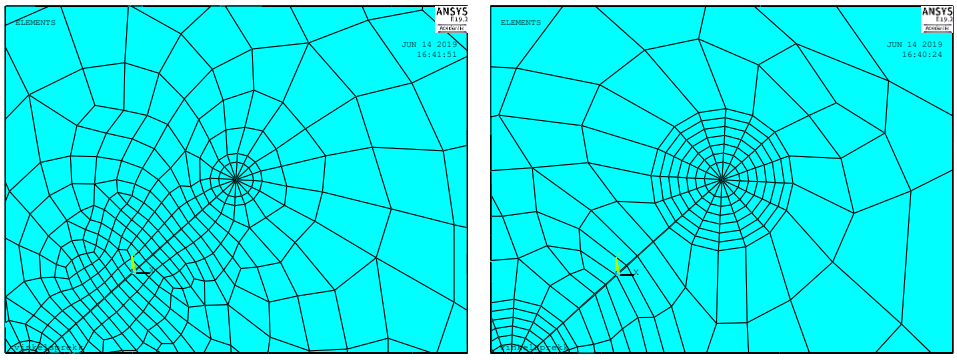

Figure 26. Example of 2 and 7 rows of elements, with NDIV square lines 8 and 5 respectively, Images used courtesy of ANSYS, Inc [11].

4.1.5.2 New rows

Some of the results obtained when the new method was used for row generation can be seen in Figure 27. The same number of rows of elements, and NDIV of square lines as the previous subsection.

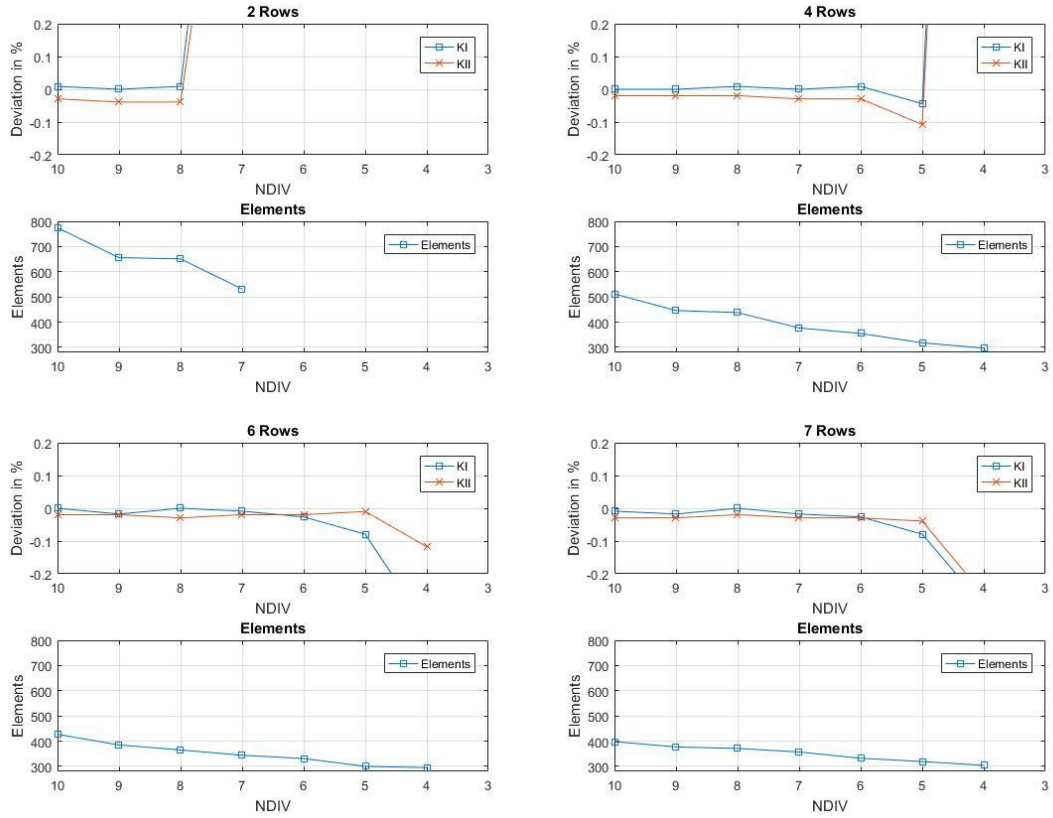

Figure 27. Plots of how square lines can be reudec further as more rows are used, ref Table A 20 in appendix.

From the plots, it can be seen that this method of meshing gives very similar results as the "traditional" method, with even further reduction of elements used.

4.1.5.3 Discussion of rows and square size.

Initially the results for 2 rows are very similar, where they fail at NDIV set to 8 where the "new" method had 651 elements, and the traditional had 529 which can be seen in Table A 19 and Table A 20 in appendix. The reason for this is because the outer edge length of the singularity element is smaller than 50% of its length, hence the second row of elements will have a shorter radial length when the "new" method is used.

As more rows are added, the benefit of the "new" method can be seen, by for example comparing the two plots for 7 rows of elements. Both of the methods fail when NDIV is set to lower than 5, but when NDIV is set to 5, the results are equal where KI miss by 0,08% and KII by 0,04%. The "traditional" method of meshing used 372 elements, whereas the "new" method used 319.

A conclusion from this section is that, increasing the user defined rows of elements surrounding the crack tip, will ensure good paths for the interaction integral. This means that the development of good paths is no longer depending on automatic mesh generation performed by ANSYS.

Adding more rows of elements is also a controlled method of refining the crack tips, which leads to the possibility of further coarsening the overall region within the inner square. This is the reduction of elements used which is seen.

4.1.6 CTSize and rows of elements.

It's been suggested that the CTSize should be equal or less than a/8 or a/10, as seen in Section 2.8.1.1. This section will use the "new" method of meshing, and compare the results obtained with various CTSize in relation to rows of elements. The form of the CTSize is always on a/n, where n is an integer going from 4-12. The divisions of the crack surface lines were determined based on the length of outer edge row element, hence as CTSize decreases, more elements will quickly be used. The square lines had a constant NDIV which was set to 7. The full test matrix can be found in Table A 21 in appendix, but the examples which are shown in Figure 28 are for n set to 4, 6, 8, 10 and 12.

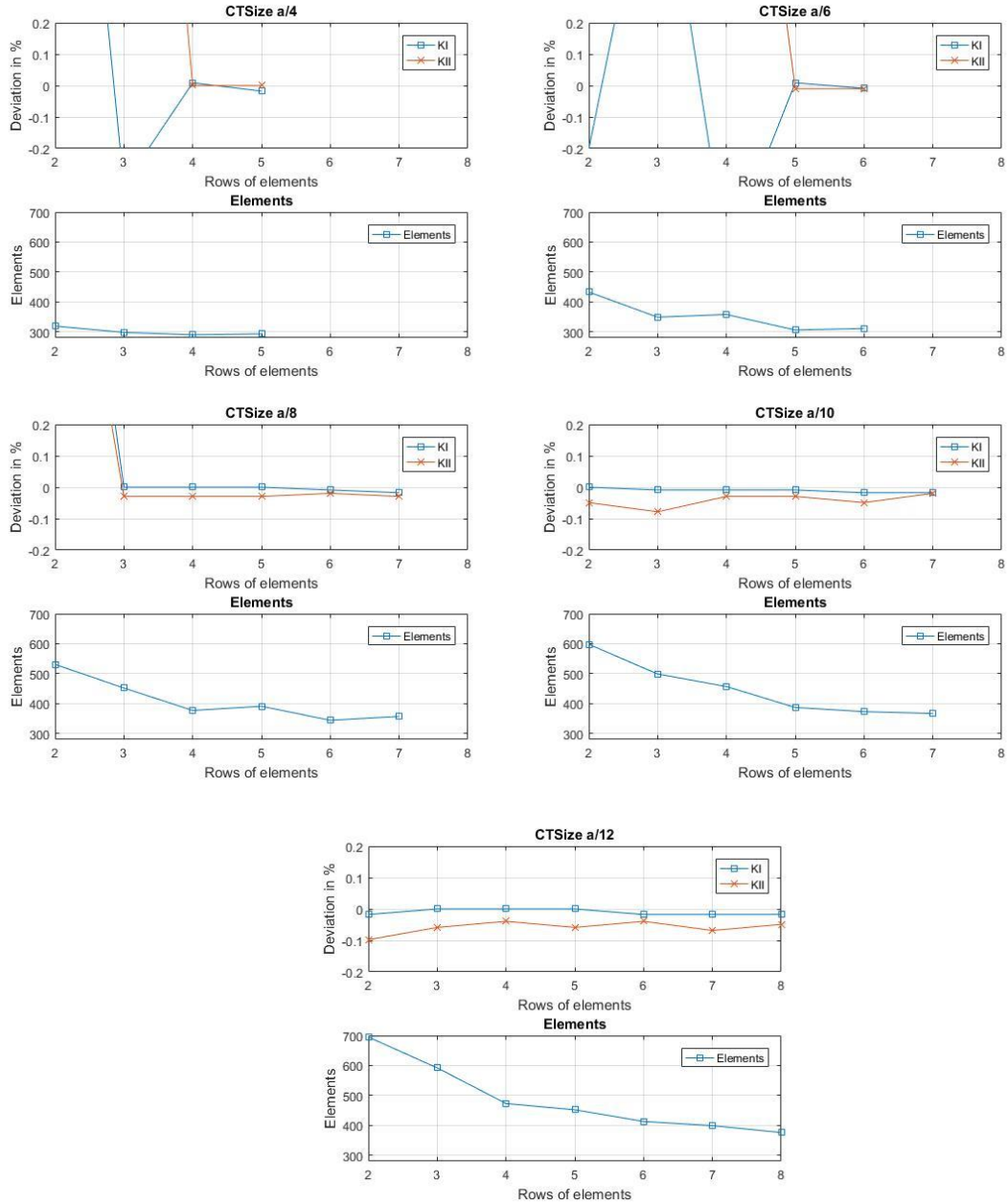

Figure 28. Plots of deviation in relation to rows of elements, for various CTSizes, ref Table A 21 in appendix.

By looking at all the plots it can be noted that when the CTSize is large, it's of high importance to add more rows of elements surrounding the singularity element row. This is most likely due to the automatic mesh generation is making the region close to the crack tip too coarse.

The results show that it's not necessarily required to have a CTSize which is a/8 or smaller. In this test, a CTsize of a/4 did also obtain good results as more rows of elements were added. In the contour study section, it is also shown that if fewer contours were to be considered, the size of the singularity zone could even be greater than what was found here.

An interesting development in this case as well, is that KII is further underestimated as the contours which were considered got closer to the crack tip. This can be clearly seen by comparing the results for a/12, a/8 and a/4 as the smaller the CTsize gets, the further KII is underestimated.

The reason why fewer rows of elements are required as the crack tip element size is reduced, is because the automatic mesh generation in ANSYS will often lead to the development of good paths surrounding the crack tip elements. The reason why this will only occur when the crack tip element is small, is because the automatic mesh generation use line size and divisions of the line in regard to the automatic mesh generation.

At this point, it was also of interest to check how KI and KII varied along the different contours, as they will not all have equal values. Figure 29 is a plot of the deviations from contours 1-8 in the case of CTSize a/4, with 4 rows of elements and a total of 290 elements used. When the average was taken for contours 3-8, the deviation was 0,01% and 0% for KI and KII respectively.

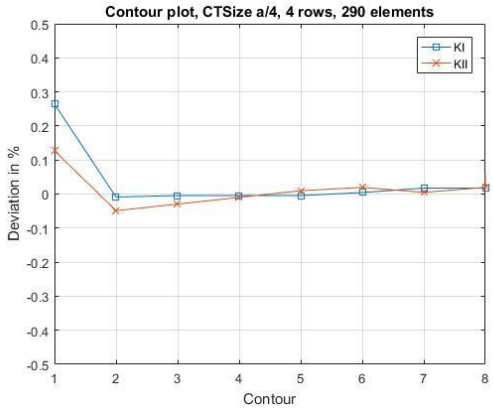

Figure 29. Plot of the deviation for various contours, for CTSize a/4 with 4 rows of elements. 290 elements in total, ref Table A 22 in appendix.

From the plot of the contours it can be seen that the first result, which is performed over the singularity elements, is overestimated for both SIFS, which is why it is generally a good practice to omit this contour. It is also noted that KI is nearly exact throughout contours 2-8, where the deviation ranges from -0,01% to 0,02%. KII starts with a deviation of -0,05% on contours 2, for then to have a deviation of 0,02% on contour 8.

4.1.7 Contour study

From the previous results, it can seem as if the solution heavily depends on how many rows of elements are used. This is indeed correct, due to the fact that the contours 3-8 are considered. Thus, another test was performed, using CTSizes a/2, a/4, a/8 and a/16, where the contours are plotted on the range -0,2% to 0,2% throughout the contours 1-12 which were checked. The reason why the

deviation was set to this limit, is to clearly show when the contours in each case will cross the ±0,1% deviation limit. The meshing method used, is the “New” method, previously described in Section 3.2.1. In all the plots in Figure 30, a total of 2 rows of elements were used, elsewhere automatic mesh generation is applied.

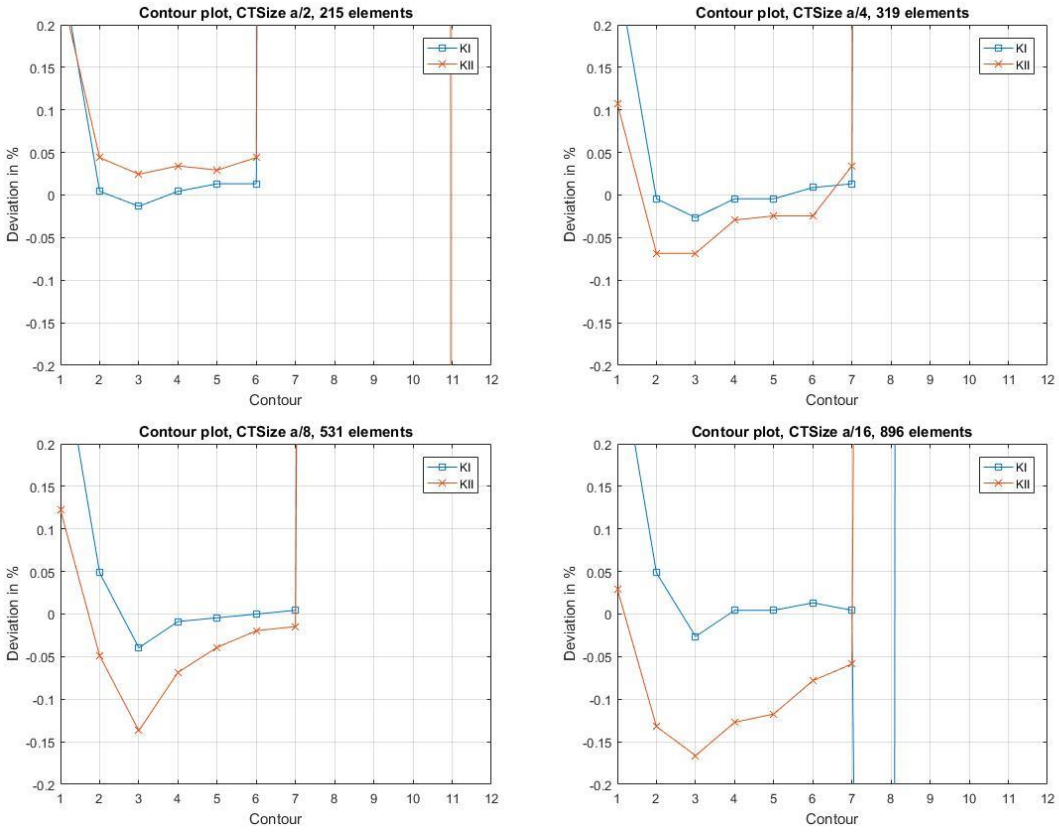

Figure 30. Plots of how the contours perform for various CTSizes. 2 rows of elements used in each test, ref Table A 23 to Table A 26 in appendix.

The first interesting observation, is that the contours 2-6 are all within the acceptable deviation of 0,1% when the CTSize is set to a/2. Further it is also seen that the contours 2-6 are mainly overestimated in this case, instead of underestimated.

The next point of interest is when CTSize is defined to be a/4. The results show that the contours for KI and KII are within an acceptable range of deviation of ±0,1% on the contours 2-7. The reason why the average of 3-8 deviated by 1,88% for KI and 3,63% for KII, as can be seen in Table A 21 in appendix, is due to the results from contour 8. It can be seen from Table A 24 in appendix, that contour 8 deviate 11,25% for KI and 21,9% for KII. When these two values are included in the average, the result will deviate. It is important to note that the addition of more rows of elements will lead to a finer mesh in the region of the crack tip, with more good paths thus making the result converge as 4 rows of elements are added, as seen in Section 4.1.6.

From the plots KII is seen to be increasingly underestimated as the CTSize is reduced. Whereas KI seems to be more stable.

As all of the results deviate by far for contour 8 and KII was further underestimated as CTSize was reduced, further testing was performed. Figure 31 displays two plots, one where the “new” method was used, and one where the “traditional” method of meshing rows was used.

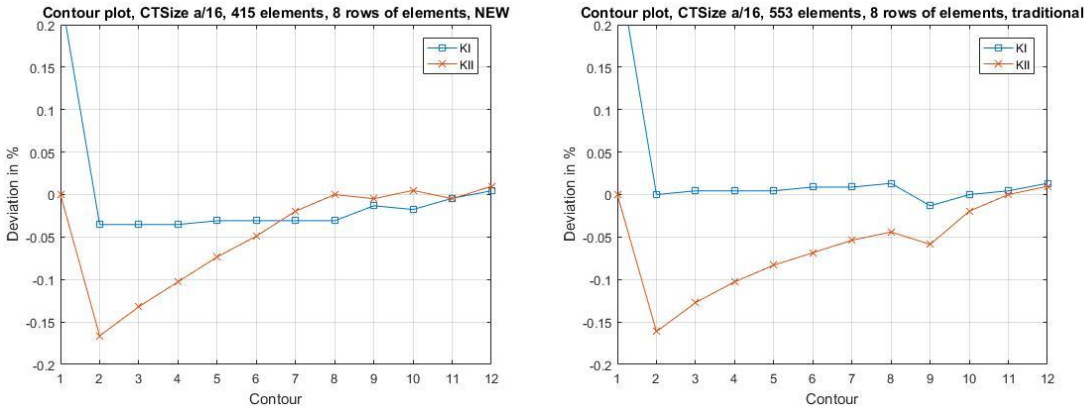

Figure 31. Plots of how the contours perform for same CTSize, with NEW and traditional meshing of rows, ref Table A 27 and Table A 28 in appendix.

The plots show that KI is within the acceptable deviation for contours 2-12, whereas KII is exact for contour 1, for then to deviate further than 0,1% on contours 2-4, and then be within the acceptable region throughout.

When the "new" method of meshing is applied, KII has higher accuracy for contours 8 to 12, whereas the results for KI are overall better for the "traditional" method.

4.1.8 Extensive refinement near the crack tip

The next section will be looking at the results obtained when CTSize initially starts at a/8 with 8 rows of elements, and the total radius of the rows of elements is 0,7568mm. The reason why the radius is now included, is that the CTSize will be divided by 2 for each step, whereas the radius will be kept so that the user defined mesh region near the crack tip will have a constant size. The radius is kept by adding more rows of elements, as the CTSize is reduced. The first case of refining the mesh in this manner will be performed using the "traditional" method, which was described in Section 3.2.1, with RRAT set to 0,5. The second example will be using the "new" method, which is somewhat different, as it's impossible to cover the exact same region.

In each case, the plotted values will be equal to the number of rows used.

4.1.8.1 Refinement near the crack tip "traditional"

The results obtained for refinement of the crack tip can be seen in Figure 32, where the results for a/8, a/16, a/32 and a/64 which had 448, 736, 1312 and 2464 elements respectively, are plotted. The refined region was kept at a total radius of 0,7568mm throughout, by the addition of more rows. RRAT was kept at 0,5 throughout, thus reducing radial length of the rows as CTSize is reduced. Further details can be found in appendix Table A 29 to Table A 32.

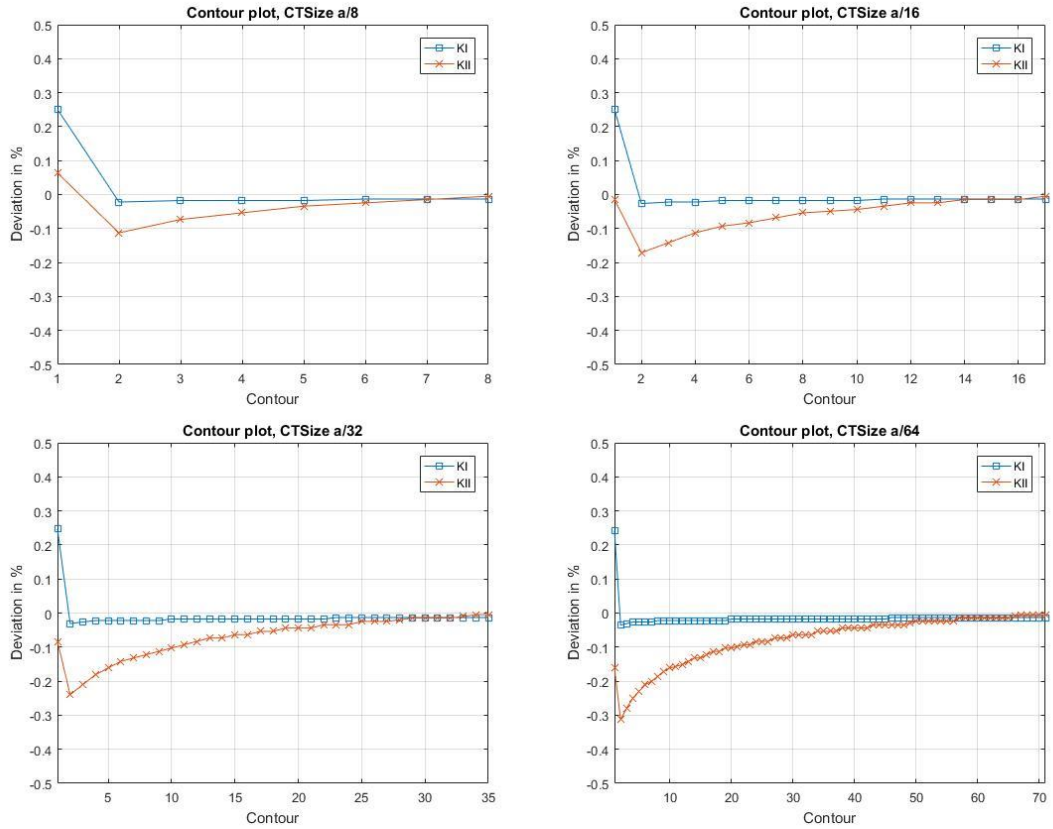

Figure 32. Plots of how the contours performs, for various initial CTSize. Refined region being constant, by adding rows of elements. Traditional rows, ref Table A 29 to Table A 32 in appendix.

From the plots, it can be seen that KI is well within the acceptable region of deviation when contour 1 is omitted. It can also be noted that KI is rather stable throughout, both in relation to refinement and contours considered.

KII is somewhat different in comparison to KI, From the first plot the result from contours 2 has a deviation of -0,11%, in comparison to -0,31% when CTSize is set to a/64. This means that as CTSize is reduced, the solution for KII diverges at contour 2. It can also be noted that the plots all have similar shape, where KII initially deviates, for then to converge towards the analytic solution, as the distance to the crack tip is increased.

For CTSize a/8, a/16, a/32 and a/64, the deviation of KII for contour number 2 is found to be -0,11%, -0,17%, -0,24%, and -0,31% respectively, whereas the last contour in every case has a deviation of 0,00%. By now looking back on how this section of the testing was performed, it can be noted that the last contour performed will always be somewhat in the same region regardless of CTSize, whereas the 2nd contour will get closer to the crack tip.

As it seems like KII starts converging towards the correct solution when the distance to the crack tip grows, an additional test was performed to check this. The test was performed with CTSize a/64, a radius of 1,0616mm and 100 rows of elements, and the result is seen in Figure 33.

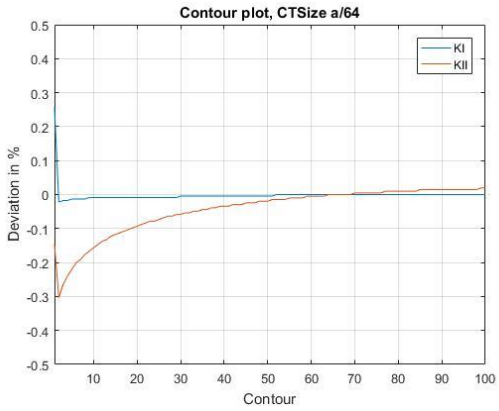

Figure 33. Plot of how the contours performs as the refined region is increased, by adding more rows of elements, ref Table A 33 in appendix.

The plot shows that KII keeps increasing as the distance to the crack tip is increased, the deviation of KII at contour 100 is 0,02%. It should be noted that all the plots show that the rate of change in regard to KII decrease as the distance to the crack tip is increased.

4.1.8.2 Refinement near the crack tip "new"

As previously stated, it is not possible to cover the exact same region, when the "new" method of making the rows of elements. This part of the testing was performed by knowing the radius of the initial test, which was set to 0,9029mm with CTSize a/4, for then to use the number of rows which led to the total radius of the refined region to be closest to the initial radius.

The test was performed ten times, where the initial CTSize was a/4, and CTSize was divided by 2 for each step. All the results can be found in appendix Table A 34 to Table A 43. The results for a/4, a/8, a/1024, a/2048, which had radius 0,9029, 0,8720, 0,9497 and 0,9172 respectively, are shown in Figure 34.

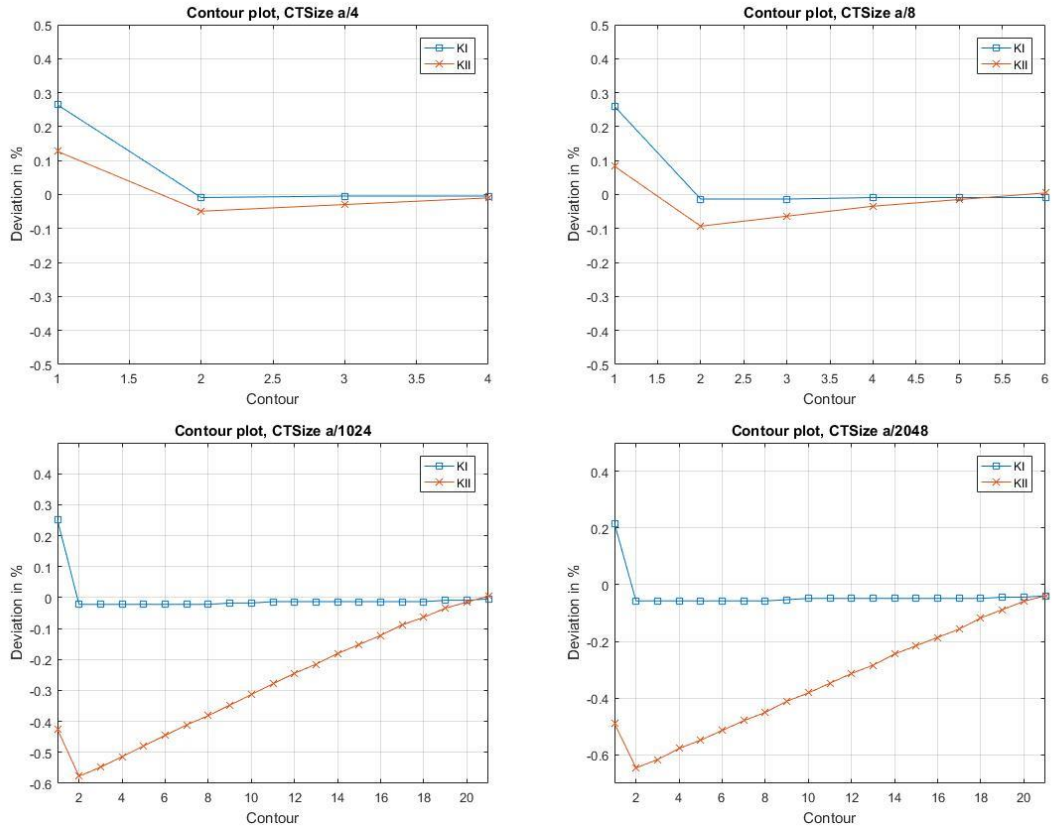

Figure 34. Plots of how the contours performs, for various initial CTSize. Refined region attempted to be constant, by adding rows of elements. Traditional rows, ref Table A 34, Table A 35, Table A 42 and Table A 43 in appendix.

CTSize a/4: This plot has 4 contours which are performed over the respective 4 rows of elements. The radius of the refined region is in this case 0,9029 and will be used as a reference to compare the other tests to. KI seems to be stable through contours 2-4, whereas KII is on a somewhat linear form.

CTSize a/8: The results are similar to the previous one, where the deviation of contour 2 for KII has increased as expected. This test was performed using a radius of 0,8720. The highest deviation of KII at contour 2 is in this case -0,09%.

CTSize a/1024: The y axis has been scaled to properly show the further reduction of KII as CTSize is decreased. The total radius of the rows is in this case 0,9833mm.

CTSize a/2048: The plot with CTSize a/2048 was added to show that a very small CTSize can still give good results for KI. KI deviates on the range -0,06% to -0,04% on the contours 2-23. The deviation of KII for contour 2 is here -0,65%.

By taking a look at the plots as a whole, it can be seen that KII deviates more for contour number 2 as it gets closer to the crack tip, which agrees with what was found in the previous tests. Similarly, as the distance from the crack tip increases, the solution converges towards the analytic solution. It should be noted that the deviation that occurs as CTSize is reduced, is a slow process as a/2048 is very small in comparison to a/4.

4.2 Slanted through thickness crack XFEM

Analysis of the slanted through thickness crack was also performed using the extended finite element method. When XFEM is used there are not as many parameters to check, as there are for FEM. This is because this method enriches the elements used, in this case Q4, instead of explicitly modelling the region in question. The geometry will still use the previously explained notation of “Connection lines and “square lines”, as this is still valid.

One new parameter in this section is the “SING” parameter, which defines the region which the singularity function will apply. The region is a circle surrounding the crack tip, with radius equal to the SING input, as shown in Figure 16.

The size of the inner and outer square found in the section for FEM will be used throughout this section as well, as the sizes are defined to reduce the finite size effect and make sure that high gradients of stress/strain are within the inner square, which is defined to be equal.

The crack is modelled into the mesh by the help of MESH200 elements, which is defined as a “mesh-only” element, and will not have any contribution to the solution obtained [11]. The MESH200 elements are used to calculate the level sets which describe the crack geometry, thus making XFEM more user friendly.

4.2.1 XFEM Q4

ANSYS mechanical APDL 19.2 is currently limited to the use of Q4 in regard to XFEM enrichment. The Q4 element will not perform as well as the Q8. To compensate for poorer performance a higher refinement was required for the outer region, namely region 1,2,3,4 in Figure 10.

4.2.1.1 Testing of refinement using only Q4 elements with SING a/8

This leads to the first test matrix, where SING is set to a/8 as this is a recommendation in regard to the singularity element size for FEM, for then to make a test matrix which increases the numbers of divisions in regard to connection lines, and square lines. The first result which is shown in Figure 35, is from testing if the connection lines still can have a division of 1, as found using FEM.

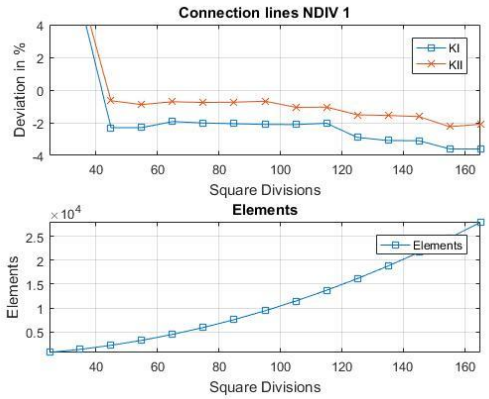

Figure 35. Plot of how the results deviate for various square line divisions, as connection lines are set to 1, ref Table B 1 in appendix.

The results obtained has a high deviation throughout where the SIFS are at first overestimated, probably due to the coarse inner region, for then to be underestimated as the inner region is further refined. The high deviations as the mesh is refined, is most likely due to the outer region being too coarse. This was expected, as the Q4 element does not perform as well as the Q8 element.

The same test was performed with connection lines NDIV set to 5, 15, 25… with further steps of 10 until it reached 75. The full test matrix can be found in Table B 1 to Table B 3.

It should be noted that as the software used is the student version of ANSYS, which means it has a limitation of nodes/elements, hence the maximum inner square divisions must be reduced as the connection lines are further refined.

The results obtained as NDIV connection lines were set to 25,35 and 55, as NDIV square lines was a variable parameter, can be seen in Figure 36.

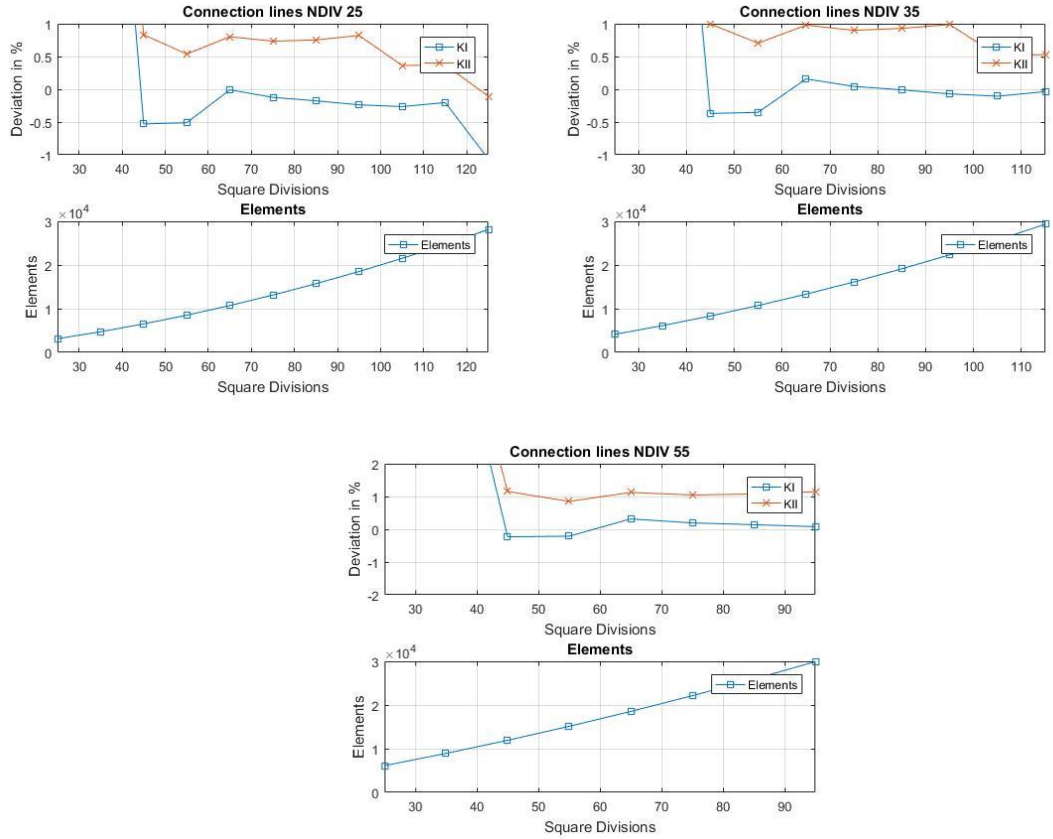

Figure 36. Plots of how the deviations, for various square divisions, for connection lines set to 25, 35 and 55. SING a/8, ref Table B 2 and Table B 3 in appendix.

When the NDIV connection lines are set to 25 and 35, it can be seen that the results are generally within 1%, when the NDIV square line divisions are on the range 45-115. Whereas for when the NDIV connection lines are set to 55, KI has a higher accuracy, and KII is slightly further overestimated.

By looking at the results shown in Figure 36, it seems as if a singularity region equal to a/8 is not necessarily giving good results, nor stabilizing the solution.

4.2.1.2 *Testing of refinement using only Q4 elements with SING 0*

The results obtained when the singularity region was set to a/8 did not seem to be very accurate or stable, as shown in Section 4.2.1.1. This led to the decision to check the results for SING 0.

For SING 0 the crack tip element will still have the singularity enrichment function. The plots in Figure 37 have the same assumptions as the plots in Figure 36, except for the SING-parameter. Comparing Figure 37 and Figure 36 gives thus a good picture of the effect of varying the SING-parameter.

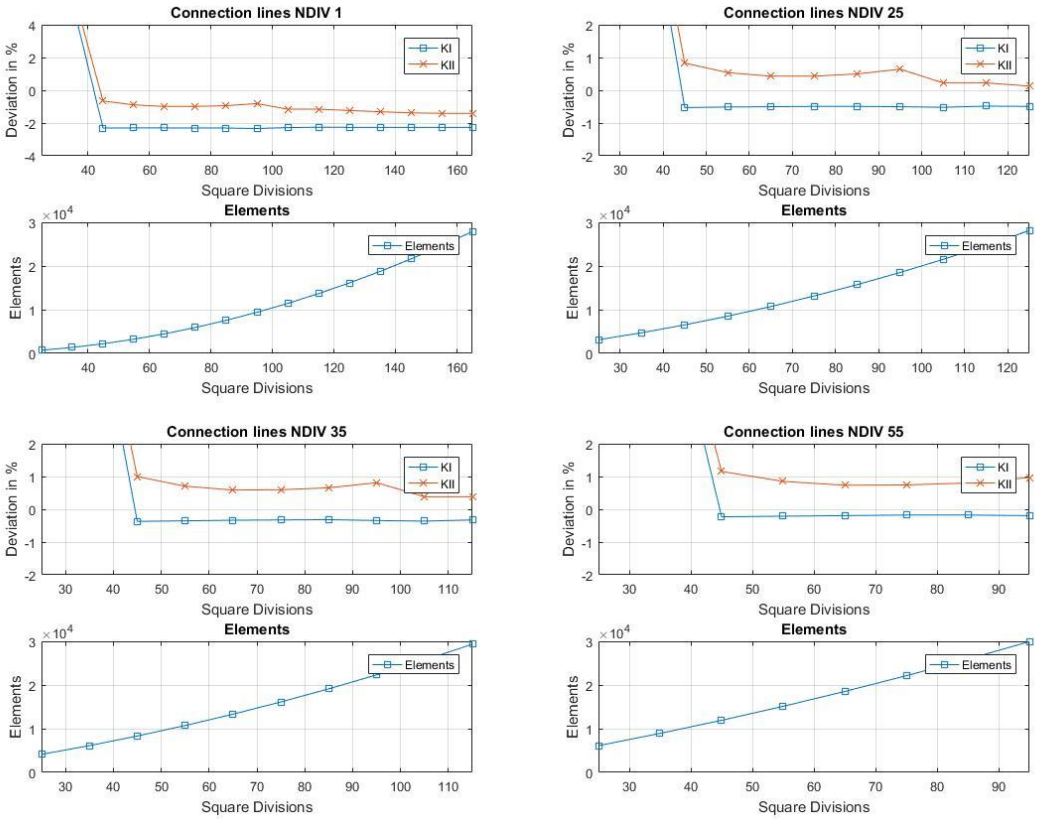

Figure 37. Plots of how the deviations, for various square divisions, for connection lines set to 1, 25, 35 and 55 with SING 0, ref Table B 4 to Table B 6 in appendix.

In this test, where the singularity enrichment function is limited to the crack tip element, the results start to look more stable throughout. Whereas for the previous section with a singularity zone equal to a/8, the results sometimes had better accuracy, but also did not seem to necessarily stabilize as the mesh was refined.

Especially by comparing the case of 55 divisions of the connection lines and 0 singularity zone, where the result for KI and KII gets within 1% deviation and is kept there as the mesh is further refined, to the case of singularity zone a/8, where the deviation of KII has higher deviation than 1% for the most part.

In the case of 35 divisions of the connection lines. The results for a singularity zone of the size a/8 leads to several of the results for KI and KII to be within 0,1% and 1% as the mesh is refined. Whereas when the singularity zone is defined to 0, the results are still within 1% deviation, but there are no results within the 0,1% limit defined earlier.

4.2.2 XFEM with Q8 elements in outer square.

As it was previously mentioned, the Q4 element does not perform as well when describing advanced strains in comparison to the Q8 element. It's also stated that Q4 elements are required in the

enriched region, for XFEM in ANSYS. This means that the outer region, ref Figure 10, can be meshed with the use of the Q8 element, and hence it's assumed that the outer region does not require refinement Beyond what was used for FEM.

In Figure 38, there are two plots where the combination of Q8 and Q4 are used, with the connection lines set to 1 division, as was performed with FEM. The difference between the plots, is that one of them use SING a/8, and the other uses SING 0.

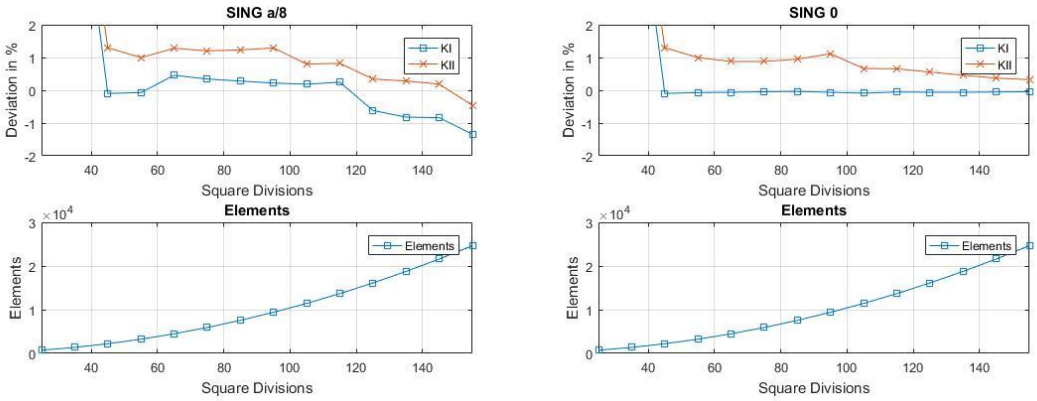

Figure 38. Plots of how refinement of the inner square, by change square divisions, for SING a/8 and SING 0, ref Table B 8 and Table B 12

The solution converges a lot better when SING 0 is used in comparison to SING a/8. It is the case where the singularity enrichment is only applied to the crack tip element which leads to a graph representing convergence. The plot where the singularity enrichment is applied, seems somewhat random.

As the singularity zone should help the result, rather than damage it, further testing was performed. The first test studied the effect of the size of the singularity region. The results, as the singularity region is reduced from a/8 is seen in Figure 39. The results were obtained for a constant mesh, which was developed with NDIV square lines set to 155 divisions, and NDIV connection lines set to 1 division.

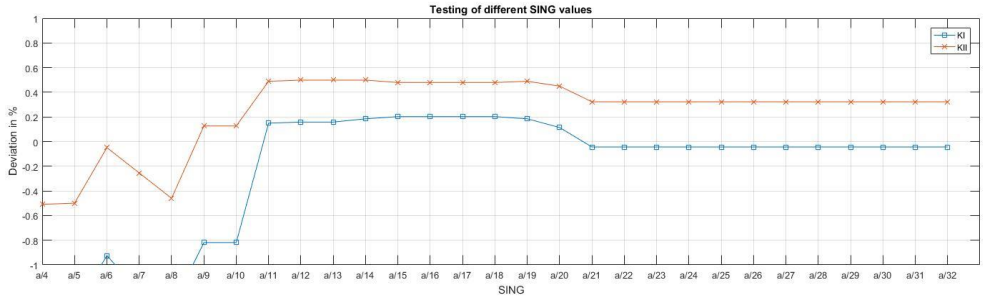

Figure 39. Plot of how the various singularity sizes, affects the solution for square line divisions set to 155, ref Table B 13 in appendix.

The constant region as a/21 is reached, is due to only the crack tip element being enriched.

Other than that, it can be seen that initially the results vary a lot, KII is within 1% deviation throughout the testing, whereas KI has a higher deviation than 1% for a/4, a/5, a/7 and a/8. This test has the highest accuracy when the singularity enrichment is only applied to the crack tip element, for all values of KI, and the highest accuracy for KII at SING a/6, where the deviation for KI is high.

As it's difficult to say something exact from just one plot, a test matrix was developed, for the steps of SING equal to 0, a/4, a/2 and a. The results are displayed in Figure 40.

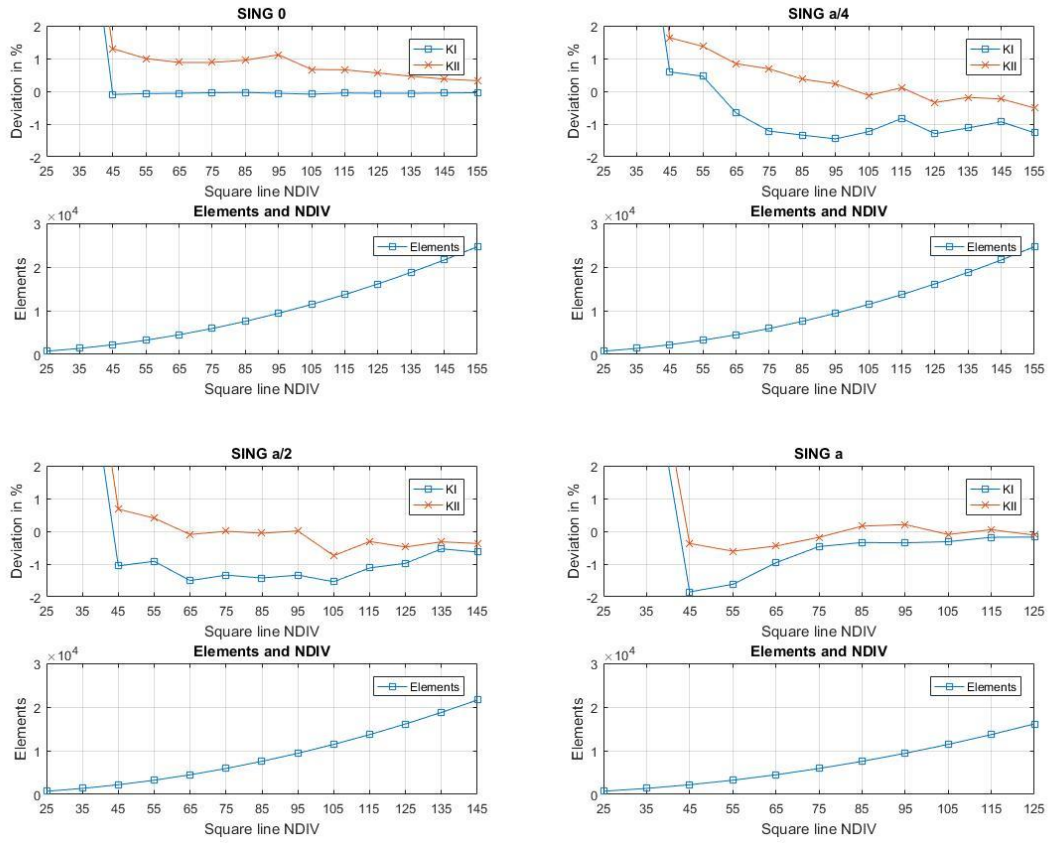

Figure 40. Plots showing the deviation as the inner square region is refined, for various singularity sizes, ref Table B 9 to Table B 12 in appendix.

The first plot where SING 0 was used, shows that KI has a rather high accuracy throughout after the square lines has reached a division of 45. KII on the other hand is overestimated throughout, but it should be noted that the results do approach the analytic solution as refinement is increased. The deviation for KI and KII as square line division is set to 155 is -0,04% and 0,32% respectively, which can be seen in Table B 12 in appendix.

From the plot where SING a/4 is used, it seems that the results are somewhat random, and the results do not necessarily approach the correct solution as the mesh is refined. The same can be said about a/2, but the results are better.

If a finite singularity zone is to be applied, the best results seem to be achieved for rather large SING-values. The case where SING = a seems somewhat random initially, but as refinement of the region is performed, the solution seems to converge towards the analytic solution. The final deviation of KI and KII were -0,18% and -0,12% respectively. The deviations for the same refinement for SING 0, were -0,06% and -0,56% for KI and KII respectively, which means a higher accuracy for KII whereas a lower accuracy for KI.

Another interesting comparison, is the fact that the last result obtained for each test, was set to limitations of nodes/elements of the software. This means that the last result obtained for each method is also a good comparison. For SING 0, the last result obtained for KI and KII were -0,04% and 0,32% respectively, whereas for SING a, the last result for KI and KII were -0,18% and -0,12% respectively, as can be seen from Table B 11 and Table B 12.

The addition of a singularity field generally seems to worsen the value of KI but improve the accuracy of KII. The results obtained, show that the addition of a singularity field, should either be large, such as SING a, or just be applied to the crack tip element, as in SING 0.

4.2.2.1 Checking of contours

It was seen that the deviation of the SIFS were initially increased when the singularity function was added, which leads to a question about how the plot of the contours looks as the singularity enrichment is added. The mesh chosen to consider is the one developed with square line divisions set to 125, as this limits the variable to the size of the singularity enrichment region. In every test, 20 contours were performed.

The first plot which is shown in Figure 41, is a plot where the singularity enrichment function is only applied to the crack tip element.

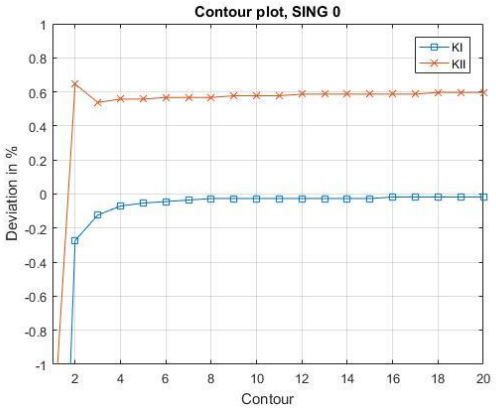

Figure 41. Plot of how the contours deviate, when the singularity region is set to 0, square line divisions set to 125, ref Table B 14 in appendix.

By looking on the plot for SING 0, it can be seen that the contours in the region 3 to 20 are all overestimated for KII and very accurate for KI. The final results for KI and KII deviated -0,02% and 0,6% respectively. The contour plots for SING a/8, a/4, a/2 and a can be seen in Figure 42.

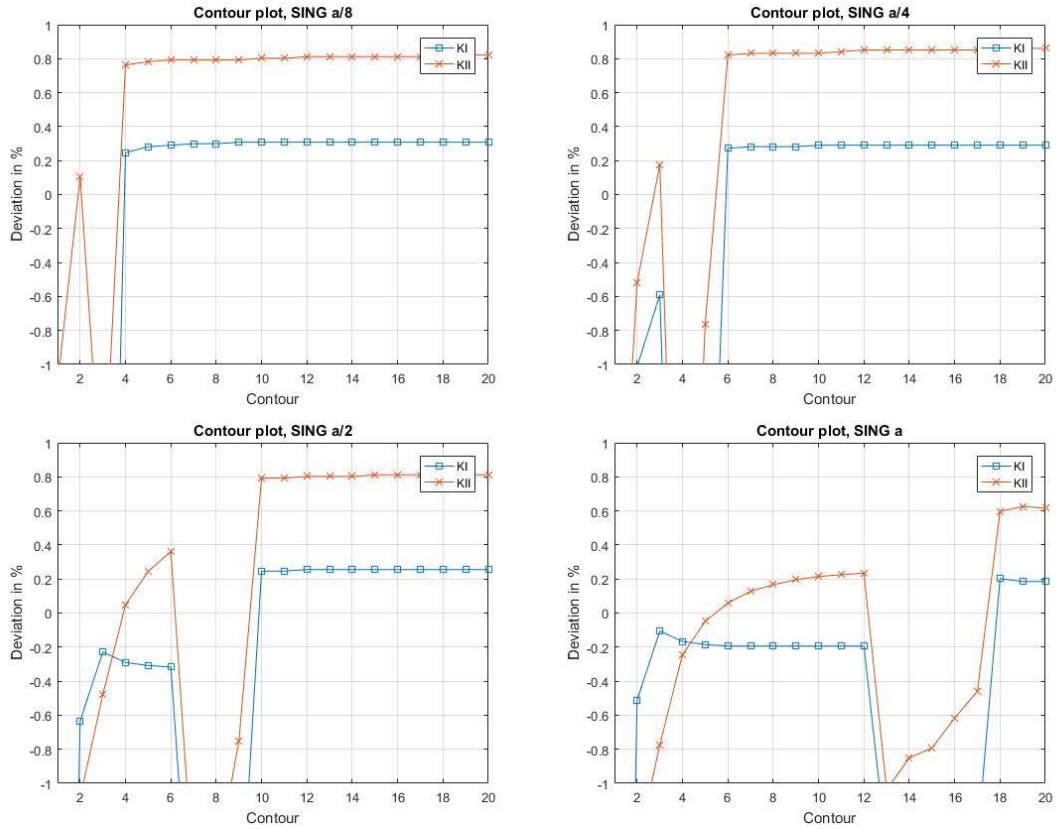

Figure 42. Plot of how the contours deviate, for various singularity sizes, and square line divisions set to 125, ref Table B 15 to Table B 18 in appendix.

From the plots, it seems that the best results are obtained from using a singularity zone equal to “a”. The only plot which represents some kind of convergence before the sudden change in deviation, is the plot of the results obtained with a singularity enriched region equal to “a”. It should also be noted that the constant region after the sudden change in deviation was worsened for KI and KII for all the results, except the results obtained with the singularity enrichment region set to a.

If more elements were to be used, there would be more contours performed within the singularity enriched region for each case, but there are a lot of elements used to obtain the results shown in Figure 42. The number of elements used in the inner square region is a total of 15625 elements.

4.3 Curved crack FEM

The second geometry is a curved through thickness crack in an infinite plate, as shown in Figure 43.

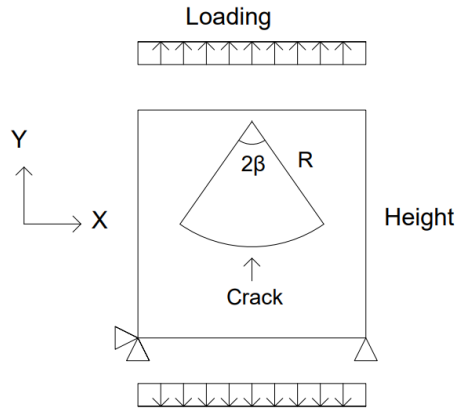

Figure 43. The geometry used for the curved crack, with loading and restraints.

The loading and restraints of the model are the same as for the previous geometry, but the parameters regarding the crack has changed, as can be seen in Figure 43. The parameters governing the geometry in this case, are R, β and the tensile stress applied. The curved crack can be seen as a section of a full circle, where R is the radius to the circle centre and 2β is the subtended angle of the arc, which is illustrated in Figure 44.

In ANSYS, the crack was plotted by coordinates, where one crack tip was located at (2, 0) and the other was located at (-2, 0) on the form (x, y). As this is an arc, it also requires a third point, to determine the curvature, which were set to (0,-0,49) for the upper crack surface line and (0,-51) for the lower crack surface line, where the middle is (0, -0,5).

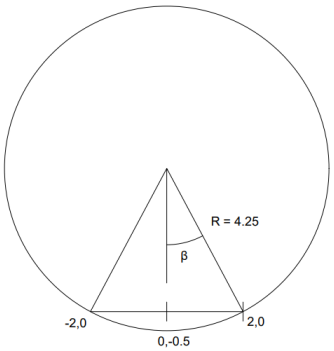

Figure 44.Display of how the curved crack should be considered.

Figure 44 illustrates the geometry of the crack. The crack itself is the section of the arc which goes through the three points (2, 0), (0, -0,5) and (-2, 0), where the radius is shown and β can be calculated.

$$\beta = \sin^{-1}\left(\frac{2}{4{,}25}\right) rad$$

$$\sigma = 100\ MPa$$

$$R = 4{,}25\ mm$$

The analytical calculations of the SIFS follow equations 5 and 6, and the numerical values are:

$$K_I \approx 201{,}46\ MPa\sqrt{mm}$$

$$K_{II} \approx 111{,}16\ MPa\sqrt{mm}$$

The calculations were performed in MATLAB, with 16 significant digits, for then to be rounded to 5 significant digits.

The meshing of the geometry is explained in Chapter 3, where the parameter "tiptofirst" has been removed, as it was found unnecessary in Section 4.1.3. The crack opens gradually from the crack tips, to the total crack opening, which was set constant to 0,02mm.

4.3.1 Start curved crack

The procedure is the same as for the slanted through thickness crack, first develop an accurate result, for then to coarsen the mesh and check parameters. The initial parameters are based on experience from the previous crack in Section 4.1 , and can be found in Table 8.

Table 8. Initial parameters used.

CTSize	a/8
LESIZE crack surface lines	Length of outer edge row element
NDIV connection line	40
NDIV square line	40
Outer square size	400x400
Inner square size	10x10
Crack opening	0,02mm
elements	8438
RRAT	0,5
Rows of elements	2

The results obtained with these parameters, had higher deviation than 0,1% in regard to the analytic solution. The results for KI and KII were 200,56 $MPa\sqrt{mm}$ and 114,55 $MPa\sqrt{mm}$ respectively, as can be seen in Table C 3 in appendix. This leads to a plot of contours to check how they perform throughout, as this was found to give insight to why the result fails, in Section 4.1 for the previous geometry. The plot obtained is shown in Figure 45.

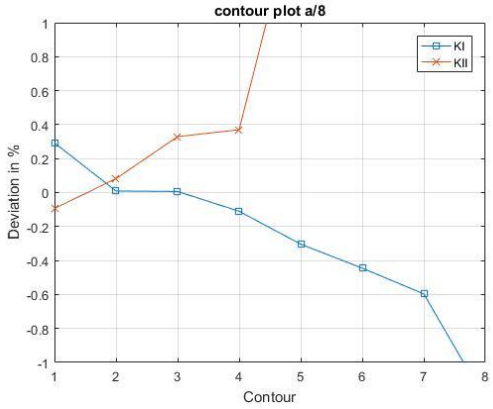

Figure 45. Plot of how the contours deviate for the initial parameters, ref Table C 2in appendix.

As can be seen in Figure 45, the results for contour 2 is rather accurate in comparison to the analytic solution, whereas the following contours quickly deviate further. This can be due to a too large initial CTSize, and that the region being considered is too far away from the crack tip. It was stated in Section 2.4.1 that the interaction integral is just defined for a straight crack, thus requiring contours to be close to the crack tip.

4.3.2 CTSize

As contour number 2 was found to be in good agreement with the analytical solution, it was assumed that size effects shouldn't be the cause of the high deviation. Thus, the next test was performed by reducing the CTSize, and the results can be seen in Figure 46.

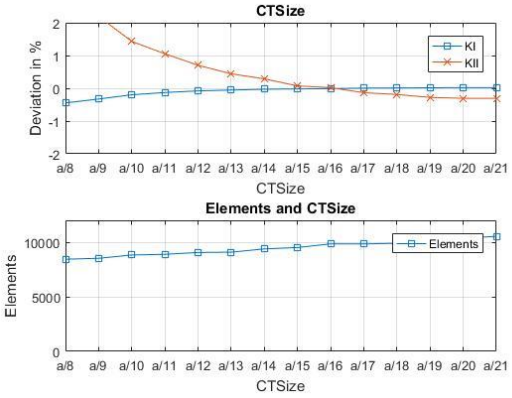

Figure 46. Plot of how the result deviate for various CTSizes, ref Table C 3 in appendix.

As the CTSize is reduced, the crack surface lines are refined, because the size of the elements along the crack is determined by the outer row edge element. This leads to the meshing being further refined as a whole.

The results show that refinement of the CTSize leads to a higher accuracy. The deviation of KI and KII for CTSize a/16 were -0,01% and 0,02% respectively, whereas the results as CTSize was set to a/21, the results for KI and KII were 0,02% and -0,31% respectively, which led to the choice of using a/16. It can be noted that the accuracy of KI has not differed much between CTSize a/16 and a/21, whereas KII is further underestimated. The deviations obtained for various CTSizes can be found in Table C 21 in appendix.

As the results seemed to be best at the region where CTSize was set to a/16, and KII deviated further as CTSize was set to a/21, two contour plots were developed one for each of the two CTSizes, as can be seen in Figure 47.

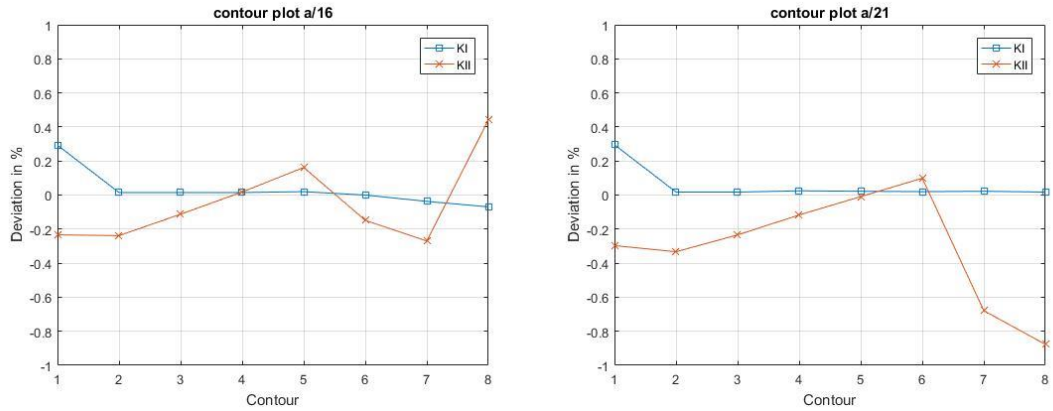

Figure 47. Plot of how the contours deviate for CTSize a/16 and a/21.

From the contours, it can be seen why the contour plot a/16 has a higher accuracy in regard to KII than for a/21. KI is more stable for the case of CTSize a/21, but it is rather stable for both cases. The sudden drop in KII, especially in the case of a/21, could be due to unfortunate paths for the interaction integral, which is checked in Section 4.3.5 where more rows of elements are added.

An extra test performed in this case of a curved crack, to decide if the first row of elements should also follow the arch of the crack, or if it should point in the initial direction of the arch. This was done by comparing the results obtained as the CTSize was reduced and see how they differed, ref Table 9.

Table 9. Results obtained, for when the crack tip elements follow the arch, and for when it is set to initial direction, ref Table C 3 and Table C 6 in appendix.

	Initial direction		Following arch	
CTSize	KI%	KII%	KI%	KII%
a/8	-0,45 %	3,06 %	-0,45 %	3,05 %
a/9	-0,32 %	2,20 %	-0,33 %	2,20 %
a/10	-0,18 %	1,46 %	-0,20 %	1,43 %
a/11	-0,13 %	1,05 %	-0,13 %	1,05 %
a/12	-0,08 %	0,71 %	-0,08 %	0,70 %
a/13	-0,05 %	0,44 %	-0,05 %	0,44 %
a/14	-0,03 %	0,29 %	-0,03 %	0,29 %
a/15	-0,02 %	0,07 %	-0,02 %	0,07 %
a/16	-0,01 %	0,02 %	-0,01 %	0,02 %
a/17	0,00 %	-0,13 %	0,00 %	-0,13 %
a/18	0,01 %	-0,19 %	0,01 %	-0,19 %
a/19	0,01 %	-0,28 %	0,01 %	-0,28 %
a/20	0,02 %	-0,31 %	0,02 %	-0,31 %
a/21	0,02 %	-0,31 %	0,02 %	-0,31 %

The results obtained are rather similar, especially as CTSize is refined. As it's practical to decide upon one of the methods, it was decided that the singularity elements should follow the arch, which was

used throughout the testing of this geometry. Throughout the testing, it's just the corner nodes that follow the arch for the row elements, the side nodes are located linearly between the corner nodes. This is because it is a known fact that when elements are further distorted, they generally perform worse.

4.3.3 Outer and inner Square sizing

As this crack is larger, and has a different shape than the previous one, size testing for the outer square size was performed. The reason why it's first performed now, is because the initial result obtained with the parameters shown in Table 8, deviated too much to be from the effect of finite size.

The parameters used for the outer and inner square size testing are seen in Table 10:

Table 10. Used parameters for outer square size testing.

CTSize	a/16
RRAT	0,5
Rows	traditional
Rows of elements	2
NDIV square lines	40
NDIV connection lines	40

The tests performed were first having the entire region as a refined mesh, which can be seen from the table above, the NDIV for square lines and connection lines are set to 40.

The initial outer square size tested was 400x400, as this functioned well for the previous geometry in Section 4.1. It was expected that the outer square size should be increased, as this crack covers a larger region along the x axis and is larger in general. The sizes which were tested was 400x400 going to 1000x1000 where the step size was 100, and the results can be seen in Figure 48.

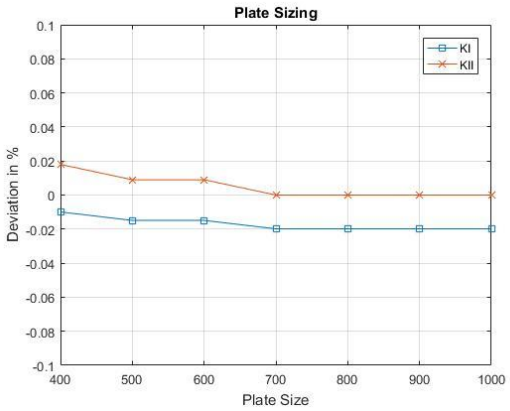

Figure 48. Plot of how the deviations vary for different plate sizes, with connection lines set to 40, ref Table C 8 in appendix.

The outer square size test shows that as the outer square size is set to 700x700, it will not have a further effect on the solution.

The next step performed, was the coarsening of the outer region. The first test performed in this relation was to reduce the divisions of the connection lines down to having 1 division, as seen from the analysis of a slanted through thickness crack. The results obtained as NDIV connection lines were set to 1 can be seen in Figure 49.

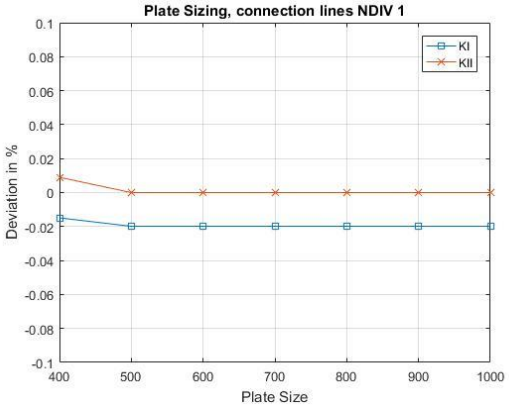

Figure 49. Plot of deviations for various outer square sizes, NDIV connection lines 1, ref Table C 10 in appendix.

The reduction of the NDIV connection lines led to a shifting of where the sizing effects seems to stop, and the values for KI and KII to have deviations of -0,02% and 0,00% respectively as seen in Figure 49. The slight change of the results obtained is due to the mesh being worsened, but it's a very small change and the results are still within the acceptable deviation, thus connection lines will continue having 1 division.

Testing was also performed with various inner square sizes, for the steps 10x10, 12x12, 14x14 and 16x16. One test matrix where the divisions of the square lines were constant set to 40, and one where they increased. The full test matrix for the two tests can be found in appendix, Table C 9 for the case where NDIV square lines are increased and Table C 10 for the case where NDIV square lines are constant. The presented results, in Figure 50, are all for a constant square line NDIV of 40.

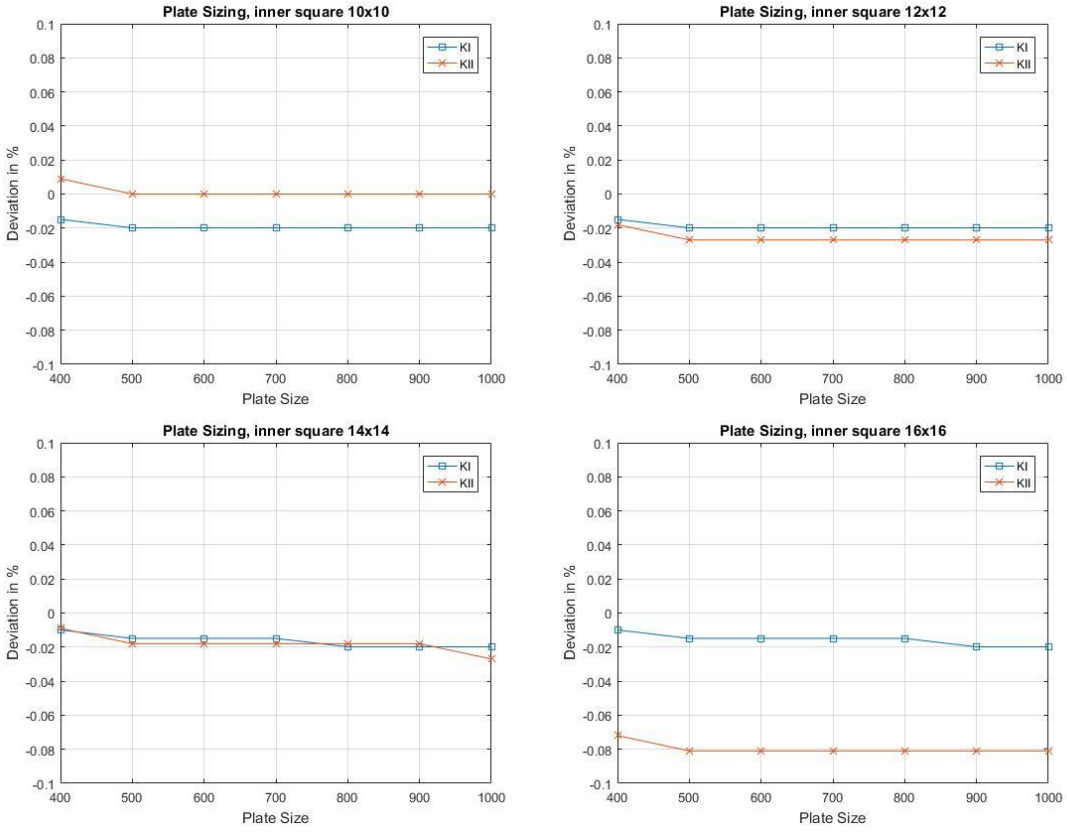

Figure 50. Plot of how the results deviate, for various inner square sizes. Connection lines set to 1, NDIV square lines set to 40, ref Table C 10 in appendix.

It can be seen that for both 10x10 and 12x12, the solution has converged for outer square size of 500x500, whereas for the 14x14 and 16x16 this is not the case. It should also be noted that 14x14 is well within the requirement of 0,1% deviation. The plot for 16x16 has a KII factor which has a nearly constant deviation of -0,08%, hence it's barely within the required deviation.

Some further testing was done in regard to the inner square sizing, to check that the region within the inner square had a high mesh density in each test previously performed. This was done by testing what happens as the NDIV square lines was reduced for the previous inner square sizes tested. As the NDIV of the square lines is the variable, the outer square size had to be a constant which was set to 500x500. The results from the further testing in regard to dimensions of the inner square sizes can be seen in Figure 51.

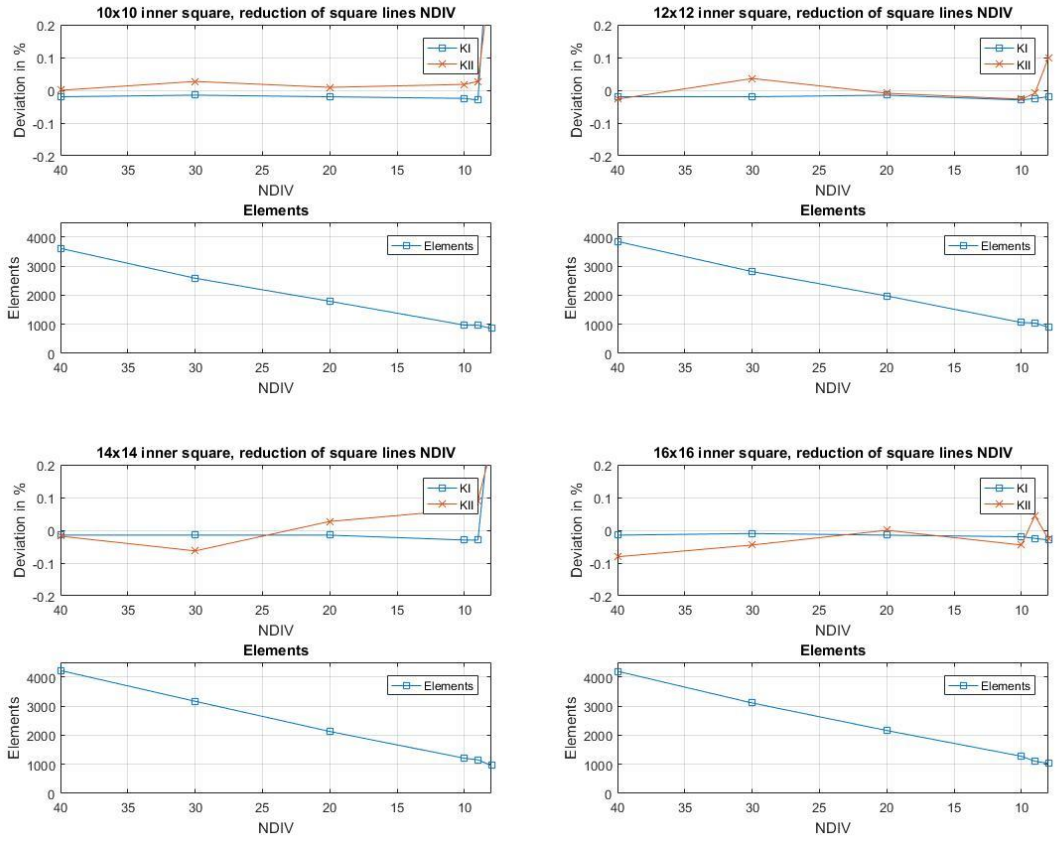

Figure 51. Plot of how the results deviate for various square sizes, as the mesh of the inner square is coarsened, ref Table C 11 in appendix.

The fact that all of the given tests, have a result within the acceptable range of deviation, as the square line divisions are reduced to 10, means that the initial mesh was more than sufficiently refined for the previous testing performed.

The paths surrounding the crack tip are of importance in regard to the results achieved, and the testing performed in the section above used 2 rows of elements, hence good paths from 3-8 in the vicinity of the crack tip are not necessarily guaranteed. The automatic mesh generation in ANSYS will typically continue making good paths when the mesh is kept refined, by using a high number of divisions for the square lines, and crack surface lines.

The inner square size and the divisions of square lines was decided upon as it can be seen that it still has rather stable results, for the values seen in Table 11.

Table 11. Defined parameters.

Defined parameters	
NDIV square lines	10
NDIV connection lines	1
Outer square size	500x500
Inner square size	10x10
CTSize	a/16

4.3.4 Crack surface line sizing

Now for taking a look on the crack surface line sizing, as mentioned before it is an important parameter in the case of few rows of elements surrounding the crack tip.

The tests performed, was first to test smaller sizes to see how it will affect the accuracy, for then to increase the size. Both plots will have an initial test, which will be equal to the length of outer edge row element, in this case it will be 0,0761mm when 2 rows of elements and CTSize a/16 is used, for then to see how the results for the contours 3-8 change throughout. The results obtained can be seen in Figure 52.

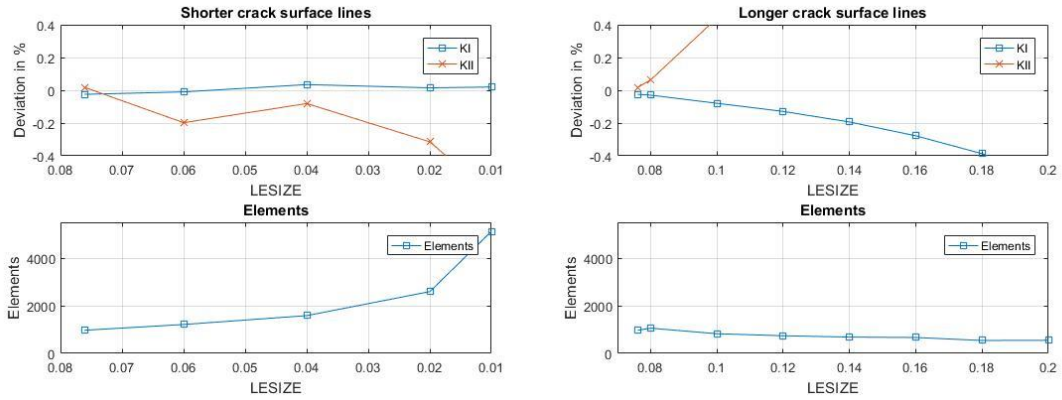

Figure 52. Plot of how the results will deviate as crack surface lines are refined and coarsened, ref Table C 13 in appendix.

When the divisions for the crack surface lines were shortened, KI remains nearly constant, whereas KII is first reduced a little bit, for then to be further underestimated. This is somewhat expected as the plots from the previous crack considered, showed that as more contours are taken closer to the crack tip, will lead to KII being further underestimated.

The other plot, where the divisions along the crack surface increases in size, it shows that the result quickly deviates from the analytic solution. This is most likely due to the mesh being too coarse as the contours 3-8 are considered, as only 2 rows of elements were defined by user input.

4.3.5 Rows of elements

The results obtained thus far, has depended on the good paths to be developed by the automatic mesh generation, in relation to the contours 3-8. This is not always practical for a coarse mesh, as was shown in Section 4.3.4.

Testing was performed using both the “traditional” and “new” method, which were described in Section 3.2.1, hence this section will be split to two subsections, but it will be shown that good paths for the interaction integral is of importance.

In this part of the testing, the division of the crack surface lines was set to 0,2mm, unless otherwise specified. The reason for the selected crack surface line sizing, is because it had a reduced number of elements, and the result is expected to converge, as more rows of elements are added.

4.3.5.1 "Traditional" method

The method for adding more rows, is by making each row of elements have a radial length which is the RRAT multiplied by the CTSize. CTSize of a/16 was used in this case, unless otherwise specified, as it was seen to be optimal from the CTSize testing in Section 4.3.2.

The first test was performed by using more rows of elements. The RRAT which was used in this case, was 0,5.

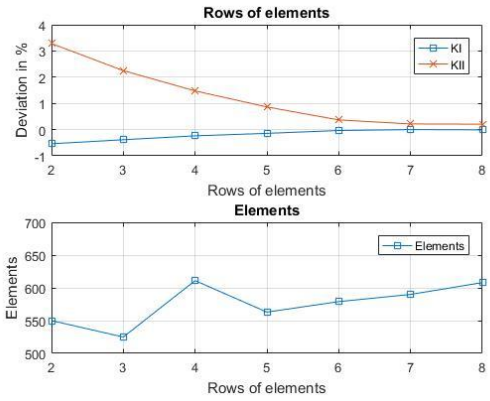

Figure 53. Plot of how the result deviate for various number of rows of elements. RRAT set to 0,5, ref Table C 15 in appendix.

As expected, the initial result for when 2 rows were used, KI and KII had a deviation of -0,54% and 3,28% respectively. Whereas when 8 rows of elements were used, KI and KII had a deviation of -0,1% and 0,21% respectively, which can be seen from Table C 15 in appendix. This means that KI has converged towards the desired accuracy, whereas KII has converged a lot, but is still overestimated.

The plots of the contours were checked for 2 and 8 rows of elements, as the results obtained differed by far. The results for the contours can be seen in Figure 54.

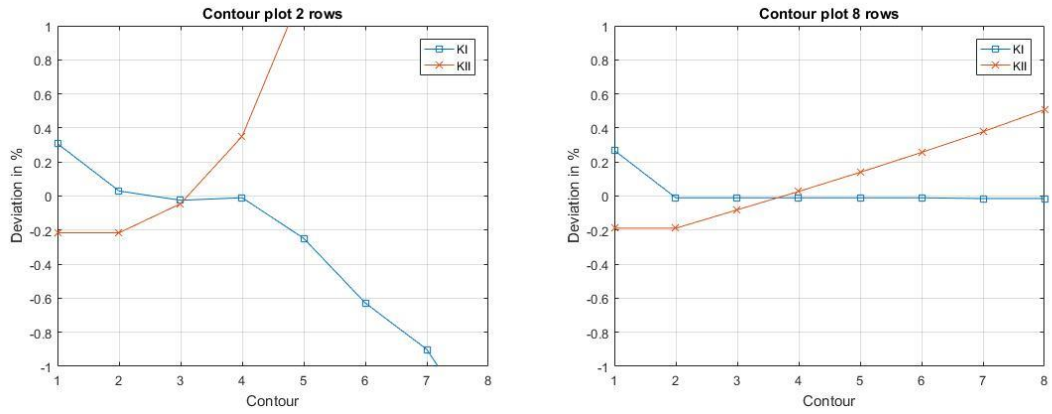

Figure 54. Plots of how the contours performs for 2 and 8 rows of elements, with same CTSize and crack surface line sizing, ref Table C 16 and Table C 17 in appendix.

From the plots, it can be seen that when 2 rows of elements were used, the results for contours 2-4 were very good for KI, whereas KII has generally a high deviation except for contour 3.

It can also be seen that when 8 rows of elements were used with RRAT set to 0,5, KI was stable for contours 2-8, whereas KII is at first underestimated and then overestimated.

The next step performed was reducing RRAT for the rows, which is now set to 0,25, and the results can be seen in Figure 55.

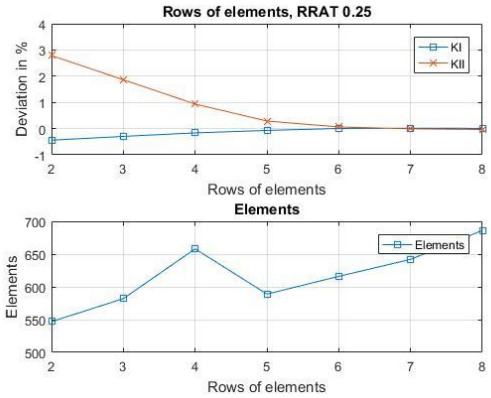

Figure 55. Plot of how the result deviate for various number of rows of elements. RRAT set to 0,25, ref Table C 18 in appendix.

This plot shows, similarly as the previous one, that as more rows of elements are added, the solution will converge towards the correct result. To compare some of the results shown in Figure 53 and Figure 55, Table 12 is developed, where the initial numbers can be found in Table C 15 and Table C 18.

Table 12. Deviations for RRAT 0,5 and 0,25 for 2 and 8 rows of elements, ref Table C 15 and Table C 18 in appendix.

	RRAT 0,5		RRAT 0,25	
	KI deviation %	KII deviation %	KI deviation %	KII deviation %
2 Rows	-0,54%	3,28%	-0,44%	2,79%
8 Rows	-0,01%	0,21%	0,01%	-0,04%

It can be seen from the table, that both results for KI as 8 rows of elements are used, will be well within the 0,1% deviation limit. Whereas KII is overestimated by 0,21% when RRAT 0,5 is used, for then to be underestimated by 0,04% as RRAT 0,25 is used. This can be due to the values of KII being underestimated for values very close to the crack tip, as previously shown.

To check if this was the case, two tests were performed with 8 rows of elements, the only difference between the two were the RRAT, and the plots are shown in Figure 56.

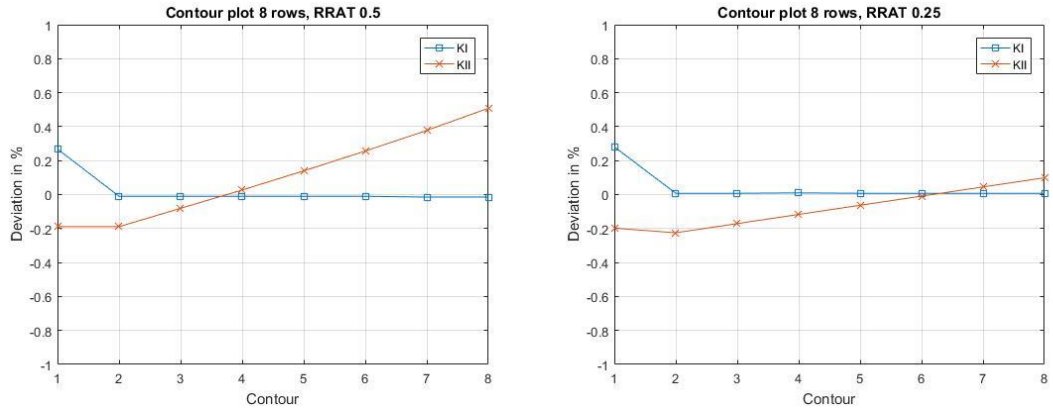

Figure 56. Plots how the contours deviate, for equal CTSize, and rows of elements, for RRAT 0,5 and 0,25, ref Table C 17 and Table C 19 in appendix.

As suspected, more of the contours are being underestimated when RRAT 0,25 is used compared to when RRAT 0,5 is used. KI is rather stable with values being constant 0,01% for RRAT 0,25 and being constant -0,01% for RRAT 0,5 which is a very small change in deviation.

The next step was to check the divisions of the crack surface lines, when 8 rows of elements were used. The choice of now reducing the crack surface line divisions, is that adoption of 8 rows of elements guarantees good paths for the interaction integral. Thus, the only requirement for additional elements along the crack surface lines, is due to display correct displacements.

The parameters used in the reduction of elements along the crack surface were 8 rows of elements, and RRAT 0,25. The results obtained can be seen in Figure 57.

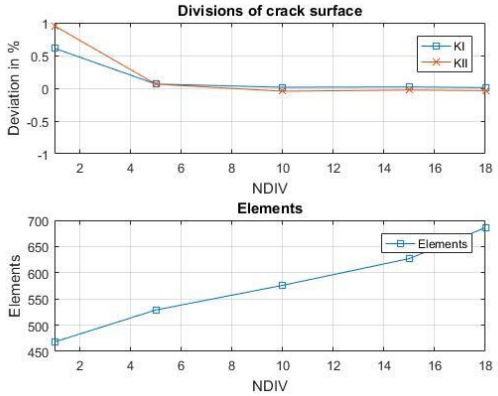

Figure 57. Deviations for various refinement of crack surface lines, by divisions, ref Table C 21 in appendix.

As seen, the results are within the 0,1% deviation requirement until the crack surface lines are set to 5 divisions, where KI and KII both have a deviation of 0,06%. As the division is set to 1, meaning one element going from one of the refined regions to the other, the results for KI and KII deviate by 0,61% and 0,95% respectively. This shows that the region between the crack surfaces can have a very coarse mesh, and still have a very accurate solution if the crack tips are meshed properly. The full table of results for the test performed, can be found in Table C 21 in appendix.

Some further testing was performed in the relation to RRAT and rows of elements used, which can be seen in Figure 58. CTSize was set to a/8, to see if this condition could still hold if RRAT was reduced.

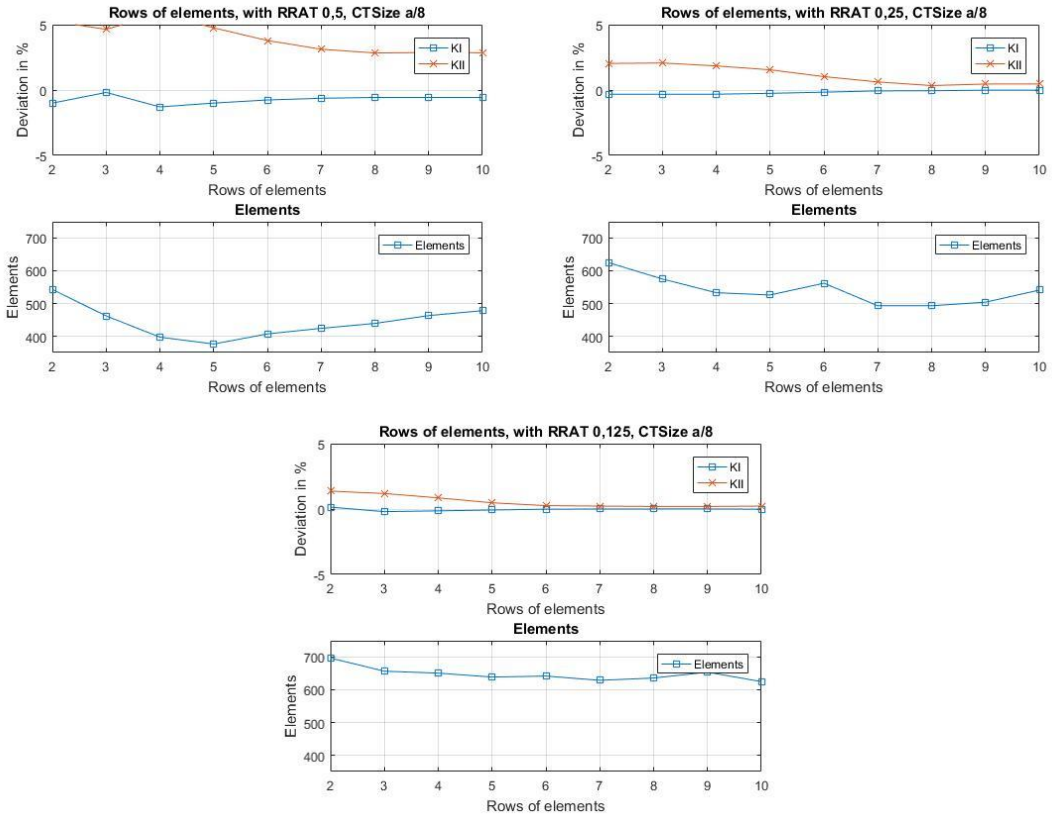

Figure 58. Constant CTSize, deviations for various number of rows, for RRAT 0,5, 0,25 and 0,125, ref Table C 23 in appendix.

From the plots in Figure 58, it can be seen that some convergence is achieved, especially in the case of KI. By looking at the results in Table C 23 in appendix, it can be seen that for example KI and KII for the case RRAT 0,125, has a deviation of -0,01% and 0,22% respectively, as 10 rows of elements are used, and 3-8 are considered.

In Figure 59 a plot of the contours 1-8 can be seen from the case of 8 rows of elements and RRAT set to 0,125.

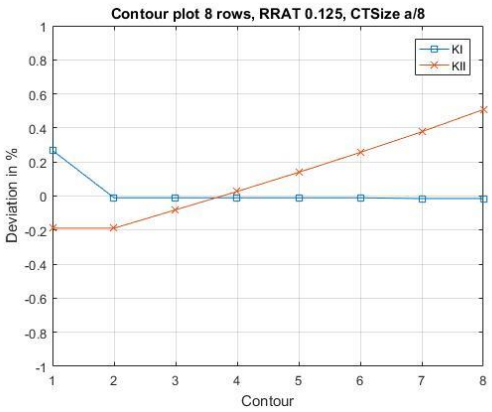

Figure 59. How the contours perform, as RRAT is set to 0,125, CTSize a/8. 8 Rows of elements, ref Table C 24 in appendix.

The KI factor remains constant throughout, with a deviation of -0,01% on the contours 2-8. Whereas KII increases about linearly through the same contours.

For comparison another plot can be made, where the parameters are exactly the same except for RRAT which is set to 0,5.

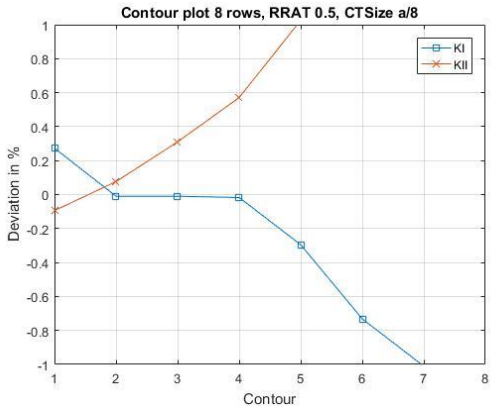

Figure 60. How the contours perform, as RRAT is set to 0,5, CTSize a/8. 8 Rows of elements, ref Table C 25 in appendix.

In the plot in Figure 60, it can be seen that KI is very accurate on the contours 2-4, whereas KII is somewhat accurate for 1 and 2. KI is on the range -0,01% to -0,02% for the contours 2-4, and KII is -0,09% and 0,08% for contour 1 and 2 respectively. Further refinement of the crack tip region, is shown in Section 4.3.7

4.3.5.2 "New" method

This section about refinement of the crack tip region, will use the method "new" which was previously explained in Chapter 3.

The fact that 8 rows of elements are advantageous as 8 contours will be considered has been showed many times, thus it was assumed to still be valid in this case, and 8 rows of elements was used from the start.

It was found that a CTSize of a/16 led to a high coarsening of the crack tip as the "new" method was used for meshing of rows. This led to the choice of first checking how refinement of the crack tip would affect the result, which can be seen in Figure 61. The size of elements along the crack surface lines was set to 0,2mm.

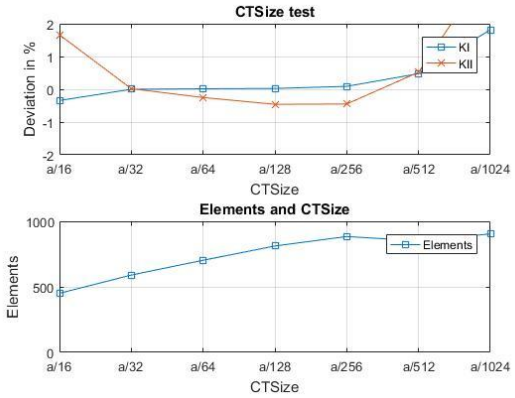

Figure 61. Deviations for various CTSizes, rows are generated by "NEW" method, ref Table C 26 in appendix.

From this plot it seems like a/32 is the better option, because this is the case where both KI and KII hit with high accuracy, the reason why further testing was performed, was to see how the result react as CTSize is reduced further. CTSize of a/32 will be used further, and also in this case to check how the contours reacts to the sizing, the results for the contours were plotted for a/16 and a/32.

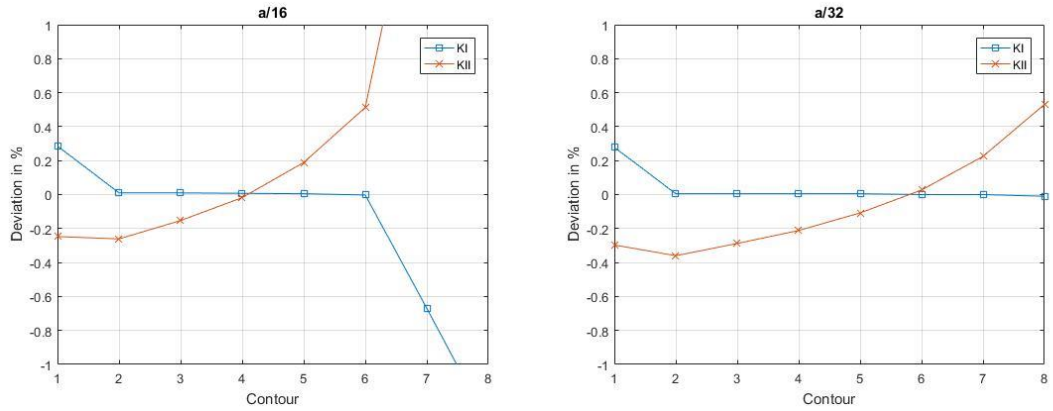

Figure 62. Deviations of contours, with CTSize a/16 and a/32, ref Table C 28 and Table C 29 in appendix.

What has been generally shown throughout, is that KI tends to be rather stable, regardless of CTSize, and distance from the crack tip. This leads to the assumption that a/16 simply is a too coarse mesh, which could be due to interaction with the curvature when the interaction integral is performed, as KI was generally stable throughout for the slanted through thickness crack.

Further testing in regard to the crack surface lines were tested in this region, to check the effects of coarsening the crack surface lines, when the crack tips would be refined with the "new" method. This time, the parameter used for divisions was the element length which was initially set to be equal to the last outer edge element, for then to be tested up to a length equal to 1mm, where the step size used was 0,1mm. The CTSize used throughout this testing was a/32. The results obtained can be seen in Figure 63.

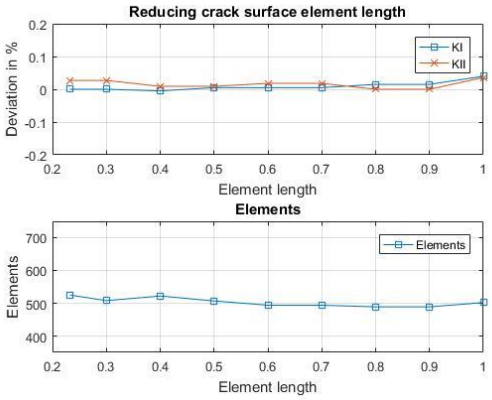

Figure 63. Enlargement of crack surface line element size, ref Table C 30 in appendix.

It can be seen from the plot, that the sizing of the crack surface lines can be reduced, if the crack tip region is properly meshed. In this case with 8 rows of elements, with CTSize a/32. It should also be mentioned that if 9 or 10 contours would be considered, the result would quickly deviate. The reason for this is that contours performed over element "paths" in coarse meshed regions, far away from the crack tip, will deviate rather quickly, as shown in Figure 64.

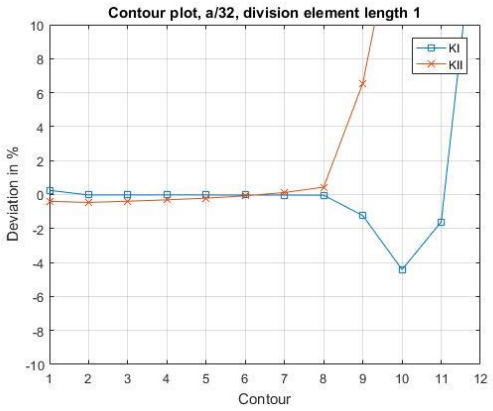

Figure 64. Contour plot of deviations of contours, CTSize a/32. Crack surface element length set to 1mm, ref Table C 31 in appendix.

From the plot, it can be seen that KI and KII are somewhat stable from contours 1-8. Usually the first contour should be omitted, hence it will be observed that KI ranges from -0,02% to -0,04% on the contours 2-8. Whereas KII ranges from -0,46% to 0,44% on the contours 2-8, as seen in Table C 31 in appendix.

KI and KII quickly deviate after the 8th contour, where the 9th contour has a deviation of KI and KII of -1,24% and 6,56% respectively. This once more stresses the requirement for good paths and refinement around the crack tip, especially in cases where a coarse mesh is used.

Further tests were performed to check the importance of crack surface line divisions, and square line divisions, as the crack tips were refined. The results obtained for each crack surface line element size is seen in Figure 65. Divisions for the square lines started at 10 for then to be reduced to 6, and crack surface line element sizes were 0,2328, equal to length of outer edge row element. Analysis were also performed for crack surface line element size of 0,3, 0,6, and 1, which is shown in Figure 65. The results obtained can be seen in Table C 32 in appendix.

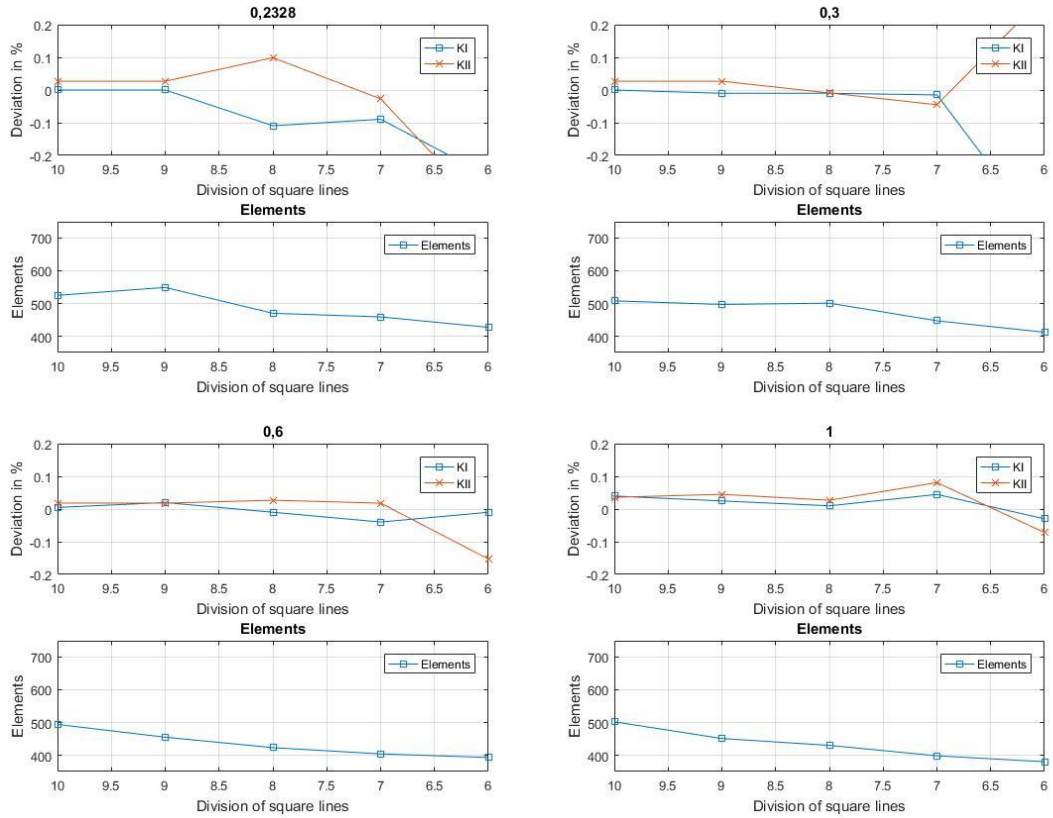

Figure 65. Plots of how the results vary, as square line divisions are reduced, for various crack surface line element lengths in mm, ref Table C 32 in appendix.

The plots in Figure 65, show that when good paths are defined by the refined region near the crack tips, the divisions of the square lines can be further reduced. Indeed, the results do start to deviate further as the mesh is coarsened, but all of the results are within ±0,1% deviation for division of square lines set to 7. The reduction of the divisions in regard to the square lines, leads to a quick reduction of elements used, especially in the case of coarse crack surface lines.

4.3.6 Contour study

A test of how the general contours perform for 2 rows of elements, for CTSizes a/2, a/4 a/8 and a/16 was performed and is presented in this section. This means that row 1 and 2 are generated by user input, whereas the rest are generated from the automatic free meshing in ANSYS.

NDIV square lines were set to 10 divisions, LESIZE crack surface lines are equal to the length of outer edge row element. The method used for rows of elements is “new”, as described in Section 3.2.1. For the exact deviations of the contours, ref Table C 34 to Table C 37 in appendix.

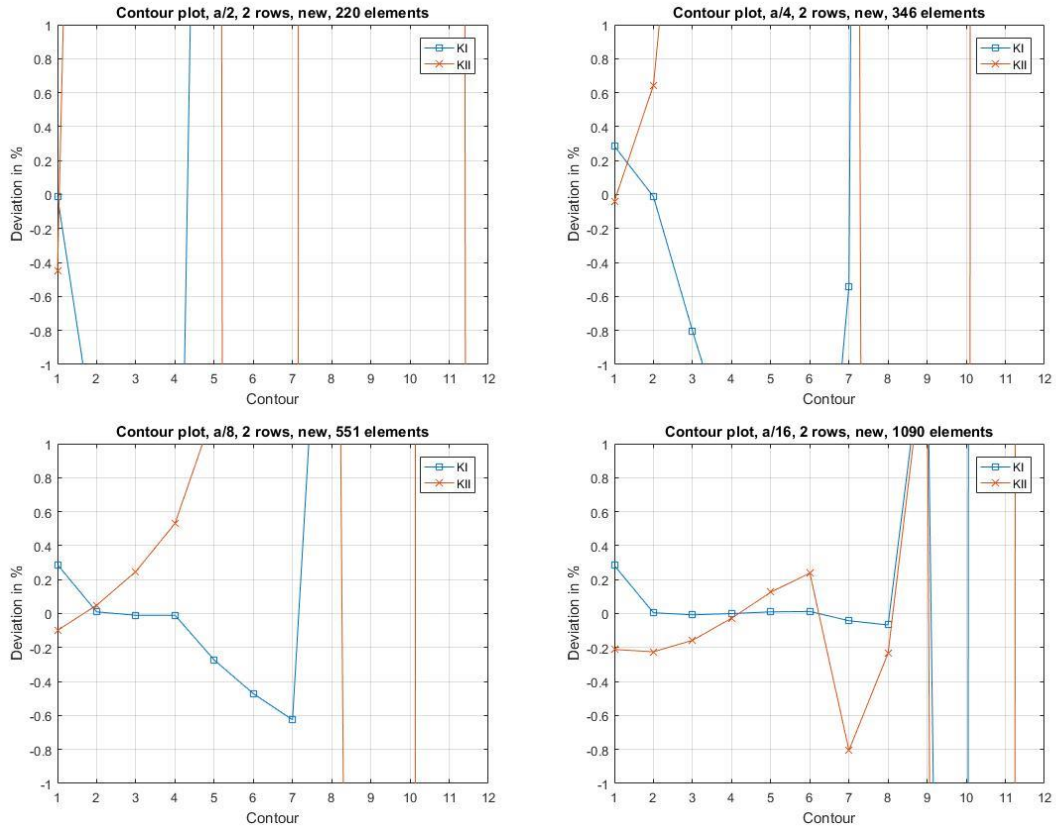

Figure 66. Deviations of contours, for CTSizesa/2, a/4, a/8 and a/16. 2 rows of elements, ref Table C 34 to Table C 37 in appendix.

The first test, with a/2 shows that contour 1 actually has an accuracy within 1%, which is interesting. Nevertheless, contour number 1 should generally be omitted, which has been seen throughout the testing previously performed. The CTSize in this case is rather large, and as it is a curved crack, the geometry will probably not be sufficiently accurate.

When CTSize is set to a/4, it can be seen that contours 2 is within a 1% deviation for KI and KII, and KI is very accurate, with a deviation of -0,01% for contour 2. Other than that, the result deviates by far, which can be due to the crack tip region not being refined enough to properly capture the geometry, as the results for the slanted through thickness crack had rather good results for some of the contours already as CTSize was set to a/2.

When the CTSize is set to be a/8, which is the largest advisable element in regard to ANSYS, it can be found that contour 2 has a high accuracy in regard to both KI and KII, with deviations 0,01% and 0,05% respectively. KI remains rather accurate on contours 2-4, whereas KII keeps deviating further, with a deviation of 0,53% for contour 4.

As the CTSize is further reduced to a/16, it can be seen that KI is rather stable on the contours 2-8, with the deviation ranging from -0,07% to 0,01%. Which probably explains why a/16 was found to be the best option in the initial testing, when the results were evaluated by the average of contours 3-8.

The requirement for higher refinement of this crack tip, than for the slanted through thickness crack can be due to two reasons:

1. The curved crack is more difficult to properly describe in FEM.
2. The interaction integral method is mainly defined for a straight crack.

4.3.7 Further refinement of the crack tip region

The refinement of the singularity element, and the region in general is of high importance for what happens as the singularity element size is reduced.

In Section 4.1 it was found that higher refinement, would lead to the 2nd contour deviating further for KII, but the overall plot of the contours being rather similar for various CTSizes. This led to the testing of further refinement being applied to the curved crack as well. This section will also be split in two parts, one for the "traditional" and one for "new" which were explained in Section 3.2.1.

4.3.7.1 Traditional

The test was performed so that the refined region will have a constant size, which is performed by adding more rows of elements as the CTSize is reduced. The initial size of the refined region had a radius of 1,6919mm. The parameters used can be seen in Table 13, and the plots in Figure 67

Table 13. Parameters used for refinement "traditional".

Parameters used	
NDIV square lines	10
NDIV Connection lines	1
LESIZE Crack surface lines	0,6591mm
Rows of elements	8
RRAT	0,5
CTSize	Variable
Radius of the refined region	1,6919

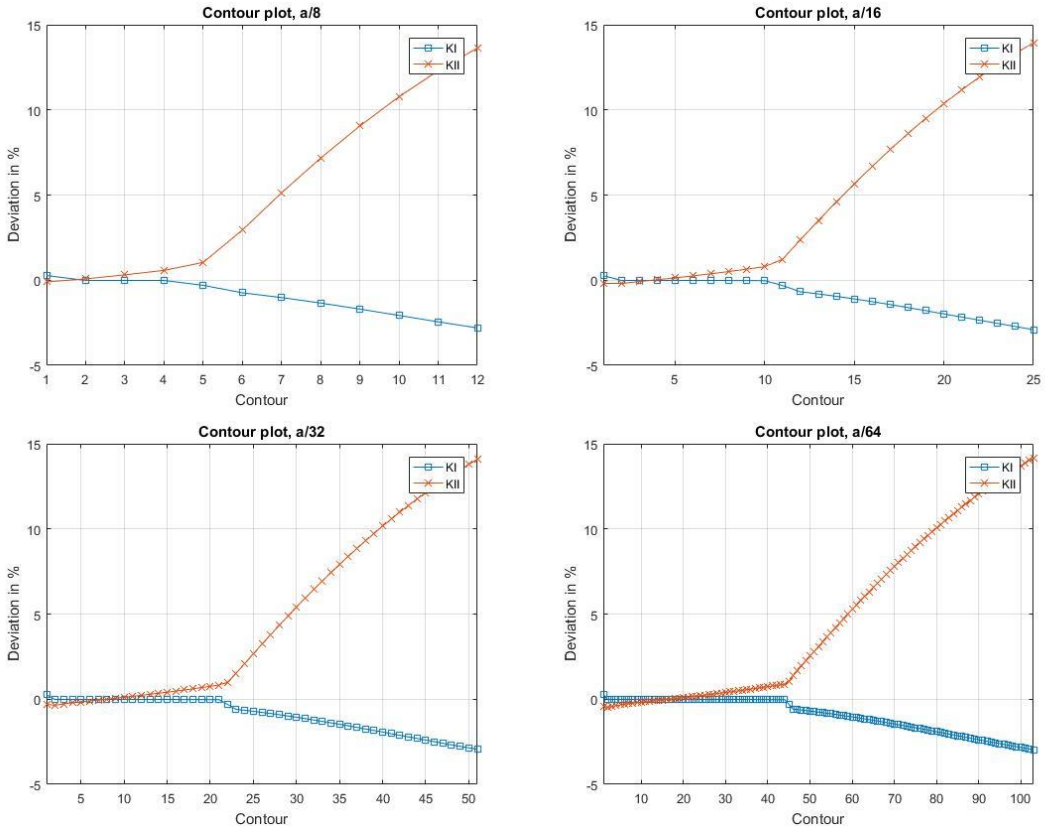

Figure 67. Contour deviations for various CTSizes, and rows of elements used. Refinement region radius 1,6919mm. Traditional rows, ref Table C 38 to Table C 41 in appendix.

It can be seen that the plots all have a similar shape, where similar deviations are in respective distances from the crack tip. This leads to the conclusion that CTSize can indeed be very small, and KI will be obtained correctly in the vicinity of the crack tip, whereas KII will be further underestimated.

It is noted that as CTSize was set to a/64, the highest underestimation of KII was -0,49%, whereas for CTSize a/8, the deviation was 0,08%.

The effect seen in Section 4.1.8.1 for the refinement of the slanted through thickness crack, where KII started approaching the analytic values as the distance to the crack tip increases, is not seen in Figure 68. The location where KI start to deviate, and KII start to deviate at a faster rate, is most likely due to the interaction integral not being valid for a curved crack.

Some further testing was done on a smaller refined region, to see how the results would compare. The size of the refined region was 1,1713mm, where all the other parameters were kept constant, and variable contours for different CTSize are presented.

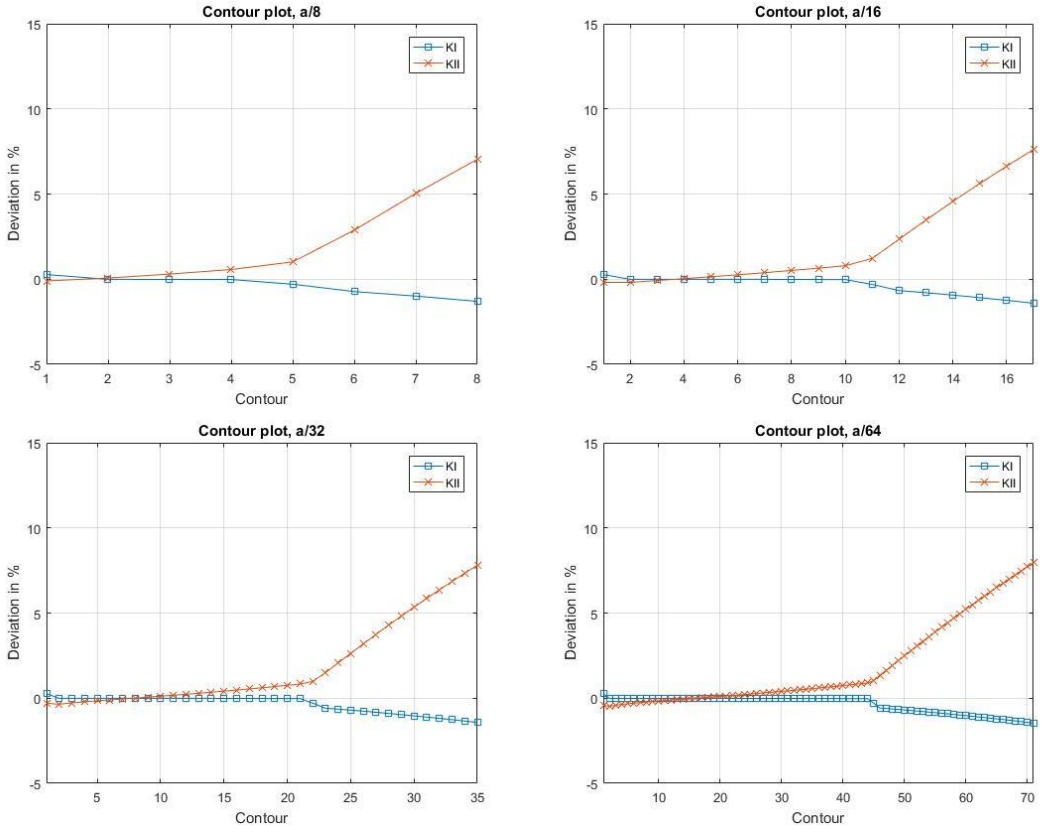

Figure 68. Contour deviations for various CTSizes, and rows of elements used. Refinement region radius 1,1713mm. Traditional rows, ref Table C 42 to Table C 45 in appendix.

It is noted that the results within the region considered in both cases are very similar, with only small deviations from each other which can be seen in Table C 38 to Table C 45.

In all 8 tests, it is seen that KI is rather stable for a while, for then to start slowly dropping. KII starts being underestimated. It should also be noted that KII starts to deviate at a faster rate, roughly at the point where KI starts to deviate. This could be due to the geometry, as this was not seen for the slanted through thickness crack.

4.3.7.2 New

The new method of meshing was also attempted refined through a reduction of CTSize. This was only performed for a refined region which had a roughly size of 0,651mm. It was attempted to maintain the region, but this is not as easily done in this case, due to how radial length of the next row of elements are defined. The parameters which were used can be seen in Table 14.

Table 14. Parameters used for refinement "NEW".

Parameters used	
NDIV square lines	10
NDIV Connection lines	1
NDIV crack surface lines	6
Rows of elements	8
CTSize	Variable
Radius of the refined region	0,651

The plots for a/32, a/64, a/128 and a/2048 can be seen in Figure 69, which had respective radiuses of 0,651, 0,6285, 0,546 and 0,5271.

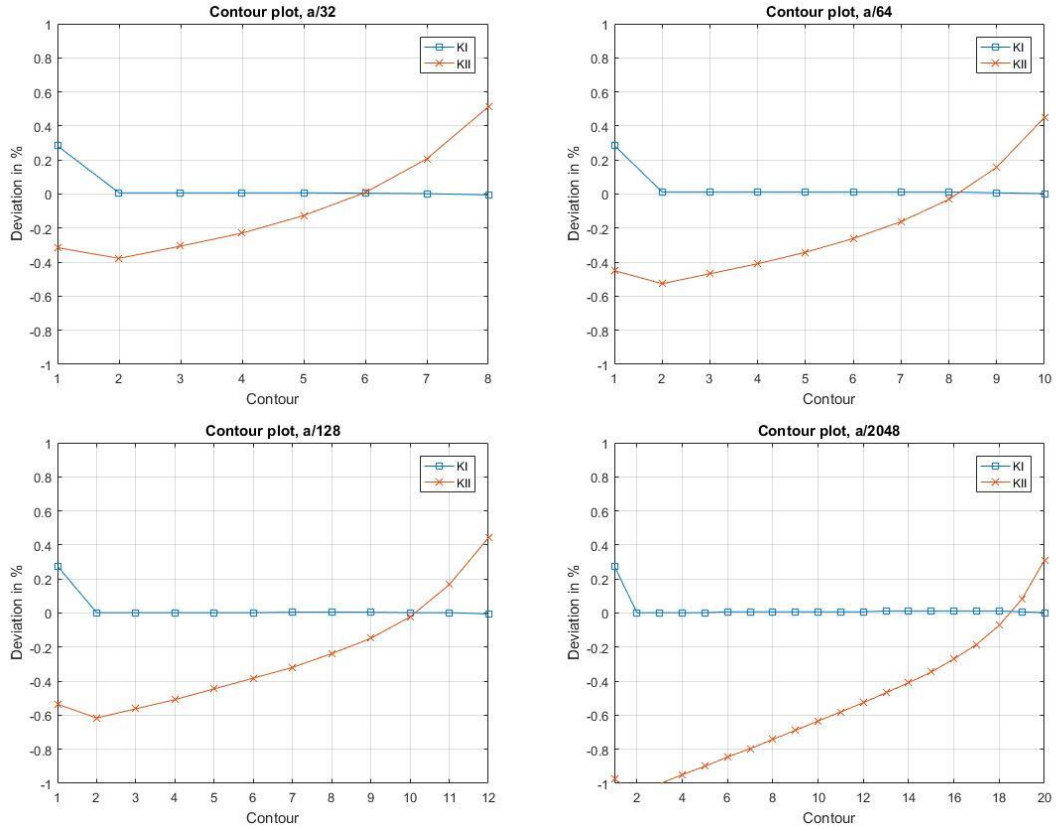

Figure 69. Contour deviations for various CTSizes, and rows of elements used. Refinement region radius is attempted to be kept constant. NEW rows, ref Table C 46 to Table C 48 and Table C 52 in appendix.

The plots show again the same as seen previously, KI remains at a constant very small deviation. Whereas KII starts to be further underestimated. The further underestimation is a slow process, as the deviation for CTSize a/32 is -0,38% and for a/2048 it is -1,06%.

4.4 Curved crack XFEM

This crack geometry was also tested using XFEM with the goal of comparing XFEM with FEM. XFEM is currently limited to Q4 when ANSYS mechanical APDL 19.2 is used.

Another important factor, as this is a curved crack, is that ANSYS is limited to the use of lines when calculating the level sets. It was attempted to use the curved MESH200 elements, to further have higher accuracy when it comes to the defined level sets for the curved crack, but this was not possible.

Inevitably, the Q4 elements would each have the fracture modelled as a line regardless, but if a curved MESH200 element could have been used, the level sets would possibly be better.

Nevertheless, it's well known that a curve can be represented by many short lines, which will here be considered a decent approximation. The number of line elements used to make the curve were normally 101 elements, with some exceptions such as 102 and 103, as ANSYS sometimes failed to calculate the level sets based on exactly 101 elements. The exact number of line elements used in each case for the crack, can be found in the tables in appendix, where the table group regarding XFEM for a curved crack is group D in appendix.

It was assumed that the inner and outer square sizes, determined in Section 4.3 for the curved through thickness crack using FEM, is still valid. Thus, the outer square size was set to 500x500, and inner square size, was set to 10x10.

4.4.1 Curved crack XFEM Q4

Initially, the testing was performed using only Q4. The parameters tested started at the NDIV connection lines had 5 divisions, for then to increase by 10 for every step, until it reached 75. The other parameter was the NDIV square line divisions, which started at 35, for then to increase by 10 until it reached 145.

Not all of the combinations of connection lines and square lines could be tested, due to the limitation of elements/nodes in the student version of the software, which was used.

Two tests were performed using the parameters mentioned above, one for SING a/8, and one for SING 0. When using SING 0, the element which contains the crack tip will still have the singularity enrichment. Whereas when SING was set to a/8, the singularity enrichment would be applied in a circle surrounding the crack tip, with the radius a/8 as shown in 3.3 of the methodology.

The first plot to be presented, is when the NDIV connection lines are set to 5, and the NDIV square lines increase, this is shown in Figure 70.

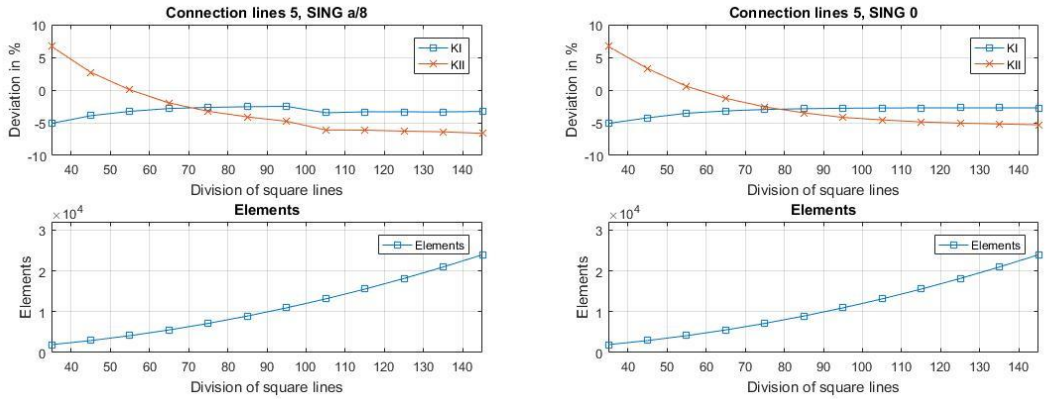

Figure 70. Refinement of square lines, as connection lines are set to 5, for SING a/8 and 0, ref Table D 1 and Table D 4 in appendix.

It can be seen from the plot, that there is some form of convergence, as the inner region is refined, but it converges towards a wrong value, and deviates more than 1%. This is probably due to the outer region being too coarse, as the elements used in that region was Q4.

The next test to be presented, is the case when the connection lines have divisions set to 25, for SING 0 and SING a/8. The results are shown in Figure 71.

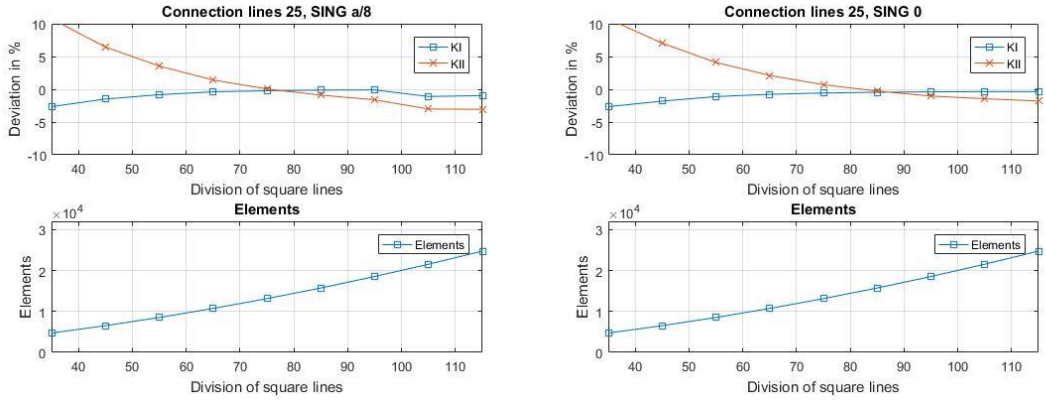

Figure 71. Refinement of square lines, as connection lines are set to 25, for SING a/8 and 0, ref Table D 1 and Table D 4 in appendix.

The results are seen to be in better agreement with the analytic solution than in the test where the connection lines had 5 divisions. It can be seen that the results converge towards better solutions for SING 0 than for SING a/8.

The results obtained with connection lines set to 35 divisions is presented in Figure 72.

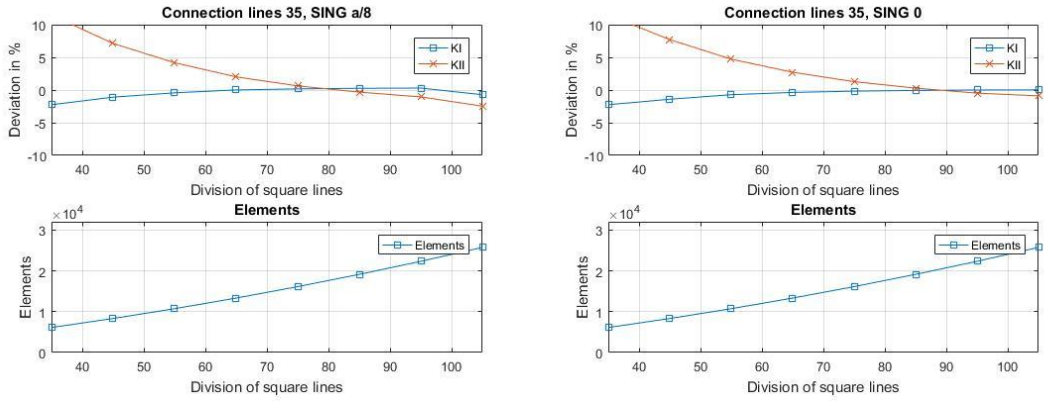

Figure 72. Refinement of square lines, as connection lines are set to 35, for SING a/8 and 0, ref Table D 2 and Table D 5 in appendix.

The results from this test are significantly better, where both converge within 1% of the analytic solution, except for KII when SING a/8 is used, and square lines are set to 95 divisions. Interestingly enough, it is the test where only the crack tip element is enriched with the singularity functions, that has the highest agreement with the analytic solution.

By comparing the data from Table D 1 to Table D 6 in appendix, and looking on the various plots in Figure 70 to Figure 72, it seems as if the better results are achieved when only the crack tip element is enriched. Further checking of contours will be performed in Section 4.4.2, where Q8 and Q4 are used together.

4.4.2 XFEM with Q8 elements in outer square

Q8 elements can be used in some regions of the mesh, namely the regions which will not be enriched, as the requirement for Q4 with XFEM is in regard to the elements being enriched.

Throughout the testing it is assumed that the NDIV connection lines can be reduced to having its divisions set to 1, as this worked well for FEM. This means that the main parameters for testing that remains, are the NDIV square lines, and the singularity enrichment region.

Figure 73 is a plot of the case where SING is set to 0 for comparison for further testing about singularity enrichment region.

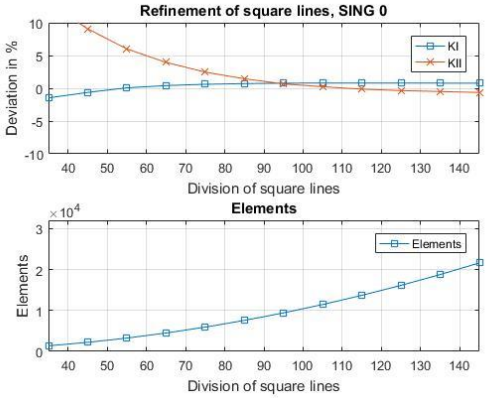

Figure 73. Refinement of square lines, as SING is set to 0, ref Table D 8 in appendix.

Used parameters 1	
NDIV Connection lines	1

Table D 8 in appendix, shows that the solution for both KI and KII will get within a 1% deviation limit. In the case of KI, it seems like it is stable with regard to further refinement, whereas for KII it keeps reducing. This could be due to the contours becoming closer to the crack tip, as will be considered later.

Some of the singularity regions which were tested, were SING a/8, a/4, a/2 and a, where the results obtained, with the addition of elements used, are presented in Figure 74.

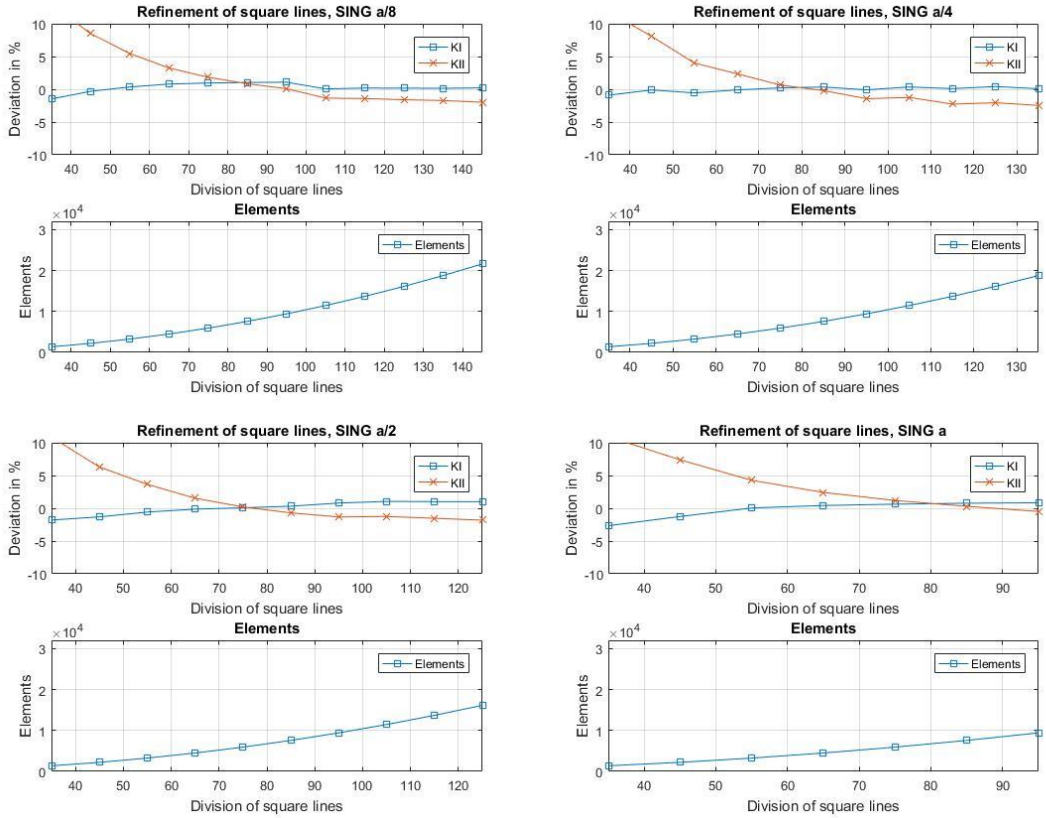

Figure 74. Refinement of square lines, as SING is set to a/8, a/4, a/2 and a, ref Table D 9 to Table D 12 in appendix.

The plots above are not necessarily the best at explaining the effects of the singularity function, as the only regions which can be properly compared throughout, are the divisions 35-95, as this is the regions which were possible to perform for all tests, due to limitation of nodes in the student version of ANSYS.

By looking at the plots and Table D 9 to Table D 12 in appendix, it can be seen that the best result for KI is achieved when SING a/8 is used, and square lines are set to 105. The proceeding results do not have a too high deviation either, with a maximum of 0,22%. By looking at the same plot, and checking KII, it can be seen that the best result is obtained as the square lines are set to 95. This can once again be in regard to how well the contour perform as they get closer to the crack tip, as KII initially is overestimated, for then to become underestimated.

When the singularity region is set to have a radius of a/4, it can be seen that all values of KI are within 1%, with two results within a 0,1% deviation, but KII deviates further than SING 0 and SING a.

When the singularity zone is further increased to a, the results once again has the shape initially found as the singularity zone was set to 0, with very similar results. The difference between the two is a slight change of when the results cross the 0% deviation line.

4.4.2.1 Curved crack XFEM contours, constant SING

The contours were also tested for various SING sizes and refinement regions, as it was expected that this would also be important information when XFEM is used. In this section, the variable is in regard to square line divisions, where the SING is kept constant.

The first part of the testing is performed using SING 0 and checking various square line sizing. The reason why SING was defined to be 0, is to easily see the change in contours, as adding the singularity function was found to make a sudden drop in deviation for the contours in the test performed with a slanted through thickness crack. The square line sizing, which was considered were 55, 105, 115, 145. The plots can be seen in Figure 75.

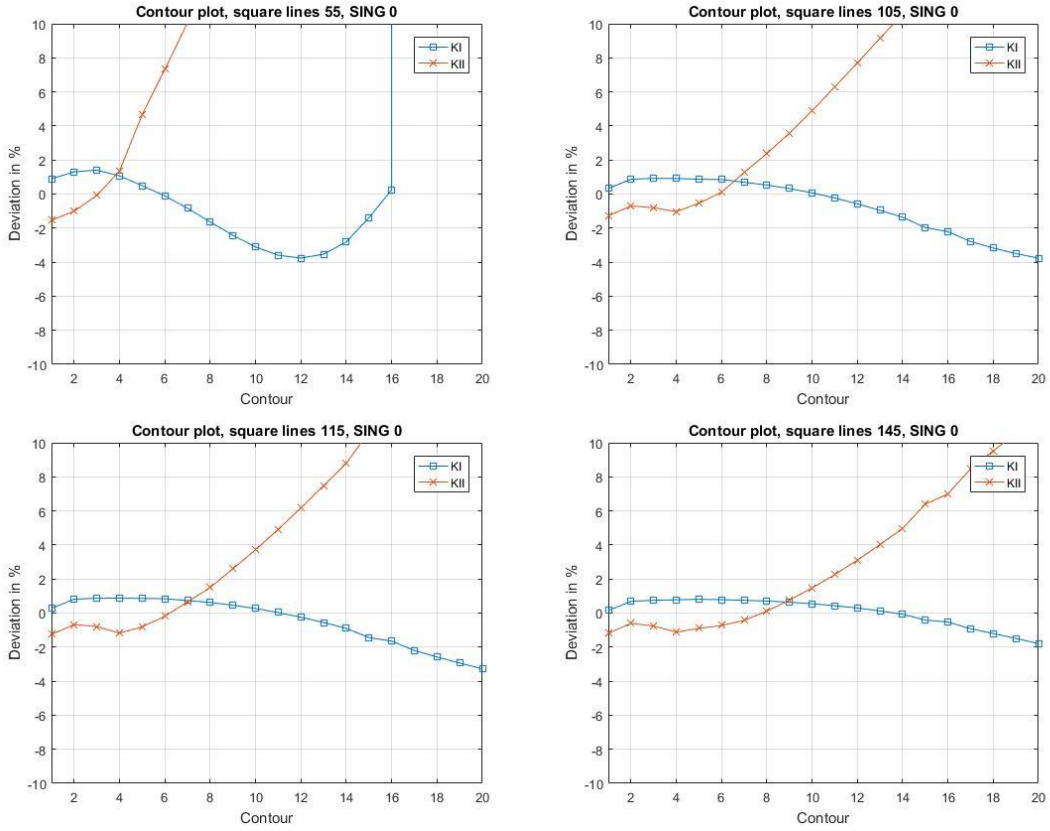

Figure 75. Contour deviations, for square lines set to 55, 105, 115 and 145 divisions. SING 0, ref Table D 13 to Table D 16 in appendix.

The number of contours were always equal, but this does not mean that the distance at which the contours are taken are equal. Each contour requires a path, and as the mesh is refined, more paths are available near the crack tip. Nevertheless, these plots do give insight in what happens in regard to which contours that are adopted.

The first graph, which was made, using square lines set equal to 55, shows the general form that the contours would take throughout. The interesting part by comparing all of the results, is that the general shape developed by the graphs are rather similar, as was seen using FEM. In every case, KII is

initially underestimated, for then to become overestimated. It should be noted that the refinement of the mesh did lead to the deviation lines getting closer to 0% deviation, which can be seen in Figure 76. This means that further refinement could lead to improved accuracy, but the mesh is already very refined. When the 145 square divisions were used, the mesh had 21025 elements in the inner square, region 5 as explained In Section 3.3.

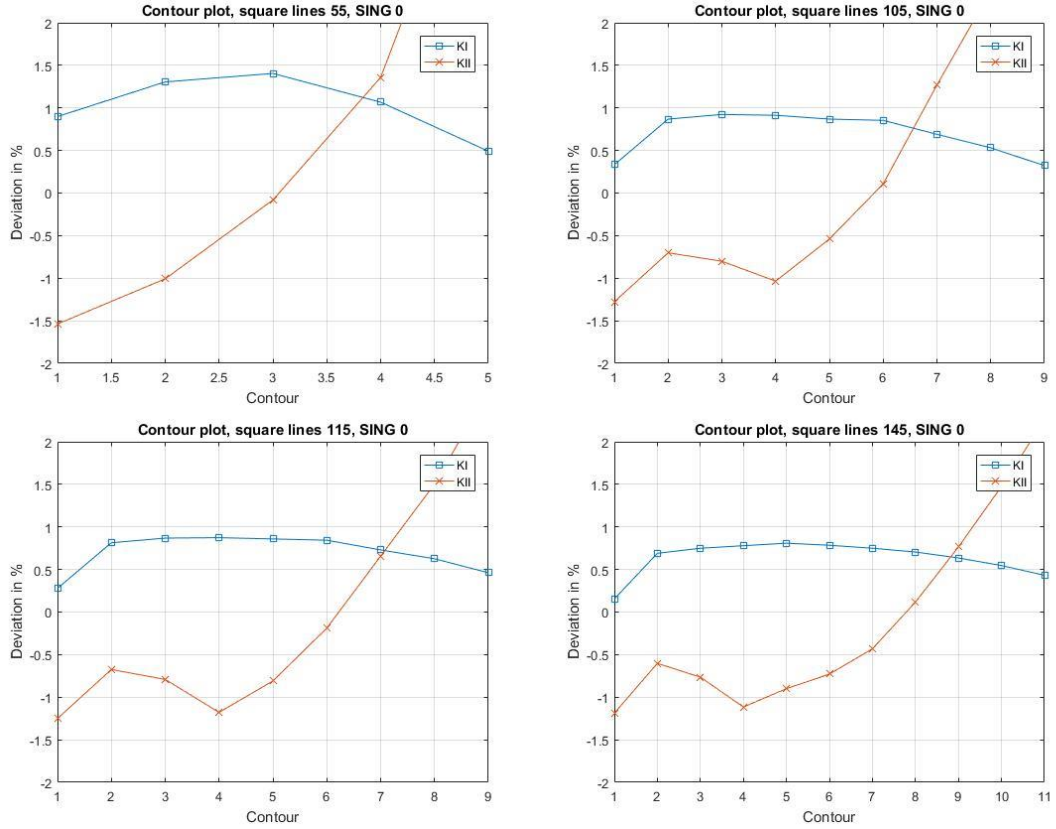

Figure 76. Contour deviations, for square lines set to 55, 105, 115 and 145 divisions. SING 0. Focusing on the region before large deviations, ref Table D 13 to Table D 16 in appendix.

All the plots in Figure 76 show that as the refinement is increased, the deviation is lowered in the vicinity of the crack tip. In the plots the number of contours differ, but the considered region is the one before the curve cross the 0% deviation line, as the results always showed that the deviation would just increase further with increasing distance.

4.4.2.2 *Curved crack XFEM contours, constant square lines*

The previous section focused on what happens as the mesh is refined with a constant singularity region, where only the crack tip element is enriched. To more clearly see the effects, this section focuses on what happens as the singularity region is modified, with a constant number for NDIV square lines. A larger singularity enriched region will lead to more degrees of freedom being added, even though the number of elements is constant. The square line divisions is set to 95 as it allows for testing up to a singularity zone equal to half the total crack length.

The first test which was performed, is the case of the singularity zone just being the crack tip element, as a practical comparison, and can be seen in Figure 77.

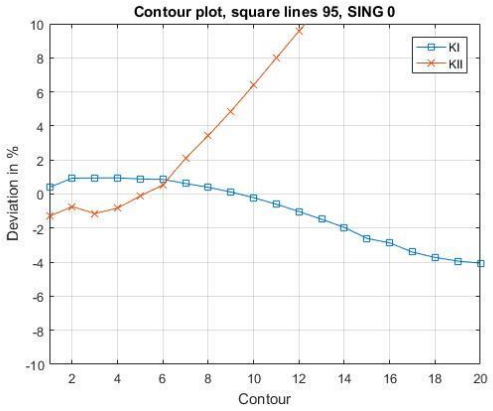

Figure 77. Contour plot for square line divisions set to 95, and SING 0, ref Table D 17 in appendix.

Figure 78 further presents the effect of SING a/8, a/4, a/2 and a. These will be compared to the results for a singularity zone which only applies the singularity enrichment to the crack tip element.

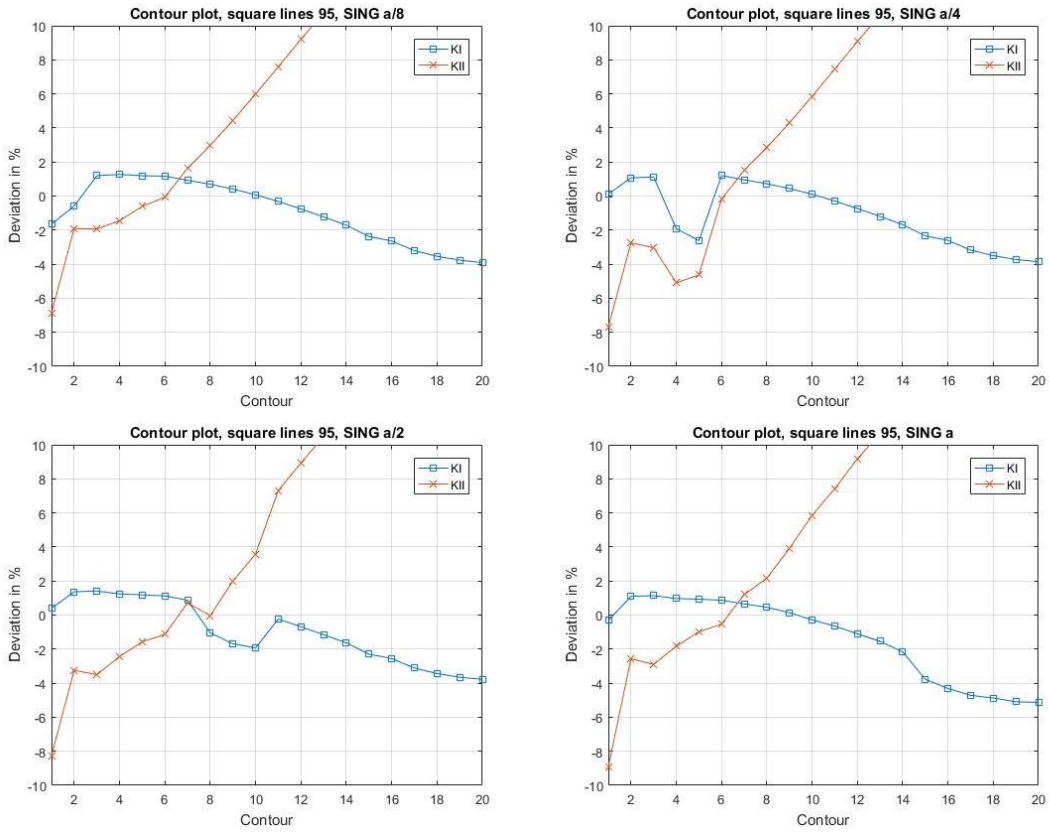

Figure 78Contour plot for square line divisions set to 95. SING a/8, a/4, a/2, a, ref Table D 18 to Table D 21 in appendix.

As was also seen for the slanted through thickness crack, when the singularity field is added, in the case of a/4 and a/2, there is a sudden change in the deviation. For a/4, the jump is between contours 3 to 6, whereas for a/2 the jump is not as drastic and located between contours 5 to 11. When the singularity region is set to a, it can be seen that most likely, the drop is at contour 14, as there is a sudden change of accuracy at that stage.

The effect of this sudden change in deviation seen in the plots for SING a/4 and a/2 in Figure 78 is most likely unfortunate for the solution, as it can be seen that it is rather drastic, and does not seem to be very consistent in magnitude. This means that the singularity enrichment zone should either be somewhat big, or just the crack tip element. The computation time is increased when a singularity enrichment is enlarged.

Further it can be noted that there is now a high deviation in the contours for KII near the crack tip, when SING a is used, where the initial contour is deviating by about 8%. This was not present when the singularity enrichment was limited to the crack tip element.

By comparing the plots for SING 0 and SING a from Figure 78, it can be seen that the enrichment applied, does not significantly improve the results obtained, and worsens some of the results, as can be seen by comparing Table D 17 with Table D 21. The increasement of the singularity region size does also increase computation time.

When the average of contours 3-8 are taken for both the previously mentioned results, it can be seen that KI and KII deviate by 0,77% and -0,64% respectively in the case of the singularity enrichment only being applied for the crack tip element. Whereas for a singularity region with a radius equal to half the total crack length, KI and KII deviate by 0,84% and -0,48% respectively. Which means a lower accuracy in regard to KI and a higher accuracy in regard to KII, which is explained by the results shown in Table 15.

Table 15. Comparison of contours 3-8, for SING a and SING 0. Square lines 95 divisions, ref Table D 17 and Table D 21 in appendix.

	SING a		SING 0	
Contour	KI%	KII%	KI%	KII%
3	1,14 %	-2,90 %	0,94 %	-1,14 %
4	0,97 %	-1,84 %	0,95 %	-0,83 %
5	0,93 %	-0,98 %	0,88 %	-0,12 %
6	0,87 %	-0,54 %	0,86 %	0,53 %
7	0,65 %	1,20 %	0,62 %	2,10 %
8	0,46 %	2,16 %	0,40 %	3,43 %

The results show that when the singularity enriched region has a radius equal to half the crack length, the value of KI is constantly further overestimated for the contours 3-8, than for SING 0. When it comes to KII, it seems as if the results are somewhat shifted. When the singularity region has a radius of a, it can be seen that KII is further underestimated than when the singularity element is just applied to the crack tip element.

From the results obtained, it seems unnecessary to add a singularity field. This is because there is no significant improvement in the accuracy, it mainly seems that the deviations have somewhat shifted as mentioned throughout, and no improvement of consistency of the results obtained.

4.5 Discussion

In this section, the discussion was split into three subsections. One for FEM, one for XFEM and one for comparing the two methods used as this is of high importance. The reason why it is decided to split it up as such, is due to the similarities and or differences between the crack geometries was discussed in FEM and XFEM, for then to compare the methods as well in the comparison section.

4.5.1 FEM – Discussion

The results show that modelling a crack by the use of general finite element method, with the help of collapsed isoparametric Q8 elements is a very accurate method. Especially when the SIFS are extracted using the interaction integral method.

4.5.1.1 Refinement of regions

In the testing section of this thesis, it has been shown that the result will not significantly change if the region with small strain gradients is very coarse. This leads to fewer elements/nodes used, and hence less computer power required. The region of high refinement must be sufficiently large to capture most of the large strain gradients for this to work, if the region is too small, the results would start to deviate from the analytical solution.

It should be noted that in practice, geometries might not be as simple as a crack in a plate. The crack in a plate will only have high gradients in the near vicinity of the crack, and small gradients everywhere else.

4.5.1.2 CTSize

When it comes to CTSize, the recommendations by ANSYS were for example a/8 or smaller. Whereas in the testing section of this thesis, it was found that for a straight crack the CTSize could be as large as a/2, and still give good results. An important thing to note, is that when the CTSize is enlarged, there will be fewer “good” contours, which is further discussed in the contour section of the discussion.

When it comes to a curved crack, the results seem to be more “sensitive” in regard to the choice of CTSize, as it was found that a CTSize of a/8 could be viable if the correct contours were considered. This could be due to the curved crack needing more elements to properly describe the actual geometry. The deviation could also be due to the choice of allowing the singularity element to also follow the curve of the crack, leading to the angle at the crack tip to be wrong, but this also comes down to describing the geometry correctly.

It should also be noted that KI tends to be stable throughout the contours considered, as CTSize is reduced. This means that KI can generally be found through making a convergence study.

KII on the other hand starts to be further underestimated as refinement of the crack tip element is continued. It should be noted that the further underestimation of KII is a slow process, thus a convergence study should be possible in this case as well, but it would be less accurate than for KI. With possibly a lower limit of CTSize set as a/64, as the deviation seems to not have become too significant at this point, and CTSize of a/16 and a/32 was more than sufficient to model the curved crack.

4.5.1.3 Contours

It was initially decided to use contours 3-8 throughout this testing section of the thesis. This was decided upon, as it was the contours which generally performed the best throughout the initial testing. The problem with these contours appears as the mesh is either very refined or coarsened.

This is because when the mesh is refined, more contours will be taken closer to the crack tip, where KII typically was underestimated, and if it's coarsened, it could lead to a too coarse mesh. When the average of contours 3-8 is taken, the reason why KII might be exact, or very accurate, is because some of the terms are overestimated, and others underestimated, thus cancelling out. KI seems to be more stable throughout, as previously stated.

When the mesh is coarsened, the higher contours, for example 7 and 8 will be far away from the crack tip, and possibly in a very coarse region. The solution can be improved by adding more rows of elements, as the integral will then be performed over good "paths".

When the curved crack is considered in Section 4.3, it was noted that the CTSize, and thus the contours had to be in the near vicinity of the crack tip to obtain results within the desired accuracy of ±0,1% deviation. This is because the interaction integral method is defined for a straight crack.

4.5.1.4 Rows of elements modelling and amount

The adding of rows of elements, can help to refine the region in the near vicinity of the crack tip, as the only parameter specifically refining the crack tip region is the number of rows of elements. Refinement of the crack surface lines would also lead to some refinement around the crack tip regions, but it would not necessarily be a practical mesh in regard to paths, and size. Another issue is that by refining the crack surface lines, many elements would be added in a region which does not necessarily require a high mesh density. By instead adding rows of elements surrounding the crack tip, leads to higher refinement in a region where it is required, and it leads to good paths for the integral to be performed over.

As the rows of elements leads to good paths for the interaction integral to be performed over, it could be good practice, to have number of rows equal or larger to the contours considered. This is why 8 rows of elements were typically used, especially in the case of the curved crack, as the contours 3-8 were generally used.

Reduction of RRAT for the "traditional" method was attempted, and did lead to obtaining more contours within the acceptable level of deviation, but it would be more beneficial to reduce CTSize or consider fewer contours, than to have 8 small rows of elements following the singularity element, to obtain 8 good paths. This is because the 8 rows would not necessarily improve the obtained results, rather than to generate more results on the region where good results can be obtained. This can for example be seen from the "very refined" regions, for both cracks in Sections 4.1.8 and 4.3.7, as the higher refinement initially gives somewhat higher accuracy, whereas further refinement after that, simply leads to more contour values in the region.

The reduction of CTSize would lead to a reduction in the radial length of the additional rows of elements, but then it is because the CTSize is reduced, not because RRAT is reduced.

4.5.2 XFEM - Discussion

The advantage of this method is as previously mentioned, no need for remeshing as the crack propagates.

4.5.2.1 Refinement

As the extended finite element method is limited to Q4 elements in the enriched region, it quickly leads to a high number of elements required to get an accurate solution.

It was found that using Q8 elements in the outer region of the plate, where the XFEM enrichment would not be applied is advantageous, as it reduced the number of elements required in the region

significantly. The inner region of the plate still requires a high level of refinement to obtain a good result, as it's limited to Q4 elements.

4.5.2.2 Singularity enrichment

The results in regard to the singularity enrichment is somewhat unclear.

In general, it seems as if it's best to allow the singularity region to be 0 or a, where 0 would limit it to the crack tip. This is due to the sudden change of deviations which was both seen for the slanted through thickness crack, and for the curved crack.

From the contour study for XFEM, it is noted that the slanted through thickness crack, experienced some improvement as the singularity enrichment function was added. For the curved crack, the change in the results were not significant.

mentioned that the enrichment will add degrees of freedom, and thus require more computing power, this leads to SING 0 being considered optimal.

4.5.3 Comparison - Discussion

By comparing some of the results and number of elements used, it can be seen that general FEM will have a higher accuracy, and lower requirement of elements used than XFEM.

It should also be emphasized that XFEM in ANSYS mechanical APDL 19.2 is limited to the use of Q4 elements, and FEM uses Q8 elements. The fact that XFEM is not implemented for Q8 elements in ANSYS means that the full potential from XFEM may not be exploited.

4.6 Conclusion

As two methods has been tested, the conclusion section will be divided into three section, one for each method in addition to a comparison.

4.6.1 Comparison - Conclusion

1. Explicitly modelling the crack using FEM will lead to a higher accuracy with a fewer number of elements required than XFEM.
2. Interaction integral method can be applied for curved cracks, if the contours considered are close to the crack tip.

4.6.2 FEM - conclusion

1. Crack tip singularity element size equal or smaller than a/8 is generally a good recommendation for the analysis, but it should be noted that it depends on the crack geometry and on how many contours will be considered.
2. The size of the singularity element can be very small, and still give accurate results for KI, whereas it will typically lead to KII being somewhat underestimated.
3. The size of the singularity element can be rather big, if the crack is straight, as the case of the slanted through thickness crack, where a size equal to a/2 could be used if only the 2nd contour was considered.
4. The number of rows of elements should be equal or larger than the number of contours performed when using the domain integral method, as it will be a controlled refinement of the crack tip region and guarantee good paths for the integral.
5. The crack surface lines can be very coarse, if the crack tip regions are refined.
6. 16 singularity elements surrounding the crack tip, is sufficient for accurate results.

4.6.3 XFEM - conclusion

1. The use of Q8 elements, in the region that is not enriched by XFEM, is an effective way of reducing the number of elements required, when XFEM enrichment is limited to Q4 elements.
2. The singularity zone should either be SING 0 or SING a.

4.7 Suggestions for further research

1. Study the benefit obtained by using XFEM over FEM for crack propagation analysis, with focus on time saved by not having to perform remeshing, in comparison to time required for having to solve a larger stiffness matrix.
2. Research into the application of XFEM for Q8 elements. Relevant topics are, availability, theoretical limitations and performance.

3.

Chapter 5 References

[1] T. L. Anderson, *Fracture mechanics : fundamentals and applications*, 3rd ed. ed. Boca Raton, Fla: Taylor & Francis, 2005.

[2] T. Næsheim, *"Alexander L. Kielland"-ulykken*. Oslo: Universitetsforlaget, 1981, p. 360 s. ill. 4°.

[3] "REPORT ON THE AIR ACCIDENT NEAR TURØY, ØYGARDEN MUNICIPALITY, HORDALAND COUNTY, NORWAY 29 APRIL 2016 WITH AIRBUS HELICOPTERS EC 225 LP, LN-OJF, OPERATED BY CHC HELIKOPTER SERVICE AS," Accident Investigation Board Norway, 2018.

[4] M. Graba, "Limit loads for centrally cracked square plates under biaxial tension," *Open Engineering,* vol. 6, no. 1, 2016.

[5] H. Tada, G. R. Irwin, and P. C. Paris, *The stress analysis of cracks handbook*, 3rd ed. ed. New York, N.Y,London: ASME Press Professional Engineering Publishing, 2000.

[6] P. C. Paris, M. P. Gomez, and W. E. Anderson, "A Rational ANalytic THeory of Fatigue," *The Trend in Engineering,* vol. 13, pp. 9-14, 1961.

[7] K. Rege and H. Lemu, *A review of fatigue crack propagation modelling techniques using FEM and XFEM*. 2017, p. 012027.

[8] T. N. Bittencourt, P. A. Wawrzynek, A. R. Ingraffea, and J. L. Sousa, "Quasi-automatic simulation of crack propagation for 2D LEFM problems," *Engineering Fracture Mechanics,* vol. 55, no. 2, pp. 321-334, 1996.

[9] D. G. Pavlou, G. N. Labeas, N. V. Vlachakis, and F. G. Pavlou, "Fatigue crack propagation trajectories under mixed-mode cyclic loading," *Engineering Structures,* vol. 25, no. 7, pp. 869-875, 2003.

[10] J. M. Alegre and I. I. Cuesta, "Some aspects about the crack growth FEM simulations under mixed-mode loading," *International Journal of Fatigue,* vol. 32, no. 7, pp. 1090-1095, 2010.

[11] *ANSYS® Academic Research Mechanical, Release 19.2, Help System, Coupled Field Analysis Guide, ANSYS, Inc.* [Online]. Available.
[12] Q. Han, Y. Wang, Y. Yin, and D. Wang, "Determination of stress intensity factor for mode I fatigue crack based on finite element analysis," *Engineering Fracture Mechanics,* vol. 138, pp. 118-126, 2015.
[13] C. Shih, B. Moran, and T. Nakamura, "Energy release rate along a three-dimensional crack front in a thermally stressed body," *International Journal of Fracture,* vol. 30, no. 2, pp. 79-102, 1986.
[14] S. Wang, J. Yau, and H. Corten, "A mixed-mode crack analysis of rectilinear anisotropic solids using conservation laws of elasticity," *International Journal of Fracture,* vol. 16, no. 3, pp. 247-259, 1980.
[15] X. Cui, H. Li, G. Cheng, C. Tang, and X. Gao, "Contour integral approaches for the evaluation of stress intensity factors using displacement discontinuity method," *Engineering Analysis with Boundary Elements,* vol. 82, pp. 119-129, 2017.
[16] F. Chen and R. Shield, "Conservation laws in elasticity of the J-integral type," *Journal of Applied Mathematics and Physics / Journal de Mathématiques et de Physique appliquées,* vol. 28, no. 1, pp. 1-22, 1977.
[17] A. E. Ismail, K. Kamarudin, and N. H. Muhd Nor, *Stress Intensity Factors of Slanted Cracks in Bi-Material Plates*. 2017, p. 012043.
[18] P. Judt and A. Ricoeur, "Consistent application of path-independent interaction integrals to arbitrary curved crack faces," *Archive of Applied Mechanics,* vol. 85, no. 1, pp. 13-27, 2015.
[19] R. D. Cook, *Concepts and applications of finite element analysis*, 4th ed. ed. New York: Wiley, 2002.
[20] R. S. Barsoum, "On the Use of Isoparametric Finite Elements in Linear Fracture Mechanics," *International Journal for Numerical Methods in Engineering,* vol. 10, pp. 25-37, 1976.

[21] R. D. Henshell and K. G. Shaw, "Crack Tip Finite Elements are Unnecessary," *International Journal for Numerical Methods in Engineering,* vol. 9, pp. 495-507, 1975.
[22] L. Banks-Sills and Y. Bortman, "Reappraisal of the quarter-point quadrilateral element in linear elastic fracture mechanics," *International Journal of Fracture,* vol. 25, no. 3, pp. 169-180, 1984.
[23] B. Ted, *Nonlinear Finite Elements for Continua and Structures*, Second edition. ed. United Kingdom: John Wiley & Sons Ltd, 2013.
[24] M. Stolarska, D. L. Chopp, N. Moës, and T. Belytschko, "Modelling crack growth by level sets in the extended finite element method," *International Journal for Numerical Methods in Engineering,* vol. 51, no. 8, pp. 943-960, 2001.
[25] T. P. Fries and T. Belytschko, "The extended/generalized finite element method: An overview of the method and its applications," vol. 84, ed. Chichester, UK, 2010, pp. 253-304.
[26] F. C. M. Menandro, E. T. Moyer, and H. Liebowitz, "A near optimal crack tip mesh," *Engineering Fracture Mechanics,* vol. 50, no. 5, pp. 703-711, 1995.
[27] Z. Fang, A. Li, H. Bao, and H. Wang, "Calculation of stress intensity factor in two-dimensional cracks by strain energy density factor procedure," *Science China Technological Sciences,* vol. 61, no. 4, pp. 542-550, 2018.
[28] F. L. Stazi, E. Budyn, J. Chessa, and T. Belytschko, "An extended finite element method with higher-order elements for curved cracks," *Computational Mechanics,* vol. 31, no. 1, pp. 38-48, 2003.
[29] R. Zhong Liang, Z. Chuan Rui, Y. Zhang, and H. Zhao, *M-integral for Stress Intensity Factor Base on XFEM*. 2019.

Chapter 6 Appendix

The appendix will have 4 sections, where they are respectively:

A- The slanted through thickness crack with FEM
B- The slanted through thickness crack with XFEM
C- The curved crack with FEM
D- The curved crack with XFEM

When the parameters are changed, a new table will be shown called “Parameters Used” which are the initial parameters used for the results obtained. Some parameters in the “Parameters Used” will definitely be changed throughout various test matrixes. The expressions used throughout the result section of the thesis will be used in this section as well.

6.1 A

Table A 1. Parameters used 1.

Parameters Used 1	
Rows of elements	2
CTSize	a/8
RRAT	0,5
LESIZE crack surface lines	Length of outer edge row element
a	1,3454
tiptofirst	a/4
Crack opening	a/200
NDIV Square lines	40
NDIV Connection lines	40
Inner square size	10x10
Outer square size	20x20
Contours	3-8
Rows	Traditional

Table A 2. Results from size testing of the outer square.

Height=width	KI	KII	KI% ERROR	KII%ERROR
20	116,19	103,98	2,30 %	1,71 %
50	114	102,48	0,37 %	0,24 %
100	113,69	102,26	0,10 %	0,03 %
200	113,61	102,21	0,03 %	-0,02 %
300	113,59	102,2	0,01 %	-0,03 %
400	113,59	102,19	0,01 %	-0,04 %
500	113,59	102,19	0,01 %	-0,04 %
600	113,59	102,19	0,01 %	-0,04 %
700	113,58	102,19	0,00 %	-0,04 %
800	113,58	102,19	0,00 %	-0,04 %

Table A 3. Results achieved for reduction of inner square size.

Elements	Height=width	KI	KII	KI% ERROR	KII%ERROR
9040	10	113,59	102,19	0,01 %	-0,04 %
8884	9	113,59	102,2	0,01 %	-0,03 %
8732	8	113,59	102,2	0,01 %	-0,03 %
8578	7	113,59	102,19	0,01 %	-0,04 %
8436	6	113,59	102,2	0,01 %	-0,03 %
8197	5	113,59	102,2	0,01 %	-0,03 %
8000	4	113,59	102,2	0,01 %	-0,03 %
7787	3	109,99	101,98	-3,16 %	-0,24 %

Table A 4. Parameters used 2.

Parameters Used 2	
Rows of elements	2
CTSize	a/8
RRAT	0,5
LESIZE crack surface lines	Length of outer edge row element
a	1,3454
tiptofirst	a/4
Crack opening	a/200
NDIV Square lines	40
NDIV Connection lines	40
Inner square size	10x10
Outer square size	400x400
Contours	3-8
Rows	Traditional

Table A 5. Reduction of number of divisions for various inner square sizes. Connection lines set to 1 division.

	Inner square size	4x4			
Elements	NDIV Square lines	KI	KII	KI% ERROR	KII%ERROR
1760	40	113,7	102,27	0,11 %	0,04 %
1238	30	113,7	102,26	0,11 %	0,03 %
751	20	108,89	96,35	-4,13 %	-5,75 %
416	10	245,53	236,28	116,17 %	131,13 %
221	1	680,64	134,48	499,26 %	31,55 %
	Inner square size	6x6			
Elements	NDIV Square lines	KI	KII	KI% ERROR	KII%ERROR
2196	40	113,59	102,2	0,01 %	-0,03 %
1586	30	113,59	102,2	0,01 %	-0,03 %
976	20	113,59	102,19	0,01 %	-0,04 %
570	10	114,26	103,05	0,60 %	0,80 %
218	1	745,41	135,17	556,29 %	32,22 %
	Inner square size	8x8			
Elements	NDIV Square lines	KI	KII	KI% ERROR	KII%ERROR
2492	40	113,59	102,19	0,01 %	-0,04 %
1844	30	113,59	102,19	0,01 %	-0,04 %
1104	20	113,59	102,19	0,01 %	-0,04 %
634	10	114,1	102,76	0,46 %	0,52 %
ERROR	1	ERROR	ERROR	#VERDI!	#VERDI!
	Inner square size	10x10			
Elements	NDIV Square lines	KI	KII	KI% ERROR	KII%ERROR
2800	40	113,59	102,19	0,01 %	-0,04 %
1909	30	113,59	102,19	0,01 %	-0,04 %
1246	20	113,58	102,19	0,00 %	-0,04 %

756	10	113,58	102,19	0,00 %	-0,04 %
241	1	626,94	76,49	451,98 %	-25,18 %
	Inner square size	10x10			
Elements	NDIV Square lines	KI	KII	KI% ERROR	KII%ERROR
756	10	113,58	102,19	0,00 %	-0,04 %
628	9	113,58	102,19	0,00 %	-0,04 %
499	8	113,58	102,18	0,00 %	-0,05 %
448	7	113,58	102,19	0,00 %	-0,04 %
431	6	140,26	131,83	23,49 %	28,95 %
355	5	166,4	154,42	46,50 %	51,05 %
334	4	289,42	155,93	154,82 %	52,53 %
234	3	556,12	97,21	389,63 %	-4,91 %
287	2	183,27	160,53	61,36 %	57,03 %
241	1	626,94	76,49	451,98 %	-25,18 %

Table A 6. Reduction of number of divisions for various inner square sizes. Connection lines set to 2 divisions.

	Inner square size	4x4			
Elements	NDIV Square lines	KI	KII	KI% ERROR	KII%ERROR
1920	40	113,58	102,19	0,00 %	-0,04 %
1358	30	113,58	102,19	0,00 %	-0,04 %
831	20	109,24	103,64	-3,82 %	1,38 %
456	10	176,39	178,75	55,30 %	74,85 %
225	1	634,69	288,74	458,80 %	182,44 %
	Inner square size	6x6			
Elements	NDIV Square lines	KI	KII	KI% ERROR	KII%ERROR
2356	40	113,59	102,2	0,01 %	-0,03 %
1706	30	113,59	102,2	0,01 %	-0,03 %
1056	20	113,58	102,19	0,00 %	-0,04 %
610	10	113,76	102,64	0,16 %	0,40 %
222	1	686,59	233,46	504,50 %	128,37 %
	Inner square size	8x8			
Elements	NDIV Square lines	KI	KII	KI% ERROR	KII%ERROR
2652	40	113,59	102,2	0,01 %	-0,03 %
1964	30	113,59	102,19	0,01 %	-0,04 %
1184	20	113,59	102,19	0,01 %	-0,04 %
674	10	113,75	102,49	0,15 %	0,25 %
ERROR	1	ERROR	ERROR	#VERDI!	#VERDI!
	Inner square size	10x10			
Elements	NDIV Square lines	KI	KII	KI% ERROR	KII%ERROR
2960	40	113,59	102,19	0,01 %	-0,04 %
2029	30	113,59	102,19	0,01 %	-0,04 %
1326	20	113,58	102,19	0,00 %	-0,04 %
796	10	113,58	102,19	0,00 %	-0,04 %
245	1	596,86	248,98	425,50 %	143,55 %
	Inner square size	10x10			
Elements	NDIV Square lines	KI	KII	KI% ERROR	KII%ERROR
796	10	113,58	102,19	0,00 %	-0,04 %
664	9	113,58	102,19	0,00 %	-0,04 %
531	8	113,58	102,18	0,00 %	-0,05 %
476	7	113,57	102,19	-0,01 %	-0,04 %
455	6	113,29	103,72	-0,26 %	1,46 %
375	5	117,34	108,75	3,31 %	6,38 %
350	4	310,07	276,61	173,00 %	170,58 %
246	3	526,63	272,56	363,66 %	166,61 %
295	2	118,93	106,07	4,71 %	3,76 %
245	1	596,86	248,98	425,50 %	143,55 %

Table A 7. Reduction of number of divisions for various inner square sizes. Connection lines set to 3 divisions.

	Inner square size	4x4			
Elements	NDIV Square lines	KI	KII	KI% ERROR	KII%ERROR
2080	40	113,59	102,19	0,01 %	-0,04 %
1478	30	113,58	102,19	0,00 %	-0,04 %
911	20	109,15	102,54	-3,90 %	0,30 %
496	10	101,72	108,17	-10,44 %	5,81 %
229	1	579,91	437,07	410,57 %	327,54 %
	Inner square size	6x6			
Elements	NDIV Square lines	KI	KII	KI% ERROR	KII%ERROR
2516	40	113,59	102,2	0,01 %	-0,03 %
1826	30	113,59	102,2	0,01 %	-0,03 %
1136	20	113,58	102,19	0,00 %	-0,04 %
650	10	113,6	102,49	0,02 %	0,25 %
226	1	643,61	392,86	466,66 %	284,29 %
	Inner square size	8x8			
Elements	NDIV Square lines	KI	KII	KI% ERROR	KII%ERROR
2812	40	113,59	102,2	0,01 %	-0,03 %
2084	30	113,59	102,19	0,01 %	-0,04 %
1264	20	113,59	102,19	0,01 %	-0,04 %
714	10	113,64	102,38	0,05 %	0,15 %
ERROR	1	ERROR	ERROR	#VERDI!	#VERDI!
	Inner square size	10x10			
Elements	NDIV Square lines	KI	KII	KI% ERROR	KII%ERROR
3120	40	113,59	102,19	0,01 %	-0,04 %
2149	30	113,59	102,19	0,01 %	-0,04 %
1406	20	113,59	102,19	0,01 %	-0,04 %
836	10	113,58	102,19	0,00 %	-0,04 %
249	1	549,85	405,25	384,11 %	296,41 %
	Inner square size	10x10			
Elements	NDIV Square lines	KI	KII	KI% ERROR	KII%ERROR
836	10	113,58	102,19	0,00 %	-0,04 %
700	9	113,58	102,19	0,00 %	-0,04 %
563	8	113,58	102,18	0,00 %	-0,05 %
504	7	113,57	102,19	-0,01 %	-0,04 %
479	6	113,17	102,9	-0,36 %	0,66 %
395	5	115,94	106,24	2,08 %	3,92 %
366	4	270,58	242,07	138,23 %	136,79 %
258	3	482,57	436,12	324,87 %	326,61 %
303	2	116,59	104,1	2,65 %	1,83 %
249	1	549,85	405,25	384,11 %	296,41 %

Table A 8. Reduction of number of divisions for various inner square sizes. Connection lines set to 4 divisions.

	Inner square size	4x4			
Elements	NDIV Square lines	KI	KII	KI% ERROR	KII%ERROR
2240	40	113,59	102,19	0,01 %	-0,04 %
1598	30	113,59	102,19	0,01 %	-0,04 %
991	20	109,26	102,01	-3,80 %	-0,22 %
536	10	102,4	105,85	-9,84 %	3,54 %
233	1	523,24	484,46	360,68 %	373,89 %
	Inner square size	6x6			
Elements	NDIV Square lines	KI	KII	KI% ERROR	KII%ERROR
2676	40	113,59	102,2	0,01 %	-0,03 %
1946	30	113,59	102,2	0,01 %	-0,03 %
1216	20	113,58	102,19	0,00 %	-0,04 %
690	10	113,53	102,41	-0,04 %	0,18 %
230	1	596,2	548,31	424,92 %	436,35 %
	Inner square size	8x8			
Elements	NDIV Square lines	KI	KII	KI% ERROR	KII%ERROR
2972	40	113,59	102,2	0,01 %	-0,03 %
2204	30	113,59	102,19	0,01 %	-0,04 %
1344	20	113,59	102,19	0,01 %	-0,04 %
754	10	113,59	102,33	0,01 %	0,10 %
ERROR	1	ERROR	ERROR	#VERDI!	#VERDI!
	Inner square size	10x10			
Elements	NDIV Square lines	KI	KII	KI% ERROR	KII%ERROR
3280	40	113,59	102,19	0,01 %	-0,04 %
2269	30	113,59	102,19	0,01 %	-0,04 %
1486	20	113,59	102,19	0,01 %	-0,04 %
876	10	113,58	102,19	0,00 %	-0,04 %
253	1	497,35	456,83	337,89 %	346,86 %
	Inner square size	10x10			
Elements	NDIV Square lines	KI	KII	KI% ERROR	KII%ERROR
876	10	113,58	102,19	0,00 %	-0,04 %
736	9	113,58	102,19	0,00 %	-0,04 %
595	8	113,58	102,18	0,00 %	-0,05 %
532	7	113,57	102,19	-0,01 %	-0,04 %
503	6	113,17	102,55	-0,36 %	0,31 %
415	5	115,33	105,07	1,54 %	2,78 %
382	4	247,57	221,86	117,97 %	117,02 %
270	3	431,33	389,91	279,76 %	281,40 %
311	2	115,51	103,2	1,70 %	0,95 %
253	1	497,35	456,83	337,89 %	346,86 %

Table A 9. Reduction of number of divisions for various inner square sizes. Connection lines set to 1 division, contours 2-5 used.

	Inner square size	4x4			
Elements	NDIV Square lines	KI	KII	KI% ERROR	KII%ERROR
1760	40	113,7	102,18	0,11 %	-0,05 %
1238	30	113,69	102,17	0,10 %	-0,06 %
751	20	113,69	102,17	0,10 %	-0,06 %
416	10	113,7	102,16	0,11 %	-0,07 %
221	1	204,26	195,36	79,84 %	91,10 %
	Inner square size	6x6			
Elements	NDIV Square lines	KI	KII	KI% ERROR	KII%ERROR
2196	40	113,59	102,11	0,01 %	-0,12 %
1586	30	113,58	102,11	0,00 %	-0,12 %
976	20	113,58	102,11	0,00 %	-0,12 %
570	10	113,58	102,11	0,00 %	-0,12 %
218	1	198,95	195,38	75,16 %	91,12 %
	Inner square size	8x8			
Elements	NDIV Square lines	KI	KII	KI% ERROR	KII%ERROR
2492	40	113,58	102,1	0,00 %	-0,13 %
1844	30	113,58	102,1	0,00 %	-0,13 %
1104	20	113,58	102,1	0,00 %	-0,13 %
634	10	113,58	102,1	0,00 %	-0,13 %
ERROR	1	ERROR	ERROR	#VERDI!	#VERDI!
	Inner square size	10x10			
Elements	NDIV Square lines	KI	KII	KI% ERROR	KII%ERROR
2800	40	113,58	102,1	0,00 %	-0,13 %
1909	30	113,58	102,1	0,00 %	-0,13 %
1246	20	113,58	102,11	0,00 %	-0,12 %
756	10	113,58	102,1	0,00 %	-0,13 %
241	1	107,04	103,87	-5,76 %	1,60 %
	Inner square size	10x10			
Elements	NDIV Square lines	KI	KII	KI% ERROR	KII%ERROR
756	10	113,58	102,1	0,00 %	-0,13 %
628	9	113,58	102,1	0,00 %	-0,13 %
499	8	113,58	102,1	0,00 %	-0,13 %
448	7	113,57	102,11	-0,01 %	-0,12 %
431	6	113,57	102,1	-0,01 %	-0,13 %
355	5	113,43	102,1	-0,13 %	-0,13 %
334	4	113,16	101,7	-0,37 %	-0,52 %
234	3	108,91	99,3	-4,11 %	-2,87 %
287	2	113,3	101,48	-0,25 %	-0,73 %
241	1	107,04	103,87	-5,76 %	1,60 %

Table A 10. Reduction of number of divisions for various inner square sizes. Connection lines set to 1 division, contours 3-6 used.

	Inner square size	4x4	Small to big	1	
Elements	NDIV Square lines	KI	KII	KI% ERROR	KII%ERROR
1760	40	113,7	102,24	0,11 %	0,01 %
1238	30	113,7	102,24	0,11 %	0,01 %
751	20	113,7	102,24	0,11 %	0,01 %
416	10	106,9	109,96	-5,88 %	7,56 %
221	1	358,4	194,44	215,55 %	90,20 %
	Inner square size	6x6			
Elements	NDIV Square lines	KI	KII	KI% ERROR	KII%ERROR
2196	40	113,59	102,17	0,01 %	-0,06 %
1586	30	113,59	102,17	0,01 %	-0,06 %
976	20	113,58	102,17	0,00 %	-0,06 %
570	10	113,59	102,17	0,01 %	-0,06 %
218	1	460,62	200,58	305,55 %	96,20 %
	Inner square size	8x8			
Elements	NDIV Square lines	KI	KII	KI% ERROR	KII%ERROR
2492	40	113,58	102,17	0,00 %	-0,06 %
1844	30	113,59	102,17	0,01 %	-0,06 %
1104	20	113,58	102,16	0,00 %	-0,07 %
634	10	113,59	102,16	0,01 %	-0,07 %
ERROR	1	ERROR	ERROR	#VERDI!	#VERDI!
	Inner square size	10x10			
Elements	NDIV Square lines	KI	KII	KI% ERROR	KII%ERROR
2800	40	113,59	102,17	0,01 %	-0,06 %
1909	30	113,58	102,17	0,00 %	-0,06 %
1246	20	113,58	102,17	0,00 %	-0,06 %
756	10	113,58	102,16	0,00 %	-0,07 %
241	1	274,62	103,6	141,79 %	1,34 %
	Inner square size	6x6			
Elements	NDIV Square lines	KI	KII	KI% ERROR	KII%ERROR
570	10	113,59	102,17	0,01 %	-0,06 %
503	9	113,59	102,16	0,01 %	-0,07 %
475	8	113,57	102,16	-0,01 %	-0,07 %
411	7	113,55	102,11	-0,03 %	-0,12 %
385	6	115,02	103	1,27 %	0,75 %
317	5	114,18	102,67	0,53 %	0,43 %
265	4	113	115,2	-0,51 %	12,69 %
242	3	121,6	114,26	7,06 %	11,77 %
241	2	112,86	107,02	-0,63 %	4,69 %
218	1	460,62	200,58	305,55 %	96,20 %
	Inner square size	8x8			
Elements	NDIV Square lines	KI	KII	KI% ERROR	KII%ERROR
634	10	113,59	102,16	0,01 %	-0,07 %
583	9	113,58	102,15	0,00 %	-0,08 %
521	8	113,59	102,15	0,01 %	-0,08 %
443	7	113,56	102,14	-0,02 %	-0,09 %
383	6	113,46	102,16	-0,11 %	-0,07 %
374	5	113,6	102,04	0,02 %	-0,19 %
314	4	164,55	157,92	44,88 %	54,48 %
297	3	118,51	111,34	4,34 %	8,91 %
233	2	180,77	118,21	59,16 %	15,63 %
ERROR	1	ERROR	ERROR	#VERDI!	#VERDI!
	Inner square size	10x10			
Elements	NDIV Square lines	KI	KII	KI% ERROR	KII%ERROR
756	10	113,58	102,16	0,00 %	-0,07 %
628	9	113,58	102,16	0,00 %	-0,07 %
499	8	113,58	102,15	0,00 %	-0,08 %
448	7	113,57	102,16	-0,01 %	-0,07 %
431	6	113,56	102,14	-0,02 %	-0,09 %
355	5	113,47	102,1	-0,10 %	-0,13 %
334	4	113,28	101,74	-0,26 %	-0,48 %
234	3	151,28	139,13	33,19 %	36,10 %
287	2	113,42	101,57	-0,14 %	-0,65 %
241	1	274,62	103,6	141,79 %	1,34 %

Table A 11. Parameters used 3.

Parameters Used 3	
Rows of elements	2
CTSize	a/8
RRAT	0,5
LESIZE crack surface lines	Length of outer edge row element
a	1,3454
tiptofirst	a/4
Crack opening	a/200
NDIV Square lines	7
NDIV Connection lines	1
Inner square size	10x10
Outer square size	400x400
Contours	3-8
Rows	Traditional

Table A 12. Initial test of the parameter tiptofirst, rows of elements set to 2.

Elements	tiptofirst	KI	KII	KI% ERROR	KII%ERROR
448	a/4	113,58	102,19	0,00 %	-0,04 %
457	a/3	113,59	102,19	0,01 %	-0,04 %
524	a/2	112,7	104,15	-0,77 %	1,88 %
458	a/1,75	114,56	102,96	0,86 %	0,71 %
487	a/1,5	113,58	102,19	0,00 %	-0,04 %
488	a/1,25	114,1	108,83	0,46 %	6,46 %
522	a/1,125	116,23	102,33	2,33 %	0,10 %

Table A 13. Adding rows of elements as tiptofirst is set to a/2.

a/2					
Elements	Rows of elements	KI	KII	KI% ERROR	KII%ERROR
524	2	112,7	104,15	-0,77 %	1,88 %
448	3	113,57	102,19	-0,01 %	-0,04 %
433	4	113,58	102,2	0,00 %	-0,03 %
430	5	113,59	102,18	0,01 %	-0,05 %
397	6	113,58	102,2	0,00 %	-0,03 %
416	7	113,59	102,18	0,01 %	-0,05 %
-	8	-	-	#VERDI!	#VERDI!

Table A 14. Adding rows of elements as tiptofirst is set to a/1.75.

a/1,75					
Elements	Rows of elements	KI	KII	KI% ERROR	KII%ERROR
458	2	114,56	102,96	0,86 %	0,71 %
439	3	113,59	102,18	0,01 %	-0,05 %
386	4	113,58	102,21	0,00 %	-0,02 %
402	5	113,58	102,19	0,00 %	-0,04 %
416	6	113,58	102,19	0,00 %	-0,04 %
464	7	113,58	102,2	0,00 %	-0,03 %
439	8	113,56	102,22	-0,02 %	-0,01 %

Table A 15. Adding rows of elements as tiptofirst is set to a/1,5.

a/1,5					
Elements	Rows of elements	KI	KII	KI% ERROR	KII%ERROR
487	2	113,58	102,19	0,00 %	-0,04 %
453	3	113,58	102,19	0,00 %	-0,04 %
395	4	113,59	102,2	0,01 %	-0,03 %
398	5	113,58	102,19	0,00 %	-0,04 %
422	6	113,57	102,2	-0,01 %	-0,03 %
423	7	113,57	102,2	-0,01 %	-0,03 %
435	8	113,59	102,18	0,01 %	-0,05 %

Table A 16. Adding rows of elements as tiptofirst is set to a/1,25.

a/1,25					
Elements	Rows of elements	KI	KII	KI% ERROR	KII%ERROR
488	2	114,1	108,83	0,46 %	6,46 %
452	3	113,58	102,21	0,00 %	-0,02 %
444	4	113,58	102,21	0,00 %	-0,02 %
392	5	113,6	102,22	0,02 %	-0,01 %
401	6	113,58	102,2	0,00 %	-0,03 %
439	7	113,57	102,1	-0,01 %	-0,13 %
448	8	113,56	102,2	-0,02 %	-0,03 %

Table A 17. Adding rows of elements as tiptofirst is set to a/1,125.

a/1,125					
Elements	Rows of elements	KI	KII	KI% ERROR	KII%ERROR
522	2	116,23	102,33	2,33 %	0,10 %
416	3	113,58	102,21	0,00 %	-0,02 %
354	4	113,57	102,17	-0,01 %	-0,06 %
380	5	113,58	102,2	0,00 %	-0,03 %
396	6	113,57	102,2	-0,01 %	-0,03 %
419	7	113,58	102,22	0,00 %	-0,01 %
440	8	113,58	102,21	0,00 %	-0,02 %

Table A 18. Changing the sizing of the crack surface lines.

Elements	LESIZE Crack surface lines	KI	KII	KI% ERROR	KII%ERROR
448	0,0981	113,58	102,19	0,00 %	-0,04 %
448	0,1	113,58	102,19	0,00 %	-0,04 %
358	0,2	114,56	102,98	0,86 %	0,73 %
334	0,3	113,57	102,23	-0,01 %	0,00 %
304	0,4	114,44	102,59	0,76 %	0,35 %
304	0,5	114,44	102,59	0,76 %	0,35 %

Table A 19. Refinement of crack tip region, with coarsening of the inner square region, with traditional rows.

Rows of elements	2				
Elements	NDIV Square lines	KI	KII	KI% ERROR	KII%ERROR
733	10	113,59	102,2	0,01 %	-0,03 %
611	9	113,58	102,2	0,00 %	-0,03 %
529	8	113,58	102,2	0,00 %	-0,03 %
488	7	114,1	108,83	0,46 %	6,46 %
435	6	119,22	103,84	4,97 %	1,57 %
Rows of elements	3				
Elements	NDIV Square lines	KI	KII	KI% ERROR	KII%ERROR
611	10	113,59	102,21	0,01 %	-0,02 %
520	9	113,58	102,21	0,00 %	-0,02 %
490	8	113,59	102,21	0,01 %	-0,02 %
452	7	113,58	102,21	0,00 %	-0,02 %
422	6	113,6	102,2	0,02 %	-0,03 %
Rows of elements	4				
Elements	NDIV Square lines	KI	KII	KI% ERROR	KII%ERROR
534	10	113,58	102,21	0,00 %	-0,02 %
550	9	113,58	102,2	0,00 %	-0,03 %
442	8	113,58	102,2	0,00 %	-0,03 %
444	7	113,58	102,21	0,00 %	-0,02 %
369	6	113,54	102,2	-0,04 %	-0,03 %
321	5	114,33	102,89	0,66 %	0,65 %
Rows of elements	5				
Elements	NDIV Square lines	KI	KII	KI% ERROR	KII%ERROR
519	10	113,58	102,2	0,00 %	-0,03 %
454	9	113,58	102,2	0,00 %	-0,03 %
427	8	113,58	102,2	0,00 %	-0,03 %
392	7	113,6	102,22	0,02 %	-0,01 %
374	6	113,57	102,22	-0,01 %	-0,01 %
360	5	113,62	102,19	0,04 %	-0,04 %
299	4	113,43	102,11	-0,13 %	-0,12 %
286	3	112,53	102,8	-0,92 %	0,56 %
Rows of elements	6				
Elements	NDIV Square lines	KI	KII	KI% ERROR	KII%ERROR
517	10	113,58	102,19	0,00 %	-0,04 %
493	9	113,58	102,2	0,00 %	-0,03 %
437	8	113,59	102,19	0,01 %	-0,04 %
401	7	113,58	102,2	0,00 %	-0,03 %
386	6	113,53	102,23	-0,04 %	0,00 %
379	5	113,53	102,17	-0,04 %	-0,06 %
346	4	113,13	100,53	-0,40 %	-1,66 %
319	3	112,48	101,24	-0,97 %	-0,97 %
Rows of elements	7				
Elements	NDIV Square lines	KI	KII	KI% ERROR	KII%ERROR
513	10	113,58	102,2	0,00 %	-0,03 %
478	9	113,58	102,2	0,00 %	-0,03 %
461	8	113,58	102,19	0,00 %	-0,04 %
439	7	113,57	102,21	-0,01 %	-0,02 %
383	6	113,56	102,2	-0,02 %	-0,03 %
372	5	113,49	102,19	-0,08 %	-0,04 %
341	4	113,1	102,33	-0,42 %	0,10 %
324	3	112,83	101,15	-0,66 %	-1,06 %
Rows of elements	8				
Elements	NDIV Square lines	KI	KII	KI% ERROR	KII%ERROR
493	10	113,57	102,2	-0,01 %	-0,03 %
480	9	113,57	102,2	-0,01 %	-0,03 %
471	8	113,57	102,2	-0,01 %	-0,03 %
448	7	113,56	102,2	-0,02 %	-0,03 %
415	6	113,62	102,15	0,04 %	-0,08 %
386	5	113,52	102,15	-0,05 %	-0,08 %
369	4	113,06	102,1	-0,46 %	-0,13 %
342	3	112,42	101,92	-1,02 %	-0,30 %

Table A 20. Refinement of crack tip region, with coarsening of the inner square region, with NEW rows.

New rows					
Rows of elements	2				
Elements	NDIV Square lines	KI	KII	KI% ERROR	KII%ERROR
774	10	113,59	102,2	0,01 %	-0,03 %
656	9	113,58	102,19	0,00 %	-0,04 %
651	8	113,59	102,19	0,01 %	-0,04 %
531	7	115,38	103,52	1,58 %	1,26 %
Rows of elements	3				
Elements	NDIV Square lines	KI	KII	KI% ERROR	KII%ERROR
619	10	113,58	102,2	0,00 %	-0,03 %
528	9	113,58	102,2	0,00 %	-0,03 %
506	8	113,58	102,2	0,00 %	-0,03 %
452	7	113,58	102,2	0,00 %	-0,03 %
417	6	113,57	102,17	-0,01 %	-0,06 %
337	5	114	110,4	0,37 %	7,99 %
Rows of elements	4				
Elements	NDIV Square lines	KI	KII	KI% ERROR	KII%ERROR
512	10	113,58	102,21	0,00 %	-0,02 %
446	9	113,58	102,21	0,00 %	-0,02 %
438	8	113,59	102,21	0,01 %	-0,02 %
377	7	113,58	102,2	0,00 %	-0,03 %
355	6	113,59	102,2	0,01 %	-0,03 %
318	5	113,53	102,12	-0,04 %	-0,11 %
297	4	117,9	105,85	3,80 %	3,54 %
Rows of elements	5				
Elements	NDIV Square lines	KI	KII	KI% ERROR	KII%ERROR
469	10	113,58	102,21	0,00 %	-0,02 %
411	9	113,58	102,21	0,00 %	-0,02 %
395	8	113,59	102,2	0,01 %	-0,03 %
391	7	113,58	102,2	0,00 %	-0,03 %
337	6	113,57	102,2	-0,01 %	-0,03 %
318	5	113,53	102,14	-0,04 %	-0,09 %
282	4	113,24	101,98	-0,30 %	-0,24 %
Circles	6				
Elements	NDIV Square lines	KI	KII	KI% ERROR	KII%ERROR
427	10	113,58	102,21	0,00 %	-0,02 %
385	9	113,56	102,21	-0,02 %	-0,02 %
365	8	113,58	102,2	0,00 %	-0,03 %
344	7	113,57	102,21	-0,01 %	-0,02 %
331	6	113,55	102,21	-0,03 %	-0,02 %
300	5	113,49	102,22	-0,08 %	-0,01 %
295	4	113,17	102,11	-0,36 %	-0,12 %
Rows of elements	7				
Elements	NDIV Square lines	KI	KII	KI% ERROR	KII%ERROR
398	10	113,57	102,2	-0,01 %	-0,03 %
377	9	113,56	102,2	-0,02 %	-0,03 %
371	8	113,58	102,21	0,00 %	-0,02 %
357	7	113,56	102,2	-0,02 %	-0,03 %
332	6	113,55	102,2	-0,03 %	-0,03 %
319	5	113,49	102,19	-0,08 %	-0,04 %
304	4	113,24	101,96	-0,30 %	-0,26 %

Table A 21. Test of various CTSizes, for various amounts of rows of elements. NEW rows.

New rows					
CTSize	a/4				
Elements	Rows of elements	KI	KII	KI% ERROR	KII%ERROR
319	2	115,71	105,94	1,88 %	3,63 %
298	3	113,22	104,75	-0,32 %	2,47 %
290	4	113,59	102,23	0,01 %	0,00 %
293	5	113,56	102,23	-0,02 %	0,00 %
CTSize	a/5				
Elements	Rows of elements	KI	KII	KI% ERROR	KII%ERROR
371	2	113,83	105,38	0,22 %	3,08 %
325	3	113,7	104,98	0,11 %	2,69 %
307	4	113,56	102,24	-0,02 %	0,01 %
296	5	113,57	102,25	-0,01 %	0,02 %
CTSize	a/6				
Elements	Rows of elements	KI	KII	KI% ERROR	KII%ERROR
433	2	113,35	105,72	-0,20 %	3,41 %
349	3	114,57	102,99	0,87 %	0,74 %
358	4	112,96	103,94	-0,55 %	1,67 %
306	5	113,59	102,22	0,01 %	-0,01 %
311	6	113,57	102,22	-0,01 %	-0,01 %
CTSize	a/7				
Elements	Rows of elements	KI	KII	KI% ERROR	KII%ERROR
451	2	113,59	102,21	0,01 %	-0,02 %
402	3	113,59	102,23	0,01 %	0,00 %
355	4	113,59	102,21	0,01 %	-0,02 %
341	5	113,59	102,21	0,01 %	-0,02 %
333	6	113,56	102,22	-0,02 %	-0,01 %
CTSize	a/8				
Elements	Rows of elements	KI	KII	KI% ERROR	KII%ERROR
531	2	115,38	103,52	1,58 %	1,26 %
452	3	113,58	102,2	0,00 %	-0,03 %
377	4	113,58	102,2	0,00 %	-0,03 %
391	5	113,58	102,2	0,00 %	-0,03 %
344	6	113,57	102,21	-0,01 %	-0,02 %
357	7	113,56	102,2	-0,02 %	-0,03 %
CTSize	a/9				
Elements	Rows of elements	KI	KII	KI% ERROR	KII%ERROR
562	2	113,58	102,18	0,00 %	-0,05 %
462	3	113,58	102,2	0,00 %	-0,03 %
449	4	113,59	102,2	0,01 %	-0,03 %
400	5	113,59	102,2	0,01 %	-0,03 %
339	6	113,57	102,21	-0,01 %	-0,02 %
346	7	113,56	102,2	-0,02 %	-0,03 %
CTSize	a/10				
Elements	Rows of elements	KI	KII	KI% ERROR	KII%ERROR
598	2	113,58	102,18	0,00 %	-0,05 %
499	3	113,57	102,15	-0,01 %	-0,08 %
457	4	113,57	102,2	-0,01 %	-0,03 %
387	5	113,57	102,2	-0,01 %	-0,03 %
373	6	113,56	102,18	-0,02 %	-0,05 %
367	7	113,56	102,21	-0,02 %	-0,02 %
CTSize	a/11				
Elements	Rows of elements	KI	KII	KI% ERROR	KII%ERROR
584	2	113,55	102,15	-0,03 %	-0,08 %
594	3	113,58	102,18	0,00 %	-0,05 %
469	4	113,59	102,19	0,01 %	-0,04 %
430	5	113,58	102,19	0,00 %	-0,04 %
394	6	113,58	102,18	0,00 %	-0,05 %
370	7	113,57	102,2	-0,01 %	-0,03 %

383	8	113,57	102,19	-0,01 %	-0,04 %
CTSize	a/12				
Elements	Rows of elements	KI	KII	KI% ERROR	KII%ERROR
695	2	113,56	102,13	-0,02 %	-0,10 %
592	3	113,58	102,17	0,00 %	-0,06 %
473	4	113,58	102,19	0,00 %	-0,04 %
452	5	113,58	102,17	0,00 %	-0,06 %
413	6	113,56	102,19	-0,02 %	-0,04 %
399	7	113,56	102,16	-0,02 %	-0,07 %
376	8	113,56	102,18	-0,02 %	-0,05 %

Table A 22. Results from contours 1-12 for the two crack tips. 4 Rows of elements and CTSize a/4. NEW rows

NEW rows								
Elements	290							
CTSize	a/4							
Rows of elements		4						
	1	2	1	2	AVG	AVG		
Contour	KI	KI	KII	KII	KI	KII	KI%	KII%
1	113,88	113,88	102,36	102,36	113,88	102,36	0,26 %	0,13 %
2	113,57	113,57	102,18	102,18	113,57	102,18	-0,01 %	-0,05 %
3	113,57	113,58	102,2	102,2	113,575	102,2	0,00 %	-0,03 %
4	113,57	113,58	102,22	102,22	113,575	102,22	0,00 %	-0,01 %
5	113,57	113,58	102,24	102,24	113,575	102,24	0,00 %	0,01 %
6	113,58	113,59	102,25	102,25	113,585	102,25	0,00 %	0,02 %
7	113,6	113,6	102,24	102,23	113,6	102,235	0,02 %	0,00 %
8	113,6	113,6	102,25	102,25	113,6	102,25	0,02 %	0,02 %
9	122,84	122,84	148,41	148,41	122,84	148,41	8,15 %	45,17 %
10	968,16	968,16	742,48	742,47	968,16	742,475	752,40 %	626,28 %
11	1122,1	1109,8	804,6	798,01	1115,95	801,305	882,52 %	683,83 %
12	2001,7	2251,4	921,05	1008,1	2126,55	964,575	1772,29 %	843,53 %

Table A 23. Results from contours 1-12 for the two crack tips. 2 Rows of elements and CTSize a/2

NEW rows								
Elements	215							
CTSize	a/2							
Rows of elements		2						
	1	2	1	2	AVG	AVG		
Contour	KI	KI	KII	KII	KI	KII	KI%	KII%
1	113,89	113,89	102,48	102,48	113,89	102,48	0,27 %	0,24 %
2	113,59	113,58	102,28	102,27	113,585	102,275	0,00 %	0,04 %
3	113,57	113,56	102,25	102,26	113,565	102,255	-0,01 %	0,02 %
4	113,6	113,57	102,27	102,26	113,585	102,265	0,00 %	0,03 %
5	113,6	113,59	102,26	102,26	113,595	102,26	0,01 %	0,03 %
6	113,6	113,59	102,28	102,27	113,595	102,275	0,01 %	0,04 %
7	127,6	127,6	157,13	157,12	127,6	157,125	12,34 %	53,70 %
8	1052,3	1052,3	793,15	793,19	1052,3	793,17	826,48 %	675,87 %
9	1075,3	1054,4	763,77	745,1	1064,85	754,435	837,53 %	637,98 %
10	1314,1	1314,1	297,06	297,05	1314,1	297,055	1056,98 %	190,58 %
11	1108,2	1108,2	94,725	94,725	1108,2	94,725	875,70 %	-7,34 %
12	1355,3	1355,3	0	0	1355,3	0	1093,26 %	-100,00 %

Table A 24. Results from contours 1-12 for the two crack tips. 2 Rows of elements and CTSize a/4 NEW rows

NEW rows								
Elements	319							
CTSize	a/4							
Rows of elements	2							
	1	2	1	2	AVG	AVG		
Contour	KI	KI	KII	KII	KI	KII	KI%	KII%
1	113,91	113,85	102,36	102,32	113,88	102,34	0,26 %	0,11 %
2	113,6	113,55	102,18	102,14	113,575	102,16	0,00 %	-0,07 %
3	113,57	113,53	102,18	102,14	113,55	102,16	-0,03 %	-0,07 %
4	113,6	113,55	102,22	102,18	113,575	102,2	0,00 %	-0,03 %
5	113,61	113,54	102,23	102,18	113,575	102,205	0,00 %	-0,02 %
6	113,59	113,59	102,26	102,15	113,59	102,205	0,01 %	-0,02 %
7	113,56	113,63	102,25	102,28	113,595	102,265	0,01 %	0,03 %
8	119,89	132,83	138,67	110,57	126,36	124,62	11,25 %	21,90 %
9	774,95	323,24	637,26	46,93	549,095	342,095	383,44 %	234,63 %
10	978,2	2185,6	703,77	959,95	1581,9	831,86	1292,76 %	713,71 %
11	1828,2	2460,2	482,66	1055,3	2144,2	768,98	1787,83 %	652,21 %
12	1355,3	1609,2	0,9991	234,16	1482,25	117,57955	1205,03 %	15,01 %

Table A 25. Results from contours 1-12 for the two crack tips. 2 Rows of elements and CTSize a/8 NEW rows

NEW rows								
Elements	531							
CTSize	a/8							
Rows of elements		2						
	1	2	1	2	AVG	AVG		
Contour	KI	KI	KII	KII	KI	KII	KI%	KII%
1	113,97	113,92	102,37	102,34	113,945	102,355	0,32 %	0,12 %
2	113,66	113,61	102,2	102,16	113,635	102,18	0,05 %	-0,05 %
3	113,54	113,53	102,1	102,08	113,535	102,09	-0,04 %	-0,14 %
4	113,59	113,55	102,18	102,14	113,57	102,16	-0,01 %	-0,07 %
5	113,59	113,56	102,2	102,18	113,575	102,19	0,00 %	-0,04 %
6	113,58	113,58	102,22	102,2	113,58	102,21	0,00 %	-0,02 %
7	113,59	113,58	102,21	102,22	113,585	102,215	0,00 %	-0,01 %
8	135,28	113,58	118,23	102,25	124,43	110,24	9,55 %	7,84 %
9	1172,7	106,22	481,83	122,71	639,46	302,27	463,00 %	195,68 %
10	2003,3	321,48	864,54	394,43	1162,39	629,485	923,41 %	515,75 %
11	2392,8	1945,7	1019,7	894,25	2169,25	956,975	1809,89 %	836,10 %
12	1677,8	2286,8	295,21	1025	1982,3	660,105	1645,29 %	545,71 %

Table A 26. Results from contours 1-12 for the two crack tips. 2 Rows of elements and CTSize a/16 NEW rows

NEW rows								
Elements	896							
CTSize	a/16							
Rows of elements		2						
	1	2	1	2	AVG	AVG		
Contour	KI	KI	KII	KII	KI	KII	KI%	KII%
1	113,93	113,96	102,26	102,26	113,945	102,26	0,32 %	0,03 %
2	113,62	113,65	102,1	102,09	113,635	102,095	0,05 %	-0,13 %
3	113,55	113,55	102,04	102,08	113,55	102,06	-0,03 %	-0,17 %
4	113,58	113,59	102,1	102,1	113,585	102,1	0,00 %	-0,13 %
5	113,59	113,58	102,12	102,1	113,585	102,11	0,00 %	-0,12 %
6	113,59	113,6	102,15	102,15	113,595	102,15	0,01 %	-0,08 %
7	113,59	113,58	102,16	102,18	113,585	102,17	0,00 %	-0,06 %
8	113,6	103,5	102,17	116,52	108,55	109,345	-4,43 %	6,96 %
9	113,6	209,04	102,18	332,93	161,32	217,555	42,03 %	112,81 %
10	135,98	599,56	113,12	584,18	367,77	348,65	223,80 %	241,04 %
11	351,98	1869	97,428	865,65	1110,49	481,539	877,72 %	371,03 %
12	2029,8	2289,5	944,13	1027,4	2159,65	985,765	1801,44 %	864,26 %

Table A 27. Results from contours 1-12 for the two crack tips. 8 rows of elements and CTSize a/16. NEW rows.

NEW rows								
Elements	415							
CTSize	a/16							
Rows of elements		8						
	1	2	1	2	AVG	AVG		
Contour	KI	KI	KII	KII	KI	KII	KI%	KII%
1	113,81	113,89	102,24	102,22	113,85	102,23	0,24 %	0,00 %
2	113,5	113,58	102,07	102,05	113,54	102,06	-0,04 %	-0,17 %
3	113,5	113,58	102,1	102,09	113,54	102,095	-0,04 %	-0,13 %
4	113,5	113,58	102,13	102,12	113,54	102,125	-0,04 %	-0,10 %
5	113,51	113,58	102,16	102,15	113,545	102,155	-0,03 %	-0,07 %
6	113,51	113,58	102,19	102,17	113,545	102,18	-0,03 %	-0,05 %
7	113,51	113,58	102,22	102,2	113,545	102,21	-0,03 %	-0,02 %
8	113,51	113,58	102,24	102,22	113,545	102,23	-0,03 %	0,00 %
9	113,56	113,57	102,22	102,23	113,565	102,225	-0,01 %	0,00 %
10	113,56	113,56	102,23	102,24	113,56	102,235	-0,02 %	0,00 %
11	113,56	113,59	102,22	102,23	113,575	102,225	0,00 %	0,00 %
12	113,58	113,59	102,25	102,23	113,585	102,24	0,00 %	0,01 %

Table A 28. Results from contours 1-12 for the two crack tips. 8 rows of elements and CTSize a/16. Traditional row method. RRAT 0,5

Elements	553							
CTSize	a/16							
Rows of elements		8						
	1	2	1	2	AVG	AVG		
Contour	KI	KI	KII	KII	KI	KII	KI%	KII%
1	113,88	113,91	102,23	102,23	113,895	102,23	0,28 %	0,00 %
2	113,57	113,59	102,07	102,06	113,58	102,065	0,00 %	-0,16 %
3	113,57	113,6	102,1	102,1	113,585	102,1	0,00 %	-0,13 %
4	113,57	113,6	102,13	102,12	113,585	102,125	0,00 %	-0,10 %
5	113,57	113,6	102,15	102,14	113,585	102,145	0,00 %	-0,08 %
6	113,58	113,6	102,16	102,16	113,59	102,16	0,01 %	-0,07 %
7	113,58	113,6	102,18	102,17	113,59	102,175	0,01 %	-0,05 %
8	113,58	113,61	102,19	102,18	113,595	102,185	0,01 %	-0,04 %
9	113,55	113,58	102,16	102,18	113,565	102,17	-0,01 %	-0,06 %
10	113,57	113,59	102,21	102,21	113,58	102,21	0,00 %	-0,02 %
11	113,57	113,6	102,23	102,23	113,585	102,23	0,00 %	0,00 %
12	113,56	113,63	102,23	102,25	113,595	102,24	0,01 %	0,01 %

Table A 29. Results for CTSize a/8, 8 rows of elements and radius of refined region 0,7568mm.

	Radius of refined region	0,7568							
	Elements	448							
	CTSize	a/8							
Rows of elements		8							
		1	2	1	2	AVG	AVG		
Distance	Contour	KI	KI	KII	KII	KI	KII	KI%	KII%
0,1681703	1	113,88	113,85	102,29	102,3	113,865	102,295	0,25 %	0,06 %
0,25225545	2	113,57	113,54	102,11	102,12	113,555	102,115	-0,02 %	-0,11 %
0,3363406	3	113,57	113,55	102,15	102,16	113,56	102,155	-0,02 %	-0,07 %
0,42042575	4	113,57	113,55	102,17	102,18	113,56	102,175	-0,02 %	-0,05 %
0,5045109	5	113,57	113,55	102,19	102,2	113,56	102,195	-0,02 %	-0,03 %
0,58859605	6	113,58	113,55	102,2	102,21	113,565	102,205	-0,01 %	-0,02 %
0,6726812	7	113,58	113,55	102,21	102,22	113,565	102,215	-0,01 %	-0,01 %
0,75676635	8	113,58	113,55	102,22	102,23	113,565	102,225	-0,01 %	0,00 %

Table A 30. Results for CTSize a/16, 17 rows of elements and radius of refined region 0,7568mm.

	Radius of refined region	0,7568							
	Elements	736							
	CTSize	a/16							
Rows of elements		17							
		1	2	1	2	AVG	AVG		
Distance	Contour	KI	KI	KII	KII	KI	KII	KI%	KII%
0,08408515	1	113,88	113,85	102,21	102,22	113,865	102,215	0,25 %	-0,01 %
0,12612773	2	113,56	113,54	102,05	102,06	113,55	102,055	-0,03 %	-0,17 %
0,1681703	3	113,57	113,54	102,08	102,09	113,555	102,085	-0,02 %	-0,14 %
0,21021288	4	113,57	113,54	102,11	102,12	113,555	102,115	-0,02 %	-0,11 %
0,25225545	5	113,57	113,55	102,13	102,14	113,56	102,135	-0,02 %	-0,09 %
0,29429803	6	113,57	113,55	102,14	102,15	113,56	102,145	-0,02 %	-0,08 %
0,3363406	7	113,57	113,55	102,16	102,16	113,56	102,16	-0,02 %	-0,07 %
0,37838318	8	113,57	113,55	102,17	102,18	113,56	102,175	-0,02 %	-0,05 %
0,42042575	9	113,57	113,55	102,18	102,18	113,56	102,18	-0,02 %	-0,05 %
0,46246833	10	113,57	113,55	102,18	102,19	113,56	102,185	-0,02 %	-0,04 %
0,5045109	11	113,58	113,55	102,19	102,2	113,565	102,195	-0,01 %	-0,03 %
0,54655348	12	113,58	113,55	102,2	102,21	113,565	102,205	-0,01 %	-0,02 %
0,58859605	13	113,58	113,55	102,2	102,21	113,565	102,205	-0,01 %	-0,02 %
0,63063863	14	113,58	113,55	102,21	102,22	113,565	102,215	-0,01 %	-0,01 %
0,6726812	15	113,58	113,55	102,21	102,22	113,565	102,215	-0,01 %	-0,01 %
0,71472378	16	113,58	113,55	102,21	102,22	113,565	102,215	-0,01 %	-0,01 %
0,75676635	17	113,58	113,55	102,22	102,23	113,565	102,225	-0,01 %	0,00 %

Table A 31. Results for CTSize a/32, 35 rows of elements and radius of refined region 0,7568mm.

	Radius of refined region	0,7568							
	Elements	1312							
	CTSize	a/32							
Rows of elements		35							
		1	2	1	2	AVG	AVG		
Distance	Contour	KI	KI	KII	KII	KI	KII	KI%	KII%
0,04204258	1	113,87	113,85	102,14	102,15	113,86	102,145	0,25 %	-0,08 %
0,06306386	2	113,56	113,53	101,98	101,99	113,545	101,985	-0,03 %	-0,24 %
0,08408515	3	113,56	113,54	102,01	102,02	113,55	102,015	-0,03 %	-0,21 %
0,10510644	4	113,57	113,54	102,04	102,05	113,555	102,045	-0,02 %	-0,18 %
0,12612773	5	113,57	113,54	102,06	102,07	113,555	102,065	-0,02 %	-0,16 %
0,14714901	6	113,57	113,54	102,08	102,09	113,555	102,085	-0,02 %	-0,14 %
0,1681703	7	113,57	113,54	102,09	102,1	113,555	102,095	-0,02 %	-0,13 %
0,18919159	8	113,57	113,54	102,1	102,11	113,555	102,105	-0,02 %	-0,12 %
0,21021288	9	113,57	113,54	102,11	102,12	113,555	102,115	-0,02 %	-0,11 %
0,23123416	10	113,57	113,55	102,12	102,13	113,56	102,125	-0,02 %	-0,10 %
0,25225545	11	113,57	113,55	102,13	102,14	113,56	102,135	-0,02 %	-0,09 %
0,27327674	12	113,57	113,55	102,14	102,15	113,56	102,145	-0,02 %	-0,08 %
0,29429803	13	113,57	113,55	102,15	102,16	113,56	102,155	-0,02 %	-0,07 %
0,31531931	14	113,57	113,55	102,15	102,16	113,56	102,155	-0,02 %	-0,07 %
0,3363406	15	113,57	113,55	102,16	102,17	113,56	102,165	-0,02 %	-0,06 %
0,35736189	16	113,57	113,55	102,16	102,17	113,56	102,165	-0,02 %	-0,06 %
0,37838318	17	113,57	113,55	102,17	102,18	113,56	102,175	-0,02 %	-0,05 %
0,39940446	18	113,57	113,55	102,17	102,18	113,56	102,175	-0,02 %	-0,05 %
0,42042575	19	113,57	113,55	102,18	102,19	113,56	102,185	-0,02 %	-0,04 %
0,44144704	20	113,57	113,55	102,18	102,19	113,56	102,185	-0,02 %	-0,04 %
0,46246833	21	113,57	113,55	102,18	102,19	113,56	102,185	-0,02 %	-0,04 %
0,48348961	22	113,57	113,55	102,19	102,2	113,56	102,195	-0,02 %	-0,03 %
0,5045109	23	113,58	113,55	102,19	102,2	113,565	102,195	-0,01 %	-0,03 %
0,52553219	24	113,58	113,55	102,19	102,2	113,565	102,195	-0,01 %	-0,03 %
0,54655348	25	113,58	113,55	102,2	102,21	113,565	102,205	-0,01 %	-0,02 %
0,56757476	26	113,58	113,55	102,2	102,21	113,565	102,205	-0,01 %	-0,02 %
0,58859605	27	113,58	113,55	102,2	102,21	113,565	102,205	-0,01 %	-0,02 %
0,60961734	28	113,58	113,55	102,21	102,21	113,565	102,21	-0,01 %	-0,02 %
0,63063863	29	113,58	113,55	102,21	102,22	113,565	102,215	-0,01 %	-0,01 %

0,65165991	30	113,58	113,55	102,21	102,22	113,565	102,215	-0,01 %	-0,01 %
0,6726812	31	113,58	113,55	102,21	102,22	113,565	102,215	-0,01 %	-0,01 %
0,69370249	32	113,58	113,55	102,21	102,22	113,565	102,215	-0,01 %	-0,01 %
0,71472378	33	113,58	113,55	102,22	102,22	113,565	102,22	-0,01 %	-0,01 %
0,73574507	34	113,58	113,55	102,22	102,23	113,565	102,225	-0,01 %	0,00 %
0,75676635	35	113,58	113,55	102,22	102,23	113,565	102,225	-0,01 %	0,00 %

Table A 32. Results for CTSize a/64, 71 rows of elements and radius of refined region 0,7568mm.

	Radius of refined region	0,7568							
	Elements	2464							
	CTSize	a/64							
Rows of elements		71							
		1	2	1	2	AVG	AVG		
Distance	Contour	KI	KI	KII	KII	KI	KII	KI%	KII%
0,02102129	1	113,87	113,84	102,06	102,07	113,855	102,065	0,24 %	-0,16 %
0,03153193	2	113,55	113,53	101,91	101,91	113,54	101,91	-0,04 %	-0,31 %
0,04204258	3	113,56	113,53	101,94	101,95	113,545	101,945	-0,03 %	-0,28 %
0,05255322	4	113,56	113,54	101,97	101,98	113,55	101,975	-0,03 %	-0,25 %
0,06306386	5	113,56	113,54	101,99	102	113,55	101,995	-0,03 %	-0,23 %
0,07357451	6	113,56	113,54	102,01	102,02	113,55	102,015	-0,03 %	-0,21 %
0,08408515	7	113,56	113,54	102,02	102,03	113,55	102,025	-0,03 %	-0,20 %
0,09459579	8	113,57	113,54	102,04	102,04	113,555	102,04	-0,02 %	-0,19 %
0,10510644	9	113,57	113,54	102,05	102,06	113,555	102,055	-0,02 %	-0,17 %
0,11561708	10	113,57	113,54	102,06	102,07	113,555	102,065	-0,02 %	-0,16 %
0,12612773	11	113,57	113,54	102,07	102,07	113,555	102,07	-0,02 %	-0,16 %
0,13663837	12	113,57	113,54	102,07	102,08	113,555	102,075	-0,02 %	-0,15 %
0,14714901	13	113,57	113,54	102,08	102,09	113,555	102,085	-0,02 %	-0,14 %
0,15765966	14	113,57	113,54	102,09	102,1	113,555	102,095	-0,02 %	-0,13 %
0,1681703	15	113,57	113,54	102,09	102,1	113,555	102,095	-0,02 %	-0,13 %
0,17868094	16	113,57	113,54	102,1	102,11	113,555	102,105	-0,02 %	-0,12 %
0,18919159	17	113,57	113,54	102,11	102,12	113,555	102,115	-0,02 %	-0,11 %
0,19970223	18	113,57	113,54	102,11	102,12	113,555	102,115	-0,02 %	-0,11 %
0,21021288	19	113,57	113,54	102,12	102,13	113,555	102,125	-0,02 %	-0,10 %
0,22072352	20	113,57	113,55	102,12	102,13	113,56	102,125	-0,02 %	-0,10 %
0,23123416	21	113,57	113,55	102,13	102,13	113,56	102,13	-0,02 %	-0,10 %
0,24174481	22	113,57	113,55	102,13	102,14	113,56	102,135	-0,02 %	-0,09 %
0,25225545	23	113,57	113,55	102,13	102,14	113,56	102,135	-0,02 %	-0,09 %
0,26276609	24	113,57	113,55	102,14	102,15	113,56	102,145	-0,02 %	-0,08 %
0,27327674	25	113,57	113,55	102,14	102,15	113,56	102,145	-0,02 %	-0,08 %
0,28378738	26	113,57	113,55	102,14	102,15	113,56	102,145	-0,02 %	-0,08 %
0,29429803	27	113,57	113,55	102,15	102,16	113,56	102,155	-0,02 %	-0,07 %
0,30480867	28	113,57	113,55	102,15	102,16	113,56	102,155	-0,02 %	-0,07 %
0,31531931	29	113,57	113,55	102,15	102,16	113,56	102,155	-0,02 %	-0,07 %
0,32582996	30	113,57	113,55	102,16	102,17	113,56	102,165	-0,02 %	-0,06 %
0,3363406	31	113,57	113,55	102,16	102,17	113,56	102,165	-0,02 %	-0,06 %
0,34685124	32	113,57	113,55	102,16	102,17	113,56	102,165	-0,02 %	-0,06 %
0,35736189	33	113,57	113,55	102,16	102,17	113,56	102,165	-0,02 %	-0,06 %
0,36787253	34	113,57	113,55	102,17	102,18	113,56	102,175	-0,02 %	-0,05 %
0,37838318	35	113,57	113,55	102,17	102,18	113,56	102,175	-0,02 %	-0,05 %
0,38889382	36	113,57	113,55	102,17	102,18	113,56	102,175	-0,02 %	-0,05 %
0,39940446	37	113,57	113,55	102,17	102,18	113,56	102,175	-0,02 %	-0,05 %
0,40991511	38	113,57	113,55	102,18	102,19	113,56	102,185	-0,02 %	-0,04 %
0,42042575	39	113,57	113,55	102,18	102,19	113,56	102,185	-0,02 %	-0,04 %
0,4309364	40	113,57	113,55	102,18	102,19	113,56	102,185	-0,02 %	-0,04 %
0,44144704	41	113,57	113,55	102,18	102,19	113,56	102,185	-0,02 %	-0,04 %
0,45195768	42	113,57	113,55	102,18	102,19	113,56	102,185	-0,02 %	-0,04 %
0,46246833	43	113,57	113,55	102,19	102,2	113,56	102,195	-0,02 %	-0,03 %
0,47297897	44	113,57	113,55	102,19	102,2	113,56	102,195	-0,02 %	-0,03 %
0,48348961	45	113,57	113,55	102,19	102,2	113,56	102,195	-0,02 %	-0,03 %
0,49400026	46	113,58	113,55	102,19	102,2	113,565	102,195	-0,01 %	-0,03 %
0,5045109	47	113,58	113,55	102,19	102,2	113,565	102,195	-0,01 %	-0,03 %
0,51502155	48	113,58	113,55	102,19	102,2	113,565	102,195	-0,01 %	-0,03 %
0,52553219	49	113,58	113,55	102,2	102,2	113,565	102,2	-0,01 %	-0,03 %
0,53604283	50	113,58	113,55	102,2	102,21	113,565	102,205	-0,01 %	-0,02 %

0,54655348	51	113,58	113,55	102,2	102,21	113,565	102,205	-0,01 %	-0,02 %
0,55706412	52	113,58	113,55	102,2	102,21	113,565	102,205	-0,01 %	-0,02 %
0,56757476	53	113,58	113,55	102,2	102,21	113,565	102,205	-0,01 %	-0,02 %
0,57808541	54	113,58	113,55	102,2	102,21	113,565	102,205	-0,01 %	-0,02 %
0,58859605	55	113,58	113,55	102,2	102,21	113,565	102,205	-0,01 %	-0,02 %
0,5991067	56	113,58	113,55	102,2	102,21	113,565	102,205	-0,01 %	-0,02 %
0,60961734	57	113,58	113,55	102,21	102,22	113,565	102,215	-0,01 %	-0,01 %
0,62012798	58	113,58	113,55	102,21	102,22	113,565	102,215	-0,01 %	-0,01 %
0,63063863	59	113,58	113,55	102,21	102,22	113,565	102,215	-0,01 %	-0,01 %
0,64114927	60	113,58	113,55	102,21	102,22	113,565	102,215	-0,01 %	-0,01 %
0,65165991	61	113,58	113,55	102,21	102,22	113,565	102,215	-0,01 %	-0,01 %
0,66217056	62	113,58	113,55	102,21	102,22	113,565	102,215	-0,01 %	-0,01 %
0,6726812	63	113,58	113,55	102,21	102,22	113,565	102,215	-0,01 %	-0,01 %
0,68319185	64	113,58	113,55	102,21	102,22	113,565	102,215	-0,01 %	-0,01 %
0,69370249	65	113,58	113,55	102,21	102,22	113,565	102,215	-0,01 %	-0,01 %
0,70421313	66	113,58	113,55	102,22	102,22	113,565	102,22	-0,01 %	-0,01 %
0,71472378	67	113,58	113,55	102,22	102,23	113,565	102,225	-0,01 %	0,00 %
0,72523442	68	113,58	113,55	102,22	102,23	113,565	102,225	-0,01 %	0,00 %
0,73574507	69	113,58	113,55	102,22	102,23	113,565	102,225	-0,01 %	0,00 %
0,74625571	70	113,58	113,55	102,22	102,23	113,565	102,225	-0,01 %	0,00 %
0,75676635	71	113,58	113,55	102,22	102,23	113,565	102,225	-0,01 %	0,00 %

Table A 33. Results for CTSize a/64, 100 rows of elements and radius of refined region 1,0616mm.

	Radius of refined region	1,0616							
	Elements	3347							
	CTSize	a/64							
Rows of elements		100							
		1	2	1	2	AVG	AVG		
Distance	Contour	KI	KI	KII	KII	KI	KII	KI%	KII%
0,02102129	1	113,88	113,86	102,07	102,09	113,87	102,08	0,26 %	-0,15 %
0,03153193	2	113,56	113,55	101,91	101,93	113,555	101,92	-0,02 %	-0,30 %
0,04204258	3	113,57	113,55	101,95	101,97	113,56	101,96	-0,02 %	-0,26 %
0,05255322	4	113,57	113,55	101,98	101,99	113,56	101,985	-0,02 %	-0,24 %
0,06306386	5	113,57	113,56	102	102,01	113,565	102,005	-0,01 %	-0,22 %
0,07357451	6	113,57	113,56	102,02	102,03	113,565	102,025	-0,01 %	-0,20 %
0,08408515	7	113,57	113,56	102,03	102,04	113,565	102,035	-0,01 %	-0,19 %
0,09459579	8	113,57	113,56	102,04	102,06	113,565	102,05	-0,01 %	-0,18 %
0,10510644	9	113,58	113,56	102,05	102,07	113,57	102,06	-0,01 %	-0,17 %
0,11561708	10	113,58	113,56	102,06	102,08	113,57	102,07	-0,01 %	-0,16 %
0,12612773	11	113,58	113,56	102,07	102,09	113,57	102,08	-0,01 %	-0,15 %
0,13663837	12	113,58	113,56	102,08	102,1	113,57	102,09	-0,01 %	-0,14 %
0,14714901	13	113,58	113,56	102,09	102,1	113,57	102,095	-0,01 %	-0,13 %
0,15765966	14	113,58	113,56	102,1	102,11	113,57	102,105	-0,01 %	-0,12 %
0,1681703	15	113,58	113,56	102,1	102,12	113,57	102,11	-0,01 %	-0,12 %
0,17868094	16	113,58	113,56	102,11	102,12	113,57	102,115	-0,01 %	-0,11 %
0,18919159	17	113,58	113,56	102,11	102,13	113,57	102,12	-0,01 %	-0,11 %
0,19970223	18	113,58	113,56	102,12	102,13	113,57	102,125	-0,01 %	-0,10 %
0,21021288	19	113,58	113,56	102,12	102,14	113,57	102,13	-0,01 %	-0,10 %
0,22072352	20	113,58	113,56	102,13	102,14	113,57	102,135	-0,01 %	-0,09 %
0,23123416	21	113,58	113,56	102,13	102,15	113,57	102,14	-0,01 %	-0,09 %
0,24174481	22	113,58	113,56	102,14	102,15	113,57	102,145	-0,01 %	-0,08 %
0,25225545	23	113,58	113,56	102,14	102,16	113,57	102,15	-0,01 %	-0,08 %
0,26276609	24	113,58	113,56	102,14	102,16	113,57	102,15	-0,01 %	-0,08 %
0,27327674	25	113,58	113,56	102,15	102,16	113,57	102,155	-0,01 %	-0,07 %
0,28378738	26	113,58	113,56	102,15	102,17	113,57	102,16	-0,01 %	-0,07 %
0,29429803	27	113,58	113,56	102,16	102,17	113,57	102,165	-0,01 %	-0,06 %
0,30480867	28	113,58	113,56	102,16	102,17	113,57	102,165	-0,01 %	-0,06 %
0,31531931	29	113,58	113,56	102,16	102,18	113,57	102,17	-0,01 %	-0,06 %
0,32582996	30	113,58	113,57	102,16	102,18	113,575	102,17	0,00 %	-0,06 %
0,3363406	31	113,58	113,57	102,17	102,18	113,575	102,175	0,00 %	-0,05 %
0,34685124	32	113,58	113,57	102,17	102,18	113,575	102,175	0,00 %	-0,05 %
0,35736189	33	113,58	113,57	102,17	102,19	113,575	102,18	0,00 %	-0,05 %
0,36787253	34	113,58	113,57	102,17	102,19	113,575	102,18	0,00 %	-0,05 %
0,37838318	35	113,58	113,57	102,18	102,19	113,575	102,185	0,00 %	-0,04 %

0,38889382	36	113,58	113,57	102,18	102,19	113,575	102,185	0,00 %	-0,04 %
0,39940446	37	113,58	113,57	102,18	102,2	113,575	102,19	0,00 %	-0,04 %
0,40991511	38	113,58	113,57	102,18	102,2	113,575	102,19	0,00 %	-0,04 %
0,42042575	39	113,58	113,57	102,19	102,2	113,575	102,195	0,00 %	-0,03 %
0,4309364	40	113,58	113,57	102,19	102,2	113,575	102,195	0,00 %	-0,03 %
0,44144704	41	113,58	113,57	102,19	102,2	113,575	102,195	0,00 %	-0,03 %
0,45195768	42	113,58	113,57	102,19	102,21	113,575	102,2	0,00 %	-0,03 %
0,46246833	43	113,58	113,57	102,19	102,21	113,575	102,2	0,00 %	-0,03 %
0,47297897	44	113,58	113,57	102,19	102,21	113,575	102,2	0,00 %	-0,03 %
0,48348961	45	113,58	113,57	102,2	102,21	113,575	102,205	0,00 %	-0,02 %
0,49400026	46	113,58	113,57	102,2	102,21	113,575	102,205	0,00 %	-0,02 %
0,5045109	47	113,58	113,57	102,2	102,21	113,575	102,205	0,00 %	-0,02 %
0,51502155	48	113,58	113,57	102,2	102,22	113,575	102,21	0,00 %	-0,02 %
0,52553219	49	113,58	113,57	102,2	102,22	113,575	102,21	0,00 %	-0,02 %
0,53604283	50	113,58	113,57	102,2	102,22	113,575	102,21	0,00 %	-0,02 %
0,54655348	51	113,58	113,57	102,21	102,22	113,575	102,215	0,00 %	-0,01 %
0,55706412	52	113,59	113,57	102,21	102,22	113,58	102,215	0,00 %	-0,01 %
0,56757476	53	113,59	113,57	102,21	102,22	113,58	102,215	0,00 %	-0,01 %
0,57808541	54	113,59	113,57	102,21	102,22	113,58	102,215	0,00 %	-0,01 %
0,58859605	55	113,59	113,57	102,21	102,23	113,58	102,22	0,00 %	-0,01 %
0,5991067	56	113,59	113,57	102,21	102,23	113,58	102,22	0,00 %	-0,01 %
0,60961734	57	113,59	113,57	102,21	102,23	113,58	102,22	0,00 %	-0,01 %
0,62012798	58	113,59	113,57	102,21	102,23	113,58	102,22	0,00 %	-0,01 %
0,63063863	59	113,59	113,57	102,22	102,23	113,58	102,225	0,00 %	0,00 %
0,64114927	60	113,59	113,57	102,22	102,23	113,58	102,225	0,00 %	0,00 %
0,65165991	61	113,59	113,57	102,22	102,23	113,58	102,225	0,00 %	0,00 %
0,66217056	62	113,59	113,57	102,22	102,23	113,58	102,225	0,00 %	0,00 %
0,6726812	63	113,59	113,57	102,22	102,23	113,58	102,225	0,00 %	0,00 %
0,68319185	64	113,59	113,57	102,22	102,24	113,58	102,23	0,00 %	0,00 %
0,69370249	65	113,59	113,57	102,22	102,24	113,58	102,23	0,00 %	0,00 %
0,70421313	66	113,59	113,57	102,22	102,24	113,58	102,23	0,00 %	0,00 %
0,71472378	67	113,59	113,57	102,22	102,24	113,58	102,23	0,00 %	0,00 %
0,72523442	68	113,59	113,57	102,22	102,24	113,58	102,23	0,00 %	0,00 %
0,73574507	69	113,59	113,57	102,22	102,24	113,58	102,23	0,00 %	0,00 %
0,74625571	70	113,59	113,57	102,23	102,24	113,58	102,235	0,00 %	0,00 %
0,75676635	71	113,59	113,57	102,23	102,24	113,58	102,235	0,00 %	0,00 %
0,767277	72	113,59	113,57	102,23	102,24	113,58	102,235	0,00 %	0,00 %
0,77778764	73	113,59	113,57	102,23	102,24	113,58	102,235	0,00 %	0,00 %
0,78829828	74	113,59	113,57	102,23	102,24	113,58	102,235	0,00 %	0,00 %
0,79880893	75	113,59	113,57	102,23	102,24	113,58	102,235	0,00 %	0,00 %
0,80931957	76	113,59	113,57	102,23	102,24	113,58	102,235	0,00 %	0,00 %
0,81983022	77	113,59	113,57	102,23	102,25	113,58	102,24	0,00 %	0,01 %
0,83034086	78	113,59	113,57	102,23	102,25	113,58	102,24	0,00 %	0,01 %
0,8408515	79	113,59	113,57	102,23	102,25	113,58	102,24	0,00 %	0,01 %
0,85136215	80	113,59	113,57	102,23	102,25	113,58	102,24	0,00 %	0,01 %
0,86187279	81	113,59	113,57	102,23	102,25	113,58	102,24	0,00 %	0,01 %
0,87238343	82	113,59	113,57	102,23	102,25	113,58	102,24	0,00 %	0,01 %
0,88289408	83	113,59	113,57	102,23	102,25	113,58	102,24	0,00 %	0,01 %
0,89340472	84	113,59	113,57	102,23	102,25	113,58	102,24	0,00 %	0,01 %
0,90391537	85	113,59	113,57	102,24	102,25	113,58	102,245	0,00 %	0,01 %
0,91442601	86	113,59	113,57	102,24	102,25	113,58	102,245	0,00 %	0,01 %
0,92493665	87	113,59	113,57	102,24	102,25	113,58	102,245	0,00 %	0,01 %
0,9354473	88	113,59	113,57	102,24	102,25	113,58	102,245	0,00 %	0,01 %
0,94595794	89	113,59	113,57	102,24	102,25	113,58	102,245	0,00 %	0,01 %
0,95646858	90	113,59	113,57	102,24	102,25	113,58	102,245	0,00 %	0,01 %
0,96697923	91	113,59	113,57	102,24	102,25	113,58	102,245	0,00 %	0,01 %
0,97748987	92	113,59	113,57	102,24	102,25	113,58	102,245	0,00 %	0,01 %
0,98800052	93	113,59	113,57	102,24	102,25	113,58	102,245	0,00 %	0,01 %
0,99851116	94	113,59	113,57	102,24	102,25	113,58	102,245	0,00 %	0,01 %
1,0090218	95	113,59	113,57	102,24	102,25	113,58	102,245	0,00 %	0,01 %
1,01953245	96	113,59	113,57	102,24	102,25	113,58	102,245	0,00 %	0,01 %
1,03004309	97	113,59	113,57	102,24	102,25	113,58	102,245	0,00 %	0,01 %
1,04055373	98	113,59	113,57	102,24	102,25	113,58	102,245	0,00 %	0,01 %
1,05106438	99	113,59	113,57	102,24	102,26	113,58	102,25	0,00 %	0,02 %
1,06157502	100	113,59	113,57	102,24	102,26	113,58	102,25	0,00 %	0,02 %

Table A 34. CTSize a/4, 4 rows of elements, radius 0,9029. NEW.

New rows	Radius of refined region	0,9029							
	Elements	290							
	CTSize	a/4							
Rows of elements		4							
		1	2	1	2	AVG	AVG		
Distance	Contour	KI	KI	KII	KII	KI	KII	KI%	KII%
0,3363406	1	113,88	113,88	102,36	102,36	113,88	102,36	0,26 %	0,13 %
0,46744533	2	113,57	113,57	102,18	102,18	113,57	102,18	-0,01 %	-0,05 %
0,64965436	3	113,57	113,58	102,2	102,2	113,575	102,2	0,00 %	-0,03 %
0,90288802	4	113,57	113,58	102,22	102,22	113,575	102,22	0,00 %	-0,01 %

Table A 35. CTSize a/8, 6 rows of elements, radius 0,872. NEW.

New rows	Radius of refined region	0,872							
	Elements	344							
	CTSize	a/8							
Rows of elements		6							
		1	2	1	2	AVG	AVG		
Distance	Contour	KI	KI	KII	KII	KI	KII	KI%	KII%
0,1681703	1	113,87	113,88	102,32	102,31	113,875	102,315	0,26 %	0,08 %
0,23372267	2	113,56	113,57	102,14	102,13	113,565	102,135	-0,01 %	-0,09 %
0,32482718	3	113,56	113,57	102,17	102,16	113,565	102,165	-0,01 %	-0,06 %
0,45144401	4	113,56	113,58	102,2	102,19	113,57	102,195	-0,01 %	-0,03 %
0,62741577	5	113,56	113,58	102,22	102,21	113,57	102,215	-0,01 %	-0,01 %
0,87198088	6	113,56	113,58	102,24	102,23	113,57	102,235	-0,01 %	0,00 %

Table A 36. CTSize a/16, 6 rows of elements, radius 0,8421. NEW.

New rows	Radius of refined region	0,8421							
	Elements	415							
	CTSize	a/16							
Rows of elements		8							
		1	2	1	2	AVG	AVG		
Distance	Contour	KI	KI	KII	KII	KI	KII	KI%	KII%
0,08408515	1	113,81	113,89	102,24	102,22	113,85	102,23	0,24 %	0,00 %
0,11686133	2	113,5	113,58	102,07	102,05	113,54	102,06	-0,04 %	-0,17 %
0,16241359	3	113,5	113,58	102,1	102,09	113,54	102,095	-0,04 %	-0,13 %
0,22572201	4	113,5	113,58	102,13	102,12	113,54	102,125	-0,04 %	-0,10 %
0,31370788	5	113,51	113,58	102,16	102,15	113,545	102,155	-0,03 %	-0,07 %
0,43599044	6	113,51	113,58	102,19	102,17	113,545	102,18	-0,03 %	-0,05 %
0,60593843	7	113,51	113,58	102,22	102,2	113,545	102,21	-0,03 %	-0,02 %
0,84213172	8	113,51	113,58	102,24	102,22	113,545	102,23	-0,03 %	0,00 %

Table A 37. CTSize a/32, 10 rows of elements, radius 0,8133. NEW.

New rows	Radius of refined region	0,8133							
	Elements	475							
	CTSize	a/32							
Rows of elements		10							
		1	2	1	2	AVG	AVG		
Distance	Contour	KI	KI	KII	KII	KI	KII	KI%	KII%
0,04204258	1	113,89	113,88	102,17	102,15	113,885	102,16	0,27 %	-0,07 %
0,05843067	2	113,58	113,57	102	101,99	113,575	101,995	0,00 %	-0,23 %
0,0812068	3	113,58	113,57	102,04	102,02	113,575	102,03	0,00 %	-0,20 %
0,112861	4	113,58	113,57	102,07	102,05	113,575	102,06	0,00 %	-0,17 %
0,15685394	5	113,58	113,57	102,1	102,09	113,575	102,095	0,00 %	-0,13 %
0,21799522	6	113,58	113,57	102,13	102,12	113,575	102,125	0,00 %	-0,10 %
0,30296921	7	113,58	113,57	102,16	102,15	113,575	102,155	0,00 %	-0,07 %
0,42106586	8	113,58	113,57	102,19	102,18	113,575	102,185	0,00 %	-0,04 %
0,58519629	9	113,58	113,57	102,22	102,2	113,575	102,21	0,00 %	-0,02 %
0,81330435	10	113,59	113,57	102,24	102,22	113,58	102,23	0,00 %	0,00 %

Table A 38. CTSize a/64, 12 rows of elements, radius 0,7855. NEW.

New rows	Radius of refined region	0,7855							
	Elements	538							
	CTSize	a/64							
Rows of elements		12							
		1	2	1	2	AVG	AVG		
Distance	Contour	KI	KI	KII	KII	KI	KII	KI%	KII%
0,02102129	1	113,86	113,88	102,08	102,08	113,87	102,08	0,26 %	-0,15 %
0,02921533	2	113,55	113,56	101,92	101,92	113,555	101,92	-0,02 %	-0,30 %
0,0406034	3	113,55	113,56	101,96	101,95	113,555	101,955	-0,02 %	-0,27 %
0,0564305	4	113,55	113,57	101,99	101,98	113,56	101,985	-0,02 %	-0,24 %
0,07842697	5	113,55	113,57	102,02	102,02	113,56	102,02	-0,02 %	-0,21 %
0,10899761	6	113,55	113,57	102,06	102,05	113,56	102,055	-0,02 %	-0,17 %
0,15148461	7	113,56	113,57	102,09	102,08	113,565	102,085	-0,01 %	-0,14 %
0,21053293	8	113,56	113,57	102,12	102,11	113,565	102,115	-0,01 %	-0,11 %
0,29259815	9	113,56	113,57	102,15	102,14	113,565	102,145	-0,01 %	-0,08 %
0,40665218	10	113,56	113,57	102,18	102,17	113,565	102,175	-0,01 %	-0,05 %
0,56516419	11	113,56	113,57	102,2	102,19	113,565	102,195	-0,01 %	-0,03 %
0,78546378	12	113,56	113,57	102,22	102,22	113,565	102,22	-0,01 %	-0,01 %

Table A 39. CTSize a/128, 14 rows of elements, radius 0,7586. NEW.

New rows	Radius of refined region	0,7586							
	Elements	612							
	CTSize	a/128							
Rows of elements		14							
		1	2	1	2	AVG	AVG		
Distance	Contour	KI	KI	KII	KII	KI	KII	KI%	KII%
0,01051064	1	113,89	113,9	102,03	102,05	113,895	102,04	0,28 %	-0,19 %
0,01460767	2	113,58	113,59	101,87	101,89	113,585	101,88	0,00 %	-0,34 %
0,0203017	3	113,58	113,59	101,9	101,92	113,585	101,91	0,00 %	-0,31 %
0,02821525	4	113,58	113,59	101,94	101,96	113,585	101,95	0,00 %	-0,27 %
0,03921349	5	113,58	113,59	101,97	101,99	113,585	101,98	0,00 %	-0,24 %
0,0544988	6	113,58	113,59	102	102,03	113,585	102,015	0,00 %	-0,21 %
0,0757423	7	113,58	113,59	102,04	102,06	113,585	102,05	0,00 %	-0,18 %
0,10526647	8	113,58	113,59	102,07	102,09	113,585	102,08	0,00 %	-0,15 %
0,14629907	9	113,58	113,59	102,1	102,12	113,585	102,11	0,00 %	-0,12 %
0,20332609	10	113,58	113,59	102,13	102,15	113,585	102,14	0,00 %	-0,09 %
0,28258209	11	113,58	113,6	102,16	102,18	113,59	102,17	0,01 %	-0,06 %
0,39273189	12	113,59	113,6	102,19	102,21	113,595	102,2	0,01 %	-0,03 %

0,54581781	13	113,59	113,6	102,22	102,24	113,595	102,23	0,01 %	0,00 %
0,75857624	14	113,59	113,6	102,24	102,26	113,595	102,25	0,01 %	0,02 %

Table A 40. CTSize a/256, 16 rows of elements, radius 0,7326. NEW.

New rows	Radius of refined region	0,7326							
	Elements	686							
	CTSize	a/256							
Rows of elements		16							
		1	2	1	2	AVG	AVG		
Distance	Contour	KI	KI	KII	KII	KI	KII	KI%	KII%
0,00525532	1	113,92	113,87	101,95	101,95	113,895	101,95	0,28 %	-0,27 %
0,00730383	2	113,61	113,56	101,79	101,79	113,585	101,79	0,00 %	-0,43 %
0,01015085	3	113,61	113,56	101,83	101,82	113,585	101,825	0,00 %	-0,40 %
0,01410763	4	113,61	113,56	101,86	101,86	113,585	101,86	0,00 %	-0,36 %
0,01960674	5	113,61	113,56	101,9	101,89	113,585	101,895	0,00 %	-0,33 %
0,0272494	6	113,61	113,56	101,93	101,92	113,585	101,925	0,00 %	-0,30 %
0,03787115	7	113,61	113,56	101,96	101,96	113,585	101,96	0,00 %	-0,26 %
0,05263323	8	113,61	113,57	102	101,99	113,59	101,995	0,01 %	-0,23 %
0,07314954	9	113,61	113,57	102,03	102,02	113,59	102,025	0,01 %	-0,20 %
0,10166304	10	113,61	113,57	102,06	102,06	113,59	102,06	0,01 %	-0,17 %
0,14129105	11	113,62	113,57	102,09	102,09	113,595	102,09	0,01 %	-0,14 %
0,19636595	12	113,62	113,57	102,13	102,12	113,595	102,125	0,01 %	-0,10 %
0,2729089	13	113,62	113,57	102,16	102,15	113,595	102,155	0,01 %	-0,07 %
0,37928812	14	113,62	113,57	102,18	102,18	113,595	102,18	0,01 %	-0,05 %
0,52713368	15	113,62	113,57	102,21	102,2	113,595	102,205	0,01 %	-0,02 %
0,73260909	16	113,62	113,57	102,23	102,23	113,595	102,23	0,01 %	0,00 %

Table A 41. CTSize a/512, 19 rows of elements, radius 0,9833. NEW.

New rows	Radius of refined region	0,9833							
	Elements	745							
	CTSize	a/512							
Rows of elements		19							
		1	2	1	2	AVG	AVG		
Distance	Contour	KI	KI	KII	KII	KI	KII	KI%	KII%
0,00262766	1	113,81	113,82	101,91	101,84	113,815	101,875	0,21 %	-0,35 %
0,00365192	2	113,5	113,51	101,75	101,68	113,505	101,715	-0,07 %	-0,50 %
0,00507542	3	113,5	113,51	101,79	101,72	113,505	101,755	-0,07 %	-0,46 %
0,00705381	4	113,5	113,52	101,82	101,75	113,51	101,785	-0,06 %	-0,44 %
0,00980337	5	113,5	113,52	101,85	101,79	113,51	101,82	-0,06 %	-0,40 %
0,0136247	6	113,5	113,52	101,89	101,82	113,51	101,855	-0,06 %	-0,37 %
0,01893558	7	113,5	113,52	101,92	101,85	113,51	101,885	-0,06 %	-0,34 %
0,02631662	8	113,5	113,52	101,96	101,89	113,51	101,925	-0,06 %	-0,30 %
0,03657477	9	113,51	113,52	101,99	101,92	113,515	101,955	-0,06 %	-0,27 %
0,05083152	10	113,51	113,52	102,02	101,96	113,515	101,99	-0,06 %	-0,23 %
0,07064552	11	113,51	113,52	102,06	101,99	113,515	102,025	-0,06 %	-0,20 %
0,09818297	12	113,51	113,52	102,09	102,02	113,515	102,055	-0,06 %	-0,17 %
0,13645445	13	113,51	113,52	102,12	102,05	113,515	102,085	-0,06 %	-0,14 %
0,18964406	14	113,51	113,52	102,15	102,08	113,515	102,115	-0,06 %	-0,11 %
0,26356684	15	113,51	113,53	102,18	102,11	113,52	102,145	-0,05 %	-0,08 %
0,36630454	16	113,51	113,53	102,21	102,14	113,52	102,175	-0,05 %	-0,05 %
0,50908915	17	113,51	113,53	102,24	102,17	113,52	102,205	-0,05 %	-0,02 %
0,70753083	18	113,51	113,53	102,26	102,19	113,52	102,225	-0,05 %	0,00 %
0,98332459	19	113,52	113,53	102,28	102,21	113,525	102,245	-0,05 %	0,01 %

Table A 42. CTSize a/1024, 21 rows of elements, radius 0,9497. NEW.

New rows	Radius of refined region	0,9497							
	Elements	827							
	CTSize	a/1024							
Rows of elements		21							
		1	2	1	2	AVG	AVG		
Distance	Contour	KI	KI	KII	KII	KI	KII	KI%	KII%
0,00131383	1	113,86	113,87	101,8	101,79	113,865	101,795	0,25 %	-0,43 %
0,00182596	2	113,55	113,56	101,64	101,64	113,555	101,64	-0,02 %	-0,58 %
0,00253771	3	113,55	113,56	101,67	101,67	113,555	101,67	-0,02 %	-0,55 %
0,00352691	4	113,55	113,56	101,71	101,7	113,555	101,705	-0,02 %	-0,51 %
0,00490169	5	113,55	113,56	101,74	101,74	113,555	101,74	-0,02 %	-0,48 %
0,00681235	6	113,55	113,56	101,78	101,77	113,555	101,775	-0,02 %	-0,45 %
0,00946779	7	113,55	113,56	101,81	101,81	113,555	101,81	-0,02 %	-0,41 %
0,01315831	8	113,55	113,56	101,84	101,84	113,555	101,84	-0,02 %	-0,38 %
0,01828738	9	113,56	113,56	101,88	101,87	113,56	101,875	-0,02 %	-0,35 %
0,02541576	10	113,56	113,56	101,91	101,91	113,56	101,91	-0,02 %	-0,31 %
0,03532276	11	113,56	113,57	101,95	101,94	113,565	101,945	-0,01 %	-0,28 %
0,04909149	12	113,56	113,57	101,98	101,98	113,565	101,98	-0,01 %	-0,24 %
0,06822723	13	113,56	113,57	102,01	102,01	113,565	102,01	-0,01 %	-0,22 %
0,09482203	14	113,56	113,57	102,05	102,04	113,565	102,045	-0,01 %	-0,18 %
0,13178342	15	113,56	113,57	102,08	102,07	113,565	102,075	-0,01 %	-0,15 %
0,18315227	16	113,56	113,57	102,11	102,1	113,565	102,105	-0,01 %	-0,12 %
0,25454457	17	113,56	113,57	102,14	102,14	113,565	102,14	-0,01 %	-0,09 %
0,35376542	18	113,56	113,57	102,17	102,16	113,565	102,165	-0,01 %	-0,06 %
0,4916623	19	113,57	113,57	102,2	102,19	113,57	102,195	-0,01 %	-0,03 %
0,68331104	20	113,57	113,57	102,22	102,21	113,57	102,215	-0,01 %	-0,01 %
0,94966399	21	113,57	113,58	102,24	102,23	113,575	102,235	0,00 %	0,00 %

Table A 43. CTSize a/2048, 23 rows of elements, radius 0,9172. NEW.

New rows	Radius of refined region	0,9172							
	Elements	874							
	CTSize	a/2048							
Rows of elements		23							
		1	2	1	2	AVG	AVG		
Distance	Contour	KI	KI	KII	KII	KI	KII	KI%	KII%
0,00065692	1	113,83	113,82	101,73	101,73	113,825	101,73	0,22 %	-0,49 %
0,00091298	2	113,52	113,51	101,57	101,57	113,515	101,57	-0,06 %	-0,65 %
0,00126886	3	113,52	113,51	101,6	101,6	113,515	101,6	-0,06 %	-0,62 %
0,00176345	4	113,52	113,51	101,64	101,64	113,515	101,64	-0,06 %	-0,58 %
0,00245084	5	113,52	113,51	101,67	101,67	113,515	101,67	-0,06 %	-0,55 %
0,00340618	6	113,52	113,51	101,71	101,7	113,515	101,705	-0,06 %	-0,51 %
0,00473389	7	113,52	113,51	101,74	101,74	113,515	101,74	-0,06 %	-0,48 %
0,00657915	8	113,52	113,51	101,77	101,77	113,515	101,77	-0,06 %	-0,45 %
0,00914369	9	113,52	113,52	101,81	101,81	113,52	101,81	-0,05 %	-0,41 %
0,01270788	10	113,53	113,52	101,84	101,84	113,525	101,84	-0,05 %	-0,38 %
0,01766138	11	113,53	113,52	101,88	101,87	113,525	101,875	-0,05 %	-0,35 %
0,02454574	12	113,53	113,52	101,91	101,91	113,525	101,91	-0,05 %	-0,31 %
0,03411361	13	113,53	113,52	101,94	101,94	113,525	101,94	-0,05 %	-0,28 %
0,04741101	14	113,53	113,52	101,98	101,98	113,525	101,98	-0,05 %	-0,24 %
0,06589171	15	113,53	113,52	102,01	102,01	113,525	102,01	-0,05 %	-0,22 %
0,09157614	16	113,53	113,52	102,04	102,04	113,525	102,04	-0,05 %	-0,19 %
0,12727229	17	113,53	113,52	102,07	102,07	113,525	102,07	-0,05 %	-0,16 %
0,17688271	18	113,53	113,52	102,11	102,11	113,525	102,11	-0,05 %	-0,12 %
0,24583115	19	113,53	113,53	102,14	102,14	113,53	102,14	-0,04 %	-0,09 %
0,34165552	20	113,53	113,53	102,17	102,17	113,53	102,17	-0,04 %	-0,06 %
0,47483199	21	113,54	113,53	102,19	102,19	113,535	102,19	-0,04 %	-0,04 %
0,65992033	22	113,54	113,53	102,22	102,22	113,535	102,22	-0,04 %	-0,01 %
0,91715563	23	113,54	113,53	102,24	102,24	113,535	102,24	-0,04 %	0,01 %

6.2 B

The dimensions of the geometry throughout XFEM testing of the crack is as was decided when FEM was applied. Meaning outer square size 400x400 and inner square size 10x10.

Table B 1. Connection lines set to 1, 5 and 15 divisions with enrichment field SING a/8 applied. Only Q4 elements.

SING a/8	Connection lines	1						5						15				
Square lines	MESH200 elements	Elements	KI	KII	KI% ERROR	KII% ERROR	MESH200 elements	Elements	KI	KII	KI% ERROR	KII% ERROR	MESH200 elements	Elements	KI	KII	KI% ERROR	KII% ERROR
25	3	725	142,49	127,71	25,45 %	24,92 %	3	1125	143,35	128,24	26,21 %	25,44 %	3	2125	144,49	129,37	27,21 %	26,55 %
35	3	1365	119,73	108,57	5,41 %	6,20 %	3	1925	120,49	109	6,08 %	6,62 %	3	3325	121,48	109,91	6,96 %	7,51 %
45	3	2205	110,96	101,56	-2,31 %	-0,66 %	3	2925	111,67	101,94	-1,68 %	-0,28 %	3	4725	112,6	102,74	-0,86 %	0,50 %
55	3	3245	110,97	101,32	-2,30 %	-0,89 %	3	4125	111,69	101,69	-1,66 %	-0,53 %	3	6325	112,63	102,45	-0,84 %	0,22 %
65	3	4485	111,39	101,5	-1,93 %	-0,71 %	3	5525	112,16	101,89	-1,25 %	-0,33 %	3	8125	113,17	102,7	-0,36 %	0,46 %
75	3	5925	111,29	101,45	-2,02 %	-0,76 %	3	7125	112,05	101,83	-1,35 %	-0,39 %	3	10125	113,04	102,63	-0,48 %	0,39 %
85	3	7565	111,24	101,47	-2,06 %	-0,74 %	3	8925	111,99	101,86	-1,40 %	-0,36 %	3	12325	112,98	102,66	-0,53 %	0,42 %
95	3	9405	111,19	101,53	-2,10 %	-0,68 %	3	10925	111,94	101,92	-1,44 %	-0,30 %	3	14725	112,92	102,72	-0,58 %	0,48 %
105	3	11445	111,18	101,15	-2,11 %	-1,06 %	3	13125	111,92	101,51	-1,46 %	-0,70 %	3	17325	112,89	102,27	-0,61 %	0,04 %
115	3	13685	111,27	101,16	-2,03 %	-1,05 %	3	15525	112,01	101,53	-1,38 %	-0,68 %	3	20125	112,97	102,29	-0,54 %	0,06 %
125	3	16125	110,29	100,68	-2,90 %	-1,52 %	3	18125	111,03	101,05	-2,25 %	-1,15 %	3	23125	111,99	101,8	-1,40 %	-0,42 %
135	3	18765	110,07	100,64	-3,09 %	-1,56 %	3	20925	110,8	101	-2,45 %	-1,20 %	3	26325	111,76	101,75	-1,60 %	-0,47 %
145	3	21605	110,06	100,57	-3,10 %	-1,62 %	3	23925	110,8	100,92	-2,45 %	-1,28 %						
155	3	24645	109,49	99,94	-3,60 %	-2,24 %	3	27125	110,22	100,29	-2,96 %	-1,90 %						
165	3	27885	109,48	100,09	-3,61 %	-2,09 %												

Table B 2. Connection lines set to 25, 35 and 45 divisions with enrichment field SING a/8 applied. Only Q4 elements.

SING a/8	Connection lines	25						35						45				
Square lines	MESH200 elements	Elements	KI	KII	KI% ERROR	KII% ERROR	MESH200 elements	Elements	KI	KII	KI% ERROR	KII% ERROR	MESH200 elements	Elements	KI	KII	KI% ERROR	KII% ERROR
	3	3125	144,94	129,86	27,61 %	27,03 %	3	4125	145,16	130,1	27,80 %	27,26 %	3	5125	145,28	130,24	27,91 %	27,40 %
25	3	4725	121,88	110,29	7,31 %	7,88 %	3	6125	122,08	110,49	7,48 %	8,08 %	3	7525	122,18	110,6	7,57 %	8,19 %
35	3	6525	112,98	103,08	-0,53 %	0,83 %	3	8325	113,16	103,25	-0,37 %	1,00 %	3	10125	113,26	103,35	-0,28 %	1,10 %
45	3	8525	113	102,78	-0,51 %	0,54 %	3	10725	113,18	102,95	-0,35 %	0,70 %	3	12925	113,28	103,04	-0,26 %	0,79 %
55	3	10725	113,57	103,05	-0,01 %	0,80 %	3	13325	113,76	103,23	0,16 %	0,98 %	3	15925	113,87	103,32	0,26 %	1,07 %
65	3	13125	113,44	102,98	-0,12 %	0,73 %	3	16125	113,63	103,15	0,04 %	0,90 %	3	19125	113,74	103,25	0,14 %	1,00 %
75	3	15725	113,38	103	-0,18 %	0,75 %	3	19125	113,57	103,18	-0,01 %	0,93 %	3	22525	113,68	103,27	0,09 %	1,02 %
85	3	18525	113,31	103,07	-0,24 %	0,82 %	3	22325	113,5	103,24	-0,07 %	0,99 %	3	26125	113,61	103,34	0,03 %	1,09 %
95	3	21525	113,28	102,6	-0,26 %	0,36 %	3	25725	113,46	102,76	-0,11 %	0,52 %	3	29925	113,57	102,85	-0,01 %	0,61 %
105	3	24725	113,35	102,61	-0,20 %	0,37 %	3	29325	113,54	102,77	-0,04 %	0,53 %						
115	3	28125	112,37	102,12	-1,07 %	-0,11 %												

Table B 3. Connection lines set to 55, 65 and 75 divisions with enrichment field SING a/8 applied. Only Q4 elements.

SING a/8	Connection lines	55						65						75				
Square lines	MESH200 elements	Elements	KI	KII	KI% ERROR	KII% ERROR	MESH200 elements	Elements	KI	KII	KI% ERROR	KII% ERROR	MESH200 elements	Elements	KI	KII	KI% ERROR	KII% ERROR
	3	6125	145,35	130,32	27,97 %	27,48 %	3	7125	145,4	130,38	28,02 %	27,54 %	3	8125	145,43	130,41	28,04 %	27,57 %
25	3	8925	122,24	110,67	7,62 %	8,26 %	3	10325	122,29	110,71	7,67 %	8,30 %	3	11725	122,31	110,74	7,69 %	8,32 %
35	3	11925	113,32	103,41	-0,23 %	1,15 %	3	13725	113,36	103,44	-0,19 %	1,18 %	3	15525	113,38	103,47	-0,18 %	1,21 %
45	3	15125	113,34	103,1	-0,21 %	0,85 %	3	17325	113,38	103,13	-0,18 %	0,88 %	3	19525	113,41	103,15	-0,15 %	0,90 %
55	3	18525	113,94	103,38	0,32 %	1,12 %	3	21125	113,98	103,42	0,35 %	1,16 %	3	23725	114	103,45	0,37 %	1,19 %
65	3	22125	113,8	103,3	0,19 %	1,05 %	3	25125	113,84	103,34	0,23 %	1,09 %	3	28125	113,87	103,37	0,26 %	1,12 %
75	3	25925	113,74	103,33	0,14 %	1,08 %	3	29325	113,78	103,37	0,18 %	1,12 %						
85	3	29925	113,67	103,4	0,08 %	1,14 %												

Table B 4. Connection lines set to 1, 5 and 15 divisions with enrichment field SING 0 applied. Only Q4 elements.

SING 0	Connection lines	1						5						15				
Square lines	MESH200 elements	Elements	KI	KII	KI% ERROR	KII% ERROR	MESH200 elements	Elements	KI	KII	KI% ERROR	KII% ERROR	MESH200 elements	Elements	KI	KII	KI% ERROR	KII% ERROR
25	3	725	142,49	127,71	25,45 %	24,92 %	3	1125	143,35	128,24	26,21 %	25,44 %	3	2125	144,48	129,37	27,21 %	26,55 %
35	3	1365	119,73	108,57	5,41 %	6,20 %	3	1925	120,49	109,01	6,08 %	6,63 %	3	3325	121,48	109,91	6,96 %	7,51 %
45	3	2205	110,96	101,56	-2,31 %	-0,66 %	3	2925	111,67	101,94	-1,68 %	-0,28 %	3	4725	112,6	102,74	-0,86 %	0,50 %
55	3	3245	110,97	101,32	-2,30 %	-0,89 %	3	4125	111,69	101,69	-1,66 %	-0,53 %	3	6325	112,63	102,45	-0,84 %	0,22 %
65	3	4485	110,97	101,22	-2,30 %	-0,99 %	3	5525	111,69	101,58	-1,66 %	-0,64 %	3	8125	112,63	102,34	-0,84 %	0,11 %
75	3	5925	110,96	101,22	-2,31 %	-0,99 %	3	7125	111,69	101,59	-1,66 %	-0,63 %	3	10125	112,64	102,35	-0,83 %	0,12 %
85	3	7565	110,96	101,27	-2,31 %	-0,94 %	3	8925	111,69	101,64	-1,66 %	-0,58 %	3	12325	112,64	102,4	-0,83 %	0,17 %
95	3	9405	110,93	101,4	-2,33 %	-0,81 %	3	10925	111,66	101,77	-1,69 %	-0,45 %	3	14725	112,62	102,56	-0,85 %	0,32 %
105	3	11445	110,99	101,05	-2,28 %	-1,15 %	3	13125	111,69	101,41	-1,66 %	-0,80 %	3	17325	112,62	102,15	-0,85 %	-0,08 %
115	3	13685	111,02	101,05	-2,25 %	-1,15 %	3	15525	111,73	101,4	-1,63 %	-0,81 %	3	20125	112,66	102,14	-0,81 %	-0,09 %
125	3	16125	111,01	100,97	-2,26 %	-1,23 %	3	18125	111,72	101,32	-1,64 %	-0,89 %	3	23125	112,65	102,05	-0,82 %	-0,18 %
135	3	18765	111,01	100,89	-2,26 %	-1,31 %	3	20925	111,72	101,24	-1,64 %	-0,97 %	3	26325	112,65	101,96	-0,82 %	-0,26 %
145	3	21605	111,01	100,82	-2,26 %	-1,38 %	3	23925	111,72	101,17	-1,64 %	-1,04 %						
155	3	24645	111,01	100,79	-2,26 %	-1,41 %	3	27125	111,72	101,13	-1,64 %	-1,08 %						
165	3	27885	111,01	100,79	-2,26 %	-1,41 %												

Table B 5. Connection lines set to 25, 35 and 45 divisions with enrichment field SING 0 applied. Only Q4 elements.

SING 0	Connection lines	25						35						45				
Square lines	MESH200 elements	Elements	KI	KII	KI% ERROR	KII% ERROR	MESH200 elements	Elements	KI	KII	KI% ERROR	KII% ERROR	MESH200 elements	Elements	KI	KII	KI% ERROR	KII% ERROR
25	3	3125	144,94	129,86	27,61 %	27,03 %	3	4125	145,16	130,1	27,80 %	27,26 %	3	5125	145,28	130,24	27,91 %	27,40 %
35	3	4725	121,88	110,29	7,31 %	7,88 %	3	6125	122,08	110,49	7,48 %	8,08 %	3	7525	122,18	110,6	7,57 %	8,19 %
45	3	6525	112,98	103,08	-0,53 %	0,83 %	3	8325	113,16	103,25	-0,37 %	1,00 %	3	10125	113,26	103,35	-0,28 %	1,10 %
55	3	8525	113	102,78	-0,51 %	0,54 %	3	10725	113,18	102,95	-0,35 %	0,70 %	3	12925	113,28	103,04	-0,26 %	0,79 %
65	3	10725	113,01	102,67	-0,50 %	0,43 %	3	13325	113,2	102,83	-0,33 %	0,59 %	3	15925	113,3	102,92	-0,25 %	0,67 %
75	3	13125	113,02	102,67	-0,49 %	0,43 %	3	16125	113,21	102,84	-0,33 %	0,60 %	3	19125	113,31	102,93	-0,24 %	0,68 %
85	3	15725	113,02	102,74	-0,49 %	0,50 %	3	19125	113,22	102,9	-0,32 %	0,66 %	3	22525	113,32	102,99	-0,23 %	0,74 %
95	3	18525	113,01	102,89	-0,50 %	0,65 %	3	22325	113,19	103,06	-0,34 %	0,81 %	3	26125	113,3	103,16	-0,25 %	0,91 %
105	3	21525	112,99	102,46	-0,52 %	0,22 %	3	25725	113,17	102,62	-0,36 %	0,38 %	3	29925	113,27	102,71	-0,27 %	0,47 %
115	3	24725	113,03	102,46	-0,48 %	0,22 %	3	29325	113,21	102,62	-0,33 %	0,38 %						
125	3	28125	113,02	102,36	-0,49 %	0,13 %												

Table B 6. Connection lines set to 55, 65 and 75 divisions with enrichment field SING 0 applied. Only Q4 elements.

SING 0	Connection lines	55						65						75				
Square lines	MESH200 elements	Elements	KI	KII	KI% ERROR	KII% ERROR	MESH200 elements	Elements	KI	KII	KI% ERROR	KII% ERROR	MESH200 elements	Elements	KI	KII	KI% ERROR	KII% ERROR
25	3	6125	145,35	130,32	27,97 %	27,48 %	3	7125	145,4	130,38	28,02 %	27,54 %	3	8125	145,43	130,41	28,04 %	27,57 %
35	3	8925	122,24	110,67	7,62 %	8,26 %	3	10325	122,29	110,71	7,67 %	8,30 %	3	11725	122,31	110,74	7,69 %	8,32 %
45	3	11925	113,32	103,41	-0,23 %	1,15 %	3	13725	113,36	103,44	-0,19 %	1,18 %	3	15525	113,38	103,47	-0,18 %	1,21 %
55	3	15125	113,34	103,1	-0,21 %	0,85 %	3	17325	113,38	103,13	-0,18 %	0,88 %	3	19525	113,41	103,15	-0,15 %	0,90 %
65	3	18525	113,36	102,98	-0,19 %	0,73 %	3	21125	113,4	103,02	-0,16 %	0,77 %	3	23725	113,43	103,04	-0,13 %	0,79 %
75	3	22125	113,38	102,99	-0,18 %	0,74 %	3	25125	113,42	103,02	-0,14 %	0,77 %	3	28125	113,44	103,05	-0,12 %	0,80 %
85	3	25925	113,38	103,05	-0,18 %	0,80 %	3	29325	113,42	103,09	-0,14 %	0,84 %						
95	3	29925	113,36	103,22	-0,19 %	0,97 %												

Table B 7. Used parameters 1.

Used parameters	
NDIV connection lines	1

Table B 8. SING a/8 for various square line divisions. Q4 + Q8. Connection lines set to 1 division.

SING	a/8					
MESH200 elements	Elements	NDIV square lines	KI	KII	KI% ERROR	KII% ERROR
3	725	25	145,53	130,53	28,13 %	27,68 %
3	1365	35	122,4	110,83	7,77 %	8,41 %
3	2205	45	113,47	103,56	-0,10 %	1,30 %
3	3245	55	113,5	103,25	-0,07 %	1,00 %
3	4485	65	114,1	103,54	0,46 %	1,28 %
3	5925	75	113,97	103,46	0,34 %	1,20 %
3	7565	85	113,9	103,49	0,28 %	1,23 %
3	9405	95	113,83	103,55	0,22 %	1,29 %
3	11445	105	113,79	103,05	0,18 %	0,80 %
3	13685	115	113,86	103,07	0,25 %	0,82 %
3	16125	125	112,88	102,58	-0,62 %	0,34 %
3	18765	135	112,65	102,52	-0,82 %	0,28 %
3	21605	145	112,63	102,42	-0,84 %	0,19 %
3	24645	155	112,05	101,76	-1,35 %	-0,46 %

Table B 9. SING a/4 for various square line divisions. Q4 + Q8. Connection lines set to 1 division.

SING	a/4					
MESH200 elements	Elements	NDIV square lines	KI	KII	KI% ERROR	KII% ERROR
3	725	25	145,53	130,35	28,13 %	27,51 %
3	1365	35	122,18	110,86	7,57 %	8,44 %
3	2205	45	114,25	103,9	0,59 %	1,63 %
3	3245	55	114,1	103,63	0,46 %	1,37 %
3	4485	65	112,83	103,09	-0,66 %	0,84 %
3	5925	75	112,2	102,93	-1,22 %	0,68 %
3	7565	85	112,06	102,61	-1,34 %	0,37 %
3	9405	95	111,93	102,46	-1,45 %	0,22 %
3	11445	105	112,18	102,1	-1,23 %	-0,13 %
3	13685	115	112,64	102,34	-0,83 %	0,11 %
3	16125	125	112,11	101,88	-1,29 %	-0,34 %
3	18765	135	112,31	102,04	-1,12 %	-0,19 %
3	21605	145	112,52	101,99	-0,93 %	-0,23 %
3	24645	155	112,14	101,71	-1,27 %	-0,51 %

Table B 10. SING a/2 for various square line divisions. Q4 +Q8. Connection lines set to 1 division.

SING	a/2					
MESH200 elements	Elements	NDIV square lines	KI	KII	KI% ERROR	KII% ERROR
3	725	25	144,07	130,27	26,84 %	27,43 %
3	1365	35	120,93	110,39	6,47 %	7,98 %
3	2205	45	112,38	102,92	-1,06 %	0,67 %
3	3245	55	112,54	102,64	-0,92 %	0,40 %
3	4485	65	111,87	102,13	-1,51 %	-0,10 %
3	5925	75	112,06	102,23	-1,34 %	0,00 %
3	7565	85	111,96	102,17	-1,43 %	-0,06 %
3	9405	95	112,06	102,24	-1,34 %	0,01 %
3	11445	105	111,83	101,47	-1,54 %	-0,74 %
3	13685	115	112,31	101,91	-1,12 %	-0,31 %
3	16125	125	112,47	101,74	-0,98 %	-0,48 %
3	18765	135	112,97	101,9	-0,54 %	-0,32 %
3	21605	145	112,86	101,85	-0,63 %	-0,37 %

Table B 11. SING a for various square line divisions. Q4 + Q8. Connection lines set to 1 division.

SING	a					
MESH200 elements	Elements	NDIV square lines	KI	KII	KI% ERROR	KII% ERROR
3	725	25	141,82	129,14	24,86 %	26,32 %
3	1365	35	120,39	109,32	6,00 %	6,94 %
3	2205	45	111,48	101,85	-1,85 %	-0,37 %
3	3245	55	111,74	101,61	-1,62 %	-0,61 %
3	4485	65	112,49	101,77	-0,96 %	-0,45 %
3	5925	75	113,05	102,04	-0,47 %	-0,19 %
3	7565	85	113,19	102,39	-0,34 %	0,16 %
3	9405	95	113,18	102,44	-0,35 %	0,21 %
3	11445	105	113,22	102,13	-0,32 %	-0,10 %
3	13685	115	113,37	102,28	-0,18 %	0,05 %
3	16125	125	113,38	102,11	-0,18 %	-0,12 %

Table B 12. SING 0 for various square line divisions. Q4 + Q8. Connection lines set to 1 division.

SING	0					
MESH200 elements	Elements	NDIV square lines	KI	KII	KI% ERROR	KII% ERROR
3	725	25	145,53	130,53	28,13 %	27,68 %
3	1365	35	122,4	110,83	7,77 %	8,41 %
3	2205	45	113,47	103,56	-0,10 %	1,30 %
3	3245	55	113,5	103,25	-0,07 %	1,00 %
3	4485	65	113,51	103,13	-0,06 %	0,88 %
3	5925	75	113,53	103,13	-0,04 %	0,88 %
3	7565	85	113,54	103,2	-0,04 %	0,95 %
3	9405	95	113,51	103,37	-0,06 %	1,12 %
3	11445	105	113,48	102,91	-0,09 %	0,67 %
3	13685	115	113,52	102,9	-0,05 %	0,66 %
3	16125	125	113,51	102,8	-0,06 %	0,56 %
3	18765	135	113,51	102,7	-0,06 %	0,46 %
3	21605	145	113,52	102,61	-0,05 %	0,37 %
3	24645	155	113,53	102,56	-0,04 %	0,32 %

Table B 13. Results for testing various singularity sizes, for a constant mesh, with NDIV square lines set to 155 divisions. Connection lines set to 1 division.

NDIV square lines	155			
ELEMENTS	24645			
MESH200 elements	3			
SING	KI	KII	KI% ERROR	KII% ERROR
a/4	112,14	101,71	-1,27 %	-0,51 %
a/5	112,03	101,72	-1,36 %	-0,50 %
a/6	112,53	102,18	-0,92 %	-0,05 %
a/7	112,2	101,97	-1,22 %	-0,25 %
a/8	112,05	101,76	-1,35 %	-0,46 %
a/9	112,65	102,36	-0,82 %	0,13 %
a/10	112,65	102,36	-0,82 %	0,13 %
a/11	113,75	102,73	0,15 %	0,49 %
a/12	113,76	102,74	0,16 %	0,50 %
a/13	113,76	102,74	0,16 %	0,50 %
a/14	113,79	102,74	0,18 %	0,50 %
a/15	113,81	102,72	0,20 %	0,48 %
a/16	113,81	102,72	0,20 %	0,48 %
a/17	113,81	102,72	0,20 %	0,48 %
a/18	113,81	102,72	0,20 %	0,48 %
a/19	113,79	102,73	0,18 %	0,49 %
a/20	113,71	102,69	0,11 %	0,45 %
a/21	113,53	102,56	-0,04 %	0,32 %
a/22	113,53	102,56	-0,04 %	0,32 %
a/23	113,53	102,56	-0,04 %	0,32 %
a/24	113,53	102,56	-0,04 %	0,32 %
a/25	113,53	102,56	-0,04 %	0,32 %
a/26	113,53	102,56	-0,04 %	0,32 %
a/27	113,53	102,56	-0,04 %	0,32 %
a/28	113,53	102,56	-0,04 %	0,32 %
a/29	113,53	102,56	-0,04 %	0,32 %
a/30	113,53	102,56	-0,04 %	0,32 %
a/31	113,53	102,56	-0,04 %	0,32 %
a/32	113,53	102,56	-0,04 %	0,32 %

Table B 14. Results for the contours 1-20. Square lines set to 125 divisions, SING 0.

NDIV square lines	125							
SING	0							
Elements	16125							
	1	2	1	2	AVG	AVG		
Contour	KI	KI	KII	KII	KI	KII	KI%	KII%
1	109,25	109,25	100,72	100,72	109,25	100,72	-3,81 %	-1,48 %
2	113,27	113,27	102,89	102,89	113,27	102,89	-0,27 %	0,65 %
3	113,44	113,44	102,78	102,78	113,44	102,78	-0,12 %	0,54 %
4	113,5	113,5	102,8	102,8	113,5	102,8	-0,07 %	0,56 %
5	113,52	113,52	102,8	102,8	113,52	102,8	-0,05 %	0,56 %
6	113,53	113,53	102,81	102,81	113,53	102,81	-0,04 %	0,57 %
7	113,54	113,54	102,81	102,81	113,54	102,81	-0,04 %	0,57 %
8	113,55	113,55	102,81	102,81	113,55	102,81	-0,03 %	0,57 %
9	113,55	113,55	102,82	102,82	113,55	102,82	-0,03 %	0,58 %
10	113,55	113,55	102,82	102,82	113,55	102,82	-0,03 %	0,58 %
11	113,55	113,55	102,82	102,82	113,55	102,82	-0,03 %	0,58 %
12	113,55	113,55	102,83	102,83	113,55	102,83	-0,03 %	0,59 %
13	113,55	113,55	102,83	102,83	113,55	102,83	-0,03 %	0,59 %
14	113,55	113,55	102,83	102,83	113,55	102,83	-0,03 %	0,59 %
15	113,55	113,55	102,83	102,83	113,55	102,83	-0,03 %	0,59 %
16	113,56	113,56	102,83	102,83	113,56	102,83	-0,02 %	0,59 %
17	113,56	113,56	102,83	102,83	113,56	102,83	-0,02 %	0,59 %

18	113,56	113,56	102,84	102,84	113,56	102,84	-0,02 %	0,60 %
19	113,56	113,56	102,84	102,84	113,56	102,84	-0,02 %	0,60 %
20	113,56	113,56	102,84	102,84	113,56	102,84	-0,02 %	0,60 %

Table B 15. Results for the contours 1-20. Square lines set to 125 divisions, SING a/8.

NDIV square lines	125							
SING	a/8							
Elements	16125							
	1	2	1	2	AVG	AVG		
Contour	KI	KI	KII	KII	KI	KII	KI%	KII%
1	103,99	103,99	101,08	101,08	103,99	101,08	-8,44 %	-1,12 %
2	111,29	111,29	102,34	102,34	111,29	102,34	-2,02 %	0,11 %
3	107,76	107,76	100,31	100,31	107,76	100,31	-5,12 %	-1,88 %
4	113,86	113,86	103,01	103,01	113,86	103,01	0,25 %	0,76 %
5	113,9	113,9	103,03	103,03	113,9	103,03	0,28 %	0,78 %
6	113,91	113,91	103,04	103,04	113,91	103,04	0,29 %	0,79 %
7	113,92	113,92	103,04	103,04	113,92	103,04	0,30 %	0,79 %
8	113,92	113,92	103,04	103,04	113,92	103,04	0,30 %	0,79 %
9	113,93	113,93	103,04	103,04	113,93	103,04	0,31 %	0,79 %
10	113,93	113,93	103,05	103,05	113,93	103,05	0,31 %	0,80 %
11	113,93	113,93	103,05	103,05	113,93	103,05	0,31 %	0,80 %
12	113,93	113,93	103,06	103,06	113,93	103,06	0,31 %	0,81 %
13	113,93	113,93	103,06	103,06	113,93	103,06	0,31 %	0,81 %
14	113,93	113,93	103,06	103,06	113,93	103,06	0,31 %	0,81 %
15	113,93	113,93	103,06	103,06	113,93	103,06	0,31 %	0,81 %
16	113,93	113,93	103,06	103,06	113,93	103,06	0,31 %	0,81 %
17	113,93	113,93	103,06	103,06	113,93	103,06	0,31 %	0,81 %
18	113,93	113,93	103,07	103,07	113,93	103,07	0,31 %	0,82 %
19	113,93	113,93	103,07	103,07	113,93	103,07	0,31 %	0,82 %
20	113,93	113,93	103,07	103,07	113,93	103,07	0,31 %	0,82 %

Table B 16. Results for the contours 1-20. Square lines set to 125 divisions, SING a/4.

NDIV square lines	125							
SING	a/4							
Elements	16125							
	1	2	1	2	AVG	AVG		
Contour	KI	KI	KII	KII	KI	KII	KI%	KII%
1	105,19	105,19	99,354	99,354	105,19	99,354	-7,39 %	-2,81 %
2	112,43	112,43	101,7	101,7	112,43	101,7	-1,01 %	-0,52 %
3	112,91	112,91	102,41	102,41	112,91	102,41	-0,59 %	0,18 %
4	108,18	108,18	98,218	98,218	108,18	98,218	-4,75 %	-3,92 %
5	109,89	109,89	101,45	101,45	109,89	101,45	-3,25 %	-0,76 %
6	113,89	113,89	103,07	103,07	113,89	103,07	0,27 %	0,82 %
7	113,9	113,9	103,08	103,08	113,9	103,08	0,28 %	0,83 %
8	113,9	113,9	103,08	103,08	113,9	103,08	0,28 %	0,83 %
9	113,9	113,9	103,08	103,08	113,9	103,08	0,28 %	0,83 %
10	113,91	113,91	103,08	103,08	113,91	103,08	0,29 %	0,83 %
11	113,91	113,91	103,09	103,09	113,91	103,09	0,29 %	0,84 %
12	113,91	113,91	103,1	103,1	113,91	103,1	0,29 %	0,85 %
13	113,91	113,91	103,1	103,1	113,91	103,1	0,29 %	0,85 %
14	113,91	113,91	103,1	103,1	113,91	103,1	0,29 %	0,85 %
15	113,91	113,91	103,1	103,1	113,91	103,1	0,29 %	0,85 %
16	113,91	113,91	103,1	103,1	113,91	103,1	0,29 %	0,85 %
17	113,91	113,91	103,1	103,1	113,91	103,1	0,29 %	0,85 %
18	113,91	113,91	103,11	103,11	113,91	103,11	0,29 %	0,86 %
19	113,91	113,91	103,11	103,11	113,91	103,11	0,29 %	0,86 %
20	113,91	113,91	103,11	103,11	113,91	103,11	0,29 %	0,86 %

Table B 17. Results for the contours 1-20. Square lines set to 125 divisions, SING a/2.

NDIV square lines	125							
SING	a/2							
Elements	16125							
	1	2	1	2	AVG	AVG		
Contour	KI	KI	KII	KII	KI	KII	KI%	KII%
1	105,56	105,56	98,677	98,677	105,56	98,677	-7,06 %	-3,48 %
2	112,86	112,86	101,12	101,12	112,86	101,12	-0,63 %	-1,09 %
3	113,32	113,32	101,74	101,74	113,32	101,74	-0,23 %	-0,48 %
4	113,25	113,25	102,28	102,28	113,25	102,28	-0,29 %	0,05 %
5	113,23	113,23	102,48	102,48	113,23	102,48	-0,31 %	0,24 %
6	113,22	113,22	102,6	102,6	113,22	102,6	-0,32 %	0,36 %
7	111,07	111,07	100,61	100,61	111,07	100,61	-2,21 %	-1,58 %
8	110,75	110,75	100,72	100,72	110,75	100,72	-2,49 %	-1,48 %
9	111,34	111,34	101,46	101,46	111,34	101,46	-1,97 %	-0,75 %
10	113,86	113,86	103,04	103,04	113,86	103,04	0,25 %	0,79 %
11	113,86	113,86	103,04	103,04	113,86	103,04	0,25 %	0,79 %
12	113,87	113,87	103,05	103,05	113,87	103,05	0,26 %	0,80 %
13	113,87	113,87	103,05	103,05	113,87	103,05	0,26 %	0,80 %
14	113,87	113,87	103,05	103,05	113,87	103,05	0,26 %	0,80 %
15	113,87	113,87	103,06	103,06	113,87	103,06	0,26 %	0,81 %
16	113,87	113,87	103,06	103,06	113,87	103,06	0,26 %	0,81 %
17	113,87	113,87	103,06	103,06	113,87	103,06	0,26 %	0,81 %
18	113,87	113,87	103,06	103,06	113,87	103,06	0,26 %	0,81 %
19	113,87	113,87	103,06	103,06	113,87	103,06	0,26 %	0,81 %
20	113,87	113,87	103,06	103,06	113,87	103,06	0,26 %	0,81 %

Table B 18. Results for the contours 1-20. Square lines set to 125 divisions, SING a.

NDIV square lines	125							
SING	a							
Elements	16125							
	1	2	1	2	AVG	AVG		
Contour	KI	KI	KII	KII	KI	KII	KI%	KII%
1	105,68	105,68	98,335	98,335	105,68	98,335	-6,96 %	-3,81 %
2	113	113	100,81	100,81	113	100,81	-0,51 %	-1,39 %
3	113,46	113,46	101,44	101,44	113,46	101,44	-0,11 %	-0,77 %
4	113,39	113,39	101,98	101,98	113,39	101,98	-0,17 %	-0,24 %
5	113,37	113,37	102,18	102,18	113,37	102,18	-0,18 %	-0,05 %
6	113,36	113,36	102,29	102,29	113,36	102,29	-0,19 %	0,06 %
7	113,36	113,36	102,36	102,36	113,36	102,36	-0,19 %	0,13 %
8	113,36	113,36	102,4	102,4	113,36	102,4	-0,19 %	0,17 %
9	113,36	113,36	102,43	102,43	113,36	102,43	-0,19 %	0,20 %
10	113,36	113,36	102,45	102,45	113,36	102,45	-0,19 %	0,22 %
11	113,36	113,36	102,46	102,46	113,36	102,46	-0,19 %	0,22 %
12	113,36	113,36	102,47	102,47	113,36	102,47	-0,19 %	0,23 %
13	111,99	111,99	101,17	101,17	111,99	101,17	-1,40 %	-1,04 %
14	111,95	111,95	101,36	101,36	111,95	101,36	-1,44 %	-0,85 %
15	111,96	111,96	101,42	101,42	111,96	101,42	-1,43 %	-0,79 %
16	111,89	111,89	101,6	101,6	111,89	101,6	-1,49 %	-0,62 %
17	112,05	112,05	101,76	101,76	112,05	101,76	-1,35 %	-0,46 %
18	113,81	113,81	102,84	102,84	113,81	102,84	0,20 %	0,60 %
19	113,79	113,79	102,87	102,87	113,79	102,87	0,18 %	0,63 %
20	113,79	113,79	102,86	102,86	113,79	102,86	0,18 %	0,62 %

6.3 C

Table C 1. Parameters used 1.

Parameters used 1	
Rows of elements	2
CTSize	a/8
RRAT	0,5
LESIZE crack surface lines	Length of outer edge row element
a	2,0823mm
Crack opening	0,02mm
NDIV Square lines	40
NDIV Connection lines	40
Inner square size	10x10
Outer square size	400x400
Rows	Traditional

Table C 2. Results obtained for contours 1-12 for the two crack tips, with the initial parameters

Elements	8438							
CTSize	a/8							
Rows of elements		2						
	1	2	1	2	AVG	AVG		
Contour	KI	KI	KII	KII	KI	KII	KI% ERROR	KII% ERROR
1	202,04	202,05	111,06	111,05	202,045	111,055	0,29 %	-0,09 %
2	201,47	201,48	111,25	111,25	201,475	111,25	0,01 %	0,08 %
3	201,47	201,47	111,53	111,52	201,47	111,525	0,01 %	0,33 %
4	201,21	201,26	111,51	111,63	201,235	111,57	-0,11 %	0,37 %
5	200,79	200,9	113,1	113,21	200,845	113,155	-0,30 %	1,79 %
6	200,47	200,65	115,24	114,99	200,56	115,115	-0,45 %	3,56 %
7	200,14	200,37	116,77	116,24	200,255	116,505	-0,60 %	4,81 %
8	199,06	198,93	119,51	119,35	198,995	119,43	-1,22 %	7,44 %
9	197,31	197,84	122,97	121,73	197,575	122,35	-1,93 %	10,07 %
10	196,26	196,7	125,11	124,06	196,48	124,585	-2,47 %	12,08 %
11	194,64	195,53	127,8	126,1	195,085	126,95	-3,16 %	14,20 %
12	193,23	193,45	130,09	129,43	193,34	129,76	-4,03 %	16,73 %

Table C 3. Results obtained for various CTSizes. Crack tip follows the arch of the crack.

Elements	CTSize	KI	KII	KI% ERROR	KII% ERROR
8438	a/8	200,56	114,55	-0,45 %	3,05 %
8524	a/9	200,8	113,6	-0,33 %	2,20 %
8825	a/10	201,06	112,75	-0,20 %	1,43 %
8889	a/11	201,2	112,33	-0,13 %	1,05 %
9056	a/12	201,3	111,94	-0,08 %	0,70 %
9084	a/13	201,35	111,65	-0,05 %	0,44 %
9383	a/14	201,4	111,48	-0,03 %	0,29 %
9510	a/15	201,42	111,24	-0,02 %	0,07 %
9846	a/16	201,44	111,18	-0,01 %	0,02 %
9837	a/17	201,47	111,01	0,00 %	-0,13 %
9902	a/18	201,48	110,95	0,01 %	-0,19 %
10339	a/19	201,49	110,85	0,01 %	-0,28 %
10381	a/20	201,5	110,82	0,02 %	-0,31 %
10526	a/21	201,5	110,82	0,02 %	-0,31 %

Table C 4. Results for the various contours for the crack tips. CTSize a/16.

Elements	9846							
CTSize	a/16							
Rows of elements	2							
	1	2	1	2	AVG	AVG		
Contour	KI	KI	KII	KII	KI	KII	KI% ERROR	KII% ERROR
1	202,05	202,05	110,9	110,9	202,05	110,9	0,29 %	-0,23 %
2	201,49	201,49	110,9	110,89	201,49	110,895	0,01 %	-0,24 %
3	201,49	201,49	111,04	111,03	201,49	111,035	0,01 %	-0,11 %
4	201,49	201,49	111,18	111,18	201,49	111,18	0,01 %	0,02 %
5	201,5	201,5	111,34	111,34	201,5	111,34	0,02 %	0,16 %
6	201,43	201,49	110,48	111,51	201,46	110,995	0,00 %	-0,15 %
7	201,38	201,39	110,65	111,07	201,385	110,86	-0,04 %	-0,27 %
8	201,34	201,3	111,77	111,53	201,32	111,65	-0,07 %	0,44 %
9	201,27	201,26	112,56	112,51	201,265	112,535	-0,10 %	1,24 %
10	201,19	201,19	113,2	113,17	201,19	113,185	-0,13 %	1,82 %
11	200,63	200,7	114,5	114,25	200,665	114,375	-0,39 %	2,89 %
12	200,5	200,6	115,31	115,02	200,55	115,165	-0,45 %	3,60 %

Table C 5. Results for the various contours for the crack tips. CTsize a/21.

Elements	10526							
CTSize	a/21							
Rows of elements	2							
	1	2	1	2	AVG	AVG		
Contour	KI	KI	KII	KII	KI	KII	KI% ERROR	KII% ERROR
1	202,06	202,05	110,83	110,83	202,055	110,83	0,30 %	-0,30 %
2	201,5	201,49	110,79	110,79	201,495	110,79	0,02 %	-0,33 %
3	201,5	201,49	110,9	110,9	201,495	110,9	0,02 %	-0,23 %
4	201,51	201,51	111,03	111,03	201,51	111,03	0,02 %	-0,12 %
5	201,5	201,51	111,15	111,15	201,505	111,15	0,02 %	-0,01 %
6	201,5	201,5	111,27	111,27	201,5	111,27	0,02 %	0,10 %
7	201,51	201,5	110,49	110,32	201,505	110,405	0,02 %	-0,68 %
8	201,5	201,49	110,28	110,09	201,495	110,185	0,02 %	-0,88 %
9	201,47	201,47	111,04	110,94	201,47	110,99	0,00 %	-0,15 %
10	201,44	201,44	111,64	111,59	201,44	111,615	-0,01 %	0,41 %
11	201,39	201,39	112,13	112,1	201,39	112,115	-0,03 %	0,86 %
12	201,11	201,23	112,64	112,57	201,17	112,605	-0,14 %	1,30 %

Table C 6. Results obtained for various CTSizes. Singularity element has the initial direction it would have if it was reduced to a point.

Elements	CTSize	KI	KII	KI% ERROR	KII% ERROR
8438	a/8	200,56	114,56	-0,45 %	3,06 %
8627	a/9	200,81	113,61	-0,32 %	2,20 %
8890	a/10	201,1	112,78	-0,18 %	1,46 %
8889	a/11	201,2	112,33	-0,13 %	1,05 %
9056	a/12	201,3	111,95	-0,08 %	0,71 %
9084	a/13	201,35	111,65	-0,05 %	0,44 %
9383	a/14	201,4	111,48	-0,03 %	0,29 %
9510	a/15	201,42	111,24	-0,02 %	0,07 %
9846	a/16	201,44	111,18	-0,01 %	0,02 %
9837	a/17	201,47	111,01	0,00 %	-0,13 %
9902	a/18	201,48	110,95	0,01 %	-0,19 %
10339	a/19	201,49	110,85	0,01 %	-0,28 %
10381	a/20	201,5	110,82	0,02 %	-0,31 %
10529	a/21	201,5	110,82	0,02 %	-0,31 %

Table C 7. Parameters Used 2.

Parameters used 2	
Rows of elements	2
CTSize	a/16
RRAT	0,5
LESIZE crack surface lines	Length of outer edge row element
a	2,0823mm
Crack opening	0,02mm
NDIV Square lines	40
NDIV Connection lines	40
Inner square size	10x10
Outer square size	400x400
Rows	Traditional

Table C 8. Plate sizing test performed using parameters defined.

a/16 outer	10x10 Elements	KI	KII	KI% ERROR	KII% ERROR
400	9846	201,44	111,18	-0,01 %	0,02 %
500	9846	201,43	111,17	-0,01 %	0,01 %
600	9846	201,43	111,17	-0,01 %	0,01 %
700	9846	201,42	111,16	-0,02 %	0,00 %
800	9846	201,42	111,16	-0,02 %	0,00 %
900	9846	201,42	111,16	-0,02 %	0,00 %
1000	9846	201,42	111,16	-0,02 %	0,00 %

Table C 9. Various inner square sizes, in combination with various outer square sizes, where the element edge length of the inner square remains constant.

NDIV Connection lines		1			
	NDIV square lines	40			
Inner	10x10				
outer	Elements	KI	KII	KI% ERROR	KII% ERROR
400	3606	201,43	111,17	-0,01 %	0,01 %
500	3606	201,42	111,16	-0,02 %	0,00 %
600	3606	201,42	111,16	-0,02 %	0,00 %
700	3606	201,42	111,16	-0,02 %	0,00 %
800	3606	201,42	111,16	-0,02 %	0,00 %
900	3606	201,42	111,16	-0,02 %	0,00 %
1000	3606	201,42	111,16	-0,02 %	0,00 %
	NDIV square lines	44			
Inner	12x12				
outer	Elements	KI	KII	KI% ERROR	KII% ERROR
400	4368	201,44	111,09	-0,01 %	-0,06 %
500	4368	201,43	111,08	-0,01 %	-0,07 %
600	4368	201,43	111,08	-0,01 %	-0,07 %
700	4368	201,43	111,08	-0,01 %	-0,07 %
800	4368	201,42	111,08	-0,02 %	-0,07 %
900	4368	201,42	111,08	-0,02 %	-0,07 %
1000	4368	201,42	111,08	-0,02 %	-0,07 %
	NDIV square lines	48			
Inner	14x14				
outer	Elements	KI	KII	KI% ERROR	KII% ERROR
400	4980	201,44	111,08	-0,01 %	-0,07 %
500	4980	201,43	111,08	-0,01 %	-0,07 %
600	4980	201,43	111,07	-0,01 %	-0,08 %
700	4980	201,42	111,07	-0,02 %	-0,08 %
800	4980	201,42	111,07	-0,02 %	-0,08 %
900	4980	201,42	111,07	-0,02 %	-0,08 %
1000	4980	201,42	111,07	-0,02 %	-0,08 %
	NDIV square lines	52			
Inner	16x16				
outer	Elements	KI	KII	KI% ERROR	KII% ERROR
400	5823	201,44	111,08	-0,01 %	-0,07 %
500	5823	201,43	111,07	-0,01 %	-0,08 %
600	5823	201,43	111,07	-0,01 %	-0,08 %
700	5823	201,43	111,07	-0,01 %	-0,08 %
800	5823	201,42	111,07	-0,02 %	-0,08 %
900	5823	201,42	111,07	-0,02 %	-0,08 %
1000	5823	201,42	111,07	-0,02 %	-0,08 %

Table C 10. Various inner square sizes, in combination with various outer square sizes, where NDIV of the square lines remains constant.

NDIV Connection lines		1			
	NDIV square lines	40			
inner	10x10				
outer	Elements	KI	KII	KI% ERROR	KII% ERROR
400	3606	201,43	111,17	-0,01 %	0,01 %
500	3606	201,42	111,16	-0,02 %	0,00 %
600	3606	201,42	111,16	-0,02 %	0,00 %
700	3606	201,42	111,16	-0,02 %	0,00 %
800	3606	201,42	111,16	-0,02 %	0,00 %
900	3606	201,42	111,16	-0,02 %	0,00 %
1000	3606	201,42	111,16	-0,02 %	0,00 %
	NDIV square lines	40			
	12x12				
outer	Elements	KI	KII	KI% ERROR	KII% ERROR
400	3843	201,43	111,14	-0,01 %	-0,02 %
500	3843	201,42	111,13	-0,02 %	-0,03 %
600	3843	201,42	111,13	-0,02 %	-0,03 %
700	3843	201,42	111,13	-0,02 %	-0,03 %
800	3843	201,42	111,13	-0,02 %	-0,03 %
900	3843	201,42	111,13	-0,02 %	-0,03 %
1000	3843	201,42	111,13	-0,02 %	-0,03 %
	NDIV square lines	40			
	14x14				
outer	Elements	KI	KII	KI% ERROR	KII% ERROR
400	4219	201,44	111,15	-0,01 %	-0,01 %
500	4219	201,43	111,14	-0,01 %	-0,02 %
600	4219	201,43	111,14	-0,01 %	-0,02 %
700	4219	201,43	111,14	-0,01 %	-0,02 %
800	4219	201,42	111,14	-0,02 %	-0,02 %
900	4219	201,42	111,14	-0,02 %	-0,02 %
1000	4219	201,42	111,13	-0,02 %	-0,03 %
	NDIV square lines	40			
	16x16				
outer	Elements	KI	KII	KI% ERROR	KII% ERROR
400	4193	201,44	111,08	-0,01 %	-0,07 %
500	4193	201,43	111,07	-0,01 %	-0,08 %
600	4193	201,43	111,07	-0,01 %	-0,08 %
700	4193	201,43	111,07	-0,01 %	-0,08 %
800	4193	201,43	111,07	-0,01 %	-0,08 %
900	4193	201,42	111,07	-0,02 %	-0,08 %
1000	4193	201,42	111,07	-0,02 %	-0,08 %

Table C 11. Results obtained as the NDIV of square lines were reduced for the various inner square sizes. Connection lines set to 1 division.

NDIV connection lines		1			
	10x10				
Elements	NDIV Square lines	KI	KII	KI% ERROR	KII% ERROR
3606	40	201,42	111,16	-0,02 %	0,00 %
2580	30	201,43	111,19	-0,01 %	0,03 %
1789	20	201,42	111,17	-0,02 %	0,01 %
971	10	201,41	111,18	-0,02 %	0,02 %
964	9	201,4	111,19	-0,03 %	0,03 %
857	8	202,63	111,57	0,58 %	0,37 %
	12x12				
Elements	NDIV Square lines	KI	KII	KI% ERROR	KII% ERROR
3843	40	201,42	111,13	-0,02 %	-0,03 %
2809	30	201,42	111,2	-0,02 %	0,04 %
1972	20	201,43	111,15	-0,01 %	-0,01 %
1060	10	201,4	111,13	-0,03 %	-0,03 %
1043	9	201,41	111,15	-0,02 %	-0,01 %
896	8	201,42	111,27	-0,02 %	0,10 %
	14x14				
Elements	NDIV Square lines	KI	KII	KI% ERROR	KII% ERROR
4219	40	201,43	111,14	-0,01 %	-0,02 %
3162	30	201,43	111,09	-0,01 %	-0,06 %
2126	20	201,43	111,19	-0,01 %	0,03 %
1206	10	201,4	111,23	-0,03 %	0,06 %
1152	9	201,4	111,26	-0,03 %	0,09 %
957	8	202,2	111,44	0,37 %	0,25 %
	16x16				
Elements	NDIV Square lines	KI	KII	KI% ERROR	KII% ERROR
4193	40	201,43	111,07	-0,01 %	-0,08 %
3104	30	201,44	111,11	-0,01 %	-0,04 %
2158	20	201,43	111,16	-0,01 %	0,00 %
1275	10	201,42	111,11	-0,02 %	-0,04 %
1101	9	201,41	111,21	-0,02 %	0,04 %
1034	8	201,4	111,13	-0,03 %	-0,03 %

Table C 12. Parameters used 3.

Parameters used 3	
Rows of elements	2
CTSize	a/16
RRAT	0,5
LESIZE crack surface lines	Length of outer edge row element
a	2,0823mm
Crack opening	0,02mm
NDIV Square lines	10
NDIV Connection lines	1
Inner square size	10x10
Outer square size	500x500
Rows	Traditional

Table C 13. Results obtained when changing the element sizes along the crack surface lines. Equal to last means 0,0761mm which is included in both tests.

Testing smaller sizes					
Elements	LESIZE crack surface lines	KI	KII	KI% ERROR	KII% ERROR
971	0,0761	201,41	111,18	-0,02 %	0,02 %
1213	0,06	201,44	110,94	-0,01 %	-0,20 %
1585	0,04	201,53	111,07	0,03 %	-0,08 %
2593	0,02	201,49	110,81	0,01 %	-0,31 %
5117	0,01	201,5	110,45	0,02 %	-0,64 %
Testing larger sizes					
Elements	LESIZE crack surface lines	KI	KII	KI% ERROR	KII% ERROR
971	0,0761	201,41	111,18	-0,02 %	0,02 %
1058	0,08	201,4	111,23	-0,03 %	0,06 %
826	0,1	201,3	111,65	-0,08 %	0,44 %
740	0,12	201,2	112,15	-0,13 %	0,89 %
684	0,14	201,07	112,67	-0,19 %	1,36 %
667	0,16	200,9	113,27	-0,28 %	1,90 %
542	0,18	200,68	113,94	-0,39 %	2,50 %
550	0,2	200,37	114,81	-0,54 %	3,28 %

Table C 14. Parameters used 4.

Parameters used 4	
Rows of elements	2
CTSize	a/16
RRAT	0,5
LESIZE crack surface lines	0,2mm
a	2,0823mm
Crack opening	0,02mm
NDIV Square lines	10
NDIV Connection lines	1
Inner square size	10x10
Outer square size	500x500
Rows	Traditional

Table C 15. Increasing rows of elements surrounding the crack tip. Traditional rows.

RRAT	0,5				
Elements	Rows of elements	KI	KII	KI% ERROR	KII% ERROR
550	2	200,37	114,81	-0,54 %	3,28 %
525	3	200,68	113,66	-0,39 %	2,25 %
611	4	200,98	112,8	-0,24 %	1,48 %
563	5	201,17	112,12	-0,14 %	0,86 %
579	6	201,39	111,57	-0,03 %	0,37 %
590	7	201,46	111,4	0,00 %	0,22 %
608	8	201,44	111,39	-0,01 %	0,21 %

Table C 16. Results for the various countours, for 2 rows of elements and CTSize a/16.

CTSize	a/16							
Rows of elements		2						
	1	2	1	2	AVG	AVG		
Contour	KI	KI	KII	KII	KI	KII	KI%	KII%
1	202,05	202,11	110,91	110,93	202,08	110,92	0,31 %	-0,22 %
2	201,49	201,55	110,91	110,93	201,52	110,92	0,03 %	-0,22 %
3	201,46	201,36	111,12	111,1	201,41	111,11	-0,02 %	-0,04 %
4	201,44	201,44	111,55	111,55	201,44	111,55	-0,01 %	0,35 %
5	200,98	200,94	112,61	112,42	200,96	112,515	-0,25 %	1,22 %
6	200,16	200,23	115,57	115,27	200,195	115,42	-0,63 %	3,83 %
7	199,48	199,81	118,18	117,52	199,645	117,85	-0,90 %	6,02 %
8	198,78	198,3	120,13	120,69	198,54	120,41	-1,45 %	8,32 %
9	195,77	196,63	125,39	124,04	196,2	124,715	-2,61 %	12,19 %
10	193,97	232,06	128,47	197,31	213,015	162,89	5,74 %	46,54 %
11	262,34	-1586,4	112,81	-808	-662,03	-347,595	-428,62 %	-412,70 %
12	-1510,5	-2829,1	15,791	-784,01	-2169,8	-384,1095	-1177,04 %	-445,55 %

Table C 17. Results for the various countours, for 8 rows of elements and CTSize a/16.

CTSize	a/16							
Rows of elements		8						
	1	2	1	2	AVG	AVG		
Contour	KI	KI	KII	KII	KI	KII	KI%	KII%
1	201,99	202,01	110,95	110,95	202	110,95	0,27 %	-0,19 %
2	201,43	201,45	110,95	110,95	201,44	110,95	-0,01 %	-0,19 %
3	201,43	201,45	111,07	111,07	201,44	111,07	-0,01 %	-0,08 %
4	201,43	201,45	111,19	111,19	201,44	111,19	-0,01 %	0,03 %
5	201,43	201,45	111,31	111,32	201,44	111,315	-0,01 %	0,14 %
6	201,43	201,45	111,44	111,45	201,44	111,445	-0,01 %	0,26 %
7	201,42	201,44	111,58	111,58	201,43	111,58	-0,01 %	0,38 %
8	201,42	201,44	111,72	111,73	201,43	111,725	-0,01 %	0,51 %
9	201,39	201,39	112,05	112,05	201,39	112,05	-0,03 %	0,80 %
10	200,27	199,86	114,31	114,81	200,065	114,56	-0,69 %	3,06 %
11	198,16	199,13	119,36	118,33	198,645	118,845	-1,40 %	6,91 %
12	197,36	198,47	122,41	120,73	197,915	121,57	-1,76 %	9,36 %

Table C 18. Results obtained when RRAT was set to 0,25. For various number of rows of elements.

RRAT	0,25				
Elements	Circles	KI	KII	KI% ERROR	KII% ERROR
547	2	200,57	114,26	-0,44 %	2,79 %
582	3	200,86	113,23	-0,30 %	1,86 %
658	4	201,13	112,2	-0,16 %	0,94 %
589	5	201,32	111,48	-0,07 %	0,29 %
616	6	201,47	111,23	0,00 %	0,06 %
642	7	201,49	111,15	0,01 %	-0,01 %
686	8	201,48	111,12	0,01 %	-0,04 %

Table C 19. Results for contours 1-12 as RRAT is set to 0,25. 8 rows of elements, traditional.

RRAT	0,25							
CTSize	a/16							
Rows of elements	8							
	1	2	1	2	AVG	AVG		
Contour	KI	KI	KII	KII	KI	KII	KI%	KII%
1	202,02	202,03	110,93	110,95	202,025	110,94	0,28 %	-0,20 %
2	201,47	201,48	110,9	110,92	201,475	110,91	0,01 %	-0,22 %
3	201,47	201,48	110,96	110,98	201,475	110,97	0,01 %	-0,17 %
4	201,48	201,48	111,02	111,04	201,48	111,03	0,01 %	-0,12 %
5	201,47	201,48	111,08	111,1	201,475	111,09	0,01 %	-0,06 %
6	201,47	201,48	111,14	111,16	201,475	111,15	0,01 %	-0,01 %
7	201,47	201,48	111,2	111,22	201,475	111,21	0,01 %	0,04 %
8	201,47	201,48	111,26	111,28	201,475	111,27	0,01 %	0,10 %
9	201,43	201,4	111,49	111,48	201,415	111,485	-0,02 %	0,29 %
10	201,06	201,05	112,02	111,96	201,055	111,99	-0,20 %	0,75 %
11	200,39	200,41	114,61	114,55	200,4	114,58	-0,53 %	3,08 %
12	199,87	199,94	117,13	117,01	199,905	117,07	-0,77 %	5,32 %

Table C 20. Results for contours 1-12 as RRAT is set to 0,5. 8 rows of elements, traditional.

RRAT	0,5							
CTSize	a/16							
Rows of elements	8							
	1	2	1	2	AVG	AVG		
Contour	KI	KI	KII	KII	KI	KII	KI%	KII%
1	201,99	202,01	110,95	110,95	202	110,95	0,27 %	-0,19 %
2	201,43	201,45	110,95	110,95	201,44	110,95	-0,01 %	-0,19 %
3	201,43	201,45	111,07	111,07	201,44	111,07	-0,01 %	-0,08 %
4	201,43	201,45	111,19	111,19	201,44	111,19	-0,01 %	0,03 %
5	201,43	201,45	111,31	111,32	201,44	111,315	-0,01 %	0,14 %
6	201,43	201,45	111,44	111,45	201,44	111,445	-0,01 %	0,26 %
7	201,42	201,44	111,58	111,58	201,43	111,58	-0,01 %	0,38 %
8	201,42	201,44	111,72	111,73	201,43	111,725	-0,01 %	0,51 %
9	201,39	201,39	112,05	112,05	201,39	112,05	-0,03 %	0,80 %
10	200,27	199,86	114,31	114,81	200,065	114,56	-0,69 %	3,06 %
11	198,16	199,13	119,36	118,33	198,645	118,845	-1,40 %	6,91 %
12	197,36	198,47	122,41	120,73	197,915	121,57	-1,76 %	9,36 %

Table C 21. Results reduction of crack surface lines, by the use of NDIV. RRAT 0,25, 8 rows of elements, traditional.

Rows of elements		8	RRAT		0.25
Elements	NDIV crack surface lines	KI	KII	KI% ERROR	KII% ERROR
686	18	201,48	111,12	0,01 %	-0,04 %
627	15	201,5	111,13	0,02 %	-0,03 %
576	10	201,49	111,11	0,01 %	-0,04 %
529	5	201,59	111,23	0,06 %	0,06 %
468	1	202,69	112,22	0,61 %	0,95 %

Table C 22. Parameters used 5.

Parameters used 5	
Rows of elements	2
CTSize	a/8
RRAT	0,5
LESIZE crack surface lines	Length of outer edge row element
a	2,0823mm
Final opening	0,02mm
NDIV Square lines	10
NDIV Connection lines	1
Inner square size	10x10
Outer square size	500x500
Rows	Traditional

Table C 23. Results obtained when using RRAT 0,5, 0,25 and 0,125, for various number of rows of elements, traditional.

CTSize	a/8				
RRAT	0,5				
Elements	Rows of elements	KI	KII	KI Deviation	KII Deviation
543	2	199,45	117,01	-1,00 %	5,26 %
462	3	201,09	116,32	-0,18 %	4,64 %
397	4	198,86	117,65	-1,29 %	5,84 %
376	5	199,45	116,45	-1,00 %	4,76 %
407	6	199,93	115,37	-0,76 %	3,79 %
424	7	200,19	114,63	-0,63 %	3,12 %
439	8	200,32	114,31	-0,57 %	2,83 %
463	9	200,32	114,35	-0,57 %	2,87 %
478	10	200,31	114,33	-0,57 %	2,85 %
RRAT	0,25				
Elements	Rows of elements	KI	KII	KI Deviation	KII Deviation
625	2	200,82	113,42	-0,32 %	2,03 %
575	3	200,8	113,46	-0,33 %	2,07 %
533	4	200,82	113,21	-0,32 %	1,84 %
526	5	200,95	112,88	-0,25 %	1,55 %
562	6	201,13	112,3	-0,16 %	1,03 %
493	7	201,33	111,85	-0,06 %	0,62 %
493	8	201,35	111,54	-0,05 %	0,34 %
504	9	201,44	111,67	-0,01 %	0,46 %
541	10	201,44	111,68	-0,01 %	0,47 %
RRAT	0,125				
Elements	Rows of elements	KI	KII	KI Deviation	KII Deviation
697	2	201,75	112,68	0,14 %	1,37 %
657	3	201,06	112,48	-0,20 %	1,19 %
651	4	201,18	112,11	-0,14 %	0,85 %
639	5	201,31	111,69	-0,07 %	0,48 %
642	6	201,44	111,45	-0,01 %	0,26 %
629	7	201,46	111,41	0,00 %	0,22 %
636	8	201,47	111,38	0,00 %	0,20 %
654	9	201,47	111,38	0,00 %	0,20 %
625	10	201,44	111,41	-0,01 %	0,22 %

Table C 24. Results obtained for the contours 1-12 for the two crack tips, when RRAT was set to 0,125 for 8 rows of elements.

Elements	636							
RRAT	0,125							
CTSize	a/8							
Rows of elements		8						
	1	2	1	2	AVG	AVG		
Contour	KI	KI	KII	KII	KI	KII	KI%	KII%
1	201,99	202,01	110,95	110,95	202	110,95	0,27 %	-0,19 %
2	201,43	201,45	110,95	110,95	201,44	110,95	-0,01 %	-0,19 %
3	201,43	201,45	111,07	111,07	201,44	111,07	-0,01 %	-0,08 %
4	201,43	201,45	111,19	111,19	201,44	111,19	-0,01 %	0,03 %
5	201,43	201,45	111,31	111,32	201,44	111,315	-0,01 %	0,14 %
6	201,43	201,45	111,44	111,45	201,44	111,445	-0,01 %	0,26 %
7	201,42	201,44	111,58	111,58	201,43	111,58	-0,01 %	0,38 %
8	201,42	201,44	111,72	111,73	201,43	111,725	-0,01 %	0,51 %
9	201,39	201,39	112,05	112,05	201,39	112,05	-0,03 %	0,80 %
10	200,27	199,86	114,31	114,81	200,065	114,56	-0,69 %	3,06 %
11	198,16	199,13	119,36	118,33	198,645	118,845	-1,40 %	6,91 %
12	197,36	198,47	122,41	120,73	197,915	121,57	-1,76 %	9,36 %

Table C 25. Results obtained for the contours 1-12 for the two crack tips, when RRAT was set to 0,5 for 8 rows of elements.

Elements	493							
RRAT	0,5							
CTSize	a/8							
Rows of elements		8						
	1	2	1	2	AVG	AVG		
Contour	KI	KI	KII	KII	KI	KII	KI%	KII%
1	202,01	202,01	111,05	111,06	202,01	111,055	0,27 %	-0,09 %
2	201,44	201,44	111,24	111,25	201,44	111,245	-0,01 %	0,08 %
3	201,44	201,44	111,5	111,51	201,44	111,505	-0,01 %	0,31 %
4	201,42	201,43	111,79	111,8	201,425	111,795	-0,02 %	0,57 %
5	200,87	200,86	112,29	112,31	200,865	112,3	-0,30 %	1,03 %
6	199,99	199,98	114,36	114,41	199,985	114,385	-0,73 %	2,90 %
7	199,44	199,41	116,76	116,83	199,425	116,795	-1,01 %	5,07 %
8	198,82	198,79	119	119,1	198,805	119,05	-1,32 %	7,10 %
9	196,71	196,94	124,02	123,69	196,825	123,855	-2,30 %	11,42 %
10	192,79	194,41	130,94	128,23	193,6	129,585	-3,90 %	16,58 %
11	194,75	191,69	134,22	133,36	193,22	133,79	-4,09 %	20,36 %
12	242,58	221,95	138,23	135,34	232,265	136,785	15,29 %	23,05 %

Table C 26. CTSize test, NEW row element method. Crack surface element length set to 0,2mm.

Rows of elements	8				
New rows					
Elements	CTSize	KI	KII	KI% ERROR	KII% ERROR
451	a/16	200,77	113,01	-0,34 %	1,66 %
590	a/32	201,46	111,18	0,00 %	0,02 %
703	a/64	201,49	110,88	0,01 %	-0,25 %
812	a/128	201,51	110,65	0,02 %	-0,46 %
884	a/256	201,64	110,66	0,09 %	-0,45 %
851	a/512	202,42	111,74	0,48 %	0,52 %
904	a/1024	205,12	115,35	1,82 %	3,77 %

Table C 27. Parameters used 6.

Parameters used 6	
Rows of elements	8
CTSize	a/32
RRAT	0,5
LESIZE crack surface lines	0,2 mm
a	2,0823mm
Final opening	0,02mm
NDIV Square lines	10
NDIV Connection lines	1
Inner square size	10x10
Outer square size	500x500
Contours	3-8

Table C 28. Results for contours 1-12, for CTSize a/16. 8 rows of elements NEW.

New rows								
CTSize	a/16							
	1	2	1	2	AVG	AVG		
Contour	KI	KI	KII	KII	KI	KII	KI%	KII%
1	202,03	202,04	110,88	110,89	202,035	110,885	0,29 %	-0,25 %
2	201,48	201,48	110,86	110,88	201,48	110,87	0,01 %	-0,26 %
3	201,48	201,48	110,98	111	201,48	110,99	0,01 %	-0,15 %
4	201,47	201,48	111,13	111,15	201,475	111,14	0,01 %	-0,02 %
5	201,47	201,47	111,36	111,38	201,47	111,37	0,00 %	0,19 %
6	201,45	201,46	111,72	111,74	201,455	111,73	0,00 %	0,51 %
7	200,11	200,11	113,62	113,66	200,11	113,64	-0,67 %	2,23 %
8	198,76	198,72	119,23	119,32	198,74	119,275	-1,35 %	7,30 %
9	196,13	196,2	125,31	125,43	196,165	125,37	-2,63 %	12,78 %
10	192,72	194,19	131	128,72	193,455	129,86	-3,97 %	16,82 %
11	205,93	191,52	137,17	133,44	198,725	135,305	-1,36 %	21,72 %
12	-178,47	211,74	-0,16234	138,26	16,635	69,04883	-91,74 %	-37,88 %

Table C 29. Results for contours 1-12, for CTSize a/32. 8 rows of elements NEW.

New rows								
CTSize	a/32							
Circles	8							
	1	2	1	2	AVG	AVG		
Contour	KI	KI	KII	KII	KI	KII	KI%	KII%
1	202,03	202,01	110,84	110,82	202,02	110,83	0,28 %	-0,30 %
2	201,48	201,46	110,77	110,75	201,47	110,76	0,00 %	-0,36 %
3	201,48	201,46	110,85	110,83	201,47	110,84	0,00 %	-0,29 %
4	201,48	201,46	110,94	110,91	201,47	110,925	0,00 %	-0,21 %
5	201,48	201,46	111,05	111,03	201,47	111,04	0,00 %	-0,11 %
6	201,47	201,45	111,2	111,18	201,46	111,19	0,00 %	0,03 %
7	201,47	201,45	111,42	111,4	201,46	111,41	0,00 %	0,22 %
8	201,45	201,43	111,76	111,74	201,44	111,75	-0,01 %	0,53 %
9	200,8	200,69	113,08	113,05	200,745	113,065	-0,35 %	1,71 %
10	199,68	199,18	116,88	117,31	199,43	117,095	-1,01 %	5,34 %
11	198,72	197,95	120,14	121,42	198,335	120,78	-1,55 %	8,65 %
12	186,77	196,74	139,06	124,25	191,755	131,655	-4,82 %	18,44 %

Table C 30 Results obtained as element edge length along the crack surface is increased.

New rows					
CTSize	a/32				
Elements	Element edge length	KI	KII	KI% ERROR	KII% ERROR
525	0,2328	201,46	111,19	0,00 %	0,03 %
508	0,3	201,46	111,19	0,00 %	0,03 %
522	0,4	201,45	111,17	0,00 %	0,01 %
507	0,5	201,47	111,17	0,00 %	0,01 %
494	0,6	201,47	111,18	0,00 %	0,02 %
494	0,7	201,47	111,18	0,00 %	0,02 %
489	0,8	201,49	111,16	0,01 %	0,00 %
489	0,9	201,49	111,16	0,01 %	0,00 %
502	1	201,54	111,2	0,04 %	0,04 %

Table C 31. Contours 1-12, for crack surface line divisions set to 1mm, CTSize a/32, NEW rows.

New rows								
LESIZE crack surface lines	1							
CTSize	a/32							
Rows of elements	8							
	1	2	1	2	AVG	AVG		
Contour	KI	KI	KII	KII	KI	KII	KI%	KII%
1	202,15	201,77	110,82	110,61	201,96	110,715	0,25 %	-0,40 %
2	201,6	201,22	110,75	110,54	201,41	110,645	-0,02 %	-0,46 %
3	201,6	201,22	110,83	110,62	201,41	110,725	-0,02 %	-0,39 %
4	201,6	201,22	110,92	110,71	201,41	110,815	-0,02 %	-0,31 %
5	201,6	201,22	111,03	110,82	201,41	110,925	-0,02 %	-0,21 %
6	201,59	201,22	111,18	110,97	201,405	111,075	-0,03 %	-0,08 %
7	201,59	201,21	111,4	111,19	201,4	111,295	-0,03 %	0,12 %
8	201,57	201,2	111,75	111,54	201,385	111,645	-0,04 %	0,44 %
9	198,36	199,56	119,2	117,7	198,96	118,45	-1,24 %	6,56 %
10	192,68	192,45	131,51	131,13	192,565	131,32	-4,42 %	18,14 %
11	201,74	194,69	132,79	134,94	198,215	133,865	-1,61 %	20,43 %
12	245,2	234,11	139,82	137,13	239,655	138,475	18,96 %	24,57 %

Table C 32. Reduction of square line divisions, for various crack surface element lengths, by the use of element size.

New rows					
Element edge length		0,2328mm (Length of outer edge row element)			
Elements	NDIV	KI	KII	KI% ERROR	KII% ERROR
525	10	201,46	111,19	0,00 %	0,03 %
549	9	201,46	111,19	0,00 %	0,03 %
470	8	201,24	111,27	-0,11 %	0,10 %
459	7	201,28	111,13	-0,09 %	-0,03 %
427	6	200,93	110,74	-0,26 %	-0,38 %
Element edge length		0,3mm			
Elements	NDIV	KI	KII	KI% ERROR	KII% ERROR
508	10	201,46	111,19	0,00 %	0,03 %
497	9	201,44	111,19	-0,01 %	0,03 %
501	8	201,44	111,15	-0,01 %	-0,01 %
447	7	201,43	111,11	-0,01 %	-0,04 %
412	6	200,55	111,48	-0,45 %	0,29 %
Element edge length		0,4mm			
Elements	NDIV	KI	KII	KI% ERROR	KII% ERROR
522	10	201,45	111,17	0,00 %	0,01 %
480	9	201,48	111,16	0,01 %	0,00 %
447	8	201,47	111,15	0,00 %	-0,01 %
424	7	201,4	111,18	-0,03 %	0,02 %
405	6	201,32	110,97	-0,07 %	-0,17 %
Element edge length		0,5mm			
Elements	NDIV	KI	KII	KI% ERROR	KII% ERROR
507	10	201,47	111,17	0,00 %	0,01 %
457	9	201,45	111,17	0,00 %	0,01 %
457	8	201,41	111,15	-0,02 %	-0,01 %
419	7	201,42	111,21	-0,02 %	0,04 %
392	6	201,01	111,08	-0,22 %	-0,07 %
Element edge length		0,6mm			
Elements	NDIV	KI	KII	KI% ERROR	KII% ERROR
494	10	201,47	111,18	0,00 %	0,02 %
455	9	201,5	111,18	0,02 %	0,02 %
423	8	201,44	111,19	-0,01 %	0,03 %
404	7	201,38	111,18	-0,04 %	0,02 %
393	6	201,44	110,99	-0,01 %	-0,15 %
Element edge length		0,8mm			
Elements	NDIV	KI	KII	KI% ERROR	KII% ERROR
489	10	201,49	111,16	0,01 %	0,00 %
459	9	201,5	111,2	0,02 %	0,04 %
438	8	201,51	111,17	0,02 %	0,01 %
404	7	201,49	111,11	0,01 %	-0,04 %
377	6	200,93	110,87	-0,26 %	-0,26 %
Element edge length		1mm			
Elements	NDIV	KI	KII	KI% ERROR	KII% ERROR
502	10	201,54	111,2	0,04 %	0,04 %
451	9	201,51	111,21	0,02 %	0,04 %
430	8	201,48	111,19	0,01 %	0,03 %
398	7	201,55	111,25	0,04 %	0,08 %
380	6	201,4	111,08	-0,03 %	-0,07 %

Table C 33. Parameters used 7.

Parameters used 7.	
Rows of elements	2
CTSize	a/32
RRAT	0,5
LESIZE crack surface lines	Length of outer edge row element
a	2,0823mm
Final opening	0,02mm
NDIV Square lines	10
NDIV Connection lines	1
Inner square size	10x10
Outer square size	500x500
Rows	Traditional

Table C 34. Results for contours 1-12 for CTSize a/2. 2 rows of elements, NEW rows.

New rows								
Elements	220							
CTSize	a/2							
	1	2	1	2	AVG	AVG		
Contour	KI	KI	KII	KII	KI	KII	KI% ERROR	KII% ERROR
1	201,44	201,44	110,67	110,65	201,44	110,66	-0,01 %	-0,45 %
2	198,43	198,32	121,6	121,61	198,375	121,605	-1,53 %	9,40 %
3	195,14	195,87	127,54	126,37	195,505	126,955	-2,96 %	14,21 %
4	192,65	192,71	131,64	131,56	192,68	131,6	-4,36 %	18,39 %
5	228,57	212,2	139,41	136,47	220,385	137,94	9,39 %	24,09 %
6	205,34	242,78	7,0821	0,38261	224,06	3,732355	11,22 %	-96,64 %
7	254,3	324,97	4,6926	26,382	289,635	15,5373	43,77 %	-86,02 %
8	1211,8	1954,4	682,81	629,81	1583,1	656,31	685,81 %	490,42 %
9	2430,5	3103,5	321,05	792,02	2767	556,535	1273,47 %	400,66 %
10	1801,2	3382,9	0,11756	854,97	2592,05	427,54378	1186,63 %	284,62 %
11	1801,2	2476,5	0	375,16	2138,85	187,58	961,67 %	68,75 %
12	1801,2	1801,2	0	0	1801,2	0	794,07 %	-100,00 %

Table C 35. Results for contours 1-12 for CTSize a/4. 2 rows of elements, NEW rows.

New rows								
Elements	346							
CTSize	a/4							
	1	2	1	2	AVG	AVG		
Contour	KI	KI	KII	KII	KI	KII	KI% ERROR	KII% ERROR
1	202,03	202,04	111,11	111,12	202,035	111,115	0,29 %	-0,04 %
2	201,43	201,44	111,87	111,88	201,435	111,875	-0,01 %	0,64 %
3	199,71	199,97	114,56	114,46	199,84	114,51	-0,80 %	3,01 %
4	197,78	198,9	120,27	119,03	198,34	119,65	-1,55 %	7,64 %
5	196,45	197,5	124,31	122,82	196,975	123,565	-2,23 %	11,16 %
6	194,25	196,19	128,07	125,32	195,22	126,695	-3,10 %	13,98 %
7	191,67	209,07	132,81	130,94	200,37	131,875	-0,54 %	18,64 %
8	275,82	268,06	118,41	1,7028	271,94	60,0564	34,98 %	-45,97 %
9	1743,3	380,96	16,86	37,523	1062,13	27,1915	427,22 %	-75,54 %
10	1949,6	1036,6	45,706	59,842	1493,1	52,774	641,14 %	-52,52 %
11	2714,2	2720	593,56	698,4	2717,1	645,98	1248,70 %	481,13 %
12	2037,3	3107,2	176,62	788,81	2572,25	482,715	1176,80 %	334,25 %

Table C 36. Results for contours 1-12 for CTSize a/8. 2 rows of elements, NEW rows.

New rows								
Elements	551							
CTSize	a/8							
	1	2	1	2	AVG	AVG		
Contour	KI	KI	KII	KII	KI	KII	KI% ERROR	KII% ERROR
1	202,04	202,04	111,04	111,06	202,04	111,05	0,29 %	-0,10 %
2	201,48	201,48	111,2	111,23	201,48	111,215	0,01 %	0,05 %
3	201,45	201,43	111,42	111,45	201,44	111,435	-0,01 %	0,25 %
4	201,46	201,42	111,72	111,78	201,44	111,75	-0,01 %	0,53 %
5	200,81	201,01	112,53	112,45	200,91	112,49	-0,27 %	1,20 %
6	200,59	200,43	114,63	114,61	200,51	114,62	-0,47 %	3,11 %
7	200,29	200,11	116,14	116,44	200,2	116,29	-0,63 %	4,61 %
8	199	217,18	119,26	120,78	208,09	120,02	3,29 %	7,97 %
9	210,29	311,93	130,68	42,21	261,11	86,445	29,61 %	-22,23 %
10	220,66	383,8	4,1875	67,002	302,23	35,59475	50,02 %	-67,98 %
11	1289,9	2196,9	711,56	467,65	1743,4	589,605	765,38 %	430,41 %
12	1562,5	2543,6	802,97	558,99	2053,05	680,98	919,09 %	512,61 %

Table C 37. Results for contours 1-12 for CTSize a/16. 2 rows of elements, NEW rows.

New rows								
Elements	1090							
CTSize	a/16							
	1	2	1	2	AVG	AVG		
Contour	KI	KI	KII	KII	KI	KII	KI% ERROR	KII% ERROR
1	202,02	202,04	110,93	110,92	202,03	110,925	0,28 %	-0,21 %
2	201,46	201,48	110,91	110,91	201,47	110,91	0,00 %	-0,22 %
3	201,46	201,43	110,98	110,99	201,445	110,985	-0,01 %	-0,16 %
4	201,49	201,43	111,13	111,13	201,46	111,13	0,00 %	-0,03 %
5	201,5	201,46	111,31	111,29	201,48	111,3	0,01 %	0,13 %
6	201,49	201,48	111,44	111,41	201,485	111,425	0,01 %	0,24 %
7	201,37	201,38	109,97	110,56	201,375	110,265	-0,04 %	-0,81 %
8	201,35	201,3	111,15	110,65	201,325	110,9	-0,07 %	-0,23 %
9	201,3	208,74	112,01	114,05	205,02	113,03	1,77 %	1,68 %
10	271,03	67,947	94,622	33,116	169,4885	63,869	-15,87 %	-42,54 %
11	1484	112,95	50,016	14,927	798,475	32,4715	296,34 %	-70,79 %
12	2749,8	1572,5	675,68	20,352	2161,15	348,016	972,74 %	213,08 %

Table C 38. Contour results for CTSize a/8, 12 rows of elements traditional. Radius 1,6919mm.

Radius of refined region		1,6919							
Elements		524							
CTSize		a/8							
Rows of elements		12							
		1	2	1	2	AVG	AVG		
Distance	Contour	KI	KI	KII	KII	KI	KII	KI% ERROR	KII% ERROR
0,26028983	1	202	202,01	111,05	111,05	202,005	111,05	0,27 %	-0,10 %
0,39043474	2	201,43	201,44	111,24	111,25	201,435	111,245	-0,01 %	0,08 %
0,52057966	3	201,43	201,44	111,51	111,51	201,435	111,51	-0,01 %	0,31 %
0,65072457	4	201,42	201,43	111,8	111,8	201,425	111,8	-0,02 %	0,58 %
0,78086949	5	200,85	200,86	112,32	112,32	200,855	112,32	-0,30 %	1,04 %
0,9110144	6	199,96	199,97	114,43	114,43	199,965	114,43	-0,74 %	2,94 %
1,04115932	7	199,4	199,41	116,86	116,86	199,405	116,86	-1,02 %	5,13 %
1,17130423	8	198,75	198,76	119,13	119,14	198,755	119,135	-1,34 %	7,17 %
1,30144915	9	198,04	198,04	121,22	121,23	198,04	121,225	-1,70 %	9,05 %
1,43159406	10	197,29	197,29	123,13	123,14	197,29	123,135	-2,07 %	10,77 %
1,56173898	11	196,54	196,53	124,83	124,84	196,535	124,835	-2,44 %	12,30 %
1,69188389	12	195,81	195,81	126,31	126,33	195,81	126,32	-2,80 %	13,64 %

Table C 39. Contour results for CTSize a/16, 25 rows of elements traditional. Radius 1,6919mm.

Radius of refined region		1,6919							
Elements		940							
CTSize		a/16							
Rows of elements		25							
		1	2	1	2	AVG	AVG		
Distance	Contour	KI	KI	KII	KII	KI	KII	KI% ERROR	KII% ERROR
0,13014491	1	201,99	202	110,95	110,95	201,995	110,95	0,27 %	-0,19 %
0,19521737	2	201,43	201,44	110,94	110,95	201,435	110,945	-0,01 %	-0,19 %
0,26028983	3	201,43	201,44	111,07	111,07	201,435	111,07	-0,01 %	-0,08 %
0,32536229	4	201,43	201,44	111,19	111,19	201,435	111,19	-0,01 %	0,03 %
0,39043474	5	201,43	201,44	111,31	111,31	201,435	111,31	-0,01 %	0,13 %
0,4555072	6	201,43	201,44	111,44	111,44	201,435	111,44	-0,01 %	0,25 %
0,52057966	7	201,42	201,43	111,58	111,58	201,425	111,58	-0,02 %	0,38 %
0,58565212	8	201,42	201,43	111,72	111,73	201,425	111,725	-0,02 %	0,51 %
0,65072457	9	201,41	201,42	111,88	111,88	201,415	111,88	-0,02 %	0,65 %
0,71579703	10	201,4	201,41	112,04	112,04	201,405	112,04	-0,03 %	0,79 %
0,78086949	11	200,82	200,83	112,53	112,53	200,825	112,53	-0,32 %	1,23 %
0,84594195	12	200,08	200,09	113,8	113,81	200,085	113,805	-0,68 %	2,38 %
0,9110144	13	199,83	199,83	115,05	115,06	199,83	115,055	-0,81 %	3,50 %
0,97608686	14	199,55	199,55	116,27	116,28	199,55	116,275	-0,95 %	4,60 %
1,04115932	15	199,24	199,25	117,45	117,45	199,245	117,45	-1,10 %	5,66 %
1,10623178	16	198,92	198,92	118,58	118,59	198,92	118,585	-1,26 %	6,68 %
1,17130423	17	198,57	198,58	119,68	119,69	198,575	119,685	-1,43 %	7,67 %
1,23637669	18	198,22	198,22	120,73	120,74	198,22	120,735	-1,61 %	8,61 %
1,30144915	19	197,85	197,85	121,73	121,74	197,85	121,735	-1,79 %	9,51 %
1,36652161	20	197,47	197,48	122,68	122,69	197,475	122,685	-1,98 %	10,37 %
1,43159406	21	197,1	197,1	123,58	123,59	197,1	123,585	-2,16 %	11,18 %
1,49666652	22	196,72	196,71	124,43	124,44	196,715	124,435	-2,36 %	11,94 %
1,56173898	23	196,35	196,34	125,22	125,24	196,345	125,23	-2,54 %	12,66 %
1,62681143	24	195,98	195,97	125,96	125,98	195,975	125,97	-2,72 %	13,32 %
1,69188389	25	195,61	195,62	126,65	126,67	195,615	126,66	-2,90 %	13,94 %

Table C 40. Contour results for CTSize a/32, 51 rows of elements traditional. Radius 1,6919mm.

Radius of refined region		1,6919							
Elements		1772							
CTSize		a/32							
Rows of elements		51							
		1	2	1	2	AVG	AVG		
Distance	Contour	KI	KI	KII	KII	KI	KII	KI% ERROR	KII% ERROR
0,06507246	1	201,98	201,99	110,82	110,83	201,985	110,825	0,26 %	-0,30 %
0,09760869	2	201,42	201,43	110,76	110,76	201,425	110,76	-0,02 %	-0,36 %
0,13014491	3	201,43	201,44	110,85	110,85	201,435	110,85	-0,01 %	-0,28 %
0,16268114	4	201,43	201,44	110,92	110,92	201,435	110,92	-0,01 %	-0,22 %
0,19521737	5	201,43	201,44	110,98	110,98	201,435	110,98	-0,01 %	-0,16 %
0,2277536	6	201,43	201,44	111,04	111,04	201,435	111,04	-0,01 %	-0,11 %
0,26028983	7	201,43	201,44	111,1	111,1	201,435	111,1	-0,01 %	-0,05 %
0,29282606	8	201,43	201,44	111,16	111,16	201,435	111,16	-0,01 %	0,00 %
0,32536229	9	201,43	201,44	111,22	111,22	201,435	111,22	-0,01 %	0,05 %
0,35789852	10	201,43	201,44	111,28	111,28	201,435	111,28	-0,01 %	0,11 %
0,39043474	11	201,43	201,44	111,35	111,35	201,435	111,35	-0,01 %	0,17 %
0,42297097	12	201,43	201,44	111,41	111,41	201,435	111,41	-0,01 %	0,22 %
0,4555072	13	201,43	201,44	111,48	111,48	201,435	111,48	-0,01 %	0,29 %
0,48804343	14	201,42	201,43	111,54	111,55	201,425	111,545	-0,02 %	0,35 %
0,52057966	15	201,42	201,43	111,61	111,62	201,425	111,615	-0,02 %	0,41 %
0,55311589	16	201,42	201,43	111,69	111,69	201,425	111,69	-0,02 %	0,48 %
0,58565212	17	201,42	201,42	111,76	111,76	201,42	111,76	-0,02 %	0,54 %
0,61818835	18	201,41	201,42	111,84	111,84	201,415	111,84	-0,02 %	0,61 %
0,65072457	19	201,41	201,42	111,92	111,92	201,415	111,92	-0,02 %	0,68 %
0,6832608	20	201,4	201,41	112	112	201,405	112	-0,03 %	0,76 %
0,71579703	21	201,4	201,41	112,08	112,08	201,405	112,08	-0,03 %	0,83 %
0,74833326	22	200,86	200,87	112,26	112,26	200,865	112,26	-0,30 %	0,99 %
0,78086949	23	200,25	200,26	112,84	112,85	200,255	112,845	-0,60 %	1,52 %
0,81340572	24	200,14	200,15	113,48	113,49	200,145	113,485	-0,65 %	2,09 %
0,84594195	25	200,02	200,03	114,12	114,12	200,025	114,12	-0,71 %	2,66 %
0,87847817	26	199,89	199,9	114,75	114,75	199,895	114,75	-0,78 %	3,23 %
0,9110144	27	199,76	199,77	115,36	115,37	199,765	115,365	-0,84 %	3,78 %
0,94355063	28	199,62	199,63	115,97	115,98	199,625	115,975	-0,91 %	4,33 %
0,97608686	29	199,47	199,48	116,57	116,58	199,475	116,575	-0,99 %	4,87 %
1,00862309	30	199,32	199,33	117,16	117,17	199,325	117,165	-1,06 %	5,40 %
1,04115932	31	199,16	199,17	117,74	117,75	199,165	117,745	-1,14 %	5,92 %
1,07369555	32	199	199,01	118,31	118,31	199,005	118,31	-1,22 %	6,43 %
1,10623178	33	198,83	198,84	118,86	118,87	198,835	118,865	-1,30 %	6,93 %
1,138768	34	198,66	198,67	119,41	119,42	198,665	119,415	-1,39 %	7,43 %
1,17130423	35	198,49	198,49	119,95	119,96	198,49	119,955	-1,47 %	7,91 %
1,20384046	36	198,31	198,31	120,47	120,48	198,31	120,475	-1,56 %	8,38 %
1,23637669	37	198,12	198,13	120,98	120,99	198,125	120,985	-1,66 %	8,84 %
1,26891292	38	197,94	197,95	121,49	121,49	197,945	121,49	-1,74 %	9,29 %
1,30144915	39	197,75	197,76	121,97	121,98	197,755	121,975	-1,84 %	9,73 %
1,33398538	40	197,57	197,57	122,45	122,46	197,57	122,455	-1,93 %	10,16 %
1,36652161	41	197,38	197,38	122,91	122,92	197,38	122,915	-2,03 %	10,57 %
1,39905783	42	197,19	197,19	123,36	123,38	197,19	123,37	-2,12 %	10,98 %
1,43159406	43	197	197	123,8	123,81	197	123,805	-2,21 %	11,38 %
1,46413029	44	196,81	196,81	124,22	124,24	196,81	124,23	-2,31 %	11,76 %
1,49666652	45	196,62	196,62	124,64	124,65	196,62	124,645	-2,40 %	12,13 %
1,52920275	46	196,44	196,43	125,03	125,05	196,435	125,04	-2,49 %	12,49 %
1,56173898	47	196,25	196,24	125,41	125,43	196,245	125,42	-2,59 %	12,83 %
1,59427521	48	196,07	196,06	125,78	125,8	196,065	125,79	-2,68 %	13,16 %
1,62681143	49	195,88	195,88	126,14	126,16	195,88	126,15	-2,77 %	13,49 %
1,65934766	50	195,7	195,7	126,48	126,5	195,7	126,49	-2,86 %	13,79 %
1,69188389	51	195,52	195,54	126,81	126,83	195,53	126,82	-2,94 %	14,09 %

Table C 41. Contour results for CTSize a/64, 103 rows of elements traditional. Radius 1,6919mm.

Radius of refined region		1,6919							
Elements		3436							
CTSize		a/64							
Rows of elements		103							
		1	2	1	2	AVG	AVG		
Distance	Contour	KI	KI	KII	KII	KI	KII	KI% ERROR	KII% ERROR
0,03253623	1	201,98	201,99	110,7	110,7	201,985	110,7	0,26 %	-0,41 %
0,04880434	2	201,42	201,43	110,62	110,62	201,425	110,62	-0,02 %	-0,49 %
0,06507246	3	201,43	201,44	110,69	110,69	201,435	110,69	-0,01 %	-0,42 %
0,08134057	4	201,43	201,44	110,74	110,74	201,435	110,74	-0,01 %	-0,38 %
0,09760869	5	201,43	201,44	110,79	110,79	201,435	110,79	-0,01 %	-0,33 %
0,1138768	6	201,43	201,44	110,83	110,83	201,435	110,83	-0,01 %	-0,30 %
0,13014491	7	201,43	201,44	110,86	110,86	201,435	110,86	-0,01 %	-0,27 %
0,14641303	8	201,43	201,44	110,9	110,9	201,435	110,9	-0,01 %	-0,23 %
0,16268114	9	201,44	201,44	110,93	110,93	201,44	110,93	-0,01 %	-0,21 %
0,17894926	10	201,44	201,44	110,96	110,96	201,44	110,96	-0,01 %	-0,18 %
0,19521737	11	201,44	201,44	110,99	110,99	201,44	110,99	-0,01 %	-0,15 %
0,21148549	12	201,44	201,44	111,02	111,02	201,44	111,02	-0,01 %	-0,13 %
0,2277536	13	201,44	201,44	111,05	111,05	201,44	111,05	-0,01 %	-0,10 %
0,24402172	14	201,44	201,44	111,08	111,08	201,44	111,08	-0,01 %	-0,07 %
0,26028983	15	201,44	201,44	111,11	111,11	201,44	111,11	-0,01 %	-0,04 %
0,27655794	16	201,44	201,44	111,14	111,14	201,44	111,14	-0,01 %	-0,02 %
0,29282606	17	201,44	201,44	111,17	111,17	201,44	111,17	-0,01 %	0,01 %
0,30909417	18	201,43	201,44	111,2	111,2	201,435	111,2	-0,01 %	0,04 %
0,32536229	19	201,43	201,44	111,24	111,24	201,435	111,24	-0,01 %	0,07 %
0,3416304	20	201,43	201,44	111,27	111,27	201,435	111,27	-0,01 %	0,10 %
0,35789852	21	201,43	201,44	111,3	111,3	201,435	111,3	-0,01 %	0,13 %
0,37416663	22	201,43	201,44	111,33	111,33	201,435	111,33	-0,01 %	0,15 %
0,39043474	23	201,43	201,44	111,36	111,36	201,435	111,36	-0,01 %	0,18 %
0,40670286	24	201,43	201,44	111,39	111,39	201,435	111,39	-0,01 %	0,21 %
0,42297097	25	201,43	201,44	111,42	111,43	201,435	111,425	-0,01 %	0,24 %
0,43923909	26	201,43	201,44	111,46	111,46	201,435	111,46	-0,01 %	0,27 %
0,4555072	27	201,43	201,44	111,49	111,49	201,435	111,49	-0,01 %	0,30 %
0,47177532	28	201,43	201,44	111,53	111,53	201,435	111,53	-0,01 %	0,33 %
0,48804343	29	201,43	201,43	111,56	111,56	201,43	111,56	-0,01 %	0,36 %
0,50431154	30	201,42	201,43	111,59	111,6	201,425	111,595	-0,02 %	0,39 %
0,52057966	31	201,42	201,43	111,63	111,63	201,425	111,63	-0,02 %	0,42 %
0,53684777	32	201,42	201,43	111,67	111,67	201,425	111,67	-0,02 %	0,46 %
0,55311589	33	201,42	201,43	111,7	111,7	201,425	111,7	-0,02 %	0,49 %
0,569384	34	201,42	201,43	111,74	111,74	201,425	111,74	-0,02 %	0,52 %
0,58565212	35	201,42	201,43	111,78	111,78	201,425	111,78	-0,02 %	0,56 %
0,60192023	36	201,41	201,42	111,82	111,82	201,415	111,82	-0,02 %	0,59 %
0,61818835	37	201,41	201,42	111,86	111,86	201,415	111,86	-0,02 %	0,63 %
0,63445646	38	201,41	201,42	111,89	111,89	201,415	111,89	-0,02 %	0,66 %
0,65072457	39	201,41	201,42	111,93	111,94	201,415	111,935	-0,02 %	0,70 %
0,66699269	40	201,41	201,42	111,98	111,98	201,415	111,98	-0,02 %	0,74 %
0,6832608	41	201,4	201,41	112,02	112,02	201,405	112,02	-0,03 %	0,77 %
0,69952892	42	201,4	201,41	112,06	112,06	201,405	112,06	-0,03 %	0,81 %
0,71579703	43	201,4	201,41	112,1	112,1	201,405	112,1	-0,03 %	0,85 %
0,73206515	44	201,4	201,41	112,14	112,14	201,405	112,14	-0,03 %	0,88 %
0,74833326	45	200,86	200,87	112,31	112,31	200,865	112,31	-0,30 %	1,03 %
0,76460137	46	200,28	200,29	112,68	112,68	200,285	112,68	-0,58 %	1,37 %
0,78086949	47	200,23	200,24	113	113,01	200,235	113,005	-0,61 %	1,66 %
0,7971376	48	200,17	200,18	113,32	113,33	200,175	113,325	-0,64 %	1,95 %
0,81340572	49	200,11	200,12	113,64	113,65	200,115	113,645	-0,67 %	2,24 %
0,82967383	50	200,05	200,06	113,96	113,97	200,055	113,965	-0,70 %	2,52 %
0,84594195	51	199,99	200	114,28	114,28	199,995	114,28	-0,73 %	2,81 %
0,86221006	52	199,93	199,93	114,59	114,59	199,93	114,59	-0,76 %	3,09 %
0,87847817	53	199,86	199,87	114,9	114,91	199,865	114,905	-0,79 %	3,37 %
0,89474629	54	199,79	199,8	115,21	115,21	199,795	115,21	-0,83 %	3,64 %
0,9110144	55	199,73	199,73	115,51	115,52	199,73	115,515	-0,86 %	3,92 %
0,92728252	56	199,66	199,66	115,82	115,83	199,66	115,825	-0,89 %	4,20 %
0,94355063	57	199,58	199,59	116,12	116,13	199,585	116,125	-0,93 %	4,47 %
0,95981875	58	199,51	199,52	116,42	116,43	199,515	116,425	-0,97 %	4,74 %
0,97608686	59	199,44	199,44	116,72	116,72	199,44	116,72	-1,00 %	5,00 %
0,99235498	60	199,36	199,37	117,01	117,02	199,365	117,015	-1,04 %	5,27 %

1,00862309	61	199,28	199,29	117,3	117,31	199,285	117,305	-1,08 %	5,53 %
1,0248912	62	199,2	199,21	117,59	117,6	199,205	117,595	-1,12 %	5,79 %
1,04115932	63	199,12	199,13	117,88	117,89	199,125	117,885	-1,16 %	6,05 %
1,05742743	64	199,04	199,05	118,16	118,17	199,045	118,165	-1,20 %	6,30 %
1,07369555	65	198,96	198,97	118,45	118,45	198,965	118,45	-1,24 %	6,56 %
1,08996366	66	198,87	198,88	118,73	118,73	198,875	118,73	-1,28 %	6,81 %
1,10623178	67	198,79	198,8	119	119,01	198,795	119,005	-1,32 %	7,06 %
1,12249989	68	198,7	198,71	119,28	119,28	198,705	119,28	-1,37 %	7,30 %
1,138768	69	198,62	198,62	119,55	119,55	198,62	119,55	-1,41 %	7,55 %
1,15503612	70	198,53	198,54	119,81	119,82	198,535	119,815	-1,45 %	7,79 %
1,17130423	71	198,44	198,45	120,08	120,09	198,445	120,085	-1,50 %	8,03 %
1,18757235	72	198,35	198,36	120,34	120,35	198,355	120,345	-1,54 %	8,26 %
1,20384046	73	198,26	198,27	120,6	120,61	198,265	120,605	-1,59 %	8,50 %
1,22010858	74	198,17	198,18	120,86	120,87	198,175	120,865	-1,63 %	8,73 %
1,23637669	75	198,08	198,08	121,11	121,12	198,08	121,115	-1,68 %	8,96 %
1,2526448	76	197,99	197,99	121,36	121,37	197,99	121,365	-1,72 %	9,18 %
1,26891292	77	197,89	197,9	121,61	121,62	197,895	121,615	-1,77 %	9,41 %
1,28518103	78	197,8	197,81	121,85	121,86	197,805	121,855	-1,81 %	9,62 %
1,30144915	79	197,71	197,71	122,09	122,1	197,71	122,095	-1,86 %	9,84 %
1,31771726	80	197,61	197,62	122,33	122,34	197,615	122,335	-1,91 %	10,05 %
1,33398538	81	197,52	197,52	122,57	122,58	197,52	122,575	-1,96 %	10,27 %
1,35025349	82	197,43	197,43	122,8	122,81	197,43	122,805	-2,00 %	10,48 %
1,36652161	83	197,33	197,33	123,03	123,04	197,33	123,035	-2,05 %	10,68 %
1,38278972	84	197,24	197,24	123,25	123,26	197,24	123,255	-2,09 %	10,88 %
1,39905783	85	197,14	197,14	123,47	123,48	197,14	123,475	-2,14 %	11,08 %
1,41532595	86	197,05	197,05	123,69	123,7	197,05	123,695	-2,19 %	11,28 %
1,43159406	87	196,95	196,95	123,91	123,92	196,95	123,915	-2,24 %	11,47 %
1,44786218	88	196,86	196,85	124,12	124,13	196,855	124,125	-2,29 %	11,66 %
1,46413029	89	196,76	196,76	124,33	124,34	196,76	124,335	-2,33 %	11,85 %
1,48039841	90	196,67	196,66	124,53	124,55	196,665	124,54	-2,38 %	12,04 %
1,49666652	91	196,58	196,57	124,73	124,75	196,575	124,74	-2,42 %	12,22 %
1,51293463	92	196,48	196,48	124,93	124,95	196,48	124,94	-2,47 %	12,40 %
1,52920275	93	196,39	196,38	125,13	125,14	196,385	125,135	-2,52 %	12,57 %
1,54547086	94	196,3	196,29	125,32	125,33	196,295	125,325	-2,56 %	12,74 %
1,56173898	95	196,21	196,19	125,51	125,52	196,2	125,515	-2,61 %	12,91 %
1,57800709	96	196,11	196,1	125,69	125,71	196,105	125,7	-2,66 %	13,08 %
1,59427521	97	196,02	196,01	125,87	125,89	196,015	125,88	-2,70 %	13,24 %
1,61054332	98	195,93	195,92	126,05	126,07	195,925	126,06	-2,75 %	13,40 %
1,62681143	99	195,84	195,83	126,23	126,24	195,835	126,235	-2,79 %	13,56 %
1,64307955	100	195,75	195,75	126,4	126,41	195,75	126,405	-2,83 %	13,71 %
1,65934766	101	195,66	195,66	126,57	126,58	195,66	126,575	-2,88 %	13,87 %
1,67561578	102	195,56	195,58	126,73	126,75	195,57	126,74	-2,92 %	14,02 %
1,69188389	103	195,47	195,5	126,89	126,91	195,485	126,9	-2,97 %	14,16 %

Table C 42. Contour results for CTSize a/8, 8 rows of elements traditional. Radius 1,1713mm.

Radius of refined region		1,1713							
Elements		479							
CTSize		a/8							
Rows of elements		8							
		1	2	1	2	AVG	AVG		
Distance	Contour	KI	KI	KII	KII	KI	KII	KI% ERROR	KII% ERROR
0,26028983	1	202,02	202	111,04	111,05	202,01	111,045	0,27 %	-0,10 %
0,39043474	2	201,45	201,43	111,23	111,24	201,44	111,235	-0,01 %	0,07 %
0,52057966	3	201,45	201,42	111,49	111,5	201,435	111,495	-0,01 %	0,30 %
0,65072457	4	201,44	201,41	111,78	111,8	201,425	111,79	-0,02 %	0,57 %
0,78086949	5	200,88	200,85	112,28	112,3	200,865	112,29	-0,30 %	1,02 %
0,9110144	6	200,02	199,97	114,34	114,38	199,995	114,36	-0,73 %	2,88 %
1,04115932	7	199,49	199,43	116,72	116,8	199,46	116,76	-0,99 %	5,04 %
1,17130423	8	198,87	198,8	118,94	119,04	198,835	118,99	-1,30 %	7,04 %

Table C 43. Contour results for CTSize a/16, 17 rows of elements traditional. Radius 1,1713mm.

Radius of refined region		1,1713							
Elements		759							
CTSize		a/16							
Rows of elements		17							
		1	2	1	2	AVG	AVG		
Distance	Contour	KI	KI	KII	KII	KI	KII	KI% ERROR	KII% ERROR
0,13014491	1	202	202,01	110,94	110,96	202,005	110,95	0,27 %	-0,19 %
0,19521737	2	201,43	201,45	110,94	110,96	201,44	110,95	-0,01 %	-0,19 %
0,26028983	3	201,44	201,46	111,07	111,08	201,45	111,075	0,00 %	-0,08 %
0,32536229	4	201,44	201,46	111,19	111,2	201,45	111,195	0,00 %	0,03 %
0,39043474	5	201,44	201,45	111,31	111,33	201,445	111,32	-0,01 %	0,14 %
0,4555072	6	201,43	201,45	111,44	111,45	201,44	111,445	-0,01 %	0,26 %
0,52057966	7	201,43	201,45	111,58	111,59	201,44	111,585	-0,01 %	0,38 %
0,58565212	8	201,42	201,44	111,72	111,74	201,43	111,73	-0,01 %	0,51 %
0,65072457	9	201,42	201,43	111,87	111,89	201,425	111,88	-0,02 %	0,65 %
0,71579703	10	201,41	201,42	112,03	112,05	201,415	112,04	-0,02 %	0,79 %
0,78086949	11	200,83	200,85	112,51	112,52	200,84	112,515	-0,31 %	1,22 %
0,84594195	12	200,1	200,12	113,76	113,78	200,11	113,77	-0,67 %	2,35 %
0,9110144	13	199,84	199,87	115,01	115,03	199,855	115,02	-0,80 %	3,47 %
0,97608686	14	199,57	199,59	116,23	116,24	199,58	116,235	-0,93 %	4,57 %
1,04115932	15	199,27	199,28	117,4	117,41	199,275	117,405	-1,08 %	5,62 %
1,10623178	16	198,95	198,97	118,53	118,54	198,96	118,535	-1,24 %	6,63 %
1,17130423	17	198,59	198,65	119,63	119,63	198,62	119,63	-1,41 %	7,62 %

Table C 44. Contour results for CTSize a/32, 35 rows of elements traditional. Radius 1,1713mm.

Radius of refined region		1,1713							
Elements		1303							
CTSize		a/32							
Rows of elements		35							
		1	2	1	2	AVG	AVG		
Distance	Contour	KI	KI	KII	KII	KI	KII	KI% ERROR	KII% ERROR
0,06507246	1	202,01	201,99	110,82	110,84	202	110,83	0,27 %	-0,30 %
0,09760869	2	201,45	201,43	110,76	110,77	201,44	110,765	-0,01 %	-0,36 %
0,13014491	3	201,45	201,44	110,84	110,86	201,445	110,85	-0,01 %	-0,28 %
0,16268114	4	201,46	201,44	110,91	110,93	201,45	110,92	0,00 %	-0,22 %
0,19521737	5	201,46	201,44	110,98	110,99	201,45	110,985	0,00 %	-0,16 %
0,2277536	6	201,46	201,44	111,04	111,05	201,45	111,045	0,00 %	-0,10 %
0,26028983	7	201,46	201,44	111,1	111,11	201,45	111,105	0,00 %	-0,05 %
0,29282606	8	201,46	201,44	111,16	111,17	201,45	111,165	0,00 %	0,00 %
0,32536229	9	201,46	201,44	111,22	111,23	201,45	111,225	0,00 %	0,06 %
0,35789852	10	201,45	201,44	111,28	111,29	201,445	111,285	-0,01 %	0,11 %
0,39043474	11	201,45	201,44	111,34	111,36	201,445	111,35	-0,01 %	0,17 %
0,42297097	12	201,45	201,43	111,41	111,42	201,44	111,415	-0,01 %	0,23 %
0,4555072	13	201,45	201,43	111,47	111,49	201,44	111,48	-0,01 %	0,29 %
0,48804343	14	201,45	201,43	111,54	111,56	201,44	111,55	-0,01 %	0,35 %
0,52057966	15	201,44	201,43	111,61	111,63	201,435	111,62	-0,01 %	0,41 %
0,55311589	16	201,44	201,42	111,68	111,7	201,43	111,69	-0,01 %	0,48 %
0,58565212	17	201,44	201,42	111,76	111,77	201,43	111,765	-0,01 %	0,54 %
0,61818835	18	201,43	201,42	111,83	111,85	201,425	111,84	-0,02 %	0,61 %
0,65072457	19	201,43	201,41	111,91	111,93	201,42	111,92	-0,02 %	0,68 %
0,6832608	20	201,43	201,41	111,99	112,01	201,42	112	-0,02 %	0,76 %
0,71579703	21	201,42	201,4	112,08	112,09	201,41	112,085	-0,02 %	0,83 %
0,74833326	22	200,89	200,87	112,24	112,26	200,88	112,25	-0,29 %	0,98 %
0,78086949	23	200,29	200,27	112,8	112,83	200,28	112,815	-0,59 %	1,49 %
0,81340572	24	200,18	200,15	113,44	113,47	200,165	113,455	-0,64 %	2,06 %
0,84594195	25	200,06	200,03	114,07	114,1	200,045	114,085	-0,70 %	2,63 %
0,87847817	26	199,94	199,91	114,69	114,73	199,925	114,71	-0,76 %	3,19 %
0,9110144	27	199,81	199,77	115,3	115,34	199,79	115,32	-0,83 %	3,74 %
0,94355063	28	199,68	199,63	115,91	115,95	199,655	115,93	-0,90 %	4,29 %
0,97608686	29	199,54	199,49	116,5	116,55	199,515	116,525	-0,97 %	4,83 %
1,00862309	30	199,4	199,34	117,07	117,14	199,37	117,105	-1,04 %	5,35 %
1,04115932	31	199,26	199,18	117,64	117,71	199,22	117,675	-1,11 %	5,86 %
1,07369555	32	199,12	199,02	118,19	118,28	199,07	118,235	-1,19 %	6,36 %
1,10623178	33	198,97	198,86	118,73	118,83	198,915	118,78	-1,26 %	6,85 %
1,138768	34	198,82	198,7	119,26	119,38	198,76	119,32	-1,34 %	7,34 %
1,17130423	35	198,65	198,53	119,78	119,91	198,59	119,845	-1,42 %	7,81 %

Table C 45. Contour results for CTSize a/64, 71 rows of elements traditional. Radius 1,1713mm.

Radius of refined region		1,1713							
Elements		2497							
CTSize		a/64							
Rows of elements		71							
		1	2	1	2	AVG	AVG		
Distance	Contour	KI	KI	KII	KII	KI	KII	KI% ERROR	KII% ERROR
0,03253623	1	201,98	201,99	110,7	110,71	201,985	110,705	0,26 %	-0,41 %
0,04880434	2	201,42	201,43	110,62	110,63	201,425	110,625	-0,02 %	-0,48 %
0,06507246	3	201,43	201,43	110,69	110,7	201,43	110,695	-0,01 %	-0,42 %
0,08134057	4	201,43	201,44	110,75	110,75	201,435	110,75	-0,01 %	-0,37 %
0,09760869	5	201,43	201,44	110,79	110,8	201,435	110,795	-0,01 %	-0,33 %
0,1138768	6	201,43	201,44	110,83	110,84	201,435	110,835	-0,01 %	-0,29 %
0,13014491	7	201,43	201,44	110,87	110,87	201,435	110,87	-0,01 %	-0,26 %
0,14641303	8	201,43	201,44	110,9	110,91	201,435	110,905	-0,01 %	-0,23 %
0,16268114	9	201,43	201,44	110,94	110,94	201,435	110,94	-0,01 %	-0,20 %
0,17894926	10	201,43	201,44	110,97	110,97	201,435	110,97	-0,01 %	-0,17 %
0,19521737	11	201,43	201,44	111	111,01	201,435	111,005	-0,01 %	-0,14 %
0,21148549	12	201,43	201,44	111,03	111,04	201,435	111,035	-0,01 %	-0,11 %
0,2277536	13	201,43	201,44	111,06	111,07	201,435	111,065	-0,01 %	-0,09 %
0,24402172	14	201,43	201,44	111,09	111,1	201,435	111,095	-0,01 %	-0,06 %
0,26028983	15	201,43	201,44	111,12	111,13	201,435	111,125	-0,01 %	-0,03 %
0,27655794	16	201,43	201,44	111,15	111,16	201,435	111,155	-0,01 %	0,00 %
0,29282606	17	201,43	201,44	111,18	111,19	201,435	111,185	-0,01 %	0,02 %
0,30909417	18	201,43	201,44	111,21	111,22	201,435	111,215	-0,01 %	0,05 %
0,32536229	19	201,43	201,44	111,24	111,25	201,435	111,245	-0,01 %	0,08 %
0,3416304	20	201,43	201,44	111,27	111,28	201,435	111,275	-0,01 %	0,10 %
0,35789852	21	201,43	201,44	111,3	111,31	201,435	111,305	-0,01 %	0,13 %
0,37416663	22	201,43	201,44	111,33	111,34	201,435	111,335	-0,01 %	0,16 %
0,39043474	23	201,43	201,44	111,36	111,37	201,435	111,365	-0,01 %	0,18 %
0,40670286	24	201,43	201,44	111,4	111,4	201,435	111,4	-0,01 %	0,22 %
0,42297097	25	201,43	201,44	111,43	111,44	201,435	111,435	-0,01 %	0,25 %
0,43923909	26	201,43	201,44	111,46	111,47	201,435	111,465	-0,01 %	0,27 %
0,4555072	27	201,43	201,43	111,5	111,5	201,43	111,5	-0,01 %	0,31 %
0,47177532	28	201,43	201,43	111,53	111,54	201,43	111,535	-0,01 %	0,34 %
0,48804343	29	201,42	201,43	111,56	111,57	201,425	111,565	-0,02 %	0,36 %
0,50431154	30	201,42	201,43	111,6	111,61	201,425	111,605	-0,02 %	0,40 %
0,52057966	31	201,42	201,43	111,63	111,64	201,425	111,635	-0,02 %	0,43 %
0,53684777	32	201,42	201,43	111,67	111,68	201,425	111,675	-0,02 %	0,46 %
0,55311589	33	201,42	201,43	111,71	111,71	201,425	111,71	-0,02 %	0,49 %
0,569384	34	201,42	201,42	111,74	111,75	201,42	111,745	-0,02 %	0,53 %
0,58565212	35	201,41	201,42	111,78	111,79	201,415	111,785	-0,02 %	0,56 %
0,60192023	36	201,41	201,42	111,82	111,83	201,415	111,825	-0,02 %	0,60 %
0,61818835	37	201,41	201,42	111,86	111,87	201,415	111,865	-0,02 %	0,63 %
0,63445646	38	201,41	201,42	111,9	111,9	201,415	111,9	-0,02 %	0,67 %
0,65072457	39	201,41	201,42	111,94	111,94	201,415	111,94	-0,02 %	0,70 %
0,66699269	40	201,4	201,41	111,98	111,99	201,405	111,985	-0,03 %	0,74 %
0,6832608	41	201,4	201,41	112,02	112,03	201,405	112,025	-0,03 %	0,78 %
0,69952892	42	201,4	201,41	112,06	112,07	201,405	112,065	-0,03 %	0,81 %
0,71579703	43	201,4	201,41	112,1	112,11	201,405	112,105	-0,03 %	0,85 %
0,73206515	44	201,4	201,4	112,15	112,15	201,4	112,15	-0,03 %	0,89 %
0,74833326	45	200,86	200,87	112,3	112,31	200,865	112,305	-0,30 %	1,03 %
0,76460137	46	200,28	200,3	112,65	112,66	200,29	112,655	-0,58 %	1,34 %
0,78086949	47	200,23	200,25	112,97	112,98	200,24	112,975	-0,61 %	1,63 %
0,7971376	48	200,17	200,19	113,3	113,3	200,18	113,3	-0,64 %	1,93 %
0,81340572	49	200,11	200,14	113,62	113,62	200,125	113,62	-0,66 %	2,21 %
0,82967383	50	200,05	200,08	113,93	113,93	200,065	113,93	-0,69 %	2,49 %
0,84594195	51	199,99	200,02	114,25	114,25	200,005	114,25	-0,72 %	2,78 %
0,86221006	52	199,92	199,96	114,57	114,55	199,94	114,56	-0,75 %	3,06 %
0,87847817	53	199,86	199,9	114,88	114,86	199,88	114,87	-0,78 %	3,34 %
0,89474629	54	199,79	199,83	115,19	115,17	199,81	115,18	-0,82 %	3,62 %
0,9110144	55	199,72	199,77	115,5	115,47	199,745	115,485	-0,85 %	3,89 %
0,92728252	56	199,65	199,7	115,8	115,77	199,675	115,785	-0,89 %	4,16 %
0,94355063	57	199,58	199,64	116,1	116,07	199,61	116,085	-0,92 %	4,43 %
0,95981875	58	199,5	199,57	116,41	116,36	199,535	116,385	-0,96 %	4,70 %
0,97608686	59	199,43	199,5	116,7	116,65	199,465	116,675	-0,99 %	4,96 %
0,99235498	60	199,36	199,43	117	116,94	199,395	116,97	-1,03 %	5,23 %

1,00862309	61	199,28	199,36	117,29	117,22	199,32	117,255	-1,06 %	5,48 %
1,0248912	62	199,2	199,29	117,58	117,51	199,245	117,545	-1,10 %	5,74 %
1,04115932	63	199,12	199,21	117,87	117,79	199,165	117,83	-1,14 %	6,00 %
1,05742743	64	199,04	199,14	118,16	118,06	199,09	118,11	-1,18 %	6,25 %
1,07369555	65	198,96	199,07	118,44	118,34	199,015	118,39	-1,21 %	6,50 %
1,08996366	66	198,88	198,99	118,72	118,61	198,935	118,665	-1,25 %	6,75 %
1,10623178	67	198,8	198,91	119	118,87	198,855	118,935	-1,29 %	6,99 %
1,12249989	68	198,72	198,83	119,27	119,14	198,775	119,205	-1,33 %	7,24 %
1,138768	69	198,63	198,74	119,54	119,4	198,685	119,47	-1,38 %	7,48 %
1,15503612	70	198,55	198,65	119,81	119,66	198,6	119,735	-1,42 %	7,71 %
1,17130423	71	198,46	198,55	120,07	119,92	198,505	119,995	-1,47 %	7,95 %

Table C 46. Contour results for CTSize a/32, 8 rows of elements new. Radius 0,651mm.

New rows									
NDIV crack surface lines		6							
Radius of refined region		0,651							
Elements		507							
CTSize		a/32							
Rows of elements		8							
		1	2	1	2	AVG	AVG		
Distance	Contour	KI	KI	KII	KII	KI	KII	KI% ERROR	KII% ERROR
0,06507246	1	202,03	202,03	110,81	110,81	202,03	110,81	0,28 %	-0,31 %
0,09042258	2	201,48	201,47	110,74	110,74	201,475	110,74	0,01 %	-0,38 %
0,12564829	3	201,48	201,47	110,82	110,82	201,475	110,82	0,01 %	-0,31 %
0,1745968	4	201,48	201,47	110,91	110,9	201,475	110,905	0,01 %	-0,23 %
0,24261406	5	201,48	201,47	111,02	111,02	201,475	111,02	0,01 %	-0,13 %
0,33712865	6	201,47	201,47	111,17	111,17	201,47	111,17	0,00 %	0,01 %
0,46846307	7	201,47	201,46	111,39	111,39	201,465	111,39	0,00 %	0,21 %
0,65096112	8	201,45	201,45	111,73	111,73	201,45	111,73	0,00 %	0,51 %

Table C 47. Contour results for CTSize a/64, 10 rows of elements new. Radius 0,6285mm.

New rows									
NDIV crack surface lines		6							
Radius of refined region		0,6285							
Elements		553							
CTSize		a/64							
Rows of elements		10							
		1	2	1	2	AVG	AVG		
Distance	Contour	KI	KI	KII	KII	KI	KII	KI% ERROR	KII% ERROR
0,03253623	1	202,07	202	110,64	110,68	202,035	110,66	0,29 %	-0,45 %
0,04521129	2	201,52	201,45	110,56	110,59	201,485	110,575	0,01 %	-0,53 %
0,06282415	3	201,52	201,45	110,62	110,66	201,485	110,64	0,01 %	-0,47 %
0,0872984	4	201,52	201,45	110,69	110,72	201,485	110,705	0,01 %	-0,41 %
0,12130703	5	201,52	201,45	110,76	110,8	201,485	110,78	0,01 %	-0,34 %
0,16856433	6	201,52	201,45	110,85	110,89	201,485	110,87	0,01 %	-0,26 %
0,23423153	7	201,52	201,45	110,96	111	201,485	110,98	0,01 %	-0,16 %
0,32548056	8	201,52	201,45	111,11	111,14	201,485	111,125	0,01 %	-0,03 %
0,45227725	9	201,51	201,44	111,32	111,35	201,475	111,335	0,01 %	0,16 %
0,62846983	10	201,5	201,43	111,64	111,68	201,465	111,66	0,00 %	0,45 %

Table C 48. Contour results for CTSize a/128, 12 rows of elements new. Radius 0,6068mm.

New rows									
NDIV crack surface lines		6							
Radius of refined region		0,6068							
Elements		619							
CTSize		a/128							
Rows of elements		12							
		1	2	1	2	AVG	AVG		
Distance	Contour	KI	KI	KII	KII	KI	KII	KI% ERROR	KII% ERROR
0,01626811	1	202	202,03	110,57	110,56	202,015	110,565	0,28 %	-0,54 %
0,02260565	2	201,45	201,48	110,48	110,47	201,465	110,475	0,00 %	-0,62 %
0,03141207	3	201,45	201,48	110,54	110,53	201,465	110,535	0,00 %	-0,56 %
0,0436492	4	201,45	201,48	110,6	110,59	201,465	110,595	0,00 %	-0,51 %
0,06065352	5	201,45	201,48	110,67	110,66	201,465	110,665	0,00 %	-0,45 %
0,08428216	6	201,45	201,48	110,74	110,73	201,465	110,735	0,00 %	-0,38 %
0,11711577	7	201,46	201,48	110,81	110,8	201,47	110,805	0,00 %	-0,32 %
0,16274028	8	201,46	201,48	110,9	110,89	201,47	110,895	0,00 %	-0,24 %
0,22613863	9	201,46	201,48	111	110,99	201,47	110,995	0,00 %	-0,15 %
0,31423492	10	201,45	201,48	111,14	111,13	201,465	111,135	0,00 %	-0,02 %
0,43665067	11	201,45	201,48	111,35	111,34	201,465	111,345	0,00 %	0,17 %
0,60675564	12	201,44	201,46	111,66	111,64	201,45	111,65	0,00 %	0,44 %

Table C 49. Contour results for CTSize a/256, 14 rows of elements new. Radius 0,5858mm.

New rows									
NDIV crack surface lines		6							
Radius of refined region		0,5858							
Elements		703							
CTSize		a/256							
Rows of elements		14							
		1	2	1	2	AVG	AVG		
Distance	Contour	KI	KI	KII	KII	KI	KII	KI% ERROR	KII% ERROR
0,00813406	1	202,04	202,02	110,44	110,44	202,03	110,44	0,28 %	-0,65 %
0,01130282	2	201,49	201,46	110,35	110,35	201,475	110,35	0,01 %	-0,73 %
0,01570604	3	201,49	201,46	110,41	110,41	201,475	110,41	0,01 %	-0,67 %
0,0218246	4	201,49	201,47	110,47	110,47	201,48	110,47	0,01 %	-0,62 %
0,03032676	5	201,49	201,47	110,53	110,53	201,48	110,53	0,01 %	-0,57 %
0,04214108	6	201,49	201,47	110,59	110,59	201,48	110,59	0,01 %	-0,51 %
0,05855788	7	201,5	201,47	110,66	110,66	201,485	110,66	0,01 %	-0,45 %
0,08137014	8	201,5	201,47	110,72	110,72	201,485	110,72	0,01 %	-0,40 %
0,11306931	9	201,5	201,47	110,8	110,8	201,485	110,8	0,01 %	-0,32 %
0,15711746	10	201,5	201,47	110,88	110,88	201,485	110,88	0,01 %	-0,25 %
0,21832534	11	201,5	201,47	110,99	110,99	201,485	110,99	0,01 %	-0,15 %
0,30337782	12	201,49	201,47	111,12	111,12	201,48	111,12	0,01 %	-0,04 %
0,421564	13	201,49	201,47	111,32	111,32	201,48	111,32	0,01 %	0,14 %
0,5857917	14	201,48	201,45	111,61	111,61	201,465	111,61	0,00 %	0,40 %

Table C 50. Contour results for CTSize a/512, 16 rows of elements new. Radius 0,5656mm.

New rows									
NDIV crack surface lines		6							
Radius of refined region		0,5656							
Elements		764							
CTSize		a/512							
Rows of elements		16							
		1	2	1	2	AVG	AVG		
Distance	Contour	KI	KI	KII	KII	KI	KII	KI% ERROR	KII% ERROR
0,00406703	1	202,04	202,25	110,33	110,33	202,145	110,33	0,34 %	-0,75 %
0,00565141	2	201,49	201,69	110,24	110,24	201,59	110,24	0,06 %	-0,83 %
0,00785302	3	201,49	201,7	110,29	110,3	201,595	110,295	0,07 %	-0,78 %
0,0109123	4	201,49	201,7	110,35	110,36	201,595	110,355	0,07 %	-0,72 %
0,01516338	5	201,49	201,7	110,41	110,41	201,595	110,41	0,07 %	-0,67 %
0,02107054	6	201,49	201,7	110,47	110,47	201,595	110,47	0,07 %	-0,62 %
0,02927894	7	201,5	201,7	110,53	110,53	201,6	110,53	0,07 %	-0,57 %
0,04068507	8	201,5	201,7	110,59	110,6	201,6	110,595	0,07 %	-0,51 %
0,05653466	9	201,5	201,7	110,66	110,66	201,6	110,66	0,07 %	-0,45 %
0,07855873	10	201,5	201,71	110,72	110,73	201,605	110,725	0,07 %	-0,39 %
0,10916267	11	201,5	201,71	110,8	110,8	201,605	110,8	0,07 %	-0,32 %
0,15168891	12	201,5	201,71	110,88	110,88	201,605	110,88	0,07 %	-0,25 %
0,210782	13	201,5	201,71	110,98	110,99	201,605	110,985	0,07 %	-0,16 %
0,29289585	14	201,5	201,7	111,11	111,12	201,6	111,115	0,07 %	-0,04 %
0,40699859	15	201,49	201,7	111,3	111,3	201,595	111,3	0,07 %	0,13 %
0,56555207	16	201,48	201,69	111,58	111,59	201,585	111,585	0,06 %	0,38 %

Table C 51. Contour results for CTSize a/1024, 18 rows of elements new. Radius 0,546mm.

New rows									
NDIV crack surface lines		6							
Radius of refined region		0,546							
Elements		821							
CTSize		a/1024							
Rows of elements		18							
		1	2	1	2	AVG	AVG		
Distance	Contour	KI	KI	KII	KII	KI	KII	KI% ERROR	KII%
0,00203351	1	202,02	202,05	110,21	110,19	202,035	110,2	0,29 %	-0,86 %
0,00282571	2	201,47	201,49	110,12	110,1	201,48	110,11	0,01 %	-0,94 %
0,00392651	3	201,47	201,5	110,18	110,16	201,485	110,17	0,01 %	-0,89 %
0,00545615	4	201,47	201,5	110,24	110,22	201,485	110,23	0,01 %	-0,84 %
0,00758169	5	201,47	201,5	110,3	110,28	201,485	110,29	0,01 %	-0,78 %
0,01053527	6	201,47	201,5	110,35	110,34	201,485	110,345	0,01 %	-0,73 %
0,01463947	7	201,48	201,5	110,41	110,4	201,49	110,405	0,01 %	-0,68 %
0,02034253	8	201,48	201,5	110,47	110,46	201,49	110,465	0,01 %	-0,63 %
0,02826733	9	201,48	201,51	110,53	110,52	201,495	110,525	0,02 %	-0,57 %
0,03927936	10	201,48	201,51	110,59	110,58	201,495	110,585	0,02 %	-0,52 %
0,05458133	11	201,48	201,51	110,66	110,64	201,495	110,65	0,02 %	-0,46 %
0,07584446	12	201,48	201,51	110,73	110,71	201,495	110,72	0,02 %	-0,40 %
0,105391	13	201,48	201,51	110,8	110,78	201,495	110,79	0,02 %	-0,33 %
0,14644792	14	201,48	201,51	110,88	110,86	201,495	110,87	0,02 %	-0,26 %
0,2034993	15	201,48	201,51	110,98	110,96	201,495	110,97	0,02 %	-0,17 %
0,28277604	16	201,48	201,51	111,11	111,09	201,495	111,1	0,02 %	-0,05 %
0,39293643	17	201,48	201,5	111,28	111,27	201,49	111,275	0,01 %	0,10 %
0,54601175	18	201,47	201,5	111,55	111,54	201,485	111,545	0,01 %	0,35 %

Table C 52. Contour results for CTSize a/2048, 20 rows of elements new. Radius 0,5271mm.

New rows									
NDIV crack surface lines		6							
Radius of refined region		0,5271							
Elements		912							
CTSize		a/2048							
Rows of elements		20							
		1	2	1	2	AVG	AVG		
Distance	Contour	KI	KI	KII	KII	KI	KII	KI%	KII% ERROR
0,00101676	1	202,03	202	110,08	110,07	202,015	110,075	0,28 %	-0,98 %
0,00141285	2	201,48	201,45	109,99	109,98	201,465	109,985	0,00 %	-1,06 %
0,00196325	3	201,48	201,45	110,05	110,04	201,465	110,045	0,00 %	-1,00 %
0,00272808	4	201,48	201,45	110,11	110,1	201,465	110,105	0,00 %	-0,95 %
0,00379084	5	201,48	201,45	110,17	110,15	201,465	110,16	0,00 %	-0,90 %
0,00526764	6	201,49	201,46	110,23	110,21	201,475	110,22	0,01 %	-0,85 %
0,00731974	7	201,49	201,46	110,28	110,27	201,475	110,275	0,01 %	-0,80 %
0,01017127	8	201,49	201,46	110,34	110,33	201,475	110,335	0,01 %	-0,74 %
0,01413366	9	201,49	201,46	110,4	110,39	201,475	110,395	0,01 %	-0,69 %
0,01963968	10	201,49	201,46	110,46	110,45	201,475	110,455	0,01 %	-0,63 %
0,02729067	11	201,49	201,46	110,52	110,51	201,475	110,515	0,01 %	-0,58 %
0,03792223	12	201,49	201,46	110,58	110,57	201,475	110,575	0,01 %	-0,53 %
0,0526955	13	201,5	201,47	110,65	110,63	201,485	110,64	0,01 %	-0,47 %
0,07322396	14	201,5	201,47	110,71	110,7	201,485	110,705	0,01 %	-0,41 %
0,10174965	15	201,5	201,47	110,78	110,77	201,485	110,775	0,01 %	-0,35 %
0,14138802	16	201,5	201,47	110,87	110,85	201,485	110,86	0,01 %	-0,27 %
0,19646821	17	201,5	201,47	110,96	110,95	201,485	110,955	0,01 %	-0,18 %
0,27300587	18	201,5	201,47	111,09	111,07	201,485	111,08	0,01 %	-0,07 %
0,37936013	19	201,49	201,46	111,26	111,24	201,475	111,25	0,01 %	0,08 %
0,52714656	20	201,48	201,45	111,51	111,5	201,465	111,505	0,00 %	0,31 %

6.4 D

The used parameters for square sizes, are, 500x500 for outer square size, and 10x10 for inner square size.

Table D 1. Connection lines set to 5, 15 and 25 divisions with enrichment field SING a/8 applied. Only Q4 elements.

SING a/8	Connection lines	5						15						25				
Square lines	MESH200 elements	Elements	KI	KII	KI% ERROR	KII% ERROR	MESH200 elements	Elements	KI	KII	KI% ERROR	KII% ERROR	MESH200 elements	Elements	KI	KII	KI% ERROR	KII% ERROR
35	101	1925	191,17	118,57	-5,11 %	6,67 %	101	3325	194,58	121,61	-3,41 %	9,40 %	101	4725	196,12	123,1	-2,65 %	10,74 %
45	102	2925	193,54	114,18	-3,93 %	2,72 %	102	4725	196,92	116,98	-2,25 %	5,24 %	102	6525	198,45	118,34	-1,49 %	6,46 %
55	101	4125	194,89	111,19	-3,26 %	0,03 %	101	6325	198,26	113,82	-1,59 %	2,39 %	101	8525	199,79	115,1	-0,83 %	3,55 %
65	103	5525	195,76	108,96	-2,83 %	-1,98 %	103	8125	199,14	111,49	-1,15 %	0,30 %	103	10725	200,68	112,73	-0,39 %	1,41 %
75	103	7125	196,11	107,55	-2,65 %	-3,25 %	103	10125	199,47	110,02	-0,99 %	-1,02 %	103	13125	201	111,21	-0,23 %	0,05 %
85	103	8925	196,31	106,59	-2,55 %	-4,11 %	103	12325	199,66	109	-0,89 %	-1,94 %	103	15725	201,19	110,17	-0,13 %	-0,89 %
95	102	10925	196,42	105,85	-2,50 %	-4,78 %	102	14725	199,75	108,23	-0,85 %	-2,63 %	102	18525	201,26	109,37	-0,10 %	-1,61 %
105	102	13125	194,45	104,37	-3,48 %	-6,11 %	102	17325	197,74	106,69	-1,84 %	-4,02 %	102	21525	199,24	107,81	-1,10 %	-3,01 %
115	102	15525	194,74	104,34	-3,33 %	-6,13 %	102	20125	198,02	106,65	-1,71 %	-4,06 %	102	24725	199,51	107,76	-0,97 %	-3,06 %
125	102	18125	194,73	104,17	-3,34 %	-6,29 %	102	23125	198	106,46	-1,72 %	-4,23 %						
135	101	20925	194,71	104,06	-3,35 %	-6,39 %												
145	102	23925	194,85	103,79	-3,28 %	-6,63 %												

Table D 2. Connection lines set to 35, 45 and 55 divisions with enrichment field SING a/8 applied. Only Q4 elements.

SING a/8	Connection lines	35						45						55				
Square lines	MESH200 elements	Elements	KI	KII	KI% ERROR	KII% ERROR	MESH200 elements	Elements	KI	KII	KI% ERROR	KII% ERROR	MESH200 elements	Elements	KI	KII	KI% ERROR	KII% ERROR
35	101	6125	196,93	123,91	-2,25 %	11,47 %	101	7525	197,4	124,39	-2,01 %	11,90 %	101	8925	197,7	124,7	-1,86 %	12,18 %
45	102	8325	199,26	119,08	-1,09 %	7,13 %	102	10125	199,73	119,52	-0,86 %	7,52 %	102	11925	200,03	119,81	-0,71 %	7,78 %
55	101	10725	200,6	115,8	-0,43 %	4,18 %	101	12925	201,07	116,21	-0,19 %	4,54 %	101	15125	201,36	116,48	-0,05 %	4,79 %
65	103	13325	201,49	113,4	0,02 %	2,02 %	103	16025	201,96	113,8	0,25 %	2,38 %	103	18525	202,25	114,05	0,39 %	2,60 %
75	103	16125	201,81	111,86	0,18 %	0,63 %	103	19125	202,28	112,25	0,41 %	0,98 %	103	22125	202,57	112,49	0,55 %	1,20 %
85	103	19125	201,99	110,8	0,26 %	-0,32 %	103	22525	202,46	111,18	0,50 %	0,02 %	103	25925	202,75	111,42	0,64 %	0,23 %
95	102	22325	202,06	109,99	0,30 %	-1,05 %	102	26125	202,53	110,37	0,53 %	-0,71 %						
105	102	25725	200,02	108,42	-0,71 %	-2,46 %												

Table D 3. Connection lines set to 65 and 75 divisions with enrichment field SING a/8 applied. Only Q4 elements.

SING a/8	Connection lines	65						75				
Square lines	MESH200 elements	Elements	KI	KII	KI% ERROR	KII% ERROR	MESH200 elements	Elements	KI	KII	KI% ERROR	KII% ERROR
35	101	10325	197,89	124,9	-1,77 %	12,36 %	101	11725	198,03	125,04	-1,70 %	12,49 %
45	102	13725	200,22	119,99	-0,61 %	7,94 %	102	15525	200,35	120,13	-0,55 %	8,07 %
55	101	17325	201,56	116,65	0,05 %	4,94 %	101	19525	201,69	116,77	0,12 %	5,05 %
65	103	21125	202,45	114,22	0,49 %	2,75 %	103	23725	202,59	114,34	0,56 %	2,86 %
75	103	25125	202,76	112,65	0,65 %	1,34 %	103	28125	202,9	112,77	0,72 %	1,45 %

Table D 4. Connection lines set to 5, 15 and 25 divisions with enrichment field SING 0 applied. Only Q4 elements.

SING 0	Connection lines	5						15						25				
Square lines	MESH200 elements	Elements	KI	KII	KI% ERROR	KII% ERROR	MESH200 elements	Elements	KI	KII	KI% ERROR	KII% ERROR	MESH200 elements	Elements	KI	KII	KI% ERROR	KII% ERROR
35	101	1925	191,17	118,57	-5,11 %	6,67 %	101	3325	194,58	121,61	-3,41 %	9,40 %	101	4725	196,12	123,1	-2,65 %	10,74 %
45	102	2925	192,89	114,81	-4,25 %	3,28 %	102	4725	196,28	117,62	-2,57 %	5,81 %	102	6525	197,81	118,98	-1,81 %	7,04 %
55	101	4125	194,3	111,79	-3,55 %	0,57 %	101	6325	197,67	114,43	-1,88 %	2,94 %	101	8525	199,21	115,71	-1,12 %	4,09 %
65	103	5525	195,03	109,75	-3,19 %	-1,27 %	103	8125	198,38	112,28	-1,53 %	1,01 %	103	10725	199,91	113,51	-0,77 %	2,12 %
75	103	7125	195,46	108,29	-2,98 %	-2,58 %	103	10125	198,8	110,74	-1,32 %	-0,38 %	103	13125	200,32	111,93	-0,56 %	0,69 %
85	103	8925	195,7	107,28	-2,86 %	-3,49 %	103	12325	199,02	109,69	-1,21 %	-1,32 %	103	15725	200,54	110,85	-0,46 %	-0,28 %
95	102	10925	195,85	106,5	-2,78 %	-4,19 %	102	14725	199,16	108,87	-1,14 %	-2,06 %	102	18525	200,67	110,01	-0,39 %	-1,03 %
105	102	13125	195,92	106,09	-2,75 %	-4,56 %	102	17325	199,22	108,43	-1,11 %	-2,45 %	102	21525	200,73	109,55	-0,36 %	-1,45 %
115	102	15525	195,96	105,73	-2,73 %	-4,88 %	102	20125	199,24	108,05	-1,10 %	-2,80 %	102	24725	200,74	109,17	-0,36 %	-1,79 %
125	102	18125	195,98	105,53	-2,72 %	-5,06 %	102	23125	199,25	107,83	-1,10 %	-2,99 %						
135	101	20925	195,97	105,39	-2,72 %	-5,19 %												
145	102	23925	195,95	105,25	-2,73 %	-5,32 %												

Table D 5. Connection lines set to 35, 45 and 55 divisions with enrichment field SING 0 applied. Only Q4 elements.

SING 0	Connection lines	35						45						55				
Square lines	MESH200 elements	Elements	KI	KII	KI% ERROR	KII% ERROR	MESH200 elements	Elements	KI	KII	KI% ERROR	KII% ERROR	MESH200 elements	Elements	KI	KII	KI% ERROR	KII% ERROR
35	101	6125	196,93	123,91	-2,25 %	11,47 %	101	7525	197,4	124,39	-2,01 %	11,90 %	101	8925	197,7	124,7	-1,86 %	12,18 %
45	102	8325	198,62	119,73	-1,41 %	7,71 %	102	10125	199,09	120,17	-1,17 %	8,11 %	102	11925	199,39	120,45	-1,03 %	8,36 %
55	101	10725	200,02	116,41	-0,71 %	4,72 %	101	12925	200,49	116,82	-0,48 %	5,09 %	101	15125	200,78	117,09	-0,34 %	5,34 %
65	103	13325	200,72	114,18	-0,37 %	2,72 %	103	16025	201,19	114,57	-0,13 %	3,07 %	103	18525	201,48	114,83	0,01 %	3,30 %
75	103	16125	201,12	112,58	-0,17 %	1,28 %	103	19125	201,59	112,96	0,07 %	1,62 %	103	22125	201,88	113,21	0,21 %	1,85 %
85	103	19125	201,33	111,48	-0,06 %	0,29 %	103	22525	201,8	111,86	0,17 %	0,63 %	103	25925	202,09	112,1	0,31 %	0,85 %
95	102	22325	201,47	110,63	0,01 %	-0,48 %	102	26125	201,93	111	0,23 %	-0,14 %						
105	102	25725	201,52	110,17	0,03 %	-0,89 %												

Table D 6. Connection lines set to 65 and 75 divisions with enrichment field SING 0 applied. Only Q4 elements.

SING 0	Connection lines	65						75				
Square lines	MESH200 elements	Elements	KI	KII	KI% ERROR	KII% ERROR	MESH200 elements	Elements	KI	KII	KI% ERROR	KII% ERROR
35	101	10325	197,89	124,9	-1,77 %	12,36 %	101	11725	198,03	125,04	-1,70 %	12,49 %
45	102	13725	199,58	120,64	-0,93 %	8,53 %	102	15525	199,72	120,77	-0,86 %	8,65 %
55	101	17325	200,97	117,26	-0,24 %	5,49 %	101	19525	201,11	117,39	-0,17 %	5,61 %
65	103	21125	201,67	114,99	0,11 %	3,45 %	103	23725	201,81	115,11	0,18 %	3,55 %
75	103	25125	202,07	113,37	0,30 %	1,99 %	103	28125	202,21	113,48	0,37 %	2,09 %

Table D 7. Used parameters 1.

Used parameters 1	
NDIV Connection lines	1

Table D 8. SING 0 for various square line divisions. Q4 + Q8. Connection lines set to 1 division.

SING	0					
MESH200 elements	Elements	NDIV square lines	KI	KII	KI% ERROR	KII% ERROR
101	1365	35	198,5	125,56	-1,47 %	12,96 %
102	2205	45	200,19	121,25	-0,63 %	9,08 %
101	3245	55	201,59	117,83	0,07 %	6,00 %
103	4485	65	202,29	115,55	0,41 %	3,95 %
103	5925	75	202,69	113,9	0,61 %	2,47 %
103	7565	85	202,89	112,77	0,71 %	1,45 %
101	9405	95	203,02	111,9	0,78 %	0,67 %
101	11445	105	203,07	111,42	0,80 %	0,23 %
101	13685	115	203,07	111,01	0,80 %	-0,13 %
101	16125	125	203,07	110,77	0,80 %	-0,35 %
101	18765	135	203,04	110,61	0,79 %	-0,49 %
102	21605	145	203	110,45	0,77 %	-0,64 %

Table D 9. SING a/8 for various square line divisions. Q4 + Q8. Connection lines set to 1 division.

SING	a/8					
MESH200 elements	Elements	NDIV square lines	KI	KII	KI% ERROR	KII% ERROR
101	1365	35	198,5	125,56	-1,47 %	12,96 %
102	2205	45	200,83	120,6	-0,31 %	8,49 %
101	3245	55	202,17	117,22	0,35 %	5,45 %
103	4485	65	203,06	114,77	0,80 %	3,25 %
103	5925	75	203,38	113,19	0,95 %	1,83 %
103	7565	85	203,55	112,1	1,04 %	0,85 %
101	9405	95	203,63	111,26	1,08 %	0,09 %
101	11445	105	201,57	109,66	0,06 %	-1,35 %
101	13685	115	201,83	109,59	0,19 %	-1,41 %
101	16125	125	201,8	109,38	0,17 %	-1,60 %
101	18765	135	201,75	109,25	0,15 %	-1,72 %
102	21605	145	201,89	108,96	0,22 %	-1,98 %

Table D 10. SING a/4 for various square line divisions. Q4 + Q8. Connection lines set to 1 division.

SING	a/4					
MESH200 elements	Elements	NDIV square lines	KI	KII	KI% ERROR	KII% ERROR
101	1365	35	199,63	124,35	-0,91 %	11,87 %
102	2205	45	201,24	120,16	-0,11 %	8,10 %
101	3245	55	200,35	115,61	-0,55 %	4,00 %
103	4485	65	201,26	113,77	-0,10 %	2,35 %
103	5925	75	201,89	111,88	0,22 %	0,65 %
103	7565	85	202,15	110,93	0,34 %	-0,21 %
101	9405	95	201,28	109,57	-0,09 %	-1,43 %
101	11445	105	202,16	109,77	0,35 %	-1,25 %
101	13685	115	201,66	108,64	0,10 %	-2,27 %
101	16125	125	202,3	108,87	0,42 %	-2,06 %
101	18765	135	201,63	108,42	0,09 %	-2,46 %

Table D 11. SING a/2 for various square line divisions. Q4 + Q8. Connection lines set to 1 division.

SING	a/2					
MESH200 elements	Elements	NDIV square lines	KI	KII	KI% ERROR	KII% ERROR
101	1365	35	197,84	123,23	-1,80 %	10,86 %
102	2205	45	198,81	118,16	-1,31 %	6,30 %
101	3245	55	200,3	115,22	-0,57 %	3,65 %
103	4485	65	201,18	112,86	-0,14 %	1,53 %
103	5925	75	201,61	111,39	0,08 %	0,21 %
103	7565	85	202,09	110,38	0,31 %	-0,70 %
101	9405	95	203,07	109,68	0,80 %	-1,33 %
101	11445	105	203,57	109,77	1,05 %	-1,25 %
101	13685	115	203,49	109,46	1,01 %	-1,53 %
101	16125	125	203,47	109,14	1,00 %	-1,82 %

Table D 12. SING a for various square line divisions. Q4 + Q8. Connection lines set to 1 division.

SING	a					
MESH200 elements	Elements	NDIV square lines	KI	KII	KI% ERROR	KII% ERROR
101	1365	35	196,1	123,3	-2,66 %	10,92 %
102	2205	45	198,93	119,38	-1,25 %	7,40 %
101	3245	55	201,55	115,9	0,05 %	4,27 %
103	4485	65	202,31	113,85	0,42 %	2,42 %
103	5925	75	202,72	112,48	0,63 %	1,19 %
103	7565	85	203,01	111,49	0,77 %	0,30 %
101	9405	95	203,15	110,62	0,84 %	-0,48 %

Table D 13. Contours 1-20 for square line division 55, SING 0.

SING	0							
NDIV square lines	55							
	1	2	1	2	AVG	AVG		
Contour	KI	KI	KII	KII	KI	KII	KI%	KII%
1	203,27	203,27	109,45	109,45	203,27	109,45	0,90 %	-1,54 %
2	204,09	204,09	110,04	110,04	204,09	110,04	1,31 %	-1,01 %
3	204,29	204,29	111,07	111,07	204,29	111,07	1,40 %	-0,08 %
4	203,61	203,61	112,67	112,67	203,61	112,67	1,07 %	1,36 %
5	202,45	202,45	116,35	116,35	202,45	116,35	0,49 %	4,67 %
6	201,24	201,24	119,3	119,3	201,24	119,3	-0,11 %	7,32 %
7	199,78	199,78	122,36	122,36	199,78	122,36	-0,83 %	10,08 %
8	198,16	198,16	125,25	125,25	198,16	125,25	-1,64 %	12,68 %
9	196,58	196,58	127,87	127,87	196,58	127,87	-2,42 %	15,03 %
10	195,19	195,19	130,04	130,04	195,19	130,04	-3,11 %	16,98 %
11	194,22	194,22	131,68	131,68	194,22	131,68	-3,59 %	18,46 %
12	193,88	193,88	132,75	132,75	193,88	132,75	-3,76 %	19,42 %
13	194,35	194,35	133,3	133,3	194,35	133,3	-3,53 %	19,92 %
14	195,8	195,8	133,39	133,39	195,8	133,39	-2,81 %	20,00 %
15	198,66	198,66	133,51	133,51	198,66	133,51	-1,39 %	20,11 %
16	201,96	201,96	132,7	132,7	201,96	132,7	0,25 %	19,38 %
17	43368	38006	18875	50970	40687	34922,5	########	########
18	40991	38114	17335	51126	39552,5	34230,5	########	########
19	40983	38097	17332	51120	39540	34226	########	########
20	40975	38080	17330	51115	39527,5	34222,5	########	########

Table D 14. Contours 1-20 for square line division 105, SING 0.

SING	0							
NDIV square lines	105							
	1	2	1	2	AVG	AVG		
Contour	KI	KI	KII	KII	KI	KII	KI%	KII%
1	202,13	202,13	109,74	109,74	202,13	109,74	0,33 %	-1,28 %
2	203,21	203,21	110,38	110,38	203,21	110,38	0,87 %	-0,70 %
3	203,32	203,32	110,27	110,27	203,32	110,27	0,92 %	-0,80 %
4	203,3	203,3	110,01	110,01	203,3	110,01	0,91 %	-1,03 %
5	203,21	203,21	110,56	110,56	203,21	110,56	0,87 %	-0,54 %
6	203,18	203,18	111,28	111,28	203,18	111,28	0,85 %	0,11 %
7	202,85	202,85	112,57	112,57	202,85	112,57	0,69 %	1,27 %
8	202,53	202,53	113,8	113,8	202,53	113,8	0,53 %	2,37 %
9	202,11	202,11	115,14	115,14	202,11	115,14	0,32 %	3,58 %
10	201,6	201,6	116,6	116,6	201,6	116,6	0,07 %	4,89 %
11	201	201	118,15	118,15	201	118,15	-0,23 %	6,29 %
12	200,3	200,3	119,73	119,73	200,3	119,73	-0,58 %	7,71 %
13	199,53	199,53	121,33	121,33	199,53	121,33	-0,96 %	9,15 %
14	198,71	198,71	122,91	122,91	198,71	122,91	-1,37 %	10,57 %
15	197,49	197,49	125,07	125,07	197,49	125,07	-1,97 %	12,51 %
16	197,01	197,01	125,91	125,91	197,01	125,91	-2,21 %	13,27 %
17	195,84	195,84	127,81	127,81	195,84	127,81	-2,79 %	14,98 %
18	195,08	195,08	129,02	129,02	195,08	129,02	-3,17 %	16,07 %
19	194,42	194,42	130,07	130,07	194,42	130,07	-3,49 %	17,01 %
20	193,87	193,87	130,99	130,99	193,87	130,99	-3,77 %	17,84 %

Table D 15. Contours 1-20 for square line division 115, SING 0.

SING	0							
NDIV square lines	115							
	1	2	1	2	AVG	AVG		
Contour	KI	KI	KII	KII	KI	KII	KI%	KII%
1	202,02	202,02	109,77	109,77	202,02	109,77	0,28 %	-1,25 %
2	203,1	203,1	110,41	110,41	203,1	110,41	0,81 %	-0,67 %
3	203,21	203,21	110,28	110,28	203,21	110,28	0,87 %	-0,79 %
4	203,22	203,22	109,85	109,85	203,22	109,85	0,87 %	-1,18 %
5	203,19	203,19	110,26	110,26	203,19	110,26	0,86 %	-0,81 %
6	203,16	203,16	110,95	110,95	203,16	110,95	0,84 %	-0,19 %
7	202,93	202,93	111,89	111,89	202,93	111,89	0,73 %	0,66 %
8	202,72	202,72	112,83	112,83	202,72	112,83	0,63 %	1,50 %
9	202,39	202,39	114,05	114,05	202,39	114,05	0,46 %	2,60 %
10	202	202	115,29	115,29	202	115,29	0,27 %	3,72 %
11	201,52	201,52	116,63	116,63	201,52	116,63	0,03 %	4,92 %
12	200,96	200,96	118,03	118,03	200,96	118,03	-0,25 %	6,18 %
13	200,34	200,34	119,48	119,48	200,34	119,48	-0,56 %	7,48 %
14	199,65	199,65	120,94	120,94	199,65	120,94	-0,90 %	8,80 %
15	198,56	198,56	122,99	122,99	198,56	122,99	-1,44 %	10,64 %
16	198,14	198,14	123,81	123,81	198,14	123,81	-1,65 %	11,38 %
17	197,02	197,02	125,73	125,73	197,02	125,73	-2,20 %	13,11 %
18	196,26	196,26	127	127	196,26	127	-2,58 %	14,25 %
19	195,54	195,54	128,16	128,16	195,54	128,16	-2,94 %	15,29 %
20	194,86	194,86	129,23	129,23	194,86	129,23	-3,28 %	16,26 %

Table D 16. Contours 1-20 for square line division 145, SING 0.

SING	0							
NDIV	145							
	1	2	1	2	AVG	AVG		
Contour	KI	KI	KII	KII	KI	KII	KI%	KII%
1	201,77	201,77	109,84	109,84	201,77	109,84	0,15 %	-1,19 %
2	202,85	202,85	110,49	110,49	202,85	110,49	0,69 %	-0,60 %
3	202,97	202,97	110,31	110,31	202,97	110,31	0,75 %	-0,76 %
4	203,03	203,03	109,92	109,92	203,03	109,92	0,78 %	-1,12 %
5	203,09	203,09	110,16	110,16	203,09	110,16	0,81 %	-0,90 %
6	203,04	203,04	110,35	110,35	203,04	110,35	0,78 %	-0,73 %
7	202,97	202,97	110,68	110,68	202,97	110,68	0,75 %	-0,43 %
8	202,88	202,88	111,29	111,29	202,88	111,29	0,70 %	0,12 %
9	202,74	202,74	112,01	112,01	202,74	112,01	0,64 %	0,76 %
10	202,56	202,56	112,8	112,8	202,56	112,8	0,55 %	1,48 %
11	202,33	202,33	113,67	113,67	202,33	113,67	0,43 %	2,26 %
12	202,05	202,05	114,61	114,61	202,05	114,61	0,29 %	3,10 %
13	201,71	201,71	115,63	115,63	201,71	115,63	0,12 %	4,02 %
14	201,32	201,32	116,69	116,69	201,32	116,69	-0,07 %	4,97 %
15	200,63	200,63	118,27	118,27	200,63	118,27	-0,41 %	6,40 %
16	200,4	200,4	118,94	118,94	200,4	118,94	-0,53 %	7,00 %
17	199,6	199,6	120,58	120,58	199,6	120,58	-0,92 %	8,47 %
18	199,05	199,05	121,75	121,75	199,05	121,75	-1,20 %	9,53 %
19	198,45	198,45	122,88	122,88	198,45	122,88	-1,49 %	10,54 %
20	197,85	197,85	124,01	124,01	197,85	124,01	-1,79 %	11,56 %

Table D 17. Contours 1-20 for square line division 95, SING 0.

SING	0							
NDIV square lines	95							
	1	2	1	2	AVG	AVG		
Contour	KI	KI	KII	KII	KI	KII	KI%	KII%
1	202,26	202,26	109,71	109,71	202,26	109,71	0,40 %	-1,30 %
2	203,34	203,34	110,34	110,34	203,34	110,34	0,93 %	-0,74 %
3	203,36	203,36	109,89	109,89	203,36	109,89	0,94 %	-1,14 %
4	203,38	203,38	110,24	110,24	203,38	110,24	0,95 %	-0,83 %
5	203,24	203,24	111,03	111,03	203,24	111,03	0,88 %	-0,12 %
6	203,19	203,19	111,75	111,75	203,19	111,75	0,86 %	0,53 %
7	202,71	202,71	113,49	113,49	202,71	113,49	0,62 %	2,10 %
8	202,26	202,26	114,97	114,97	202,26	114,97	0,40 %	3,43 %
9	201,7	201,7	116,57	116,57	201,7	116,57	0,12 %	4,87 %
10	201,03	201,03	118,27	118,27	201,03	118,27	-0,21 %	6,40 %
11	200,26	200,26	120,04	120,04	200,26	120,04	-0,60 %	7,99 %
12	199,39	199,39	121,8	121,8	199,39	121,8	-1,03 %	9,57 %
13	198,47	198,47	123,54	123,54	198,47	123,54	-1,48 %	11,14 %
14	197,52	197,52	125,2	125,2	197,52	125,2	-1,96 %	12,63 %
15	196,2	196,2	127,37	127,37	196,2	127,37	-2,61 %	14,58 %
16	195,69	195,69	128,17	128,17	195,69	128,17	-2,86 %	15,30 %
17	194,59	194,59	129,95	129,95	194,59	129,95	-3,41 %	16,90 %
18	193,96	193,96	130,99	130,99	193,96	130,99	-3,72 %	17,84 %
19	193,53	193,53	131,82	131,82	193,53	131,82	-3,94 %	18,59 %
20	193,29	193,29	132,49	132,49	193,29	132,49	-4,06 %	19,19 %

Table D 18. Contours 1-20 for square line division 95, SING a/8.

SING	a/8							
NDIV	95							
	1	2	1	2	AVG	AVG		
Contour	KI	KI	KII	KII	KI	KII	KI%	KII%
1	198,13	198,13	103,52	103,52	198,13	103,52	-1,65 %	-6,87 %
2	200,29	200,29	109,04	109,04	200,29	109,04	-0,58 %	-1,91 %
3	203,87	203,87	109,01	109,01	203,87	109,01	1,20 %	-1,93 %
4	204,02	204,02	109,55	109,55	204,02	109,55	1,27 %	-1,45 %
5	203,86	203,86	110,48	110,48	203,86	110,48	1,19 %	-0,61 %
6	203,82	203,82	111,09	111,09	203,82	111,09	1,17 %	-0,06 %
7	203,32	203,32	112,97	112,97	203,32	112,97	0,92 %	1,63 %
8	202,86	202,86	114,47	114,47	202,86	114,47	0,69 %	2,98 %
9	202,29	202,29	116,09	116,09	202,29	116,09	0,41 %	4,44 %
10	201,6	201,6	117,82	117,82	201,6	117,82	0,07 %	5,99 %
11	200,82	200,82	119,6	119,6	200,82	119,6	-0,32 %	7,59 %
12	199,93	199,93	121,39	121,39	199,93	121,39	-0,76 %	9,20 %
13	198,99	198,99	123,15	123,15	198,99	123,15	-1,23 %	10,79 %
14	198,02	198,02	124,83	124,83	198,02	124,83	-1,71 %	12,30 %
15	196,67	196,67	127,06	127,06	196,67	127,06	-2,38 %	14,30 %
16	196,14	196,14	127,85	127,85	196,14	127,85	-2,64 %	15,01 %
17	195	195	129,68	129,68	195	129,68	-3,21 %	16,66 %
18	194,33	194,33	130,73	130,73	194,33	130,73	-3,54 %	17,61 %
19	193,87	193,87	131,59	131,59	193,87	131,59	-3,77 %	18,38 %
20	193,59	193,59	132,27	132,27	193,59	132,27	-3,91 %	18,99 %

Table D 19. Contours 1-20 for square line division 95, SING a/4.

SING	a/4							
NDIV Square lines	95							
	1	2	1	2	AVG	AVG		
Contour	KI	KI	KII	KII	KI	KII	KI%	KII%
1	201,72	201,72	102,62	102,62	201,72	102,62	0,13 %	-7,68 %
2	203,61	203,61	108,1	108,1	203,61	108,1	1,07 %	-2,75 %
3	203,72	203,72	107,79	107,79	203,72	107,79	1,12 %	-3,03 %
4	197,6	197,6	105,5	105,49	197,6	105,495	-1,92 %	-5,10 %
5	196,19	196,19	106,01	106,01	196,19	106,01	-2,62 %	-4,63 %
6	203,89	203,89	110,96	110,96	203,89	110,96	1,21 %	-0,18 %
7	203,38	203,38	112,84	112,84	203,38	112,84	0,95 %	1,51 %
8	202,92	202,92	114,33	114,33	202,92	114,33	0,72 %	2,85 %
9	202,35	202,35	115,94	115,94	202,35	115,94	0,44 %	4,30 %
10	201,67	201,67	117,67	117,67	201,67	117,67	0,10 %	5,86 %
11	200,88	200,88	119,45	119,45	200,88	119,45	-0,29 %	7,46 %
12	199,99	199,99	121,24	121,24	199,99	121,24	-0,73 %	9,07 %
13	199,05	199,05	122,99	122,99	199,05	122,99	-1,20 %	10,64 %
14	198,08	198,08	124,67	124,67	198,08	124,67	-1,68 %	12,15 %
15	196,74	196,74	126,9	126,9	196,74	126,9	-2,34 %	14,16 %
16	196,21	196,21	127,69	127,69	196,21	127,69	-2,61 %	14,87 %
17	195,07	195,07	129,51	129,51	195,07	129,51	-3,17 %	16,51 %
18	194,41	194,41	130,57	130,57	194,41	130,57	-3,50 %	17,46 %
19	193,95	193,95	131,42	131,42	193,95	131,42	-3,73 %	18,23 %
20	193,68	193,68	132,1	132,1	193,68	132,1	-3,86 %	18,84 %

Table D 20. Contours 1-20 for square line division 95, SING a/2.

SING	a/2							
NDIV Square lines	95							
	1	2	1	2	AVG	AVG		
Contour	KI	KI	KII	KII	KI	KII	KI%	KII%
1	202,26	202,26	101,96	101,97	202,26	101,965	0,40 %	-8,27 %
2	204,21	204,21	107,55	107,55	204,21	107,55	1,37 %	-3,25 %
3	204,31	204,31	107,27	107,27	204,31	107,27	1,41 %	-3,50 %
4	203,96	203,96	108,45	108,45	203,96	108,45	1,24 %	-2,44 %
5	203,85	203,85	109,41	109,41	203,85	109,41	1,19 %	-1,57 %
6	203,73	203,73	109,9	109,9	203,73	109,9	1,13 %	-1,13 %
7	203,22	203,22	111,95	111,95	203,22	111,95	0,87 %	0,71 %
8	199,34	199,34	111,12	111,12	199,34	111,12	-1,05 %	-0,04 %
9	198,06	198,06	113,38	113,38	198,06	113,38	-1,69 %	2,00 %
10	197,58	197,58	115,14	115,14	197,58	115,14	-1,93 %	3,58 %
11	200,99	200,99	119,29	119,29	200,99	119,29	-0,23 %	7,31 %
12	200,08	200,08	121,09	121,09	200,08	121,09	-0,68 %	8,93 %
13	199,13	199,13	122,82	122,82	199,13	122,82	-1,16 %	10,49 %
14	198,17	198,17	124,49	124,49	198,17	124,49	-1,63 %	11,99 %
15	196,83	196,83	126,69	126,69	196,83	126,69	-2,30 %	13,97 %
16	196,31	196,31	127,48	127,48	196,31	127,48	-2,56 %	14,68 %
17	195,19	195,19	129,28	129,28	195,19	129,28	-3,11 %	16,30 %
18	194,54	194,54	130,32	130,32	194,54	130,32	-3,43 %	17,24 %
19	194,1	194,1	131,17	131,17	194,1	131,17	-3,65 %	18,00 %
20	193,85	193,85	131,84	131,84	193,85	131,84	-3,78 %	18,60 %

Table D 21. Contours 1-20 for square line division 95, SING a.

SING	a							
NDIV Square lines	95							
	1	2	1	2	AVG	AVG		
Contour	KI	KI	KII	KII	KI	KII	KI%	KII%
1	200,83	200,84	101,25	101,26	200,835	101,255	-0,31 %	-8,91 %
2	203,66	203,67	108,31	108,3	203,665	108,305	1,09 %	-2,57 %
3	203,76	203,76	107,94	107,93	203,76	107,935	1,14 %	-2,90 %
4	203,41	203,42	109,12	109,12	203,415	109,12	0,97 %	-1,84 %
5	203,34	203,34	110,07	110,07	203,34	110,07	0,93 %	-0,98 %
6	203,21	203,22	110,57	110,56	203,215	110,565	0,87 %	-0,54 %
7	202,77	202,78	112,49	112,49	202,775	112,49	0,65 %	1,20 %
8	202,38	202,39	113,57	113,56	202,385	113,565	0,46 %	2,16 %
9	201,73	201,74	115,51	115,51	201,735	115,51	0,14 %	3,91 %
10	200,89	200,9	117,67	117,66	200,895	117,665	-0,28 %	5,85 %
11	200,15	200,16	119,41	119,4	200,155	119,405	-0,65 %	7,42 %
12	199,24	199,25	121,36	121,35	199,245	121,355	-1,10 %	9,17 %
13	198,34	198,36	123,03	123,02	198,35	123,025	-1,54 %	10,67 %
14	197,1	197,12	124,87	124,86	197,11	124,865	-2,16 %	12,33 %
15	193,85	193,86	125,35	125,34	193,855	125,345	-3,77 %	12,76 %
16	192,77	192,78	126,92	126,91	192,775	126,915	-4,31 %	14,17 %
17	191,96	191,97	128,13	128,12	191,965	128,125	-4,71 %	15,26 %
18	191,64	191,64	128,96	128,96	191,64	128,96	-4,87 %	16,01 %
19	191,3	191,1	130,01	130,24	191,2	130,125	-5,09 %	17,06 %
20	191,14	191,13	131,04	131,04	191,135	131,04	-5,13 %	17,88 %